Karlsruhe Institute of Technology

Synthesis of 4f and 3d-4f Homo and Hetero-metallic Complexes: Magnetism, Photoluminescence and Catalytic Studies

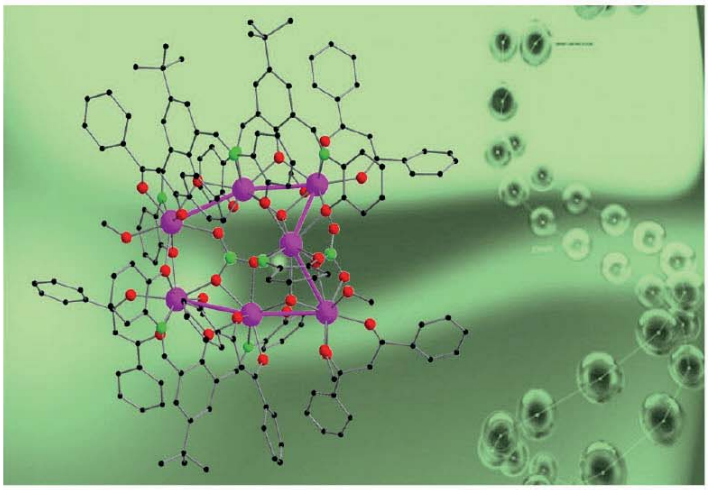

Munendra Yadav

Cuvillier Verlag Göttingen
Internationaler wissenschaftlicher Fachverlag

Synthesis of 4f and 3d-4f Homo and Heterometallic Complexes: Magnetism, Photoluminescence and Catalytic Studies

Dieses Werk ist copyrightgeschützt und darf in keiner Form vervielfältigt werden noch an Dritte weitergegeben werden.
Es gilt nur für den persönlichen Gebrauch.

Dieses Werk ist copyrightgeschützt und darf in keiner Form vervielfältigt werden noch an Dritte weitergegeben werden.
Es gilt nur für den persönlichen Gebrauch.

Synthesis of 4f and 3d-4f Homo and Heterometallic Complexes: Magnetism, Photoluminescence and Catalytic Studies

Zur Erlangung des akademischen Grades eines

DOKTORS DER NATURWISSENSCHAFTEN

(Dr. rer. nat.)

Fakultät für Chemie und Biowissenschaften

Karlsruher Institut für Technologie (KIT) - Universitätsbereich

Genehmigte

DISSERTATION

von

M. S.-Chem. Munendra Yadav

aus

Etah Uttar Pradesh, Indien

Dekan: Prof. Dr. P. W. Roesky

Referent: Prof. Dr. P. W. Roesky

Korreferent: Prof. Dr. Mario Ruben

Tag der mündlichen Prüfung: 24.10.2014

Dieses Werk ist copyrightgeschützt und darf in keiner Form vervielfältigt werden noch an Dritte weitergegeben werden.
Es gilt nur für den persönlichen Gebrauch.

Bibliografische Information der Deutschen Nationalbibliothek
Die Deutsche Nationalbibliothek verzeichnet diese Publikation in der
Deutschen Nationalbibliografie; detaillierte bibliografische Daten sind im Internet
über http://dnb.d-nb.de abrufbar.
1. Aufl. - Göttingen : Cuvillier, 2015
Zugl.: Karlsruhe (KIT), Univ., Diss., 2014

Die vorliegende Arbeit wurde in der Zeit vom 01. Sepetember 2011 bis zum 10. September 2014 am Institut für Anoganische chemie des Karlsruher Institut für Technologie (KIT) unter der Leitung von Prof. Dr. Peter W. Roesky durchgeführt.

© CUVILLIER VERLAG, Göttingen 2015
Nonnenstieg 8, 37075 Göttingen
Telefon: 0551-54724-0
Telefax: 0551-54724-21
www.cuvillier.de

Alle Rechte vorbehalten. Ohne ausdrückliche Genehmigung des Verlages ist
es nicht gestattet, das Buch oder Teile daraus auf fotomechanischem Weg
(Fotokopie, Mikrokopie) zu vervielfältigen.
1. Auflage, 2015
Gedruckt auf umweltfreundlichem, säurefreiem Papier aus nachhaltiger Forstwirtschaft.

ISBN 978-3-95404-961-5
eISBN 978-3-7369-4961-4

Dieses Werk ist copyrightgeschützt und darf in keiner Form vervielfältigt werden noch an Dritte weitergegeben werden.
Es gilt nur für den persönlichen Gebrauch.

Dedicated to my Parents

Dieses Werk ist copyrightgeschützt und darf in keiner Form vervielfältigt werden noch an Dritte weitergegeben werden.
Es gilt nur für den persönlichen Gebrauch.

Dieses Werk ist copyrightgeschützt und darf in keiner Form vervielfältigt werden noch an Dritte weitergegeben werden.
Es gilt nur für den persönlichen Gebrauch.

Contents

1 Introduction 1
1.1 Lanthanides 1
1.1.1 Oxidation states 1
1.1.2 Lanthanide contraction 1
1.1.3 Optical properties 1
1.1.4 Luminescence 2
1.2 Magnetism 4
1.2.1 Diamagnetism 4
1.2.2 Paramagnetism 5
1.2.3 Ferromagnetism 6
1.2.4 Antiferromagnetism 6
1.2.5 Ferrimagnetism 7
1.2.6 Canted Antiferrimagnetism 7
1.3 Magnetic behaviour 8
1.4 Single Molecule Magnets (SMM) 9
1.4.1 4f-based SMM 11
1.4.2 3d-4f-based SMM 13
1.4.3 SMM Applications 14
1.5 Metal Organic Frameworks (MOFs) 14
1.5.1History of MOF based catalysis 15
1.5.2 Basic Catalytic Requirements of CMOFs 18
1.5.3 Enantioselective Sulfoxidation 19
2 Research Objectives 21
3 Results and Discussion 23
3.1 Mononuclear and Tetranuclear Compounds of Yttrium and Dysprosium: Synthesis, Photoluminescence and Magnetism 23
3.1.1 Synthesis and Structures 23
3.1.2 Photoluminescence (PL) properties 27
3.1.3 Magnetic Properties of Compounds 31
3.2 Mononuclear dysprosium compound 35
3.3 Synthesis and Characterization of Binuclear (Ni-Ln) and Trinuclear (Ni-Ln-Ni) Complexes 37
3.3.1 Synthesis and Structures 37
3.4 Tetranuclear and Pentanuclear Clusters of Lanthanides: Synthesis and Magnetic Studies 41

Dieses Werk ist copyrightgeschützt und darf in keiner Form vervielfältigt werden noch an Dritte weitergegeben werden.
Es gilt nur für den persönlichen Gebrauch.

3.4.1 Synthesis and structures....42
3.4.2 Magnetic Properties....46
3.5 See-Saw and Square Planar Shaped Tetranulcear and Pentagonal prism Shaped Pentanuclear Complexes of Lanthanides: Synthesis and Magnetic study....50
3.5.1 Synthesis and Structures....50
3.5.2 Magnetic Properties....55
3.6 Mononuclear, Pentanculear and Hepatenuclear Complexes of Lanthanides: Synthesis and Magnetism.58
3.6.1 Synthesis and Structures....58
3.6.2 Magnetic Properties....63
3.7 Binuclear and Trinuclear complexes of Dysprosium: Synthesis....71
3.7.1 Synthesis and Structures....71
3.8 Salen-Based 1-D Coordination Polymers of Manganese and lanthanides: Synthesis and Catalytic sulfoxidation....76
3.8.1 Synthesis and Structures....76
3.8.2 Catalysis....79
4 Experimental sections....83
4.1 General considerations:....83
4.2 Photoluminescence (PL) Measurements....83
4.3 Magnetic Measurements....83
4.4 Synthesis of Compounds....84
4.4.1 Synthesis of {[Ln(HL)$_4$][ETAH]} (1,2)....84
4.4.2 Synthesis of {[Y$_4$(HL)$_2$(L)$_4$(μ_3-OH)$_2$]·4(MeOH)·4(H$_2$O)} (3)....84
4.4.3 Synthesis of {[Dy$_4$(HL)$_2$(L)$_4$(μ_3-OH)$_2$]·5(MeOH)·7(H$_2$O)} (4)....85
4.4.4 Synthesis of {[Dy$_4$(HL)$_8$(L)$_2$]·4(MeOH)·2(H$_2$O)} (5)....85
4.4.5 Synthesis of {[Dy(HL^1)$_2$(H$_2$O)$_3$]·(NO$_3$)} (6)....85
4.4.6 Synthesis of [NiLnL(acac)$_2$] (7-9)....86
4.4.7 Synthesis of {[NiDyL(Ph$_2$acac)$_2$]$_2$·4(CH$_2$Cl$_2$)·(MeOH)} (10)....87
4.4.8 Synthesis of [Ni$_2$Ln(L1)$_2$] (11- 13)....87
4.4.9 Synthesis of {[Dy$_4$(L^2)$_3$(Ph$_2$acac)$_4$]·(Et$_3$NH)·4(MeOH)·(MeCN)·(H$_2$O)} (14)....88
4.4.10 Synthesis of {[Ln$_5$(μ_3-OH)$_2$(L^2)$_2$(Ph$_2$acac)$_7$(Ph$_2$acacH)]·7(PhMe)} (15,16)....89
4.4.11 Synthesis of {[Ln$_4$(μ_3-OH)$_2$(L^2)(HL^2)(acac)$_5$(H$_2$O)]·(NO$_3$)·(HNEt$_3$)·2(Et$_2$O)} (17-21)....89
4.4.12 Synthesis of {[Dy$_4$(μ_4-OH)(L^2)$_2$(acac)$_4$(MeOH)$_2$(EtOH)(H$_2$O)]·(NO$_3$)·2(MeOH)·3(EtOH)} (22)....91
4.4.13 Synthesis of {[Dy$_5$(μ_5-NO$_3$)(L^2) (L^{2a})$_2$(acac)$_6$(iPrOH)$_2$(HO)(H$_2$O)]·4(H$_2$O)} (23)....91
4.4.14 Synthesis of {[Ln(Ph$_2$acac)$_4$](Et$_3$NH)}(24, 25)....92
4.4.15 Synthesis of {[Dy$_5$(μ_3-OH)$_2$(L^2)$_3$(Ph$_2$acac)$_4$(MeOH)$_4$]·4(MeOH)} (26)....92
4.4.16 Synthesis of {[Tb$_7$(μ_3-OH)$_2$(μ_5-(NO$_3$)(μ_3-NO$_3$)(L^2)$_3$(Ph$_2$acac)$_5$(H$_2$N-Ph-O)(MeO)$_2$(MeOH)$_3$]·(MeOH)$_3$·(MeCN)·15(H$_2$O)} (27)....93

Dieses Werk ist copyrightgeschützt und darf in keiner Form vervielfältigt werden noch an Dritte weitergegeben werden.
Es gilt nur für den persönlichen Gebrauch.

4.4.17 Synthesis of {[Dy_2L_3]·3(OH)·6(H_2O)·(C_6H_{12})} (28). 93
4.4.18 Synthesis of{[Dy_2L_3(OH)]·[$Dy(NO_3)_3(H_2O)_3$]·3(Py)·2(HO)·7(H_2O)·6(MeOH)·($CHCl_3$)} (29)....93
4.4.19 Synthesis of {[$Dy_2L_3(H_2O)$]·[$Dy(NO_3)(H_2O)_7$]·5(NO_3)·3(MeOH)·7(H_2O)} (30). 94
4.4.20 General procedure for the synthesis of complexes (31- 34). 94
4.4.21 General procedure for catalysis 95
4.4.22 NMR data of Sulfoxides 95
5 Crystal Structure Measurements....97
5.1 Data collection and refinement....97
5.1.1 {[$Y(HL)_4$][ETAH]·(H_2O)} (1)....98
5.1.2 {[$Dy(HL)_4$][ETAH]·(3MeOH)·(H_2O)} (2). 98
5.1.3 {[$Y_4(HL)_2(L)_4(\mu_3\text{-}OH)_2$]·4(MeOH)·4($H_2O$)} (3)....99
5.1.4 {[$Dy_4(HL)_2(L)_4(\mu_3\text{-}OH)_2$]·5(MeOH)·7($H_2O$)} (4)....99
5.1.5 {[$Dy_4(HL)_8(L)_2$]·4(MeOH)·2(H_2O)} (5). 100
5.1.6 {[$Dy(HL^1)_2(H_2O)_3](NO_3)$} (6). 100
5.1.7 {NiGdL$(acac)_2$} (7). 101
5.1.8 {NiTbL$(acac)_2$} (8)....101
5.1.9 {[NiDyL$(acac)_2]_2$·7(MeOH)} (9). 102
5.1.10 {[NiDyL$(Ph_2acac)_2]_2$·4(CH_2Cl_2)·(MeOH)} (10). 102
5.1.11 {[$Ni_2Gd(L^1)_2$]·(NO_3)·2(H_2O)} (11). 103
5.1.12 {[$Ni_2Tb(L^1)_2]_4$·4(NO_3)·3(MeCN)·5(MeOH)·(H_2O)} (12). 103
5.1.13 {[$Ni_2Dy(L^1)_2$]·(NO_3)(MeOH)·(H_2O)} (13). 104
5.1.14 {[$Dy_4(L^2)_3(Ph_2acac)_4$](Et_3NH)·4(MeOH)·(MeCN)·(H_2O)} (14)....104
5.1.15 {[$Tb_5(\mu_3\text{-}OH)_2(L^2)_2(Ph_2acac)_7(Ph_2acacH)$]·7(PhMe)} (15). 105
5.1.16 {[$Dy_5(\mu_3\text{-}OH)_2(L^2)_2((Ph_2acac)_7(Ph_2acacH)$]·7(PhMe)} (16). 105
5.1.17 {[$Tb_4(\mu_3\text{-}OH)_2(L^2)(HL^2)(acac)_5(H_2O)$]·($NO_3$)·($HNEt_3$)·2($Et_2O$)} (17). 106
5.1.18 {[$Dy_4(\mu_3\text{-}OH)_2(L^2)(HL^2)(acac)_5(H_2O)$]·($NO_3$)·($HNEt_3$)·2($Et_2O$)} (18)....106
5.1.19 {[$Ho_4(\mu_3\text{-}OH)_2(L^2)(HL^2)(acac)_5(H_2O)$]·($NO_3$)·($HNEt_3$)·2($Et_2O$)} (19)....107
5.1.20 {[$Er_4(\mu_3\text{-}OH)_2(L^2)(HL^2)(acac)_5(H_2O)$]·($NO_3$)·($HNEt_3$)·2($Et_2O$)} (20)....107
5.1.21 {[$Tm_4(\mu_3\text{-}OH)_2(L^2)(HL^2)(acac)_5(H_2O)$]·($NO_3$)·($HNEt_3$)·2($Et_2O$)} (21). 108
5.1.22 {[$Dy_4(\mu_4\text{-}OH)(L^2)_2(acac)_4(MeOH)_2(EtOH)(H_2O)$]·($NO_3$)·2(MeOH)·3(EtOH)} (22). 108
5.1.23 {[$Dy_5(\mu_5\text{-}NO_3)(L^2)(L^{2a})_2(acac)_6(iPrOH)_2(HO)(H_2O)$]·4($H_2O$)} (23). 109
5.1.24 {[$Tb(Ph_2acac)_4$]·(Et_3NH)} (24). 109
5.1.25 {[$Dy(Ph_2acac)_4]_2$·2(Et_3NH)·3(CH_2Cl_2)} (25)....110
5.1.26 {[$Dy_5(\mu_3\text{-}OH)_2(L^2)_3(Ph_2acac)_4(MeOH)_4$]·4(MeOH)} (26). 110
5.1.2{[$Tb_7(\mu_3\text{-}OH)_2(\mu_5\text{-}NO_3)(\mu_3\text{-}NO_3)(L^2)_3(Ph_2acac)_5(H_2N\text{-}PhO)(MeO)_2(MeOH)_3$]·3(MeOH)
·(MeCN)·15(H_2O) (27)....111

Dieses Werk ist copyrightgeschützt und darf in keiner Form vervielfältigt werden noch an Dritte weitergegeben werden.
Es gilt nur für den persönlichen Gebrauch.

5.1.28 {[Dy_2L_3]·3(OH)·6(H_2O)·(C_6H_{12})}(28). 111
5.1.29 {[Dy_2L_3(OH)]·[$Dy(NO_3)_3(H_2O)_3$]·3(Py)·2(HO)·7(H_2O)·6(MeOH)·($CHCl_3$)} (29). 112
5.1.30 {[$Dy_2L_3(H_2O)$][$Dy(NO_3)(H_2O)_7$]·5(NO_3)·3(MeOH)·7(H_2O)} (30). 112
5.1.31 {[$Pr_2(MnLClNO_3)_2(dmf)_6(H_2O)_2$]·($H_2O$)}$_n$ (31). 113
5.1.32 {[$Nd_2(MnLClNO_3)_2(dmf)_6(H_2O)_2$]·($H_2O$)}$_n$ (32). 113
5.1.33 {[$Sm_2(MnLClNO_3)_2(dmf)_6(H_2O)_2$]·($H_2O$)}$_n$ (33). 114
5.1.34 {[$Gd_2(MnLClNO_3)_2(dmf)_6(H_2O)_2$]·($H_2O$)}$_n$ (34). 114
6 Summary/ Zusammenfassung 115
6.1 Summary 115
6.2 Zusammenfassung 119
7 References 123
8 Appendices 131
8.1 Directory of Abbreviations 131
8.1.1 NMR Abbreviations 132
8.1.2 IR Abbreviations 133
8.1.3 Magnetic Abbreviations 133
8.2 Directory of Compounds 134

Dieses Werk ist copyrightgeschützt und darf in keiner Form vervielfältigt werden noch an Dritte weitergegeben werden.
Es gilt nur für den persönlichen Gebrauch.

1 Introduction

1.1 Lanthanides

The term “lanthanide” was introduced by Victor Goldschmidt with the name of its first element “lanthanum”.[1] It has the outer electronic configuration $6s^2 5d^1 4f^0$, so it can either be considered as a d-block elements or an f-block element. The relative energy of the 5d and 4f orbitals are very similar and sensitive to occupancy of orbitals but on the basis of stability of 4f shell which is slightly more compare to 5d shell, it was considered as f-block element. This criterion was followed by next 14 elements and electrons enter in the 4f shell until at lutetium.[2] The lanthanides are 15 elements in the periodic table considered as the first f-block elements, starting from lanthanum ($_{59}$La) to lutetium ($_{71}$Lu), which are commonly referred as “rare earth metals” along with scandium and yttrium. They are chemically represented by the symbol “Ln”.

1.1.1 Oxidation states

The most characteristic oxidation of the lanthanides is +3 and the electronic configurations for +3 oxidations states (Ln^{3+}) are represented as $4f^n 5d^0 6s^0$ with strict regularity.[2] Other oxidation states like +2 and +4 also exist but they are not generally stable as by losing or gaining one electron they can revert to +3. Eu(II) and Yb(II) are quite stable as they have half ($4f^7$) and completely filled ($4f^{14}$) subshells respectively. Eu(II), Sm(II) and Yb(II) can be prepared in aqueous solution but they can reduce water easily and are oxidized by oxygen. The lanthanides Nd, Dy, Tm and Ho can also form some compounds in the +2 oxidation state but they are stable in the solid state. The +4 oxidation state is shown by Ce, Pr and Tb but only Ce^{4+} is stable in water.[2]

1.1.2 Lanthanide contraction

In lanthanides due to shape of f-orbitals, shielding of one f-electron by another from the effects of nuclear charge is quite weak. So with increasing atomic number and nuclear charge, the effective nuclear charge experienced by each 4f electrons increases and it is apparent from atomic radii of the lanthanides. The atomic radius or ionic radius decreases from La to Lu with increase in atomic number due to lanthanide contraction.[3] The shrinking of atomic radii for Ln^{3+} is shown in Table 1.1.[4] Lanthanide contraction can also be explained in terms of bond lengths. This phenomena was reported in trinuclear series Ni-Ln-Ni (Ln= La to Tb).[5]

1.1.3 Optical properties

The absorption spectra of Ln^{3+} result from f-f transitions unlike the absorption spectra of transition metal result from d-d transitions.[6] The 4f orbitals are deep within atom, thus broadening effect of

Dieses Werk ist copyrightgeschützt und darf in keiner Form vervielfältigt werden noch an Dritte weitergegeben werden.
Es gilt nur für den persönlichen Gebrauch.

ligand vibrations are minimized and the absorption spectra of Ln^{3+} ions are typically very narrow in comparison with the d-d absorption bands of transition metals.[7, 8] The parity of ground state and excited state do not change due to laporte forbidden parity of f-f transitions so the absorption coefficient of lanthanides normally becomes very low. The spectral properties of Ln(III) ions are little influenced by external field generated by counter ions or ligand molecules.[6, 7, 9]

Table 1.1 General Properties of lanthanides.[2,4]

Atomic number	Name (symbol)	Electronic configurations	(M^{3+})	Oxidation states	Atomic radius (Ln^{3+}) Å	Ground state
57	Lanthanum (La)	$5d^16s^2$	f^0	+3	1.216	^1S_o
58	Cerium (Ce)	$4f^15d^16s^2$	f^1	+3, +4	1.196	$^2F_{5/2}$
59	Praseodymium(Pr)	$4f^36s^2$	f^2	+3, +4	1.179	$^3H_4$
60	Neodymium (Nd)	$4f^46s^2$	f^3	+2,+3, +4	1.163	$^4I_{9/2}$
61	Promethium (Pm)	$4f^56s^2$	f^4	+3	1.144	$^6H_{5/2}$
62	Samarium (Sm)	$4f^66s^2$	f^5	+2,+3	1.132	$^7F_0$
63	Europium (Eu)	$4f^76s^2$	f^6	+2,+3	1.120	$^8S_{3/2}$
64	Gadolinium (Gd)	$4f^75d^16s^2$	f^7	+3	1.107	$^8S_{3/2}$
65	Terbium (Tb)	$4f^96s^2$	f^8	+3, +4	1.095	$^7F_6$
66	Dysprosium (Dy)	$4f^{10}6s^2$	f^9	+2,+3, +4	1.083	$^6H_{15/2}$
67	Holmium (Ho)	$4f^{11}6s^2$	f^{10}	+2,+3	1.072	$^5I_8$
68	Erbium (Er)	$4f^{12}6s^2$	f^{11}	+3	1.062	$^4I_{15/2}$
69	Thulium (Tm)	$4f^{13}6s^2$	f^{12}	+2,+3	1.052	$^3H_6$
70	Ytterbium (Yb)	$4f^{14}6s^2$	f^{13}	+2,+3	1.042	$^2F_{7/2}$
71	Lutetium (Lu)	$4f^{14}5d^16s^2$	f^{14}	+3	1.032	^1S_o

1.1.4 Luminescence

Luminescence refers to the emission of light from a chemical substance when it is excited photonically, chemically or electrically. In photoluminescence, due to absorption (A) of light,

Dieses Werk ist copyrightgeschützt und darf in keiner Form vervielfältigt werden noch an Dritte weitergegeben werden.
Es gilt nur für den persönlichen Gebrauch.

electron is excited from ground state to excited states and it comes back to its ground state by loss of thermal energy and emission of a photon of lower energy. If the thermal loss is rapid and excited electron goes directly to the ground state {singlet (S) to singlet (S)} the process is called fluorescence (F). When the excited electron undergoes intersystem crossing (ISC) to a metstable triplet state and then it returns to ground state causing delay due to interconversion of states {singlet (S) to triplet (T)} then the process is called phosphorescence (P). In lanthanides, when the excitation and emission do not become analogous to fluorescence, then the emission of light is generally mentioned as time-resolved fluorescence.10

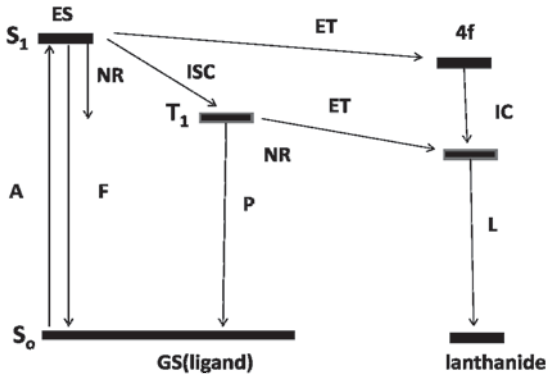

Figure 1.1 Energy diagram showing representation of photoluminescence[6], Abbreviations: L = lanthanide-centered luminescence; ET = energy transfer; IC = internal conversion; GS = ground state, ES = excited state.

Low extinction coefficients dominate the lanthanides luminescence. In general, the lanthanides luminescence[8, 9] is quenched by non-radiative (NR) process. The lanthanides have little luminescence background under ambient conditions; this may be an advantage in applications.[10]

Lanthanides shows very interesting luminescence properties[11] and their two main characteristics are long life times of emission and line-like emission spectrum.[6, 8] In the interest of luminescence, lanthanides have application in luminescent probes,[9] sensors, light amplification,[9] frequency conversion[12-14] and biomedical applications.[15] Anhydrous salts of Ln(III) ions show luminescence and they can be used in solid state laser materials and phosphors for color televisions while the hydrated lanthanides show lower luminescence intensity or no luminescence.[15]

In some applications, water-soluble complexes of Ln(III) are required. One of the drawbacks of lanthanides is that they have high affinity for water molecules, which can quench the excited states.[7] To overcome this problem, it becomes necessary to prevent the water molecules from binding. This can be possible with the help of suitable organic chromophores which can act as an efficient sensitizers for lanthanides.[7] To achieve such behaviour in lanthanide complexes, the ligand must

Dieses Werk ist copyrightgeschützt und darf in keiner Form vervielfältigt werden noch an Dritte weitergegeben werden.
Es gilt nur für den persönlichen Gebrauch.

have one or more chromophores and should be able to effectively pass the energy to excited states of Ln(III) ion.[7, 9, 16]

To detect *time-resolved fluorescence*, the lanthanide is sensitized with the help of an organic chromophore and it is called as "antenna" which can act to absorb the excitation light. The absorbed energy is transferred from excited singlet state of antenna to triplet state of Ln(III) ion after that it emits as a photon, this process is shown in Figure 1.2. The energy of triplet state should be little higher than the Ln(III) ion emitting levels, if the energy of triplet state is lower, then reverse transfer (Ln(III) ion to ligand) take place which can reduce the efficiency of sensitized emission.[6, 7]

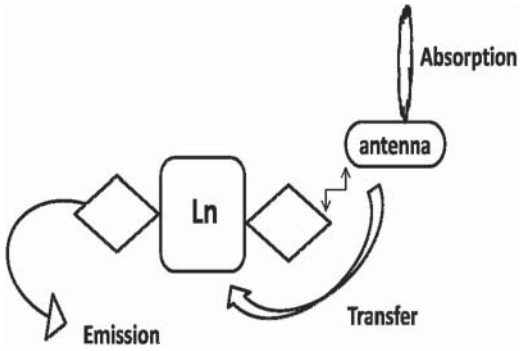

Figure 1.2 Representation of chromophore to acts as an antenna and absorb light which transfer the energy to the lanthanide excited state consequently emitted as a fluorescent signal with a long lifetime.[10]

1.2 Magnetism

Michal Faraday categorised substances either as diamagnetic or paramagnetic. It was followed up to many years, later it has been studied in terms of electronic structure. The origin of magnetism is due to orbital and spin motion of electrons as well as the interaction of these electrons with one another. Some substances have no interaction between the moments of neighbouring atoms, whereas other substances have very strong interactions with the moments of neighbouring atoms. On the basis of these interactions, the magnetic behaviour of substances is divided into six major classes.

1.2.1 Diamagnetism

When a substance is placed in an external magnetic field, there is an induced circulation of electrons producing a net magnetic moment aligned in or against the applied magnetic field. It emerges due to paired electrons of the sample hence it is called diamagnetic effect. These substances do not have net magnetic moments since all the occupied orbital's are containing a pair of electrons. When a substance has all of its electrons paired, this effect dominates and the material is classified as diamagnetic and producing negative magnetization and negative susceptibility. These substances are

Dieses Werk ist copyrightgeschützt und darf in keiner Form vervielfältigt werden noch an Dritte weitergegeben werden.
Es gilt nur für den persönlichen Gebrauch.

repelled by magnetic fields. In general, magnetic susceptibility is independent of the temperature and the strength of the applied field.

1.2.2 Paramagnetism

The origin of paramagnetism is due to unpaired electrons in the sample. The spin and orbital motions of electrons gives rise to permanent molecular magnetic moments which align themselves with an applied field. The paramagnetic effect is much stronger in comparison with the diamagnetic effect because it cancels any repulsion between an applied field and paired electrons in the sample. Substances which only have one unpaired electron per molecule also show the net attraction towards magnetic field. In the absence of an externally applied magnetic field, the paramagnetic effect is not observed as the thermal motion in bulk sample has no overall moment (Figure 1.3a). In the presence of applied magnetic field, there is counteraction between the thermal tendency towards randomness and the field capacity to force alignment (Figure 1.3b). As a result paramagnetic effect decreases in magnitude as the temperature is increased. Paramagnetic substances have positive magnetization and positive susceptibility due to partial alignment of the atomic magnetic moments in the direction of the field.

(a) (b)

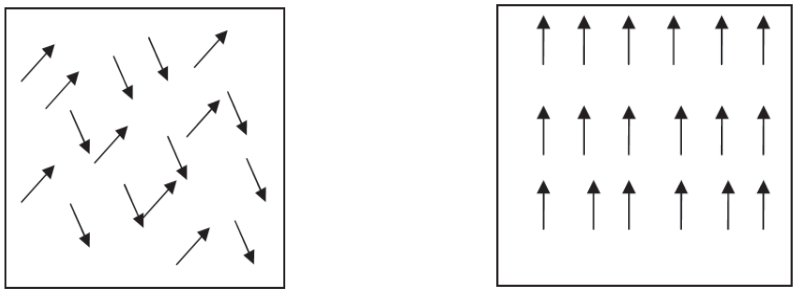

Figure 1.3 (a) In the absence of an external magnetic field electron orientation is random (b) In the presence of an external magnetic field electron oriented in one direction.[2]

The paramagnetic moment originates from spin and orbital motions of unpaired electrons and they have three modes of coupling (spin-spin, orbital-orbital and spin-orbital). In case of the lanthanides, all types of coupling and theoretical paramagnetic moments are considered.[2]

$$\mu = g[\, j(j+1)]^{1/2}$$

Where j is total angular momentum and g is the Lande splitting factor.

$$g = 1 + \frac{j(j+1) + S(S+1) - L(L+1)}{2j(j+1)}$$

Dieses Werk ist copyrightgeschützt und darf in keiner Form vervielfältigt werden noch an Dritte weitergegeben werden.
Es gilt nur für den persönlichen Gebrauch.

So the values of j depend upon total orbital angular momentum quantum number (L) and total spin angular momentum quantum number (S).

Complexes in which the spin-orbit coupling is negligible or nonexistent but they have significant spin and orbital contributions then the theoretical paramagnetic moment, value of μ can be given by,

$$\mu = [4S(S+1) + L(L+1)]^{1/2}$$

It is never completely realized in complexes because the orbital contribution is always less than ideal value. For the first raw transition metal, orbital contribution may be ignored; for the $L = 0$ condition, the value of μ can be given by,

$$\mu = 2[S(S+1)]^{1/2}$$

This is the spin-only formula for magnetic moment. The S will be related to the number of unpaired electrons.

1.2.3 Ferromagnetism

A substance which has interacting magnetic dipoles from its neighbouring paramagnetic centres in such a way that the individual moment is oriented in parallel alignment, then the substance is called ferromagnetic. Parallel alignment leads to an increase in the magnetic moment. In general ferromagnetic substances consist of domains to minimize its free energy. A spontaneous magnetization emerges in each domain even in the absence of a magnetic field. Normally, these substances have very large and positive magnetic susceptibly.[17] Ferromagnetic substances have certain temperature below which magnetic exchange dominates; this temperature value is called the Curie temperature (T_C). Above the Curie temperature, interactions are not strong enough to keep the individual moments in alignment and the substance behaves as a simple paramagnet.

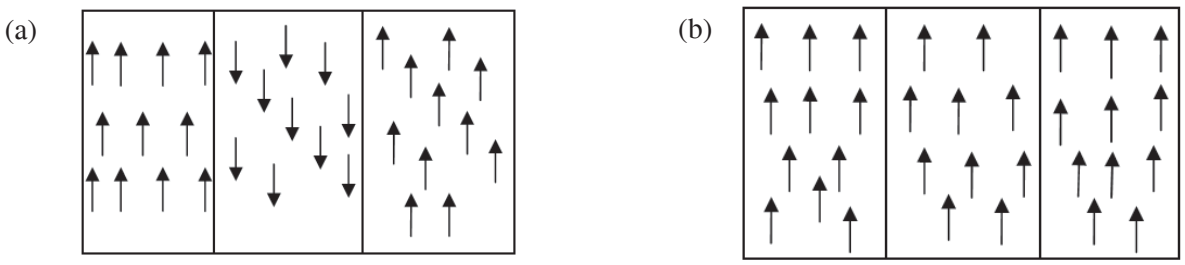

Figure 1.4 (a) In the absence of an external magnetic field the orientation of domains is random. (b) In the presence of an external magnetic field domains oriented in one direction.[2]

1.2.4 Antiferromagnetism

A substance which has interacting magnetic dipoles from its neighbouring paramagnetic centres in such a way that individual moment is oriented in antiparallel alignment then the substance is called

Dieses Werk ist copyrightgeschützt und darf in keiner Form vervielfältigt werden noch an Dritte weitergegeben werden.
Es gilt nur für den persönlichen Gebrauch.

antiferromagnetic. Due to complete antiparallel alignment of magnetic moments these substances do not show any spontaneous magnetization. Antiferromagnetic substances have a certain temperature below which magnetic exchange dominates; this temperature value is called the Neel temperature (T_N). Above the Neel temperature, interactions are no longer strong enough to keep the individual moments in alignment analogous to ferromagnetic substances, and they behave as a simple paramagnet.

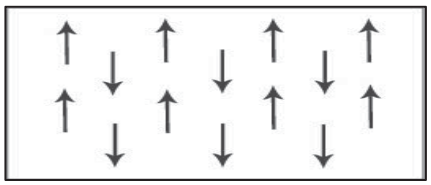

Figure 1.5 In the presence of an external magnetic field orientation of domains.[2]

1.2.5 Ferrimagnetism

In the case of ferrimagnetism,[18] magnetic moments are aligned antiparallel but they have incomplete compensation of the spins. In general, it is due to the unequal number of spins oriented in two directions or two types of spin centres have unequal number of unpaired electrons. Similar to ferromagnets, ferrimagnets also show spontaneous magnetization.

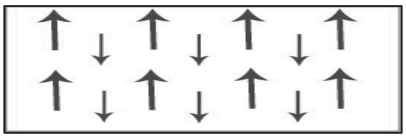

Figure 1.6 In the presence of an external magnetic field orientation of domains.

1.2.6 Canted Antiferrimagnetism

In the case of canted antiferrimagnetism,[19] the equilibrium distribution of moments is not collinear below the Neel temperature. The orientation of spins become canted and due to their incomplete compensation, passes the spontaneous magnetization called as canted antiferromagnetism or weak ferromagnetism.

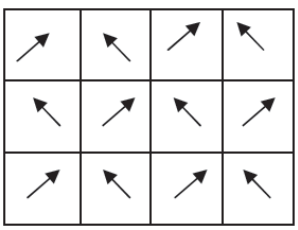

Figure 1.7 In the presence of an external magnetic field orientation of domains.

Dieses Werk ist copyrightgeschützt und darf in keiner Form vervielfältigt werden noch an Dritte weitergegeben werden.
Es gilt nur für den persönlichen Gebrauch.

1.3 Magnetic behaviour

In 1895 Pierre Curie stated that paramagnetic susceptibility is inversely proportional to absolute temperature. This law is known as *Curie's law*.

$$\chi_M = C / T$$

Where χ_M is molar susceptibility, C is the Curie constant and T is the temperature.

The Curie law is fairly applicable for paramagnetic substances, which are magnetically dilute, i.e. the substances, in which paramagnetic centers are well separated from each other by diamagnetic atoms. In materials, which are not magnetically dilute, unpaired spins on neighbouring centers may interact with each other and they do not follow the Curie law. The modified Curie-Weiss law for these substances can be given as below:

$$\chi_M = C / (T- \Theta)$$

Where, Θ is constant with units of temperature.

The magnetic susceptibility v/s temperature can be plotted in three ways. Commonly researchers use the χT versus T to determine the magnetic behaviour of the substances which is as shown in Figure 1.8.

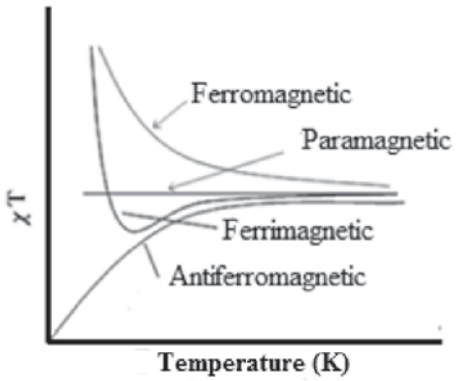

Figure 1.8 Plots of χT *v/s* temperature for paramagnetic, ferromagnetic, antiferromagnetic and ferrimagnetic materials.

In the case of paramagnetic substances, χT is independent of temperature and a horizontal straight-line is observed in the plot. In the case of antiferromagnets, χT is decreased with lowering in temperature and can be extended to zero (ground state S = 0). In the case of ferromagnets, χT increases as the temperature is decreased, whereas for ferrimagnets, χT first decreases to a minimum and after that it increases abruptly as the temperature is further decreased.

Dieses Werk ist copyrightgeschützt und darf in keiner Form vervielfältigt werden noch an Dritte weitergegeben werden.
Es gilt nur für den persönlichen Gebrauch.

1.4 Single Molecule Magnets (SMM)

It is a class of molecular compounds which shows supermagnetic behaviour below a certain temperature called as the blocking temperate (T_B). These complexes act as nanomagnets, in which every single molecule behaves like an independent magnet. The first time SMM behaviour was observed in manganese cluster (Mn_{12}) of formula $[Mn_{12}O_{12}(O_2CR)_{16}(H_2O)_4]$, after that in the last two decades many mono and polynulcear complexes have been discovered. SMM have magnetic relaxation many times slower (10^8) than normal molecular paramagnets.[20]

The basic requirement to show SMM behaviour is that the complex should have negative uni-axial magnetic anisotropy (D) and a non zero spin ground state (S). These two parameters combine to give an energy barrier by which slow relaxation of magnetization can take place. This energy barrier for integral spin is calculated by $U_{eff} = |D|S^2$ and for half integral spin $U_{eff} = |D|(S^2\text{-}1/4)$. The negative uni-axial anisotropy ($D < 0$) removes the degeneracy of ground spin states $(M_S) = \pm S$.

A known example of Mn_{12}-cluster[21-24] has taken to discuss about the SMM. Twelve manganese ions have two types of valencies, four Mn(IV) ions and eight Mn(III) ions are independently coupled with $S = 2$ and $S = 3/2$ respectively. The four Mn(IV) ions are antiferromagnetically coupled with eight Mn (III) ions in the complex so the total spin is $S = 8\times2 - 4\times3/2 = 10$, therefore $M_S = \pm10$ (Figure 1.9).

When no external field is applied to the system, energy levels degenerate and probability to find the molecule in either potential well should be equal.[24] In the presence of an applied magnetic field, the degeneracy of energy levels is removed, therefore one potential well preferentially will be more populated in comparison to other.[24] When the applied field is removed then the system will try to come back to thermal equilibrium (relaxation) through the thermally activated energy levels. If the two microstates have equal energy then the probability of quantum tunnelling is increased which is called quantum tunnelling of magnetization.[23, 24]

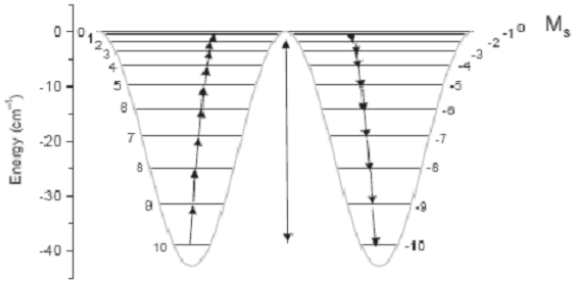

Figure 1.9 Plots of energies of the microstates in S = 10 system.[24]

Dieses Werk ist copyrightgeschützt und darf in keiner Form vervielfältigt werden noch an Dritte weitergegeben werden.
Es gilt nur für den persönlichen Gebrauch.

Magnetisation can be monitored as a function of time. If the energy barrier is high then it is possible to characterise in phase (χ'), out of phase signal (χ'') and hysteresis loops for a molecule. AC-susceptibility measurement of a sample produces two components, one component is susceptibility (χ) and other component is phase shift (ϕ). The phase shift produces a real component of susceptibility and an imaginary component of susceptibility. When real component of susceptibility starts to increase time imaginary component of susceptibility part starts to decrease as shown in Figure 1.10 as a function of frequency and temperature.

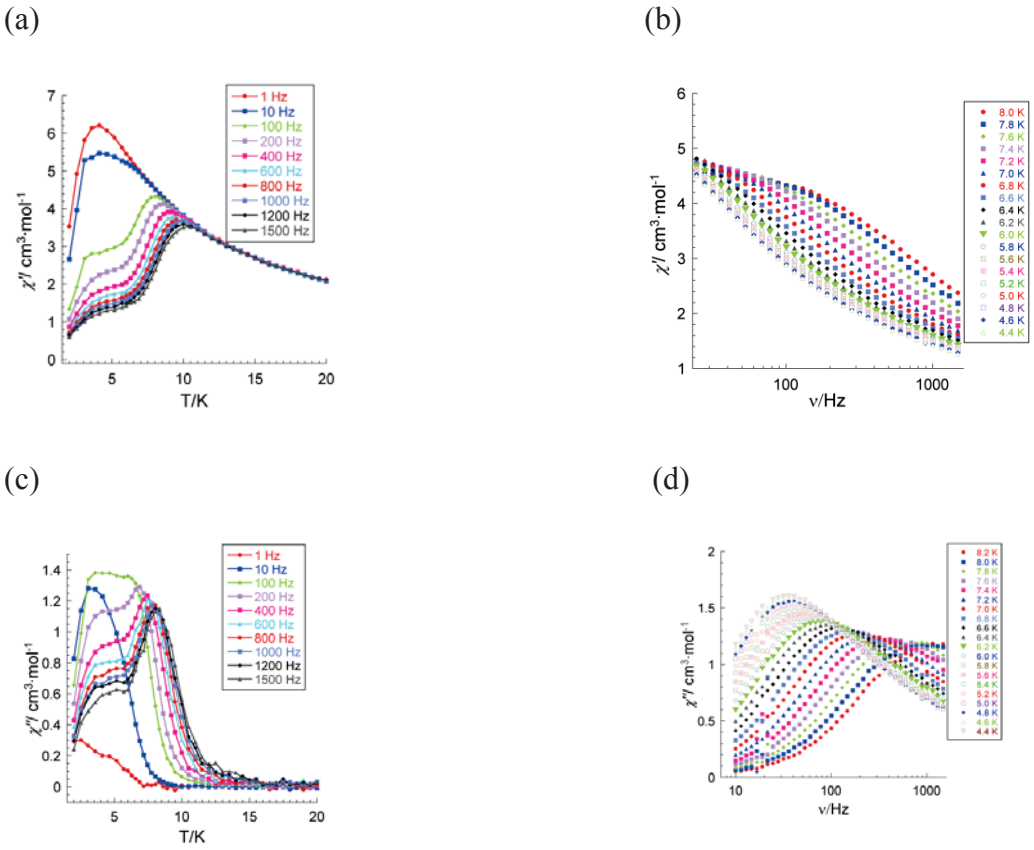

Figure 1.10 AC susceptibility measurements as a function of temperature at different frequencies, and as a function of frequency at different temperatures in-phase (a, b) and out-of-phase signals (c, d).

While the energy levels are thermally activated, energy barrier (U_{eff}) and the relaxation time (τ) can be calculated with the help of Arrhenius expression,

$$\tau = \tau_0 . e^{\left(\frac{Ueff}{K_B T}\right)}$$

If the energy barrier is small enough then the frequency of spin reorientation will be faster and maxima is not observed in out of phase signal or may be no out of phase signal (χ'') is perceived.

Dieses Werk ist copyrightgeschützt und darf in keiner Form vervielfältigt werden noch an Dritte weitergegeben werden.
Es gilt nur für den persönlichen Gebrauch.

1.4.1 4f-based SMM

Interest in lanthanide ions has been revived and 4f coordination compounds have been extensively investigated for their single-molecule magnet (SMM) and single-ion magnet (SIM) properties.[25] The large spin multiplicity and large magnetic anisotropies of lanthanides ions in the ground state plays a key role to get the SMM behaviour.[26] Strong single ion anisotropy of lanthanides and flexibility in anisotropy is another advantage by which it is easy to design the ligand so that it can create the ligand field anisotropy. These anisotropies are correlated as :

$$^{n}B_{m} = {}^{n}A_{m} \langle r^{m} \rangle \Theta_{m}$$

Where Θ_m is Stevens's factor, $^{n}B_m$ is m^{th}-order magnetic anisotropy parameters; $^{n}A_m \langle r^m \rangle$ denotes the ligand field anisotropy.[27]

The Θ_m parameter for lanthanides like Er(III) ion is positive so they require the equatorial ligand field to exhibit the SMM behaviour which is difficult to obtain as a result Er-based complexes are rarely reported in literature.[27] While the Θ_m parameter for lanthanides like Dy(III), Tb(III), and Ho(III) is negative so they require an axial ligand field to exhibit the SMM behaviour which is easy to achieve.[27] The symmetry at the individual Ln sites is crucial for the construction of SMMs and SIMs and for the control of the single-axial anisotropy.[13, 16-22]

The ligand should be designed on the basis of basic shape of free ion electron density. It is oblate for Ce(III), Pr(III), Nd(III), Tb(III), Dy(III), and Ho(III) ions, thus they prefer the axial coordinating geometry to minimize the charge contact and for prolate like Pm(III), Sm(III), Er(III), Tm(III), and Yb(III) ions prefer the equatorial coordinating geometry.[26]

In general for lanthanides, the spin-orbit coupling energy becomes larger than the crystal field energy so the quantum number *j* is extremely important. The interaction of the ground spin–orbit coupled *j* state with the crystal field gives the magnetic anisotropy barrier, which separates the opposite orientations of the spin ground state.

Two major requirements are essential to explore the anisotropy of lanthanides. Firstly ground state should be double degenerate with high magnitude. This means highly populated ground state can maintain the high magnetic moment at particular temperatures. Double degeneracy is essential because SMM are explained in terms of bistabilty of ground states.[26] For Dy(III) ion which can always maintain the degeneracy in ground state but for Tb(III) ion strictly axial symmetry is required to maintain it.[26] Secondly a large separation is required between the bistable ground state and the first excited state.

Dieses Werk ist copyrightgeschützt und darf in keiner Form vervielfältigt werden noch an Dritte weitergegeben werden.
Es gilt nur für den persönlichen Gebrauch.

As most of the complexes have axial coordinating ligands, the Dy(III) ion is an ideal candidate to function as SMM. Tb(III) ion shows similar behaviour but they require an extremely axial symmetry to get the bistable ground state. This ideal geometry for Tb(III) ion is obtained in bis-phthalocyanine sandwich-type complexes and as a result they have the highest anisotropy energy barrier yet discovered.

In 2003 first report of a mononuclear lanthanide complex, which showed slow relaxation of the magnetization at low temperature, $(Bu_4N)[Tb(Pc)_2]$ (H_2Pc = phthalocyanine)[28, 29] with energy barrier of 230 cm^{-1} led to acceptance of the lanthanides in single molecule magnetism. Since this discovery, there has been increasing interest in this area. From the study of Dy(III) ion, it undoubtedly has much more interest for SMM. A large number of mononuclear,[30-36] binuclear,[37-42] trinuclear,[43-46] tetranuclear,[47-51] and multinuclear[52-56] compounds of Dy(III) have been reported.

Lanthanide ions with high spins and intrinsic magnetic anisotropy along with strong orbital coupling [Dy(III), Tb(III), and Ho(III)] have been the focus of most research in this area.[57] Mononuclear,[28,29,58-60] binuclear,[61,62] and multinuclear[63-65] complexes of dysprosium and terbium have been reported. Some of them show a high energy barrier due to large intrinsic magnetic anisotropy and reduced quantum tunnelling of magnetization (QTM) at low temperature.

The drawback of magnetic behaviour in lanthanides is difficult to explain by spin models. It is difficult to support the magnetic interactions between neighbouring metal atoms. If one can achieve the ferromagnetic interactions then it may be possible to get the novel magnetic properties due to the large magnetic anisotropy of lanthanides.[66] To increase the knowledge based on magnetic data base, there is a continuous need to design new ligands to get more fascinating structures.[50,51,56, 67-69] In the last couple of years, many multinuclear clusters have been reported.[70, 71]

In terms of cluster size, an Er-based chiral 60 sodalite cage has been recently reported.[72] The magnetic properties of multinuclear clusters, especially the compounds of Dy(III) ion have been reported.[50,52,64,73] The metal ions of Dy(III) ion upto 26 nuclearity have been investigated for slow relaxation of magnetization.[74-76] The tetranuclear Dy_4 with defect dicubane[63] have the high anisotropic energy barrier of 170k and a square pyramid shaped pentanuclear[52] $[Dy_5O(OiPr)_{13}]$ has been investigated which have the highest energy barrier of 530K and slow magnetic relaxation at 40 K. Extending this work, same group has synthesized a Dy_4K_2 complex[77] which exhibited the highest energy barrier of all reported Dy-based complexes. When they diluted this complex with yttrium (Dy-doped Y complexes) an energy barrier of more than 800K is reached.

Dieses Werk ist copyrightgeschützt und darf in keiner Form vervielfältigt werden noch an Dritte weitergegeben werden.
Es gilt nur für den persönlichen Gebrauch.

If we deliberate more about fascinating structures, a detailed study of dysprosium triangle has been reported due its novel magnetic behaviour.[45,65,66,78,79] Dysprosium triangle which has non magnetic ground state has been investigated for its typical SMM behaviour[78], this is quite unfrequented. In a further study, this triangle was opened to a linear trinuclear structure where the near ions are ferromagnetically coupled and AC-susceptibility measurements showed slow relaxation of magnetization.[44] In another study, dysprosium triangle get coupled and a hexanuclear complex $\{[Dy_6(\mu_3\text{-}OH)_4L_4L'_2\text{-}(H_2O)_9Cl]Cl_5 \cdot 15H_2O\}$ (L = o-vanillato, H_2L' = 2-hydroxymethyl-6-methoxyphenol) has been reported, which has the high energy barrier of 139 cm^{-1}.[65] In terms of linear shaped geometry of Dy(III) ion, few binuclear,[62] trinuclear[44,80] and tetranuclear[64,81,82] clusters were reported. Out of these, some of them show interesting magnetic properties. The tetranuclear Dy_4 with linear shaped geometry showed two step relaxations with effective energy barriers (Δ) of 19.7 and 173 K.[64]

If we deliberate more about lanthanides highest anisotropy energy barrier and hysteresis temperature, a tetranuclear complexes $[Dy_4(\mu_3\text{-}OH)_2(bmh)_2(msh)_4Cl_2]$ (bmh = 1,2- bis(2-hydroxy-3-methoxybenzylidene) hydrazone, msh = 3-methoxysalicylaldehyde hydrazone) with defect dicubane central core have the energy barrier U_{eff} =170 K and hysteresis at 7K.[63] A dinuclear complexes $[K(18\text{-crown-}6)]\{[(Me_3Si)_2N]_2(THF)Dy\}_2$ core have the energy barrier U_{eff} = 123 cm^{-1} and hysteresis at 8.3 K.[83]

A terbium complex bridged by a N_2^{3-} radical has an energy barrier U_{eff} = 227 cm^{-1} and shows the hysteresis at 14 K.[37] The first phthalocyanine complex with mononuclear Tb(III) ions has been modified with the ligand by its chiral derivative, a double-decker terbium complex has been synthesized with an energy barrier U_{eff} = 422 cm^{-1}.[84] Another study of double decker phthalocyanine with intimate contact at graphite surface have the energy barrier U_{eff} = 566 cm^{-1} and shows the hysteresis at 7 K. This is the highest energy barrier known for mononuclear Tb-complexes.[85]

An Er-Single-Ion Magnet was reported which have the high energy barrier of 225 cm^{-1} and hysteresis at 1.8 K.[86]

1.4.2 3d-4f-based SMM

In the last two decades, many 3d–4f heterometallic complexes have been studied for their magnetic properties. The inspiration to combine 3d and 4f in one molecule comes through achievement of high spin ground states via the involvement of 3d metals and large single-ion anisotropy from 4f ions. In the beginning, work was concentrated mostly on Cu–Gd system and majority of coordination complexes have been investigated for ferromagnetic interactions.[85,86] By keeping in mind ferro- and

Dieses Werk ist copyrightgeschützt und darf in keiner Form vervielfältigt werden noch an Dritte weitergegeben werden.
Es gilt nur für den persönlichen Gebrauch.

ferrimagnet type of interactions may be helpful to get SMM behaviour, many 3d-4f heterometallic complexes have been synthesized.[87-89] To avoid the formation of either pure 3d or pure 4f metal complexes the choice of right ligand is essential and with the help of *o*-vanillin and its derivative ligands many complexes have been synthesized.[90,91] Some of them exhibit the SMM behaviour.[92] There are few reasons for the relatively small number of studies of 3d-4f complexes,[93] such as controlling the nuclearity of the metal complex, right choice of the ligand etc. A suitable ligand can control the nuclearity of complexes and also plays an important role to examine the construction of SMMs.[92, 94]

Few di-, tri-, and multinuclear Mn-Ln,[73,95,96] Fe-Ln,[97] Co-Ln[95,98] and Ni-Ln[5,88,99-102] complexes have been investigated for their magnetic properties. The Ni^{II}-Ln^{III} were also investigated for ferromagnetic behaviour like the Cu-Gd systems and found that Ni^{II}-Dy^{III} and Ni^{II}-Tb^{III} compounds exhibited the slow magnetic relaxation.

1.4.3 SMM Applications

It is possible to create molecular scale devices that can store information by using their orientation of molecular spin with the help of SMM.[103-105] They have potential applications in quantum computation due to their quantum coherent properties[106] and high density data storage.[107,108] SMM applications are limited as this behaviour can be obtained at extremely low temperature. Mn_{12}-cluster was the first complex which was investigated for SMM behaviour after that to achieve high blocking temperature is the major goal for chemist. In last two decades many complexes have been reported and in case of transition metal complexes anisotropy has been increased approximately 60% and highest hysteresis temperature is increased approximately 70%.[26] In case of f-elements anisotropy has increased approximately 1200% and highest hysteresis temperature is increased approximately 370%.[26] Still researchers in this area have the huge possibility to explore the new substance for magnetic study.

1.5 Metal Organic Frameworks (MOFs)

Metal organic frameworks are porous coordination polymers; they are a class of crystalline materials, which have potential voids between an infinite network of metal ions and organic ligands. Due to their very large surface areas, they have extremely high capability to adsorb gases of interest.

The first MOF was discovered in 1943, further a series of metal complexes were synthesized by Tomic et al. in 1965 with the help of aromatic carboxylic acid.[109] This field was further elaborated by R. Robson and co-workers in early 1990 by giving a beautiful concept of "node and-spacer" to design

Dieses Werk ist copyrightgeschützt und darf in keiner Form vervielfältigt werden noch an Dritte weitergegeben werden.
Es gilt nur für den persönlichen Gebrauch.

the porous coordination polymers.[110] First time by using the concept of "node and-spacer" it was possible to construct the 3D-metal organic frameworks.

A breakthrough came in research when the concept of rational design or reticular synthesis was initiated by Yaghi et al.[111-113] By using the concepts of secondary building units (SBUs) and isoreticular frameworks, we can conveniently design a series of highly porous and stable metal organic frameworks with various pore sizes, for example $[Zn_4(\mu_4\text{-}O)(O_2CR)_6]$.[114] It has been a good approach to synthesize microporous MOFs and they have been found interesting for gas storage and separation such gases as hydrogen, methane and carbon dioxide.[115,116]

In MOFs, metal ions or metal clusters act as nodes, and linker bridging organic ligands act as spacers or “struts”. With the help of this technique predictable network architectures were successfully synthesized as crystalline solids.[11] It is easy to modify the nodes and linkers to get the functional diversity of MOFs. By changing the size of the ligand, it is possible to change the porosity of MOFs from several angstroms to nanometres. Due to the stability of MOFs, they are promising for gas storage[115,116] and heterogeneous catalytic applications.[117,118]

1.5.1History of MOF based catalysis

In 1994, Makoto Fujita reported the $\{[Cd(4,4'\text{-}bpy)_n](NO_3)\}$ (bpy = Bipyridine) crystalline 2D-porous coordination polymer, which has the inner cavities surrounded by 4,4′-bipyridine units.[119] This complex has high shape selectivity towards some aromatic guests and it has been used as heterogeneous catalyst for the cyanosilylation of aldehydes.

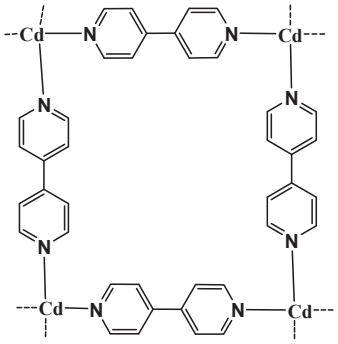

Scheme 1.1 A two-dimensional square network material with inner cavities and surrounded by 4,4’-bpy units.[119]

After that, in 1998 Aoyama reported the Ti- complex with hydrogen-bonded network. It has been used as a catalyst for the Diels-Alder reaction of ethyl acrylate with 1,3-cyclohexadiene and has been proved for the heterogeneous catalysis.[120]

Dieses Werk ist copyrightgeschützt und darf in keiner Form vervielfältigt werden noch an Dritte weitergegeben werden.
Es gilt nur für den persönlichen Gebrauch.

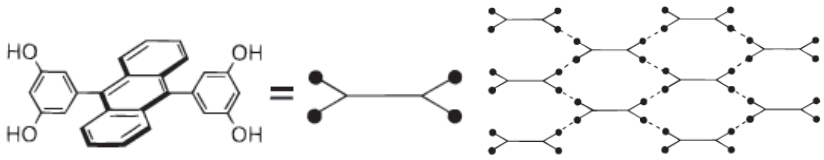

Scheme 1.2 The hydrogen-bonded network of a metal-coordination network.[120]

In 2000, the first asymmetric catalysis by MOFs was reported by Kim *et al*. First homochiral MOF was synthesized by solvothermal process $\{[Zn_3(\mu_3\text{-}O)(L_4\text{-}H)_6]2H_3O.12H_2O\}$.[121] It was used as a catalyst for the transesterification between an aromatic ester and ethanol. This work promoted the researcher to design the chiral ligands and homochiral metal organic systems for heterogeneous asymmetric catalysis. One year later Lin reported a series of homochiral MOFs, based on lanthanide phosphonate $[Ln(L_3\text{-}H_2)(L_3\text{-}H_3)(H_2O)_4]xH_2O$ (L-H_4 = 2,2′-diethoxy-1,1′-binaphthalene-6,6′-bisphosphonic acid) and used it as a catalyst.[122] This was the first asymmetric catalysis of MOFs which was promoted by metal ions at the nodes. This catalyst was examined for catalytic activity as a Lewis acid, unfortunately the enantiomeric excess (ee) was negligible.[122] Furthermore they designed the 2,2'-bis(diphenylphosphino)-1,1'-binaphthyl (BINAP) based homochiral bridging ligand with ruthenium complexes[123] and it was found to display excellent enantioselectivity in the asymmetric hydrogenation of aromatic ketones (up to 99.2% ee).[123] In 2005 Lin had synthesized the first crystalline 1,1'-Bi-2-naphthol (BINOL) based homochiral MOF. It was highly enantioselective and heterogeneous in asymmetric catalysis.[124]

In 2006, Hupp and co-workers reported the first chiral Mn(salen) MOF and examined the olefin epoxidation reaction.[125] This catalyst has higher catalytic activity in comparison to its homogeneous counterpart and it was recycled three times without loss of enantioselectivity.

Scheme 1.3 A chiral bridging Mn-salen complex and the achiral H_2bpdc.[125]

In 2009, Kim introduced organocatalyst units into preassembled achiral frameworks by postsynthetic modifications.[126] In this investigation, L-proline-based chiral ligands were connected to the open metal coordination sites of MIL-101. The resulting chiral metal-organic porous materials (MOPMs) showed remarkable catalytic activities in asymmetric aldol reactions and have much higher enantioselectivity compare to chiral ligands themselves.

Dieses Werk ist copyrightgeschützt und darf in keiner Form vervielfältigt werden noch an Dritte weitergegeben werden.
Es gilt nur für den persönlichen Gebrauch.

In 2010, Lin reported a series of isoreticular chiral metal–organic frameworks from copper paddle-wheels and BINOL-derived tetracarboxylic acid, which act as bridging ligands with the formula $[LCu_2(solvent)_2]$ (L = chiral tetracarboxylate ligand derived from 1,1′-bi-2-naphthol) and they were post-synthetically functionalized with $Ti(OiPr)_4$.[127] All the CMOFs have the same non-interpenetrating framework structures but different open channel sizes and they provided an ideal platform for generating the heterogeneous catalysts. Figure 1.11 is represented from their publication.[127]

The CMOF/$Ti(O^iPr)_4$ combinations are highly active catalysts for the additions of diethylzinc and ethyl(phenylalkynyl)zinc to a wide range of the aromatic aldehydes, which is fruitful for the synthesis of chiral secondary alcohols. The detailed study make it clear that the ee results in all reactions are dependent on the open channel sizes since there is competition between the enantioselective $(BINOL_{ate})Ti(O^iPr)_2$-catalysed reaction and the non-enantioselective background reaction as the rates of diffusion of organic substrates in the open channels of varied sizes were different.

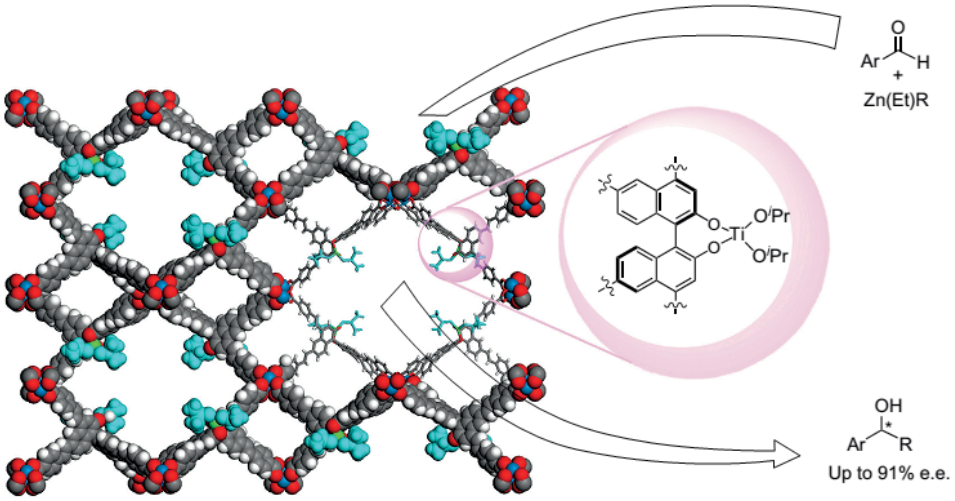

Figure 1.11 Representation of asymmetric alkyl- and alkynylzinc additions catalysed by the CMOF/Ti-BINOLate catalyst within large open channels and binding of Ti(IV) to the CMOF framework.[127]

In 2011, Telfer reported a new strategy for the introduction of organocatalytic groups into MOFs. This study explored the synthesis of a Chiral-MOF by protecting catalytically active sites with the help of protecting group. It was removed after synthesis of CMOF, which convert the framework into an active catalyst.[128]

In 2013 we reported a series of 1D achiral coordination polymers (CPs) based on manganese- and lanthanide metal atoms.[129] The polymers consist of manganese–salen-based metalloligands having carboxylate linkers connected to lanthanide atoms to form 1D CPs as shown in Figure 1.12. The CPs

Dieses Werk ist copyrightgeschützt und darf in keiner Form vervielfältigt werden noch an Dritte weitergegeben werden.
Es gilt nur für den persönlichen Gebrauch.

were tested for heterogeneous catalysis and during the study found that they were catalytically active for epoxidation. It was the first example of 1D-coordination polymers which were used as heterogeneous catalysts in an epoxidation reaction of an alkene with molecular oxygen or synthetic air. The comparison of CPs with homogeneous Jacobsen-type catalyst shows that heterogeneous CPs are well-stabilized since more conversion was obtained in comparison to Jacobsen-type catalyst and the later started to decompose after few hours.

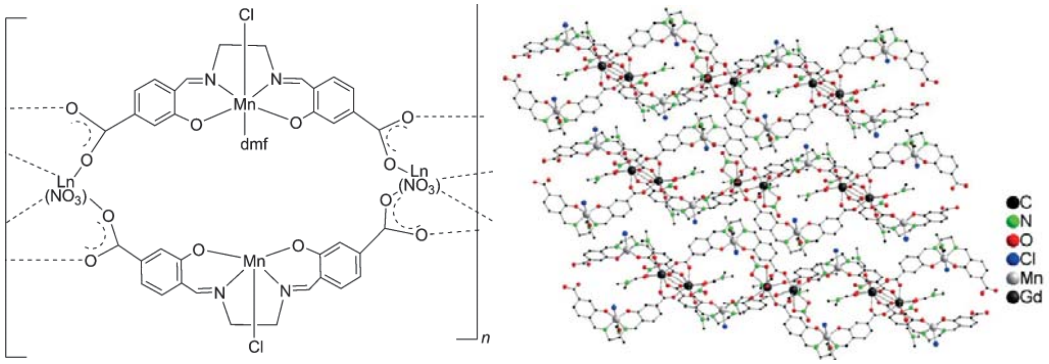

Figure 1.12 Simplified drawing of 1D achiral coordination polymer (left) and polymeric structure (right).[129]

In 2014, Lin introduced the first phosphine based metal−organic frameworks for hydrogenation and aryl/alkyl addition reactions.[130] In asymmetric catalysis, it was found that the Rh-complex, which worked as heterogeneous catalyst was 3 times more active in comparison to its homogeneous counterpart and produced the aryl addition products with ee values of more than 99%.

1.5.2 Basic Catalytic Requirements of CMOFs

A CMOF should have following characteristics to act as a catalyst, for the high enantioselectivity and high conversion.[117]

1. Chiral catalytically active centers and chiral induction should be in proper position to achieve high enantioselectivity in products.
2. The frameworks should have large pores or channels to get higher diffusion of substrates into pores to achieve the high catalytic activity. In CMOFs chiral pores also helps to achieve the high enantioselectivity.
3. The frameworks should be stable enough to maintain its structural integrity during catalysis, and separation of the catalyst from reactions mixtures should be easy.

Dieses Werk ist copyrightgeschützt und darf in keiner Form vervielfältigt werden noch an Dritte weitergegeben werden.
Es gilt nur für den persönlichen Gebrauch.

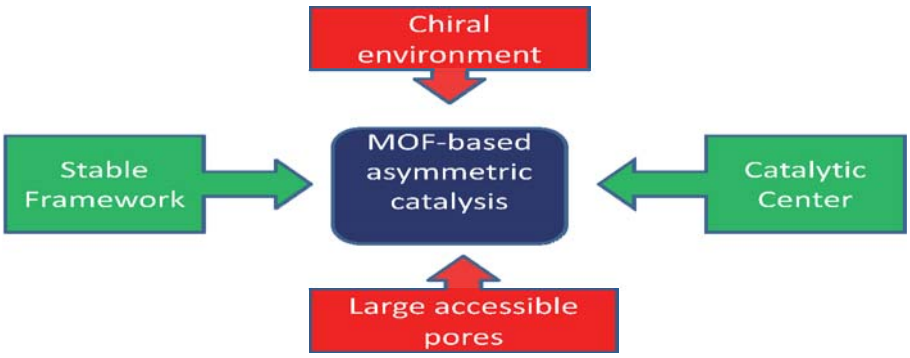

Figure 1.13 Simplified drawing of general requirements for MOF-based asymmetric catalyst.[117]

1.5.3 Enantioselective Sulfoxidation

The significance of enantioselective sulfoxides[131] in biological systems cannot be underestimated, as they have application in medicinal and pharmaceutical chemistry.[132] The enantiomeric rich sulfoxides play a very important role in biological systems.[133] Sulfoxides can be synthesized starting form achiral molecules with the help of enantiomeric pure catalyst which play a key role in asymmetric sulfoxides synthesis.[132] Recently, researchers have been much influenced by the concept of heterogeneous catalysis especially for chiral metal organic framework (CMOF) which can be synthesized by using enantiomeric pure salen ligands.[134-136] With the help of CMOFs it is easy to synthesize chiral molecule starting from achiral substrate where CMOFs work as a catalyst.[137] In the last two decades, metal complexes of titanium, vanadium, chromium, manganese and iron[138] with chiral moieties have shown exceptional efficiency in the enantioselective oxidation of sulfides and they have been extensively studied for homogenous catalysis.[139] In heterogeneous catalysis,[131,140] catalyst can be separated from reaction mixtures and they can be reused. They are also helpful in obtaining high enantiomeric purity since sometimes reactions occur inside the chiral pores of CMOF.[137]

Dieses Werk ist copyrightgeschützt und darf in keiner Form vervielfältigt werden noch an Dritte weitergegeben werden.
Es gilt nur für den persönlichen Gebrauch.

Dieses Werk ist copyrightgeschützt und darf in keiner Form vervielfältigt werden noch an Dritte weitergegeben werden.
Es gilt nur für den persönlichen Gebrauch.

2 Research Objectives

The main objective of thesis was the synthesis of 4f and 3d-4f homo- and heterometallic complexes and to investigate their magnetic, luminescent and catalytic properties. The first strategy was to synthesize the Schiff base 2-aminoethyl-hydroxybenzoic acid (H_2L), which contains carboxylic and hydroxyl groups as linkers. Other derivatives of this ligand have been reported by our group and investigated for magnetic behaviour.[73] H_2L was chosen to synthesize the Dy and Y-based metal complexes and the plan was to study their magnetic and fluorescence properties. This ligand was later modified to 2-hydroxy-3-(pyridine-4-carbonyl)-hydrazonomethyl-benzoic acid (H_2L^1). The H_2L^1 proligand is more rigid than H_2L and the target was to synthesize mononuclear lanthanide complexes.

Scheme 2.1 Chemical structure of the proligands H_2L and H_2L^1.

The next idea was to synthesize 3d-4f metal complexes with bulky flexible polydentate ligands. Tris-((2-hydroxybenzyliden)-aminoethyl)amine (H_3L) and tris-((2-hydroxy-3-methoxybenzyliden)-aminoethyl)amine (H_3L^1) ligands were prepared. These ligands were selected to obtain binuclear and trinuclear 3d-4f complexes.

Scheme 2.2 Chemical structure of the proligands H_3L and H_3L^1.

In another synthesis, the target was to synthesize lanthanide clusters of various nuclearity in order to examine their magnetic behaviour. Thus, a bulky and slightly more rigid polydentate ligand, 4-tert-butyl-2,6-bis-[(2-hydroxy-phenylimino)-methyl]-phenol (H_3L^2), was prepared. H_3L^2 was used to synthesize more interesting multinuclear lanthanide compounds for magnetic studies.

Dieses Werk ist copyrightgeschützt und darf in keiner Form vervielfältigt werden noch an Dritte weitergegeben werden.
Es gilt nur für den persönlichen Gebrauch.

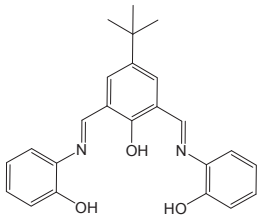

Scheme 2.3 Chemical structure of the proligand H_3L^2.

After this, the goal was to get more fascinating structures. Thus, the proligand H_3L^2 was modified to (3-{5-tert-butyl-2-hydroxy-3-[(2-hydroxy-phenylimino)-methyl]-benzylidene}-pentane-2,4-dione) (H_2L^{2a}). This work was extended to control the nuclearity of the metal complexes and synthesized the 4-tert-butyl-2,6-bis-[(pyridine-4-cabonyl)-hydrazonomethyl]-phenol proligand (HL) was synthesized to get binuclear complexes.

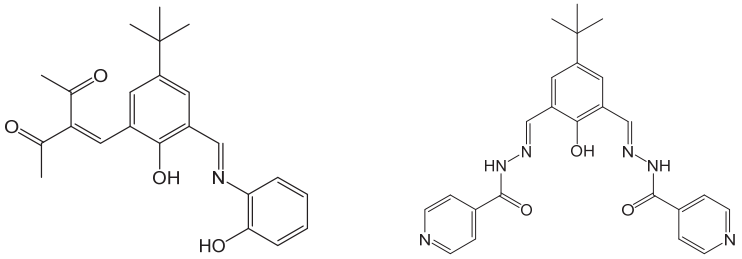

Scheme 2.4 Chemical structure of the proligands H_2L^{2a} and HL.

Previously, in our group 1D coordination polymers (CPs) have been reported with *N,N′*-bis(4-carboxysalicylidene) ethylenediamine (H_4L) ligand and investigated for catalytic[129] and magnetic properties. Continuing this work, the aim was to synthesize new chrial-1D CPs, which could be used in catalysis. So, the new chiral salen proligand, *N,N′*-bis(4-carboxysalicylidene)cyclohexanediamine (H_4L), was prepared and used for coordination polymer formation.

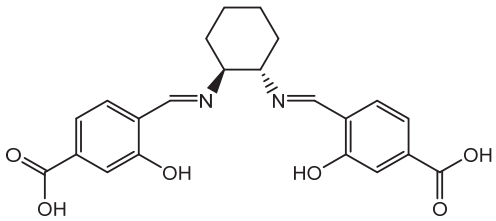

Scheme 2.5 Chemical structure of the chiral proligand H_4L.

Dieses Werk ist copyrightgeschützt und darf in keiner Form vervielfältigt werden noch an Dritte weitergegeben werden.
Es gilt nur für den persönlichen Gebrauch.

3 Results and Discussion

3.1 Mononuclear and Tetranuclear Compounds of Yttrium and Dysprosium: Synthesis, Photoluminescence and Magnetism

3.1.1 Synthesis and Structures

The proligand Schiff-base 2-aminoethyl-hydroxybenzoic acid (H_2L) was described before.[141] We prepared this ligand and fully characterized it again. During our investigation we realized that an *in situ* preparation from 3-formylsalicylic and ethanolamine without an isolation of H_2L is most efficient for the synthesis of lanthanides compounds. Thus, 3-formylsalicylic acid was reacted with ethanolamine (ETA) in different ratios and different reaction conditions in the presence of the metal salts $[Ln(NO_3)_3 \cdot (H_2O)_6]$ (Ln = Y, Dy). By using pyridine as base in methanol and 1:4 (Ln/ H_2L) ratio, the mononuclear $\{[Y(HL)_4][ETAH] \cdot (H_2O)\}$ (**1**), $\{[Dy(HL)_4][ETAH] \cdot 3(MeOH) \cdot (H_2O)\}$ (**2**) were obtained at room temperature (Scheme 3.1). By using triethylamine as base and 1:2 (Ln/ H_2L) ratio under similar reaction conditions the planer tetranuclear clusters with butterfly structures $\{[Y_4(HL)_2(L)_4(\mu_3\text{-}OH)_2] \cdot 4(MeOH) \cdot 4(H_2O)\}$ (**3**) and $\{[Dy_4(HL)_2(L)_4(\mu_3\text{-}OH)_2] \cdot 5(MeOH) \cdot 7(H_2O)\}$ (**4**) were obtained (Scheme 3.1). On changing the metal to ligand ratio to 1:3 (Ln/ H_2L) and increasing the reaction temperature to 80 °C the tetranuclear cluster $\{[Dy_4(HL)_8(L)_2] \cdot 4(MeOH) \cdot 2(H_2O)\}$ (**5**) was obtained (Scheme 3.1). All compounds could be isolated as single crystalline material directly from the reaction mixture. Obviously, the stoichiometric ratio and the reaction conditions play a key role in the formation of different type of compounds. Compounds **1-5** were characterized by spectroscopic and analytical techniques. All complexes are poorly soluble in common organic solvents and it was not possible to acquire NMR data. The solid state structures were established by single X-ray diffraction.

Dieses Werk ist copyrightgeschützt und darf in keiner Form vervielfältigt werden noch an Dritte weitergegeben werden.
Es gilt nur für den persönlichen Gebrauch.

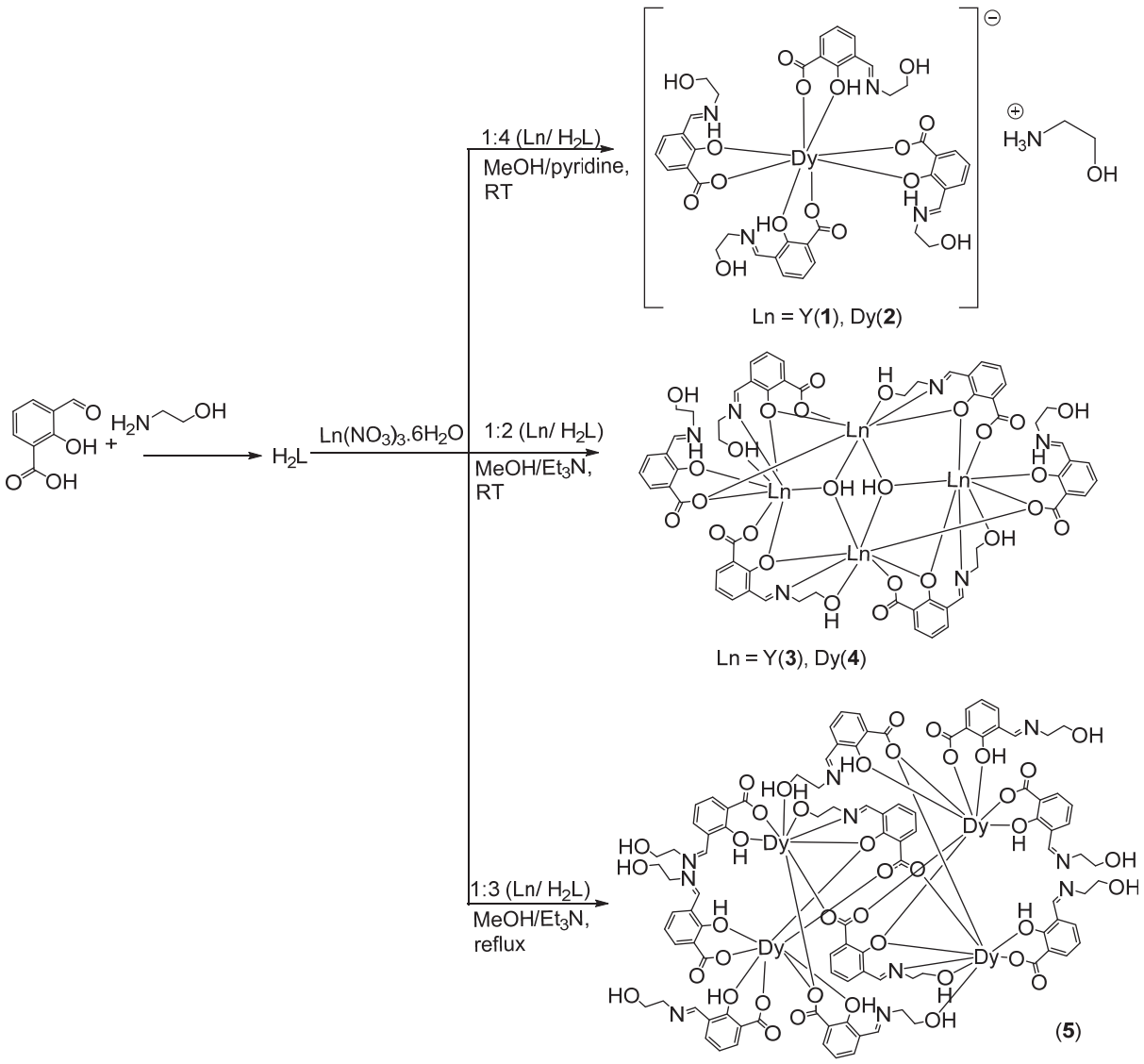

Scheme 3.1 Synthesis of compounds **1-5**.

Although the yttrium complex **1** crystallized in the monoclinic space group *C*2/*c*, whereas complex **2** crystallized in the monoclinic space group $P2_1/c$ the structures of the ionic complexes **1** and **2** are similar, differing only in the number of solvent molecules (MeOH and H_2O). Compound and **1** and **2** consist of a $[Ln(HL)_4]^-$ coordination anion and protonated disordered ethanolamine $(ETAH)^+$ cation as well as disordered H_2O (**1**) or CH_3OH and H_2O molecules (**2**) (Figure 3.1). In compound **1** a crystallographic *C*2 through the Y atom is observed, whereas in **2** this symmetry axis is not observed and only a non-crystallographic pseudo *C*2-axis thru the Dy atom is seen in the anion. However, the structural parameters of both compounds are similar. The structures of the anions are supported by ESI-MS data. The $[Ln(HL)_4]^-$ anion consists of one Ln(III) ion coordinated by monoanionic Schiff-base ligands. Thus, the metal atom is 8-fold coordinated by four phenol oxygen atoms and four carboxyl oxygen atoms from the ligands, resulting in a distorted square anti-prismatic coordination polyhedron. Although, we can observe some electron density between the phenol oxygen atom and the Schiff-base nitrogen atom (see Scheme 3.1), it is not possible to unambiguously assign the

Dieses Werk ist copyrightgeschützt und darf in keiner Form vervielfältigt werden noch an Dritte weitergegeben werden.
Es gilt nur für den persönlichen Gebrauch.

position of the remaining acidic proton of the ligand. However, based on the *pK*a values we consider the benzoate function as deprotonated and the phenol as protonated in the ligand. The Ln-O (phenolate) and Ln-O (carboxyl) distances are in the range of 2.261(3) Å - 2.264(3) Å (**1**); 2.261(6) Å -2.330(6) Å (**2**) and 2.391(3) Å -2.392(3) Å (**1**); 2.371(6) Å - 2.383(6) Å (**2**), respectively. There is a very slight difference in the Ln-O bond lengths of the phenolic and the carboxyl groups. Hydrogen bonds are observed between the proton of the alcohol function and the non-coordinating oxygen atom of the benzoate group. These bonds cause a folding of the ligand to compact structure without dangling arms.

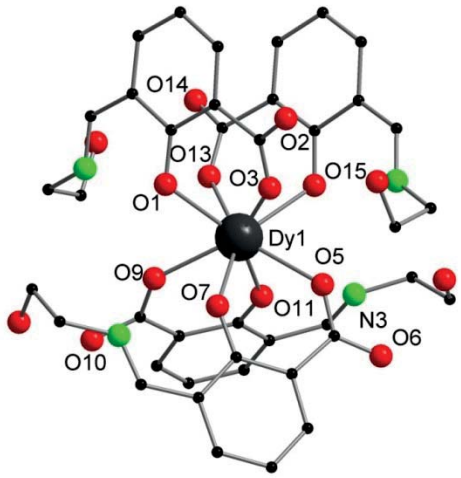

Figure 3.1 Solid state structure of the anion of **2**, shown is the coordination arrangement of a dysprosium, omitted hydrogen atoms for clarity. The color codes of balls: Dy, dark gray; O, red; N, green; C, black.

Complexes **3** and **4** are isostructural and crystallize in the monoclinic space group $P2_1/c$ with half of the cluster and some disordered CH_3OH and H_2O molecules in the asymmetric unit (Figure 3.2). Only the number of solvent molecules (MeOH and H_2O), which could be refined differ. Thus, we describe here the structure of compound **4** in detail.

A crystallographic inversion center is observed in the center of **4**. The Dy atoms are arranged with a planar rhomboid scaffold. Such planar Dy_4 complexes are relatively rare.[48,49,63,142] The metal core of **4** consists of four Dy (III) ions (Dy1, Dy2, Dy1', and Dy2'). In the center of the complex two μ_3-hydroxide ligands bridge the central Dy1 and Dy1' ions and one of the outer ions (Dy2 or Dy2'). These two μ_3-OH groups are nearly symmetrically arranged between the metal centers. The oxygen atom (O1 and O1') are located 0.923 Å out of the plane of the metal cores. The Dy2-O1 and Dy1-O1 distances are 2.327(3) Å and 2.356(3) Å respectively and of Dy1'-O1-Dy1 and Dy2-O1-Dy1 are angles are 108.00(12)° and 109.97(12)°, respectively. The periphery of the complex is bridged by the six Schiff-base ligands. Four ligands bind in a tetradentate μ_2-coordination mode with one carboxyl oxygen atom, the phenolate and the alcohol oxygen atoms as well as the Schiff-base nitrogen atom.

Dieses Werk ist copyrightgeschützt und darf in keiner Form vervielfältigt werden noch an Dritte weitergegeben werden.
Es gilt nur für den persönlichen Gebrauch.

We consider these four ligands as deprotonated at the phenol and at the acid function. The carboxyl oxygen atom and the phenolate oxygen atoms of these ligands bind to Dy2 whereas the phenolate and the alcohol oxygen atoms as well as the Schiff-base nitrogen atom bind to Dy1. The phenolate oxygen atoms of the four Schiff-base ligands adopt a μ_2-bridging mode. The remaining two Schiff-base ligands coordinate as observed in compound **2** in a κ^2-mode with the phenol oxygen and the carboxyl oxygen atoms to the metal center. These two ligands are only single negative charged. The ligands adopt a μ_2-bridging mode in which the carboxylate oxygen atoms coordinate to Dy1 and Dy2. As already reported for **1** and **2**, we can observe some electron density between the phenol oxygen atom and the Schiff-base nitrogen atom of these ligands (see Scheme 3.1) but we cannot unambiguously assign the position of the remaining acidic proton. All Dy ions are eight-fold coordinated from seven oxygen atoms and one imine nitrogen atom. All Dy-atoms adopt a distorted square anti-prismatic coordination geometry. The two square bases of the square antiprism for Dy1 consist of O1, O1', O2, O4, and O6, O12, O13, N3, whereas for Dy2, the two square bases are defined by the atoms O1, O4, O5, N1 and O6, O8, O11, O12. A significant intramolecular hydrogen bonding interaction has been observed between hydroxyl, carboxylic and imines part of the complex in the range of 2.588-2.627 Å and intermolecular hydrogen bonding was observed due presence of methanol and water molecules in the lattice which are in the range of 2.680-2.947 Å.

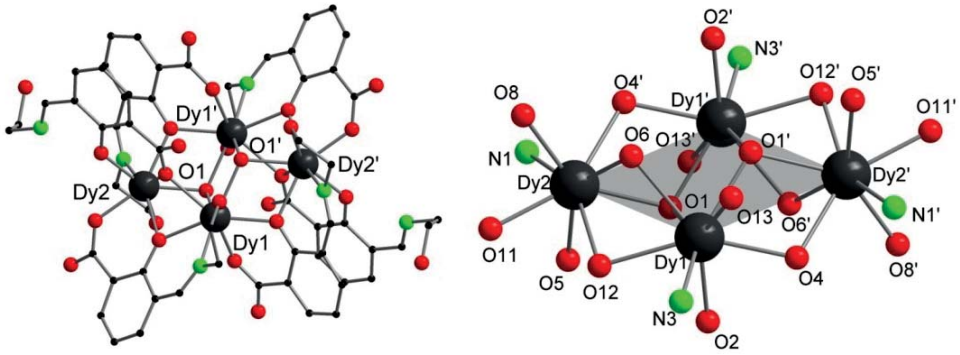

Figure 3.2 Solid state structure of **4** (left), and side view of the planar Dy_4 core (right). Hydrogen atoms have been omitted for clarity.

The tetranuclear complex **5** crystallizes in the monoclinic space group $P2_1/n$ with half of the molecule and some disordered CH_3OH and H_2O molecules in the asymmetric unit (Figure 3.3). A crystallographic inversion center is observed in the center of **5**. The four dysprosium ions, which are coordinated by ten Schiff-base ligands, are arranged in a planar rectangular scaffold. The molecular structure consists of two binuclear subunits, in which each unit has two different types of dysprosium ions and four molecules of the ligand acting as a bridge to connect these subunits. To the best of our knowledge this is unique structure among all the reported Dy_4 cluster arrangements. Out of the ten ligands, which are coordinated to the metal two are double deprotoned whereas eight are only single

Dieses Werk ist copyrightgeschützt und darf in keiner Form vervielfältigt werden noch an Dritte weitergegeben werden.
Es gilt nur für den persönlichen Gebrauch.

negative charged. As observed for **3** and **4** the double deprotoned ligands ($[L]^{2-}$) bind in a tetradentate mode to the metals. They are localized in the center of the cluster and bridge three dysprosium atoms each. The bridges are formed by the carboxylate and the phenolate groups. Two single negative charged ligands ($[HL]^-$) bind as it was observed in compound **2** in a κ^2-mode with the phenol oxygen and the carboxyl oxygen atoms in a chelating fashion to Dy1 and Dy1'. A third equivalent of $[HL]^-$ binds in the same chelating mode to Dy1 or Dy1' but also coordinates in a metal bridging mode via the carboxylate group to Dy2 or Dy2'. Furthermore, the alcohol function coordinates to a third dysprosium atom.

All dysprosium ions are eight coordinated with different oxygen and nitrogen atoms of the Schiff-base ligands. Each dysprosium ion has a distorted square anti-prismatic geometry formed by eight O-atoms for Dy1 and seven O-atoms and one N-atom for Dy2. The two square bases of the square anti-prism for Dy1 consist of O1, O3, O5, O7, and O9, O11, O12, O19, whereas for Dy2, the two square bases are defined by the atoms O14, O16, O18, O20 and N4, O12, O9, O13. Dy1 and Dy2 are μ_2-bridging mode with the phenol oxygen and carboxylic oxygen atoms of the Schiff-base with a Dy1-Dy2 distance of 3.8954 (5) Å.

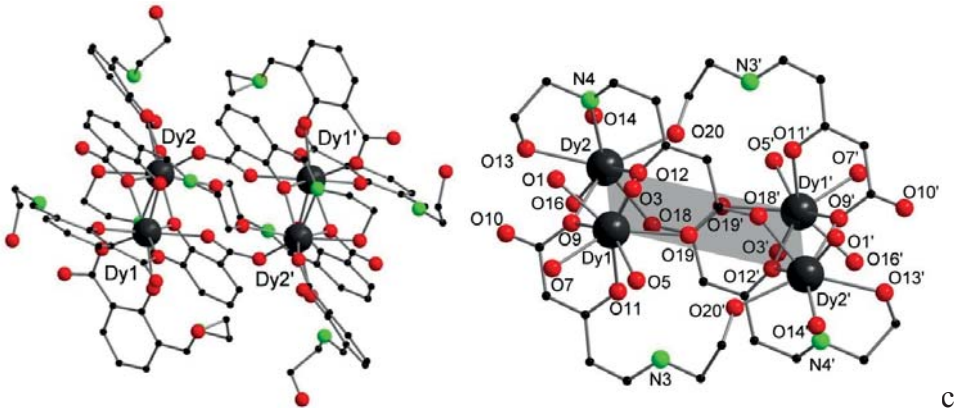

c

Figure 3.3 Solid state structure of **5** (right), and side view of the planar rhombus Dy_4 core (left). Hydrogen atoms have been omitted for clarity.

3.1.2 Photoluminescence (PL) properties

The photoluminescence of compounds were studied by Dr. Sergei Lebedkin (Prof. Manfred M. Kappes). Ligand (H_2L) shows bright greenish emission in the solid state. The intensity depends only moderately on the temperature within the range of 20-290 K. The emission is fluorescence with a lifetime shorter than 5 nsec as estimated using a nsec-pulsed nitrogen laser for excitation at 337 nm. The fluorescence spectrum of H_2L is centered at ~490 nm at 290 K, but shifts to 540 nm at 20 K (Figure 3.4). The PLQY was determined to be 0.20 (20%) at ambient temperature. This relatively high value can even be slightly underestimated because of the overlap (relatively small Stokes shift)

Dieses Werk ist copyrightgeschützt und darf in keiner Form vervielfältigt werden noch an Dritte weitergegeben werden.
Es gilt nur für den persönlichen Gebrauch.

between the PL excitation (absorption) and emission spectra, resulting in reabsorption of the shorter-wavelength emission in the bulk (crystalline powder) sample of H_2L. Note that the same remark is also true for complexes **1**, **4** and in particular for **3**, whose PL properties have been studied in this work (Figure 3.4-3.9).

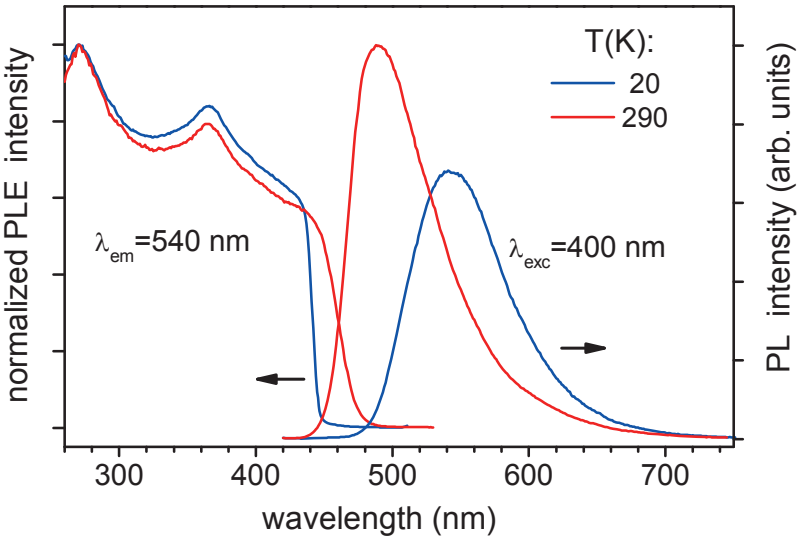

Figure 3.4. Photoluminescence excitation (PLE) and emission (PL) spectra (left and right panels, respectively) of solid compound H_2L at the temperatures of 20 and 290 K. The PL and PLE spectra were excited and recorded at 400 and 540 nm, respectively.

PLE and PL spectra of the above complexes, as well as their emission lifetimes (< 5 nsec), are roughly similar to those of H_2L (cf. Figures 3.4-3.7). There are also similar (less pronounced) red shifts of the PL maximum and PLE absorption onset, which are observed by decreasing the temperature. Therefore we conclude that the visible PL of complexes **1**, **3** and **4** is ligand-based, with a moderate influence by ligand-metal and ligand-ligand interactions in the solid state. Similar to H_2L, the greenish emission of Y and Y_4 complexes **1** and **3** is rather strong. The corresponding PLQY values amount to 11.5 and 13%, respectively, at ambient temperature. The PL intensity increases by decreasing the temperature, e.g., by a factor of ~4 for complex **3** below ~100 K (Figure 3.6). As a result, PLQY of about 60% is expected for this complex at lowest temperatures. In difference to H_2L and Dy_4 complex **4**, the emission band of **1** and particularly of **3** is broadened and asymmetrically shaped, both at ambient and low temperatures (Figures 3.5, 3.6). This likely indicates a contribution of several excited ligand substates/configurations, emitting at slightly different energies. A distorted, "hat-like" shape of the emission band of **3** can also be explained in part by the strong overlap (small Stokes shift) of the PLE and PL spectra of this complex and emission reabsorption effects.

Dieses Werk ist copyrightgeschützt und darf in keiner Form vervielfältigt werden noch an Dritte weitergegeben werden.
Es gilt nur für den persönlichen Gebrauch.

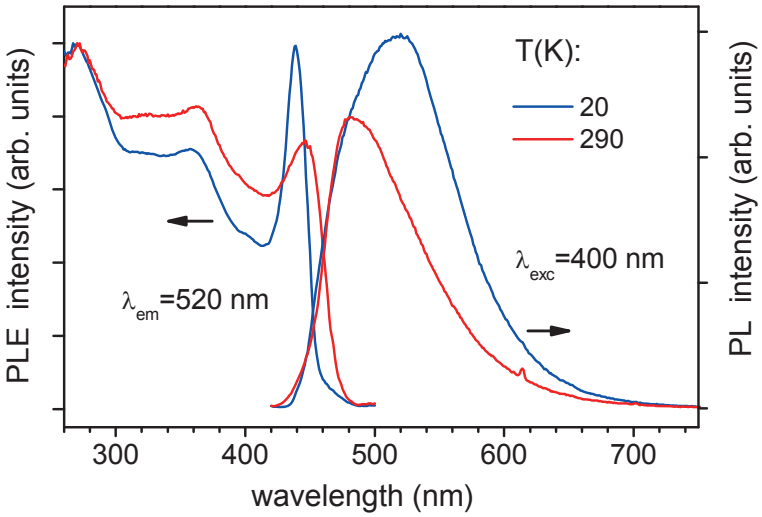

Figure 3.5 Photoluminescence excitation (PLE) and emission (PL) spectra of solid compound **1** at 20 K and 290 K.

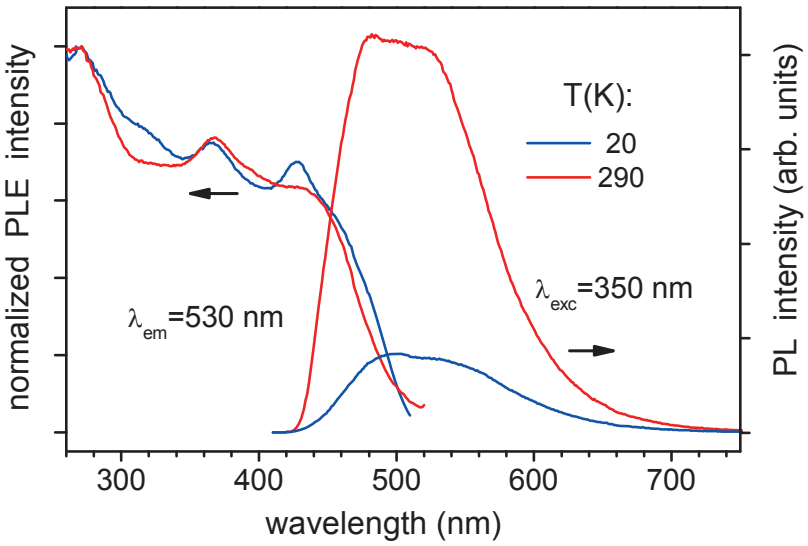

Figure 3.6. Photoluminescence excitation (PLE) and emission (PL) spectra (left and right panels, respectively) of solid compound **3** at the temperatures of 20 and 290 K. The PL and PLE spectra were excited and recorded at 400 and 540 nm, respectively.

In difference to **1** and **3**, the dysprosium complex **4** shows relatively weak ligand-based fluorescence centered at ~455 and 465 nm at 20 and 295 K, respectively (Figure 3.7). Its PLQY was determined to be only 0.7% at T = 295 K, which is probably due to a quenching effect of the Dy ions. There is some energy transfer to excited electronic levels of dysprosium as evidenced by the characteristic f-f emission lines of Dy(III) in the visible spectral range at ~485 and 577 nm (observed at low temperatures), as well as in the NIR region, e.g., at 845, 940, 1015 and 1184 nm (Figure 3.8).

Dieses Werk ist copyrightgeschützt und darf in keiner Form vervielfältigt werden noch an Dritte weitergegeben werden.
Es gilt nur für den persönlichen Gebrauch.

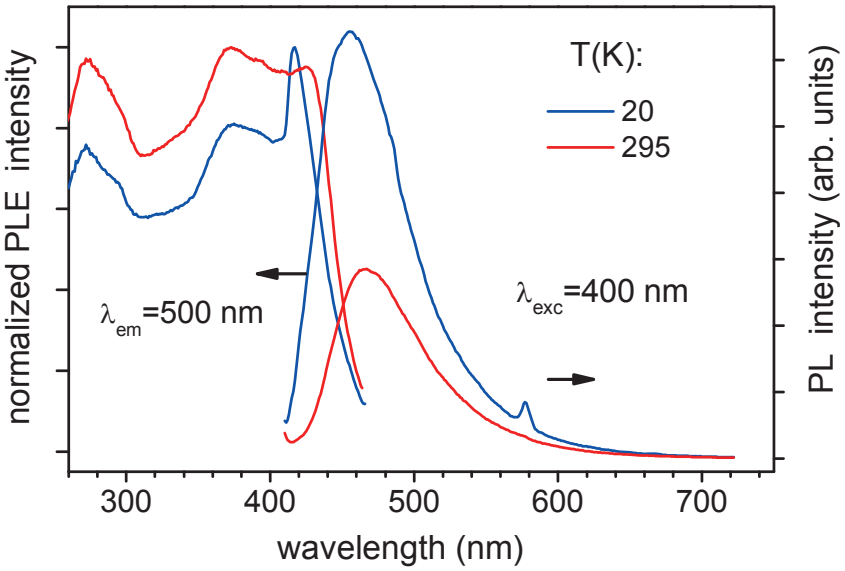

Figure 3.7 Photoluminescence excitation (PLE) and emission (PL) spectra of solid complex **4** at the temperatures of 20 and 295 K. The PL and PLE spectra were excited and recorded at 300 and 500 nm, respectively. A "shoulder" on the emission curve (T = 20K) at ~485 nm and a peak at 577 nm are due to f-f emission lines of Dy(III).

However, the energy transfer efficiency is apparently low since the Dy(III) emission is weak. Interestingly, although the integrated emission intensity of Dy(III) in **4** increases only moderately by decreasing the temperature, the relative intensities of particular f-f transitions vary strongly. For instance, a peak at ~845 nm assigned to the $^4F_{9/2} \rightarrow {}^6H_{5/2}$ transition is quite prominent at 20 K, but nearly missing at 290 K (Figure 3.9).

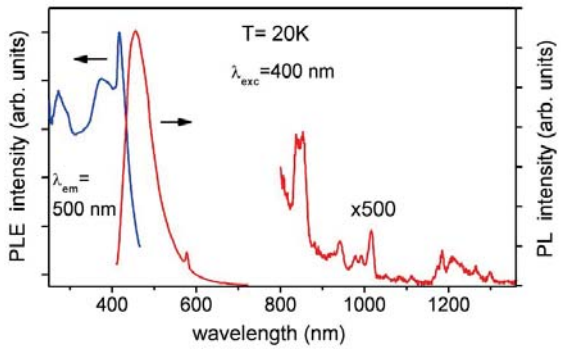

Figure 3.8 Combined visible and near-infrared emission spectra (shown on the same intensity scale) of solid complex **4** recorded at 20 K and excitation wavelength 400 nm. The narrow emission lines can be assigned to f-f transitions of Dy(III) ions.

Dieses Werk ist copyrightgeschützt und darf in keiner Form vervielfältigt werden noch an Dritte weitergegeben werden.
Es gilt nur für den persönlichen Gebrauch.

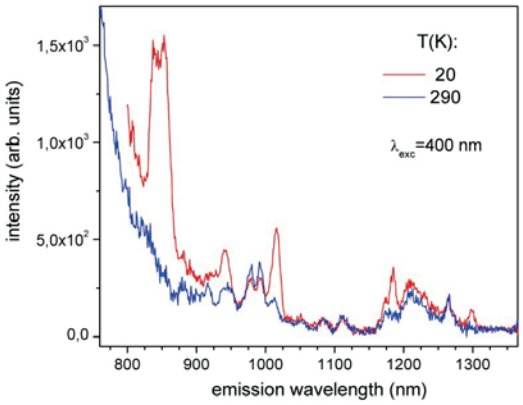

Figure 3.9 Near-infrared emission spectra of solid complex **4** recorded at 20 K and 290 K. The excitation wavelength is 400 nm. The emission lines can be assigned to f-f transitions of Dy(III) ions.

3.1.3 Magnetic Properties of Compounds

The magnetic properties of compounds **2**, **4** and **5** were studied by Dr. Valeriu Mereacre (Prof. Annie K. Powell).

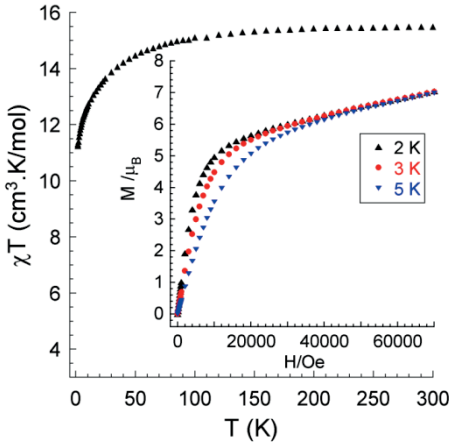

Figure 3.10 Temperature dependence of χT for compound **2** at 1000 Oe. Inset: molar magnetization versus field at 2-5 K

The static *dc* magnetic susceptibility studies of **2** were performed in the 1.8–300 K range under an applied magnetic field of 1000 Oe (Figure 3.10). The χT value of 15.0 cm^3 K mol^{-1} at 300 K for **2** is close to the calculated value of 14.17 cm^3 K mol^{-1} for the ground state of the Dy(III) ion ($4f^9$, J = 15/2, S = 5/2, L = 5, g = 4/3, $_6H^{15/2}$). On cooling, the χT product gradually decreases to achieve a value of 11.1 cm^3 K mol^{-1} at 1.8 K. Such behaviour is primarily owing to the depopulation of the Stark sublevels of the dysprosium ion, which occurs from the splitting of the $_6H^{15/2}$ ground term by the ligand field. The M versus H plot at 2-5 K (inset in Figure 3.10) shows a quite fast increase in the magnetization at low field (till 1 T) and then a slow linear increase to achieve a value of 7.0 μ_B at the maximum applied field of 7 T. This value is lower than the expected saturation value for Dy(III) of

Dieses Werk ist copyrightgeschützt und darf in keiner Form vervielfältigt werden noch an Dritte weitergegeben werden.
Es gilt nur für den persönlichen Gebrauch.

~10 μ_B and such behaviour is likely due to crystal-field effects leading to significant magnetic anisotropy. Dynamic *ac* magnetic susceptibility measurements as a function of the temperature were carried out, but this complex did not show any out-of-phase signal under zero or dc external field.

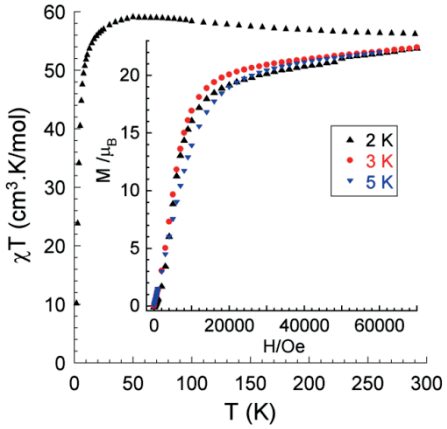

Figure 3.11 Temperature dependence of χT for compound **4** at 1000 Oe. Inset: molar magnetization versus field at 2 - 5 K.

The dc magnetic data for complex **4** shows a little temperature dependent value of χT of 56.1 to 59.0 cm^3 K mol^{-1} over the temperature range 300−50 K (Figure 3.11). On lowering the temperature χT drops abruptly to a minimum value of 10 cm^3 K mol^{-1} at 2K, indicating depopulation of exited Stark sublevels. Magnetization data at low temperatures are shown in the inset of Figure 3.11. The magnetization at all temperatures (2 - 5 K) reaches a maximum value of 22.8 μ_B at 70000 Oe, without showing true saturation. This is noticeably lower than the theoretical value for four Dy^{3+} ions (~ 40 μ_B), indicating a much smaller effective spin in **4**. Isothermal magnetization experiments done at 2.0 K have shown hysteresis with a small coercive field of 9 Oe and a small remenant magnetization of 0.012 μ_B (Figure 3.12). From the magnetization curve at 2 K two inflections (one at ~1500 Oe, second at ~ 40000 Oe) are observed. Such types of inflections are usually observed when the applied magnetic fields overcome intra- and/or intermolecular antiferromagnetic interactions and alignment of the spins occurs. Since the spin ground state in a Dy(III) containing compound is difficult to characterize, it is also difficult to conclude about the degree of the magnetic interactions and processes responsible for the features observed at those two regions.

Dieses Werk ist copyrightgeschützt und darf in keiner Form vervielfältigt werden noch an Dritte weitergegeben werden.
Es gilt nur für den persönlichen Gebrauch.

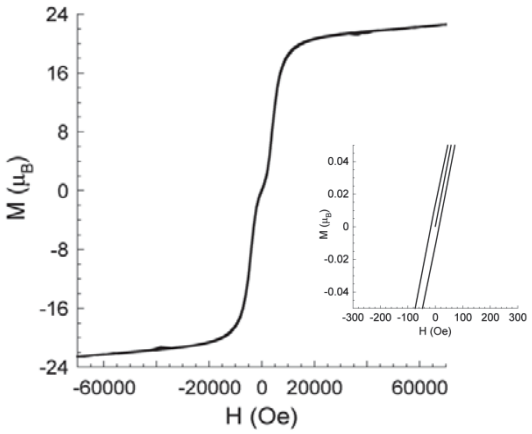

Figure 3.12 Hysteresis loop of **4** recorded at 2.0 K and (inset) expansion of hysteresis to highlight it at low field.

The relaxation of the magnetization in polycrystalline sample **4** was studied using temperature and frequency dependent *ac* susceptibility measurements (Figure 3.13 and 3.14). The ac data measured at zero applied field for frequencies between 1 and 1500 Hz, show frequency dependence of the out-of-phase signals belonging to two relaxation processes (Figure 3.13).

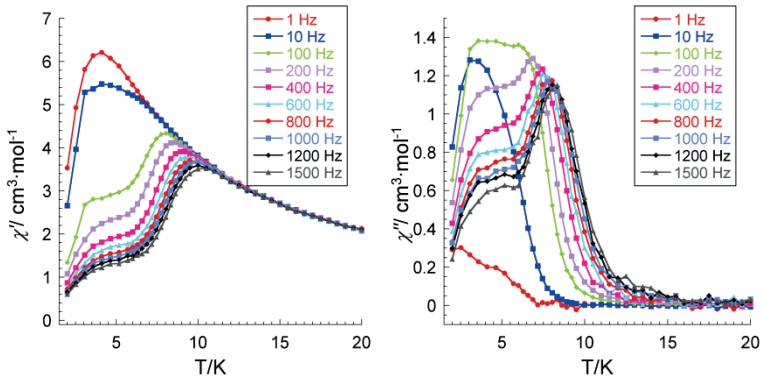

Figure 3.13 In- (χ') and out-of-phase (χ'') ac susceptibility of **4** in zero field as a function of temperature at frequencies from 1 Hz to 1500 Hz.

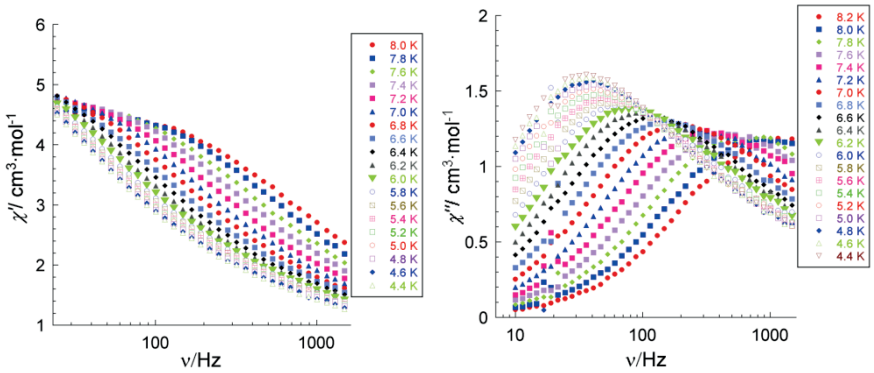

Figure 3.14 In- (χ') and out-of-phase (χ'') ac susceptibility vs frequency ν on a logarithmic scale for **4** over the temperature range 4.4-8.0 K.

Dieses Werk ist copyrightgeschützt und darf in keiner Form vervielfältigt werden noch an Dritte weitergegeben werden.
Es gilt nur für den persönlichen Gebrauch.

The data in the χ'' *vs* frequency plot (Figure 3.14) were extracted into an Arrhenius plot ($\ln\tau$ *vs* 1/T) (Figure 3.15) and the linear fitting of high temperature region (slow relaxation, SR) of which resulted in a relaxation time of τ_0 = 5.1 10^{-9} s and a barrier of U_{eff} = 84 cm^{-1}, pertaining to the relaxation mechanism assigned to a thermally activated process. The Figure 3.13 also shows a second relaxation mechanism that is essential below 6 K (fast relaxation, FR), with τ_0 = 2.5 10^{-3} s and a barrier of U_{eff} = 3 cm^{-1}. Arrhenius analysis confirms that both processes are thermally activated, but the τ_0 value obtained for the FR is much bigger than expected for a SMM[59, 143, 144] and strongly suggests that this process is dominated by quantum effects. An alternative reason for the appearance of the low temperature relaxation might be due to weak dipolar or intermolecular interactions through hydrogen bonds.

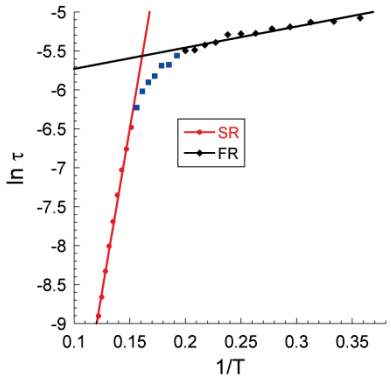

Figure 3.15 Arrhenius plot and linear fit of the maxima at high and low temperatures.

The dc magnetic data (Figure 3.16) for complex **5** show only small differences compared with compound **4**. However, it shows no frequency dependence of the ac susceptibility in zero and non-zero applied field.

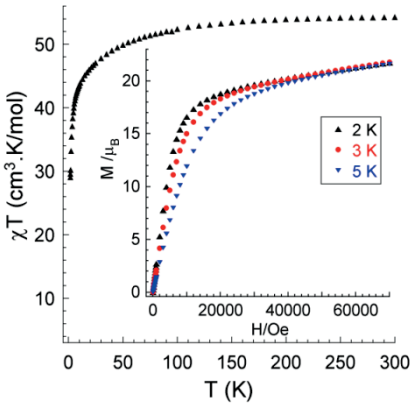

Figure 3.16. Temperature dependence of χT for compound **5** at 1000 Oe. Inset: molar magnetization versus field at 2 - 5 K.

In summary, five new rare earth compounds which are ligated by 2-aminoethyl-hydroxybenzoate (HL^-) and in some case also with the corresponding dianion L^{2-} were prepared. Depending on the

Dieses Werk ist copyrightgeschützt und darf in keiner Form vervielfältigt werden noch an Dritte weitergegeben werden.
Es gilt nur für den persönlichen Gebrauch.

stoichiometric ratio either mononuclear or tetranuclear complexes were obtained. The clusters are either in a butterfly or in a rectangular scaffold arrangement. The proligand H_2L and all yttrium complexes show fluorescence with quantum yields of up to 13%. In contrast the dysprosium compound **4** shows weak fluorescence due to quenching effects. In the magnetic studies, the tetranuclear compound **4** with the butterfly structure shows SMM behavior with two relaxation processes. In comparison to the tetranuclear compound **4**, the mononuclear compound **2** and the tetranuclear compound **5** with the rectangular arrangement show no slow relaxation of the magnetization.

3.2 Mononuclear dysprosium compound

The proligand (H_2L^1) was prepared as by condensation of 3-formylsalicylic acid and isoniazid in methanol. H_2L^1 was further reacted with dysprosium salt $[Dy(NO_3)_3 \cdot 5(H_2O)]$ to get the mononuclear compound $\{[Dy(HL^1)_2(H_2O)_3] \cdot (NO_3)\}$ (**6**). Pyridine acts as a base to deprotonate the ligand. Compound was isolated as single crystalline material directly from the reaction mixture. The solid state structure was established by single crystal-X-ray diffraction and characterized by spectroscopic and analytical techniques. The molecular structure of cation was supported by ESI-MS.

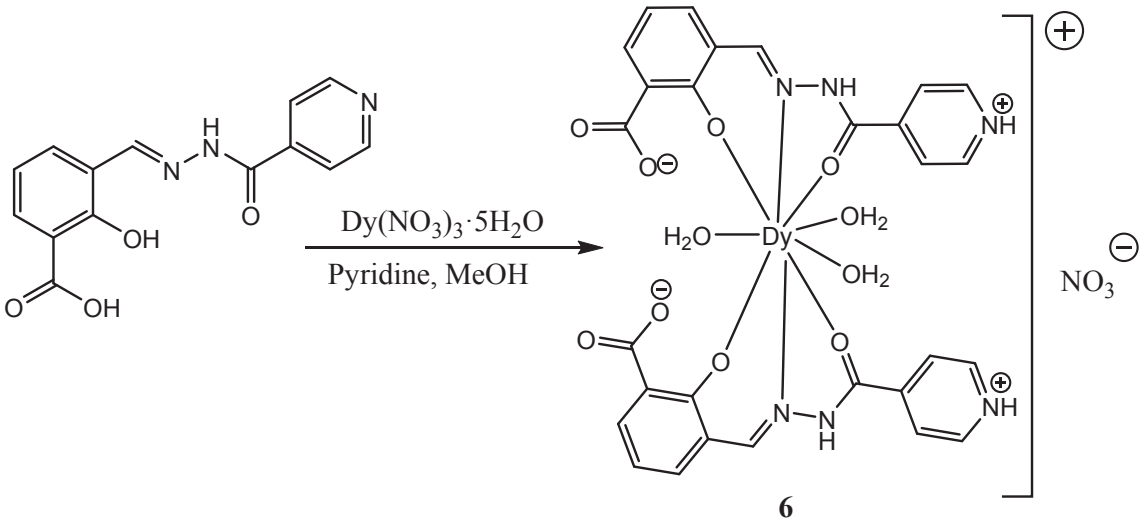

6

Scheme 3.2 Synthesis of compound **6**

The mononuclear dysprosium complex **6** crystallized in the monoclinic space group *P*2/*n* with two molecules per unit cell. A perspective view of complex **6** is represented in Scheme 3.2. Compound **6** consists of a $[Dy(HL^1)_2]^+$ coordination cation and a nitrate counter anion. It has a crystallographic *P*2-axis through the Dy-atom. The $[Dy(HL^1)_2]^+$ cation consists of one Dy(III) ion coordinated by two monoanionic ligands and three water molecules. Thus, the metal atom is 9-fold coordinated by four O atoms and two N atoms of two HL^1 ligands; and three O atoms from water molecules, resulting in a distorted trigonal prismatic coordination geometry (Figure 3.17).

Dieses Werk ist copyrightgeschützt und darf in keiner Form vervielfältigt werden noch an Dritte weitergegeben werden.
Es gilt nur für den persönlichen Gebrauch.

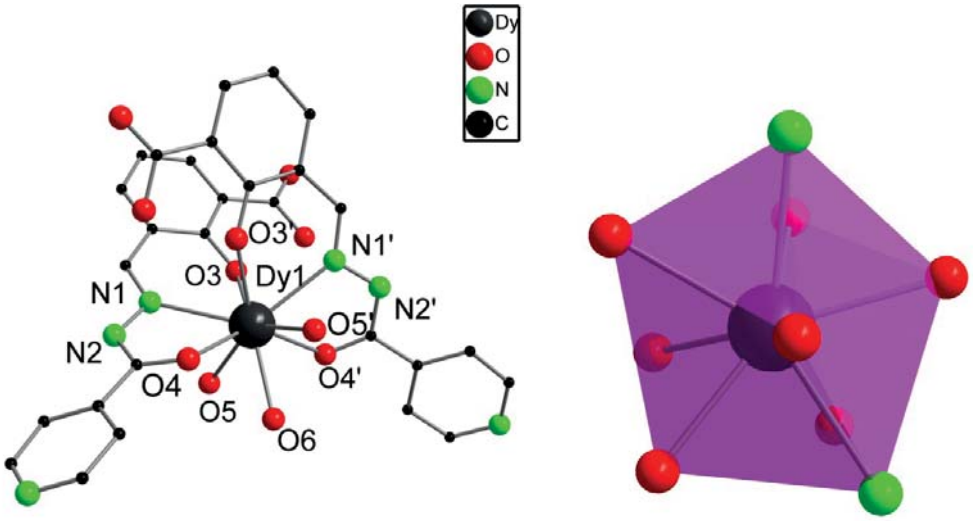

Figure 3.17 Solid state structure of **6** (left) and the arrangement of the coordinating atoms around the dysprosium (right). Hydrogen atoms have been omitted for clarity.

The Dy-O bond lengths for the phenolate oxygen atom Dy1-O3 2.345(3) Å are comparable to the coordinated water molecules Dy1-O5 2.398(3) Å and Dy1-O6 2.379(3) Å. The Dy-O(phenolate) bond lengths are comparable to our previously reported mononuclear dysprosium compound $[Dy(H_3L)^2]^+$ (L = 2,2′-{[(2-aminoethyl)imino]bis[2,1-ethanediylnitriloethylidyne]}bis-2-hydroxy-benzoic acid) 2.324(2)−2.374(2) Å.[73] But the bond length of the ketonic oxygen atom of the ligand is slightly longer Dy1-O4 2.418(3) Å. The bond angles O-Dy-O are O4-Dy1-N1 62.23(11)°, O5-Dy1-O4 88.69(11)°, O3-Dy1-N1 68.32(11)°.

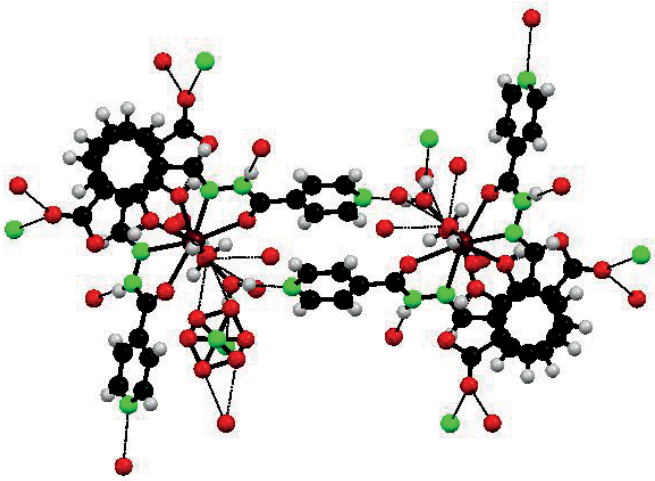

Figure 3.18 Hydrogen bonding interactions in near moieties is shown by dotted lines.

Significant intermolecular and intramolecular hydrogen bonding are observed in the moieties which are shown in Figure 3.18. Intramolecular hydrogen bonding was observed between phenolate oxygen atoms and the carboxylic groups at a distance of 2.471 Å. Intermolecular hydrogen bonding was

Dieses Werk ist copyrightgeschützt und darf in keiner Form vervielfältigt werden noch an Dritte weitergegeben werden.
Es gilt nur für den persönlichen Gebrauch.

observed between the nitrogen atoms of ligand, the coordinated water molecules and the nitrate anions with a range of 2.672-2.813 Å.

3.3 Synthesis and Characterization of Binuclear (Ni-Ln) and Trinuclear (Ni-Ln-Ni) Complexes

3.3.1 Synthesis and Structures

The Schiff base (H_3L) was prepared *in situ* by reflulxing salicylaldehyde and tris(2-aminoethyl)amine in methanol for 1 hour. H_3L ligand was further stirred with $[Ni(NO_3)_2 \cdot 6(H_2O)]$ and the lanthanide salts $[Ln(NO_3)_3 \cdot x(H_2O)]$ (Ln = Gd, Tb, Dy) to obtain the binuclear complexes $[NiGdL(acac)_2]$ (**7**) and $[NiTbL(acac)_2]$ (**8**), and $\{[NiDyL(acac)_2]_2 \cdot 7(MeOH)\}$ (**9**). Triethylamine acts as a base to deprotonate the proligand and acetylacetone (acacH). These compounds were isolated as single crystalline material directly from the reaction mixtures. When the proligand acetylacetone was replaced by dibenzoylmethane another binuclear compound $\{[NiDyL(Ph_2acac)_2]_2 \cdot 4(CH_2Cl_2) \cdot (MeOH)\}$ (**10**) was obtained. A diffusion process was found helpful to obtain **c**ompound **10** as single crystalline materials, whereas direct addition leads to precipitation. This work was further extended with the H_3L^1-proligand, which is a methoxy derivative of the H_3L ligand. It was prepared *in situ* as by refluxing 3-methoxysalicylaldehyde and tris(2-aminoethyl)amine in methanol. H_3L^1 was reacted with $[Ni(NO_3)_2 \cdot 5(H_2O)]$ and the lanthanide salts $[Ln(NO_3)_3 \cdot x(H_2O)]$ (Ln = Gd, Tb, Dy) to obtain the trinuclear complexes $\{[Ni_2Gd(L^1)_2] \cdot (NO_3) \cdot 2(H_2O)\}$ (**11**), $\{[Ni_2Tb(L^1)_2]_4 \cdot 4(NO_3) \cdot 3(MeCN) \cdot 5(MeOH) \cdot (H_2O)\}$(**12**), $\{[Ni_2Dy(L^1)_2](NO_3) \cdot ((MeOH) \cdot (H_2O)\}$ (**13**). The trinuclear linear complexes were obtained directly from the reaction mixtures. The solid state structures of all compounds were established by single crystal-X-ray diffraction and characterized by spectroscopic and analytical techniques. The molecular structure cations of **11**, **12** and **13** were supported by ESI-MS.

Dieses Werk ist copyrightgeschützt und darf in keiner Form vervielfältigt werden noch an Dritte weitergegeben werden.
Es gilt nur für den persönlichen Gebrauch.

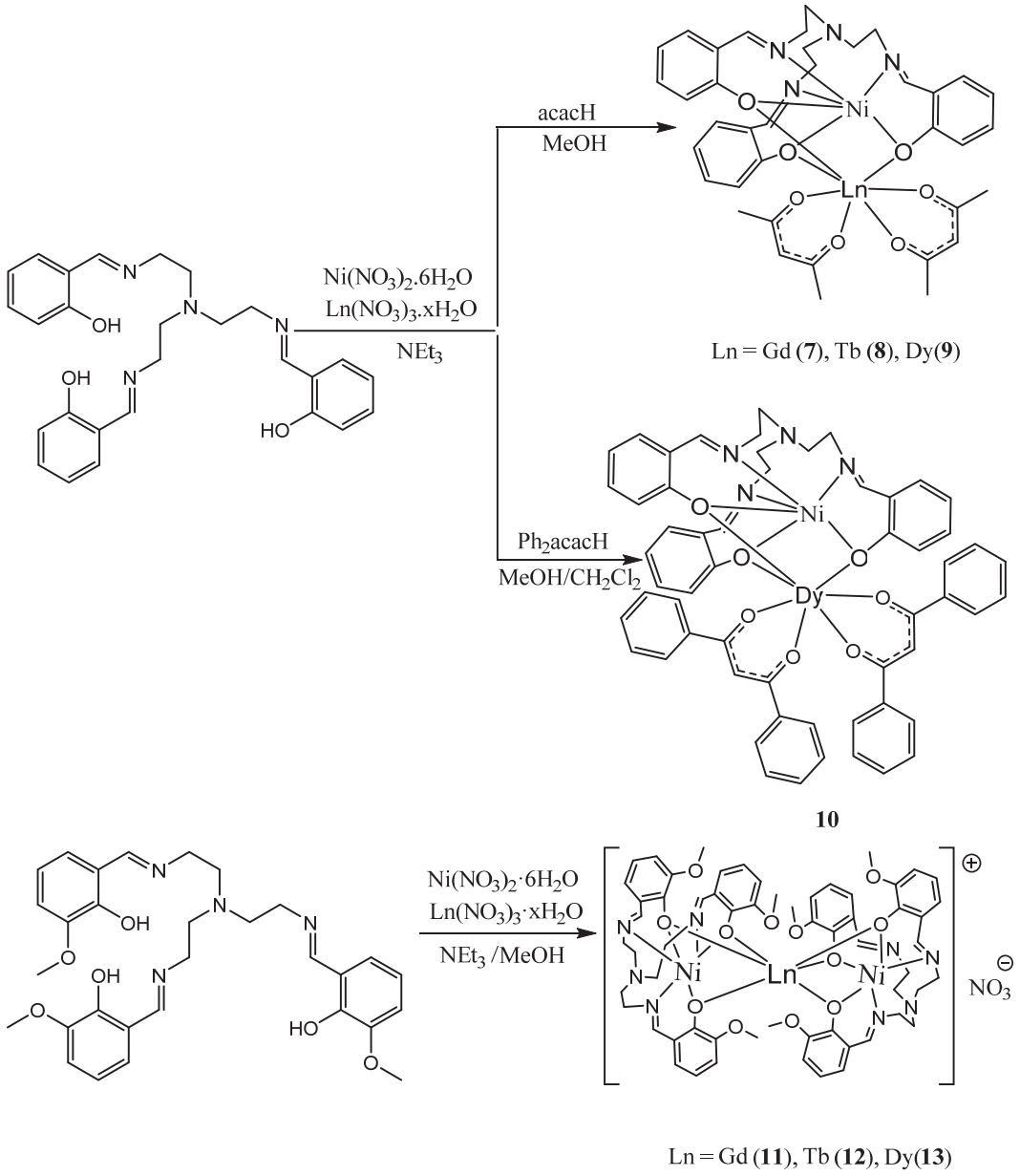

Scheme 3.3 Synthesis of compound **7-13**

Complexes **7**, **8** and **9** are isostructural and have a binuclear metal core as shown in Scheme 3.3. Complexes **7** and **8** crystallized in monoclinic space group $P2_1/n$ whereas **9** crystallized in the triclinic space group *P*-1 only. The representative structural parameters of **7** are discussed in detail (Figure 3.19). The asymmetric unit contains face-sharing binuclear molecules, in which the Ni ion occupies an inner N_3O_3 coordination site and features a distorted octahedral coordination geometry. The Gd ion occupies the outer O_3O_4 coordination site and it is seven coordinated. The Ni-O bond distances of **7**, **8** and **9** are between 2.078(2)-2.0951(2) Å, 2.074(2)-2.094 Å and 2.064(2)-2.0948(2) Å, respectively. Ni-O bond lengths are in comparable range of reported binuclear complexes $[(H_2O)_2NiL\text{-}Y(NO_3)_3]$ (L = N,N′-2,2-dimethylpropylenedi(3-methoxy-salicylideneiminato)) 2.032(3)-2.159(3) Å.[99] The Ni-Gd, Ni-Tb and Ni-Dy, bond distances are 3.1587(6) Å, 3.1365(6) Å

Dieses Werk ist copyrightgeschützt und darf in keiner Form vervielfältigt werden noch an Dritte weitergegeben werden.
Es gilt nur für den persönlichen Gebrauch.

and 3.1188(11) Å respectively. The four O_{acac} atoms are in κ^2-mode and the other three phenolate oxygen atoms are in μ_2-bridging mode with Ni and Tb ions.

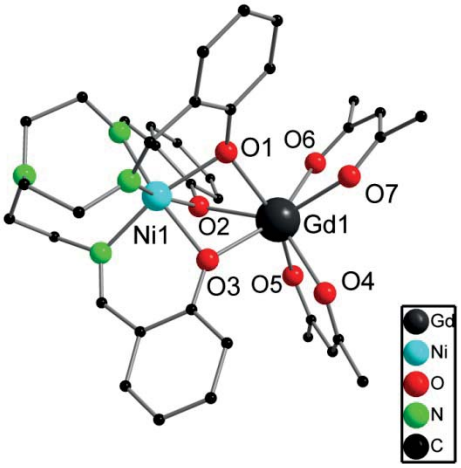

Figure 3.19 Solid state structure of **7** and hydrogen atoms have been omitted for clarity.

The distances of chelating the Ln-O_{acac} and the bridging Ln- $O_{phenolate}$ bonds are close to each other. The Ln-$O_{phenolate}$ bond lengths of **7** are in the range of 2.345(2)-2.3613(2) Å and the Ln-O_{acac} ones are in the range of 2.319(2)-2.340(2) Å. These compounds are isostructural and an inspection of the bond distances for compounds **7**, **8** and **9** shows that the bond lengths decrease in the order Ni-O_{avg} 2.089 Å (Gd) > 2.085 Å (Tb) > 2.0799 Å (Dy). Ln-$O_{(phenolate)avg}$ bond lengths also decrease in the order 2.3545 Å (Gd), > 2.3363 Å (Tb) >2.3262 Å (Dy) respectively. The average of Ln-$O_{(phenolate)}$ bond distances decreases as the atomic number increases, it correspondence to lanthanide contraction. This phenomena was earlier reported in the binuclear Ni-Ln complexes [(NiL)Ln(hfac)$_2$(EtOH)] (hfac = hexafloroacetyacetonate).[88]

Complex **10** crystallized in the triclinic space group *P*-1. The Ni ion occupies an inner N_3O_3 coordination site and has distorted octahedral coordination geometry (Figure 3.10). The Dy-ion occupies an outer O_3O_4 coordination site and it is seven coordinated. The molecule structure is similar to complex **7** but the acetylacetone ligand is replaced by the dibenzoylmethane ligand. The bond lengths and angles of **10** are also comparable to those of compound **7**.

Dieses Werk ist copyrightgeschützt und darf in keiner Form vervielfältigt werden noch an Dritte weitergegeben werden.
Es gilt nur für den persönlichen Gebrauch.

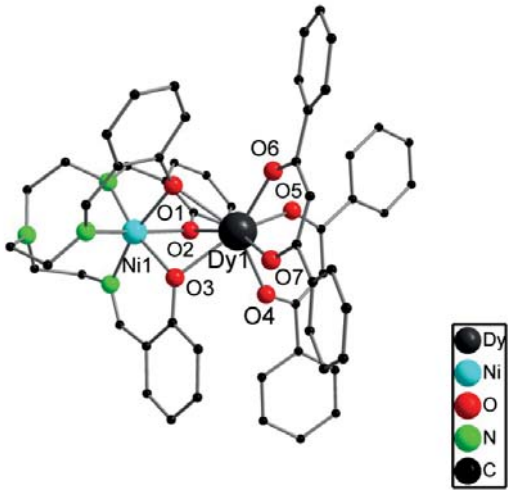

Figure 3.20 Solid state structure of **10** and hydrogen atoms have been omitted for clarity.

The Ni-Dy bond distance of **10** is 3.1380(11) Å, which is slightly larger than that of complex **9** [3.1188(11) Å]. The Ni-O bond distances of **10** are in the range of 2.065(2)-2.089(2) Å and are comparable to those of complex **9** [2.064(2)-2.0948(2) Å]. The Ln-$O_{phenolate}$ bond lengths are in the range of 2.331(2)-2.360(2) Å and the Ln-O_{Phacac} bond lengths are in the range of 2.272(3)-2.287(2) Å.

Complexes **11** and **12** crystallized in triclinic space group *P*-1, whereas complex **13** crystallized in the monoclinic space group $P2_1/n$. The trinuclear metal core is analogous in **11**, **12** and **13,** as shown in Scheme 3.3. Thus, representative structural parameters of complex **11** are discussed in detail (Figure 3.21). The asymmetric unit contains a face sharing trinuclear molecule $[L^1{}_2Ni_2Ln]^+$ and a nitrate as counter anion. The molecular structure of cation is also supported by ESI-MS.

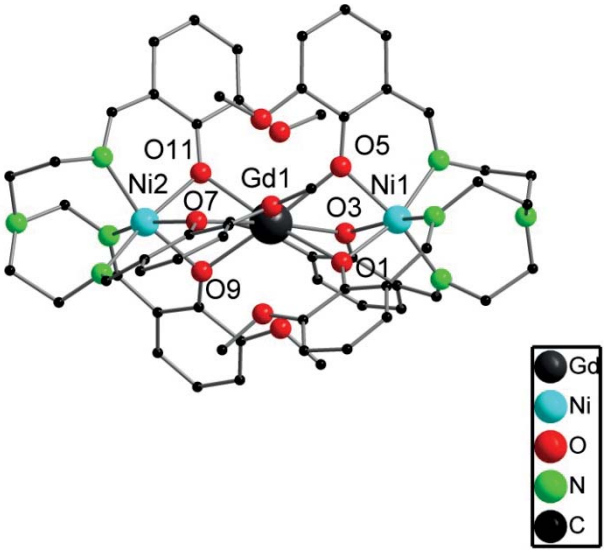

Figure 3.21 Solid state structure of cation **11** and hydrogen atoms have been omitted for clarity.

Dieses Werk ist copyrightgeschützt und darf in keiner Form vervielfältigt werden noch an Dritte weitergegeben werden.
Es gilt nur für den persönlichen Gebrauch.

The trinuclear metal core consists of two Ni ions and one Ln ion. The metal core is almost linear having the Ni-Ln-Ni bond angles 177.966(15)° [NiGdNi], 176.662(19)° [NiTbNi], and 176.94(2)° [NiDyNi] respectively. The Ni(II) ions are coordinated in a distorted octahedral manner by the $(L^1)^{3-}$ ligand in N_3O_3 coordination site. The Ln(III) ion is central in metal core and coordinated by two $[NiL^1]^{-1}$ moiety. The Ln ion is six-coordinate by μ_2-bridged phenolate oxygen atoms of L^1 and the methoxy groups of the ligands have interactions with the Ln ion. The coordination environments of the two Ni-ions are slightly different in the bonding parameters. The Ni1-Gd1 and Ni2Gd1 bond distances are 3.3244(9) Å, and 3.3125(9) Å respectively. In the metal core the Ni1-O bond distances are in the range of 2.067(3)-2.077(3) Å and the Ni2-O bond distances are between 2.076(3)-2.082(3) Å. Ni-O bond distances are comparable to reported trinuclear complexes $[L_2Ni_2Ln][ClO4]$ (Ln = La, Ce, Pr, Nd, Sm, Eu, Gd, Tb, Dy, Ho, Er) which have $Ni\text{-}O_{avg}$ bond distances in the range from 2.056 to 2.063 Å and in this series they have been found the lanthanide contraction phenomena.[5] The Gd-O bond lengths can be divided into two types; $Gd\text{-}O_{phenolate}$ bond distances are in the range of 2.365(3)-2.421(3) Å and the $Gd\text{-}O_{methoxy}$ are characterized longer than 2.926(3) Å. As compounds **11**, **12** and **13** are isostructural with one another and their bond lengths are $Ni\text{-}O_{avg}$ 2.075 Å (Gd), > 2.070 Å (Tb), < 2.076 Å (Dy) Å and $Ln\text{-}O_{(phenolate)avg}$ 2.3985 Å (Gd), > 2.3656 Å (Tb), >2.3598 Å (Dy) respectively. The $Ln\text{-}O_{(phenolate)avg}$ bond distances decrease with increasing atomic number due to lanthanide contraction like the binuclear complexes **7**, **8** and **9** and their $Ln\text{-}O_{(phenolate)avg}$ bond lengths are 2.3545 Å (Gd), > 2.3363 Å (Tb) and >2.3262 Å (Dy).

In summary, seven new Ni-Ln compounds were synthesized, which are ligated by the L^{3-} ligand in compounds **7**, **8**, **9** and **10.** Compounds **11**, **12** and **13** are ligated by the corresponding methoxy derivative $(L^1)^{3-}$. Binuclear or trinuclear complexes were obtained depending upon the type of ligand used and the reaction stoichiometry. The close inspection of bond lengths for binuclear and trinuclear complexes showed that bond distances decrease with increasing atomic number due to lanthanide contraction. In binuclear compounds, the lanthanide ions are seven coordinated and in trinuclear complexes; lanthanide ions are six coordinated and having interaction to near methoxy groups of the $(L^1)^{3-}$ ligands.

3.4 Tetranuclear and Pentanuclear Clusters of Lanthanides: Synthesis and Magnetic Studies

By using dibenzoylmethane as a ligand in our group and other groups few lanthanides clusters have been reported.[145-149] Recently, by using dibenzoylmethane as a ligand and peptoids as a supporting ligands, we synthesized the novel pentadecanuclear lanthanide hydroxyl clusters $[\{Ln_{15}(\mu_3\text{-}OH)_{20}(PepCO_2)_{10}(Ph_2acac)_{10}Cl\}Cl_4]$ ($PepCO_2.HCl$ = 2-[{3-(((tert-butoxycabonyl)amino)methyl) benzyl}amino-aceticacid hydrochloride) and studied the luminescent properties of the metal

Dieses Werk ist copyrightgeschützt und darf in keiner Form vervielfältigt werden noch an Dritte weitergegeben werden.
Es gilt nur für den persönlichen Gebrauch.

clusters.[150] Further we altered the amino acids supporting ligand and synthesized the pentanuclear dysprosium hydroxo clusters $[Dy_5(OH)_5(\alpha\text{-}AA)_4(Ph_2acac)_6]$ (α-AA = amino acids, Ph_2acac = dibenzoylmethanide) in which all the pentanuclear clusters showed the single molecule magnet behaviour below 10 K.[151] It is interesting to continue this work together with a Schiff base ligand and dibenzoylmethane as a supportive ligand.

3.4.1 Synthesis and structures

The Schiff base (H_3L^2) was prepared *in situ* as proligand by refluxing 4-tert-butyl-2,6-diformylphenol and 2-aminophenol in methanol. Then, it was reacted with different ratio of metal salts $[Ln(NO_3)_3 \cdot x(H_2O)]$ (Ln = Tb, Dy) to obtain the complexes $\{[Dy_4(L^2)_3(Ph_2acac)_4] \cdot (Et_3NH) \cdot 4(MeOH) \cdot (MeCN) \cdot (H_2O)\}$ (**14**), $\{[Tb_5(\mu_3\text{-}OH)_2(L^2)_2(Ph_2acac)_7(Ph_2acacH)] \cdot 7(PhMe)\}$ (**15**) and $\{[Dy_5(\mu_3\text{-}OH)_2(L^2)_2((Ph_2acac)_7(Ph_2acacH)] \cdot 7(PhMe)\}$ (**16**). Compounds **14**, **15** and **16** were isolated as single crystalline material. Triethylamine was used to deprotonate a solution of the H_3L^2 ligand and dibenzoylmethane. Obviously the stoichiometry ratio of metal to ligand and the used solvents played a key role in the formation of the compounds. The tetranuclear compound **14** was obtained by using acetonitrile as a solvent and 3:4:4 (H_3L^2 :Ln:Ph_2acacH) stoichiometric ratio. By altering the solvent to methanol and stoichiometry ratio to 2:5:8 (H_3L^2 :Ln:Ph_2acacH), the pentanuclear clusters **15** and **16** were obtained as the products. Compound **15** and **16** were separated as powder form by filtration and than recrystallized from toluene to get single crystalline material. The solid state structures of **14**, **15** and **16** were established by single crystal-X-ray diffraction and characterized by spectroscopic and analytical techniques. The anionic structure of **14** was supported by ESI-MS.

Dieses Werk ist copyrightgeschützt und darf in keiner Form vervielfältigt werden noch an Dritte weitergegeben werden.
Es gilt nur für den persönlichen Gebrauch.

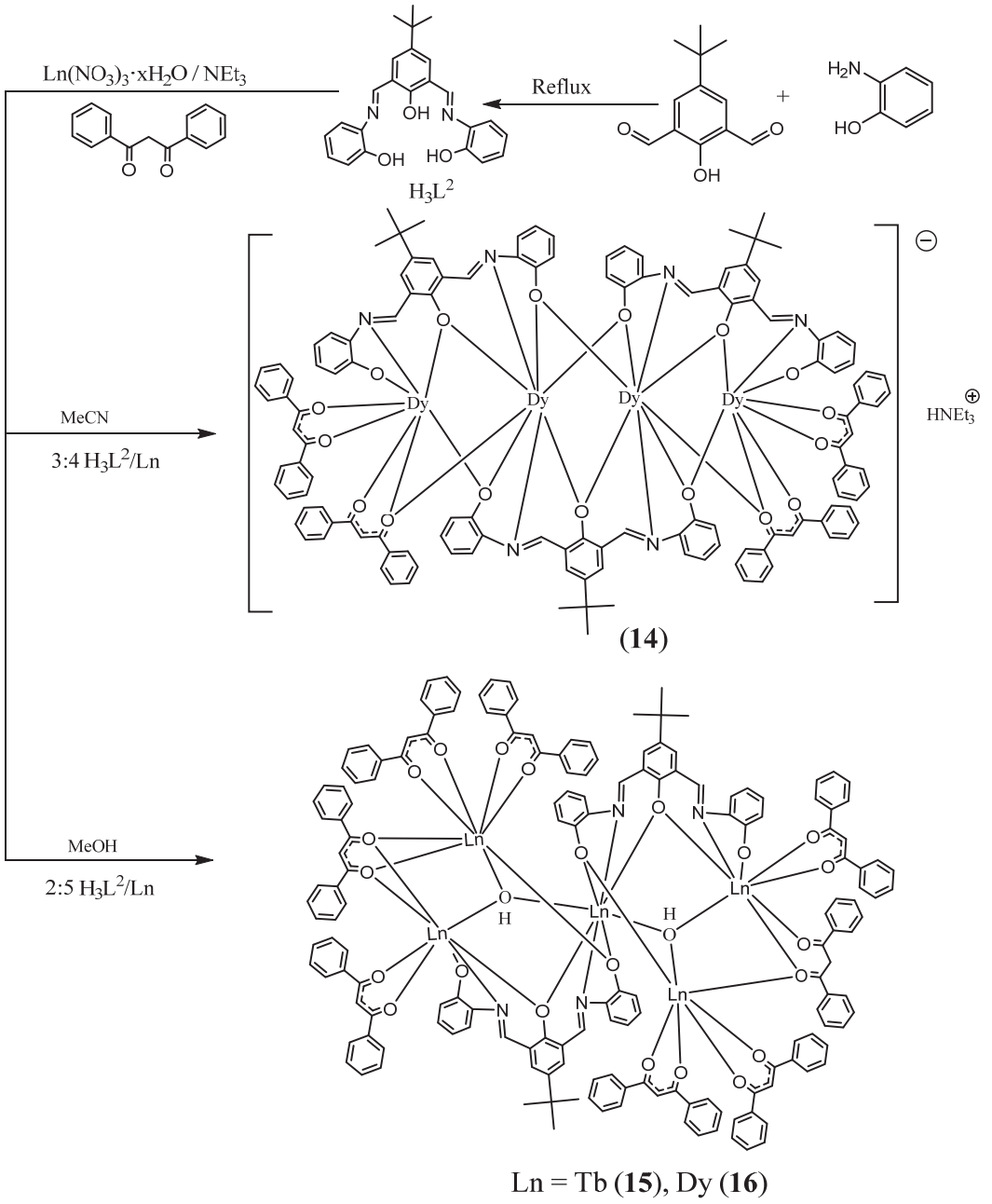

Scheme 3.4 Synthesis of compound **14-16.**

The centrosymmetrical complex **14** crystallized in the triclinic space group *P*-1 with two molecules in the unit cell. A perspective view of compound **14** is shown in Scheme 3.4. Compound **14** consists of $[Dy_4(Ph_2acac)_4(L^2)_3]^-$ anion and a protonated triethylamine counter cation. The $[Dy_4(Ph_2acac)_4(L^2)_3]^-$ anion consists of four Dy(III) ions coordinated by three central trianionic Schiff-base ligands $(L^2)^{3-}$ and four peripheral monoanionic Ph_2acac ligands. The molecular structure of the anion $[Dy_4(Ph_2acac)_4(L^2)_3]^-$ is shown in Figure 3.22 and it is supported by ESI-MS.

Dieses Werk ist copyrightgeschützt und darf in keiner Form vervielfältigt werden noch an Dritte weitergegeben werden.
Es gilt nur für den persönlichen Gebrauch.

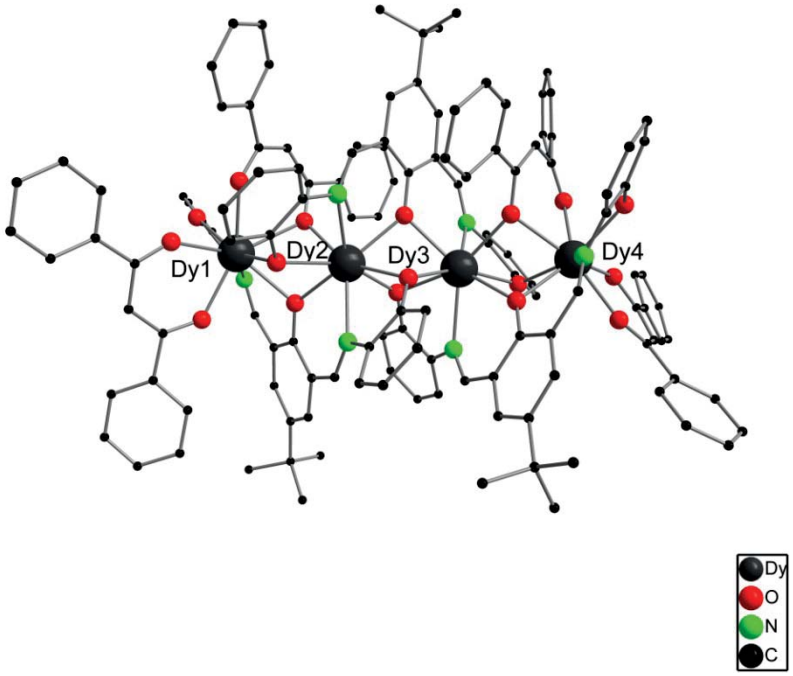

Figure 3.22 Perspective view of the molecular structure of the anion **14**. Hydrogen atoms have been omitted for clarity.

The dysprosium atoms in compound **14** are eight fold coordinated and features a distorted square antiprism coordination geometry. The central Dy atoms (Dy2 and Dy3) are coordinated by two nitrogen atoms and five oxygen atoms (μ_2-bridging modes) of the Schiff base ligand and one μ_2-bridging atom of the Ph_2acac ligand. The peripheral Dy atoms (Dy1 and Dy4) are coordinated to one nitrogen atom and seven oxygen atoms; two oxygen atoms of the Schiff base ligand and one oxygen atom of the Ph_2acac ligand are in μ_2-bridging coordination modes. The Dy_4 metal core of complex is precisely linear as evidenced by angles of Dy3–Dy2–Dy1 163.798(12)° and Dy2–Dy3–Dy4 165.562(12)°. Previously reported tetranuclear dysprosium complexes $[Dy_4(L)_4(MeOH)_6]$[64] (H_3L = 2-hydroxy-3-methoxybenzoic acid [(2-hydroxy-3-methoxyphenyl)methylene] hydrazide) and $[Dy_4(L)_2(C_6H_5COO)_{12}(MeOH)_4]$[82] (HL = 2,6-bis((furan-2-ylmethylimino)methyl)-4-methylphenol) have the Dy–Dy–Dy angles of 149.99° and 175.673° respectively.[81] The bond distances between Dy(III) metal ions in **14** are Dy1-Dy2 3.5126(9) Å, Dy2-Dy3 3.4497(9) Å and Dy3-Dy4 3.4805(8) Å, which are slightly shorter than previously reported linear tetranuclear compounds.[64, 81, 82] The reported linear tetranuclear compound has the Dy-Dy bond distances between 4.055-4.241 Å.[81] The bond distances between Dy–O and Dy–N are in the range of 2.259(4)–2.411(4) Å and 2.486(5)-2.542(5) Å respectively, which are comparable to reported complexes.[81, 82]

Compound **15** and **16** crystallized in the monoclinic space group *C*2/*c*. The structures of compounds **15** and **16** are shown in Scheme 3.4. Compound **15** and **16** are isostructural with each other. Only representative bonding parameters of compound **16** are discussed in detail (see Figure 3.23).

Dieses Werk ist copyrightgeschützt und darf in keiner Form vervielfältigt werden noch an Dritte weitergegeben werden.
Es gilt nur für den persönlichen Gebrauch.

Complex **16** is encapsulated by seven peripheral Ph_2acac ligands, one dibenzoylmethane and two central Schiff base ligands. Complex **15** and **16** are neutral as charge of the five Ln(III) ions is balanced by seven monoanionic dibenzoylmethanide (Ph_2acac) ligands, two trianionic Schiff base ligands $(L^2)^{3-}$ and two hydroxide ions.

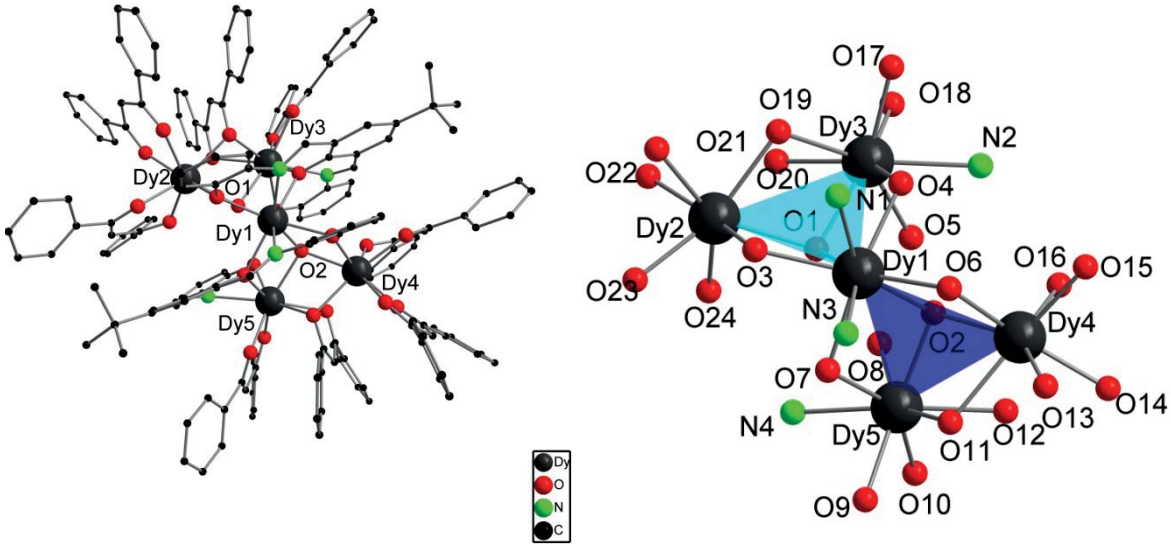

Figure 3.23 Perspective view of the molecular structure of **16** (left) and metal core of complex **16** (right). Triangle unit A (skyblue) and B (blue) are shown in metal core. Hydrogen atoms have been omitted for clarity.

The pentanuclear complex is made up of a central Dy_5O_9 metal core. This metal core consists of two corner sharing triangle units A (Dy1, Dy2, Dy3) and B (Dy1, Dy4, Dy5). The triangles A and B are shown in metal core by sky-blue and blue color respectively (see Figure 3.23). Each triangle is bridged by a central μ_3-(OH) group. In compounds **16**, two μ_3-(OH) groups (O1 and O2) are nearly symmetrical bridge to the near metal centres and the hydroxide ions lie 0.896 Å and 0.914 Å below the plane of the metal cores, respectively. Dy1 is the central metal atom in the metal core of compound **16**. It connects the triangles A and B to form the deltawing shaped arrangement of five dysprosium atoms. In triangle unit A, oxygen atom (O19) of the Ph_2acac ligand coordinate in a μ_2-bridging to Dy2 and Dy3 and other oxygen atom (O20) coordinate to Dy3 in η^1-mode giving a seven coordination number to Dy2 and eight coordination number to Dy3. In triangle unit B, oxygen atom (O11) of the Ph_2acac ligand coordinate in μ_2-bridging mode to Dy4 and Dy5 and oxygen atom (O12) is coordinate in κ^1- mode to Dy5. Thus, Dy4 is seven fold coordinated to seven oxygen atoms, wheras Dy5 is eight fold coordinated seven oxygen atoms and a nitrogen atom. These trinagles are analogous and the Dy-O distances of the Ph_2acac ligands are Dy2-O19 2.39(4) Å, Dy2-O20 2.963 Å, Dy3-O20 2.39(4) Å, Dy4-O11 2.42 Å, and Dy4O12 2.734(19) Å. Dy-O distances of the Ph_2acac ligand in compound **16** is comparable to reported pentanuclear dysprosium compound $[Dy_5(\mu 3\text{-}OH)_3(opch)_6(H_2O)_3]$ (H_2opch = (E)-N'-(2-hyborxy-3-methoxybenzylidene)pyrazine-2-carbo-

Dieses Werk ist copyrightgeschützt und darf in keiner Form vervielfältigt werden noch an Dritte weitergegeben werden.
Es gilt nur für den persönlichen Gebrauch.

hydrazide) 2.195(8)–2.642(10) Å.[67] The distances between the Dy(III) metal ions in **16** are Dy1-Dy2 3.82(6) Å, Dy1-Dy3 3.7225(5) Å, Dy1-Dy4 3.83(5) Å and Dy1-Dy5 3.732(5) Å, which are slightly longer than the linear complex **14** but they are comparable to the isostructural Tb-compound **16.** The Tb-Tb distances in compound **15** are Tb1-Tb2 3.7496(7) Å, Tb1-Tb3 3.8461(6) Å, Tb1-Tb4 3.7427(6) Å and Tb1-Tb5 3.8580(12) Å.

3.4.2 Magnetic Properties

The magnetic properties of compounds **14-16** were studied by Dr. Abhishake Mondal (Prof. Annie K. Powell). The dc magnetic susceptibility data for compound **14** were collected over a temperature range of 1.8-300 K and a field of 0.1 T (Figure 3.24). At 300 K, the $\chi_M T$ value of **14** is 56.5 cm^3 mol^{-1} K, is in good agreement with the expected value of 56.7 cm^3 K mol^{-1} for four non-coupled Dy(III) metal ions ($S = {}^5/_2$, $L = 5$, $g = {}^4/_3$). Upon cooling, the $\chi_M T$ value decreases smoothly down to 7 K with a value 46.7 cm^3 K mol^{-1}. After that point the $\chi_M T$ product increases at lower temperatures to a maximum value of 53.2 cm^3 K mol^{-1} at 1.8 K. This low temperature increase is suggestive of very weak ferromagnetic exchange between the constituent Dy(III) ions.[65] Magnetization (M) data was collected in the 0–70 kOe field range at different temperatures.

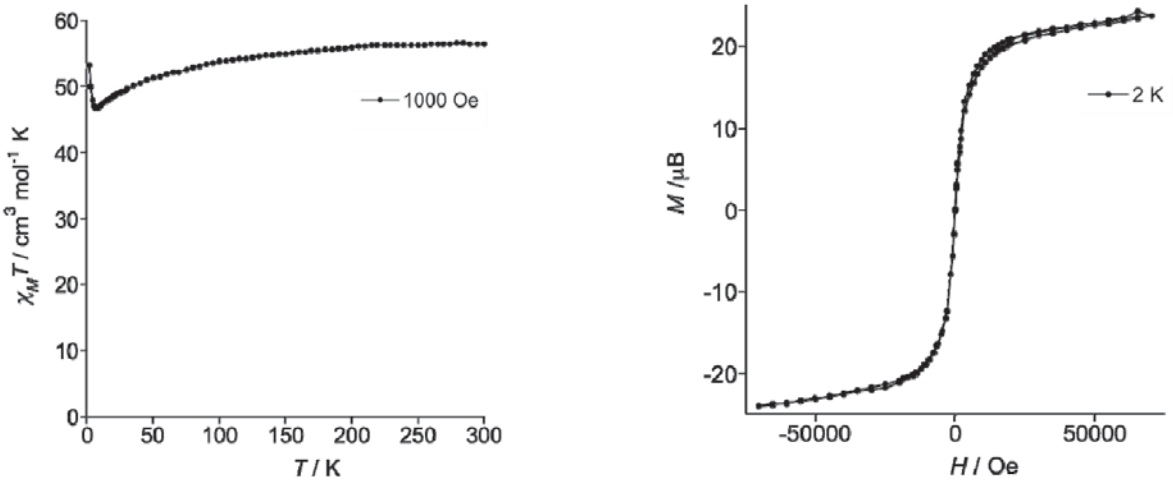

Figure 3.24 Plots of $\chi_M T$ vs. T (left) and M vs. H (right) for compound **14**.

The non-superposition of the *M vs. H/T* data (Figure 3.25) suggests the presence of significant magnetic anisotropy and/or low-lying excited states. The magnetization increases rapidly at low field and eventually reaches a value of 23.5 μB at 70 kOe without clear saturation. This value is much lower than the expected saturation value of 40 μB for four non-interacting Dy(III) ions, most likely due to the crystal-field effect at the Dy(III) ion that eliminates the 16-fold degeneracy of the $^6H_{15/2}$ ground state.[152]

Dieses Werk ist copyrightgeschützt und darf in keiner Form vervielfältigt werden noch an Dritte weitergegeben werden.
Es gilt nur für den persönlichen Gebrauch.

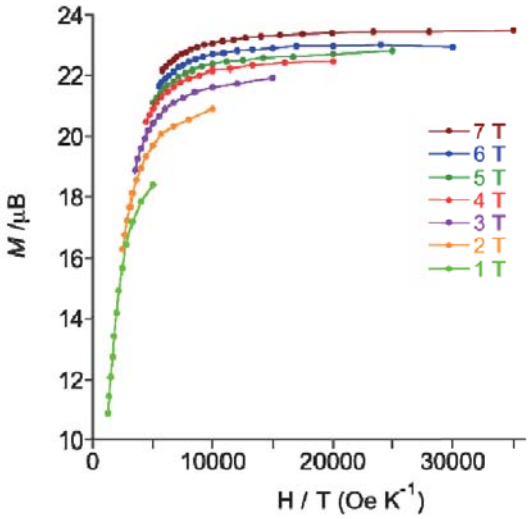

Figure 3.25 *M* vs. *H/T* curve for **14** in the 1–7 T magnetic field range and between 1.8 and 12 K.

Due to the presence of magnetic anisotropy, the magnetization relaxation of this system was probed under zero dc fields, using ac susceptibility measurements as a function of the temperature at different frequencies. Clearly this compound exhibits non-zero out-of-phase ac susceptibility with a weak intensity (Figure 3.27), indicating an absence of any appreciable barrier to relaxation of the magnetization, which could be due to strong quantum tunnelling resonance at zero dc field. The maximum of out-of-phase signal could not be observed above 1.8 K at a frequency of 1500 Hz. The out-of-phase ac susceptibilities are weakly frequency dependent, indicating that this compound exhibits slow magnetic relaxation and is probably a single-molecule magnet (SMM).

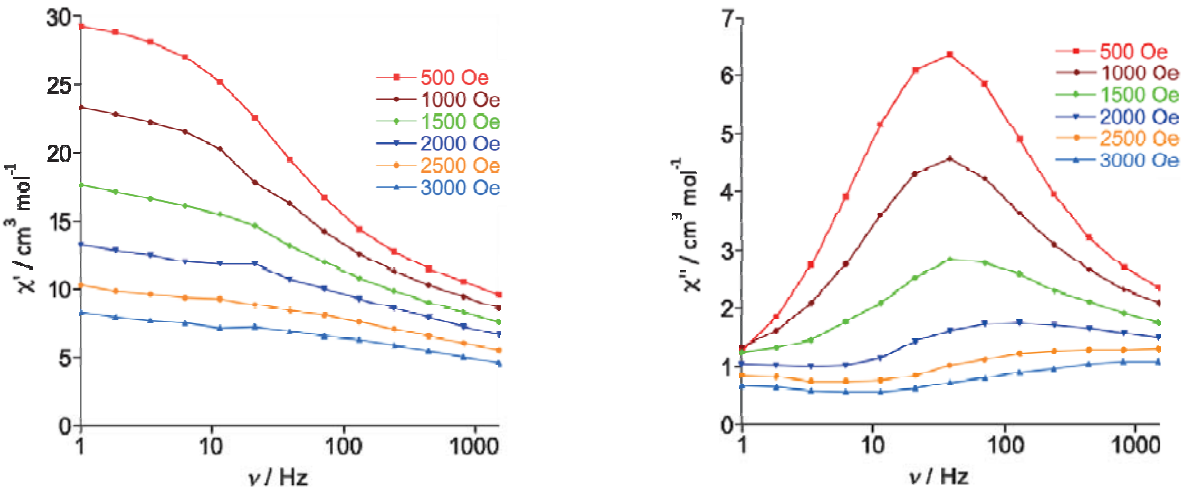

Figure 3.26 Plots of χ' vs. ν (left) and χ'' vs. ν (right) at 1.8 K with different applied dc fields for compound **14.**

In order to further investigate the dynamic magnetic properties of this complex, ac susceptibility measurements in the presence of a weak dc field were performed. Indeed this compound shows the field-induced slow relaxation of the magnetization. With the application of an external dc field, the intensity of the out-of-phase ac susceptibility is more enhanced (Figure 3.27). This type of behavior

Dieses Werk ist copyrightgeschützt und darf in keiner Form vervielfältigt werden noch an Dritte weitergegeben werden.
Es gilt nur für den persönlichen Gebrauch.

further suggests that this complex has a very fast tunnelling process in the absence of static field. The tunnelling effect is most efficiently suppressed with a dc field of 700 Oe (Figure 3.26). Under these fields, the ac response at different temperatures increases by an order of magnitude and shows classic SMM behaviour with strong frequency dependence (Figure 3.27). However, hysteresis of the magnetization is not observable at 2 K (Figure 3.24).

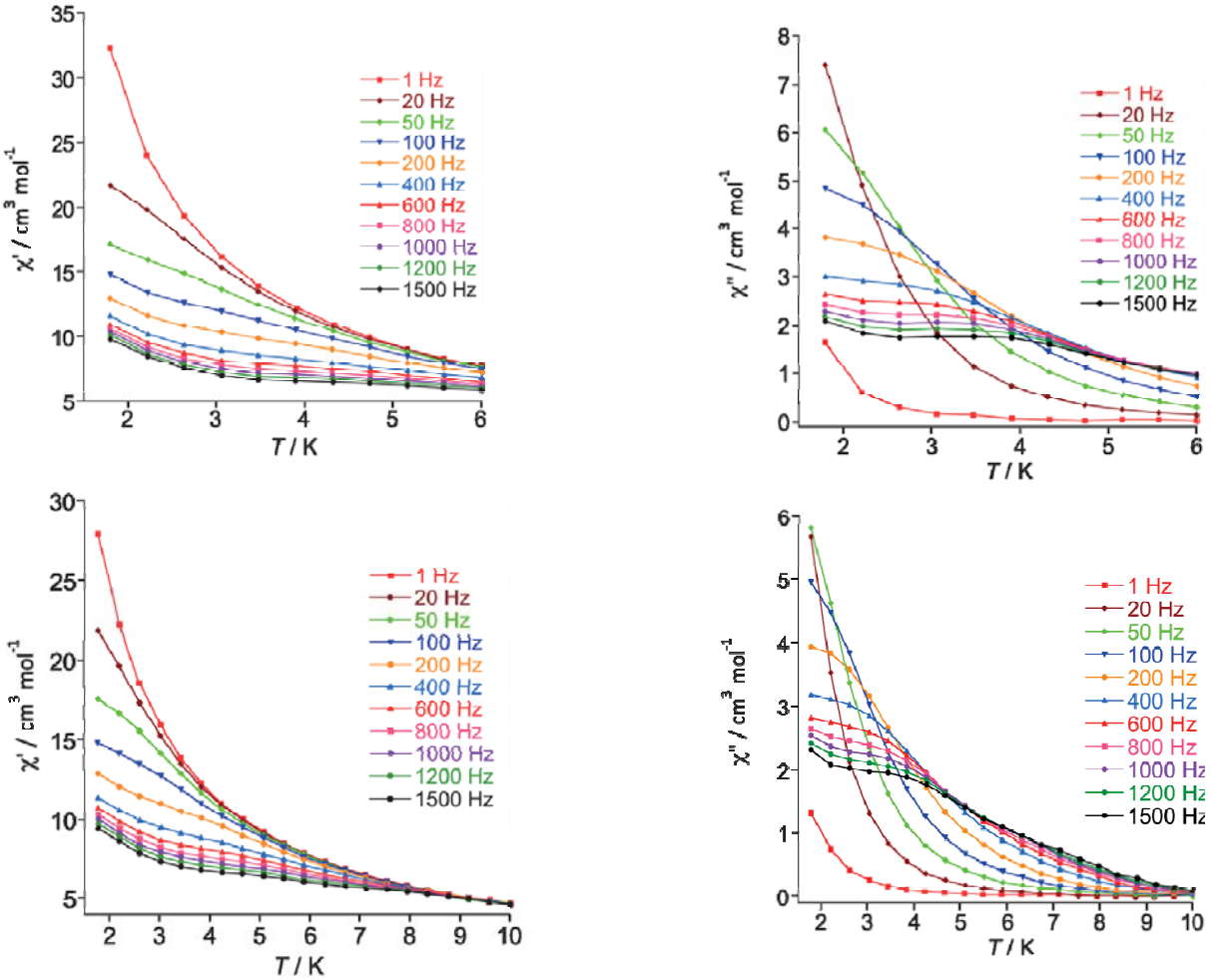

Figure 3.27 Frequency dependence of the in-phase (left) and out-of-phase (right) ac susceptibility under zero dc field (above) and 700 Oe dc field (below).

The dc molar magnetic susceptibilities $\chi_M T$, of the two pentanuclear complexes of **15** and **16** have also been measured over the 1.8 to 300 K temperature range in an applied magnetic field of 0.1 T. The experimental results for these complexes are plotted as shown in Figure 3.28 and Figure 3.29.

Dieses Werk ist copyrightgeschützt und darf in keiner Form vervielfältigt werden noch an Dritte weitergegeben werden.
Es gilt nur für den persönlichen Gebrauch.

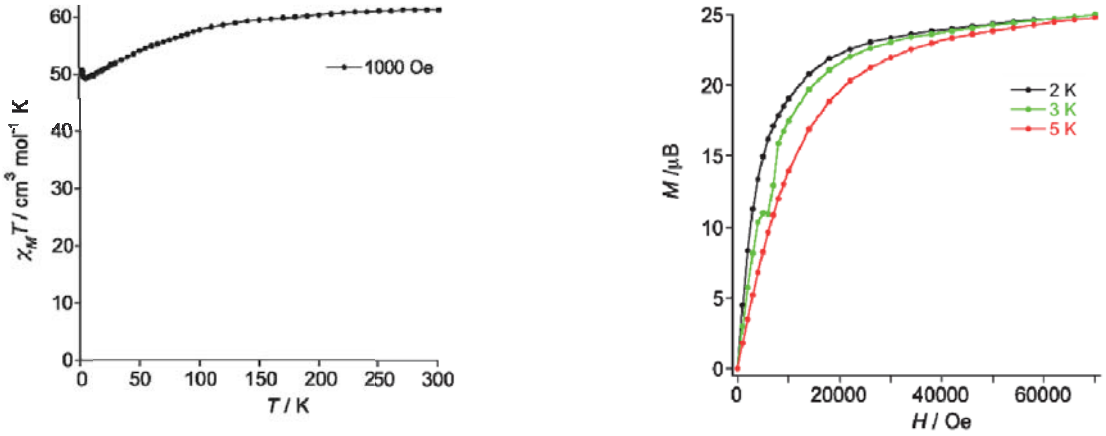

Figure 3.28 Plots of $\chi_M T$ vs. T (left) and M vs. H (right) for compound **15**.

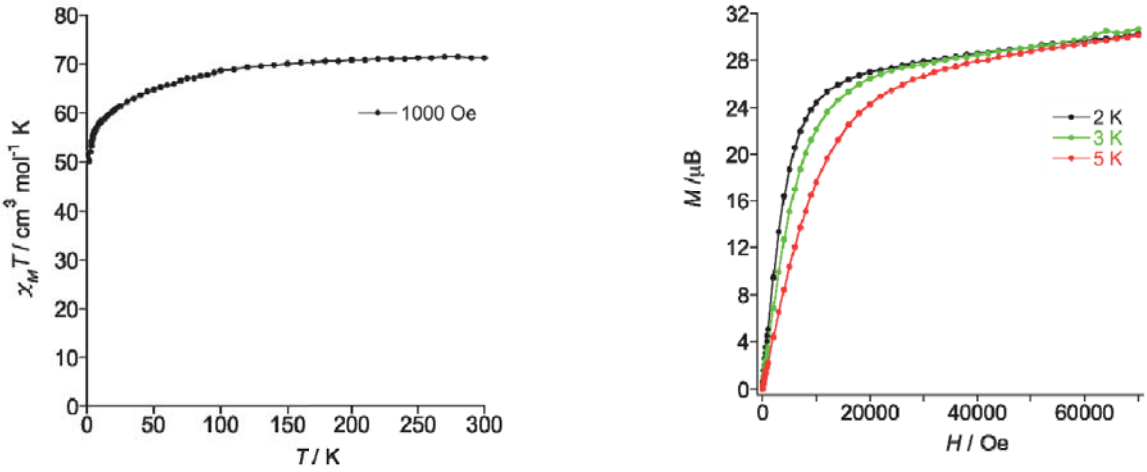

Figure 3.29 Plots of $\chi_M T$ vs. T (left) and M vs. H (right) for compound **16**.

At 300 K, the $\chi_M T$ products of **15** (61.2 cm^3 mol^{-1} K) and **16** (71.5 cm^3 mol^{-1} K) are close to that expected for five non-interacting Tb(III) (S = 3, L = 3, J = 6, g = 3/2, $^7F_6$) and Dy(III) (S = 5/2, L = 5, J = 15/2; g = 4/3, $^6H_{15/2}$) ions, respectively. On cooling in both cases, the $\chi_M T$ product remains essentially constant until approximately 100 K, below which the value begins to slowly decrease. Upon cooling, the $\chi_M T$ product of **15** decreases smoothly down to 5 K with a value 49.2 cm^3 mol^{-1} K. After that point the $\chi_M T$ product increases at lower temperatures to a maximum value of 50.7 cm^3 mol^{-1} K at 1.8 K. The low temperature increase is suggestive of very weak ferromagnetic exchange between the constituent Tb(III) ions. However, for complex **16**, this decrease continues down to 1.8 K, indicative of the thermal depopulation of the single-ion ligand-field states and/or very weak antiferromagnetic exchange between the Dy centres.

Magnetization (M) data were collected in the 0–70 kOe field range at 2-5 K. The field dependence of the magnetization shows a rapid increase of the magnetization at low field and a linear increase at high field to reach values of 25.0 and 30.2 μB for compounds **15** and **16** (Figure 3.28 and Figure 3.29) at 2 K, respectively, which are considerably smaller than the expected saturation magnetization

Dieses Werk ist copyrightgeschützt und darf in keiner Form vervielfältigt werden noch an Dritte weitergegeben werden.
Es gilt nur für den persönlichen Gebrauch.

values, for five Ln(III) ions. This behavior suggests the presence of a significant magnetic anisotropy arising from the ligand-field effects and/or low-lying excited states. Nonetheless, no out-of-phase ac magnetic susceptibility signal were observed down to 1.8 K, thus discarding the occurrence of slow magnetic relaxation of these two complexes.

In summary, unique tetranuclear $\{[Dy_4(L^2)_3(Ph_2acac)_4]\cdot(Et_3NH)\cdot 4(MeOH)\cdot(MeCN)\cdot(H_2O)\}$ (**14**) and the pentanuclear $\{[Tb_5(\mu_3\text{-}OH)_2(L^2)_2(Ph_2acac)_7(Ph_2acacH)]\cdot 7(PhMe)\}$ (**15**), $\{[Dy_5(\mu_3\text{-}OH)_2(L^2)_2((Ph_2acac)_7(Ph_2acacH)]\cdot 7(PhMe)\}$ (**16**) compounds were prepared and structurally characterized. The solid state structures of compounds were established by single crystal x-ray diffraction. A molecular peak corresponding to $[Dy_4(L^2)_3(Ph_2acac)_4]^-$ is observed in the ESI mass spectrum (negative mode) of compound **14**. Magnetic studies of compounds **14** and **15** shows weak ferromagnetic interactions, whereas compound **16** shows antiferromagnetic interactions between neighboring ions. In addition compound **14** shows the SMM behavior with the application of an external dc field.

3.5 See-Saw and Square Planar Shaped Tetranulcear and Pentagonal prism Shaped Pentanuclear Complexes of Lanthanides: Synthesis and Magnetic study

3.5.1 Synthesis and Structures

The proligand (H_3L^2) was prepared *in situ* by condensation of 4-tert-butyl-2,6-diformylphenol and 2-aminophenol in methanol. It was reacted with the metal salts $[Ln(NO_3)_3\cdot x(H_2O)]$ (Ln = Tb, Dy, Er, Ho, Tm) in the presence of acetyacetone (acacH) to obtain compounds $\{[Ln_4(\mu_3\text{-}OH)_2(L^2)(HL^2)(acac)_5(H_2O)]\cdot(NO_3)\cdot(HNEt_3)\cdot 2(Et_2O)\}$ Ln = Tb (**17**), Dy (**18**), Ho (**19**), Er (**20**), Tm (**21**). These compounds were isolated as single crystalline material by recrystallization of the reaction mixtures in diethyether. Another tetranuclear planar compound $\{[Dy_4(\mu_4\text{-}OH)(L^2)_2(acac)_4(MeOH)_2(EtOH)(H_2O)]\cdot(NO_3)\cdot 2(MeOH)\cdot 3(EtOH)\}$ (**22**) was isolated as single crystalline material from the same ligand (H_3L^2) by altering the reaction time and temperature. When ligand H_3L^2 was refluxed with acetylacetone and lanthanide salts for 2 hours compounds **17-21** were isolated. By altering the reaction time to 2 minutes at room temperature; compound **22** was obtained directly from the reaction mixture. In next synthesis, we prepared the new ligand (H_2L^{2a}), by condensing one formyl group of 4-tertbutyl-2,6-diformylphenol with 2-aminophenol and the other formyl group with acetylacetone. Both H_2L^{2a} and H_3L^2 were used in the synthesis of complex and the ligands were reacted with the metal salt $[Dy(NO_3)_3\cdot 5(H_2O)]$ to obtain the unique coplanar pentanuclear $\{[Dy_5(\mu_5\text{-}NO_3)(L^2)(L^{2a})_2(acac)_6(iPrOH)_2(H_2O)(OH)]\cdot 4(H_2O)\}$ (**23**) complex. The solid state structures of compounds **17-23** were established by single crystal-X-ray diffraction and characterized by

Dieses Werk ist copyrightgeschützt und darf in keiner Form vervielfältigt werden noch an Dritte weitergegeben werden.
Es gilt nur für den persönlichen Gebrauch.

spectroscopic and analytical techniques. The molecular structure of anions (**17-22**) were supported by ESI-MS.

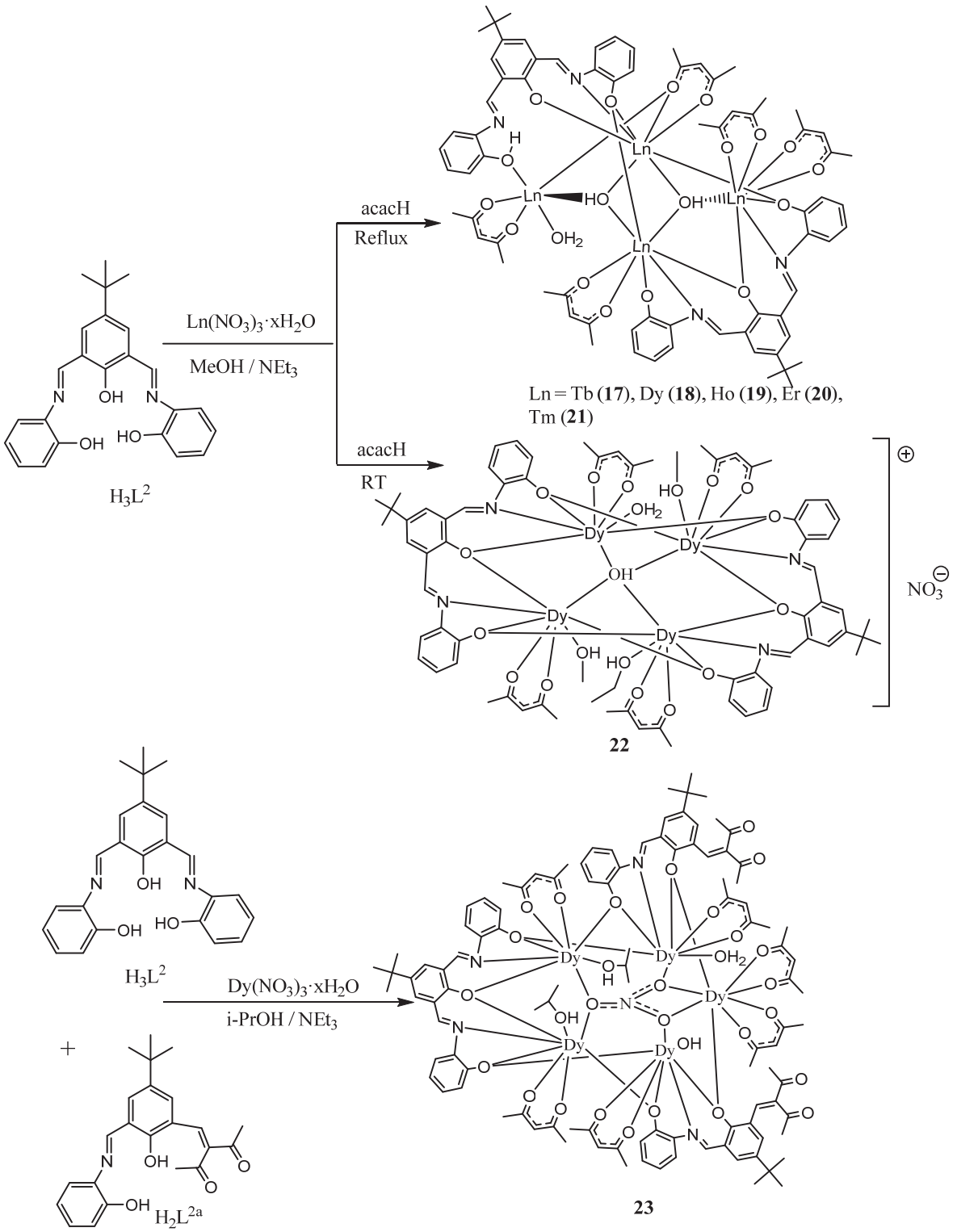

Scheme 3.5 Synthesis of compounds **17-23**.

Complex **17- 21** crystallized in the triclinic space group *P*-1 with two molecules in the unit cell. They are isostructural with one another as shown in Scheme 3.5. The representative bonding parameters of cation **17** are discussed in detail (Figure 3.30). The asymmetric unit of compounds **17-21** contains

Dieses Werk ist copyrightgeschützt und darf in keiner Form vervielfältigt werden noch an Dritte weitergegeben werden.
Es gilt nur für den persönlichen Gebrauch.

one $[Ln_4(\mu_3\text{-}OH)_2(L^2)(HL^2)(acac)_5(H_2O)]$ molecule. Furthermore, one triethylamonium nitrate ion pair and two diethyl ether molecules are present in the crystal lattice. The charge of the four Dy(III) ions is balanced by one trianionic Schiff-bases $(L^2)^{3-}$, one dianionic Schiff-bases $(L^2)^{3-}$, five monoanionic acac and two hydroxide ions. The compostion of the compounds (**17-21)** is characterized by ESI-MS. Although in the singly crystal X-ray structures some electron density is located between the phenol oxygen atom and the Schiff-base nitrogen atom for $(HL)^{2-}$ (see Scheme 3.5), it is not possible to unambiguously assign the position of the remaining acidic proton without doubt. Since one nitrogen atom (N3) of the dianionic Schiff-base $(HL)^{2-}$ ligand is not coordinating to the metal atom, we anticipate that the proton is localized between N3 and O5.

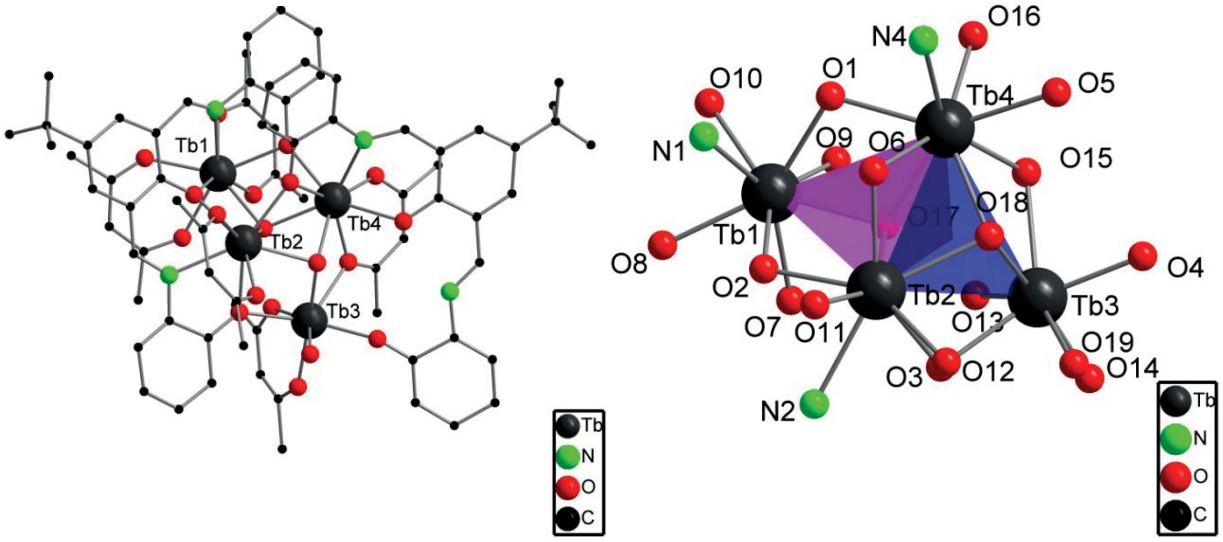

Figure 3.30 Solid state structure of **17** (left) and the metal core (right). Triangle A (pink) and B (blue) are shown in the metal core. Hydrogen atoms have been omitted for clarity.

The metal core consists of a tetranuclear arrangement of Ln(III) ions in a see-saw shape. Such see-saw shaped geometry for tetranuclear rare earth metals $[Ln_4(L)_4(\mu_4\text{-}OH)(\mu_3\text{-}OH)_2(NO_3)_4]\cdot(NO3)$ (LH = 2-methoxy-6-(pyridin-2-ylhydrazonomethyl)phenol) are rarely reported in literature.[153] The see-saw shaped is made up by two edge sharing triangles A (Tb1Tb2Tb4) and B (Tb2Tb4Tb3). The triangles A and B are shown in metal core by pink and blue color, respectively (see Figure 3.30). In triangle A, μ_3-hydroxyalte (O17) bridged 0.960 Å below the plane of triangle. In triangle B, μ_3-hydroxyalte (O18) bridged 1.047 Å above the plane of triangle. These triangles planes are oriented at an angle of 71.23° from each other. The angles between the Tb(III) ions are 56.18(2)° (Tb2-Tb3-Tb4) and 54.12(2)° (Tb2-Tb1-Tb4). Tb1, Tb2 and Tb4 are eight fold coordinated to seven oxygen atoms and one nitrogen atom. Tb1 is distorted square-antiprismatic coordinate to four O-atoms of acac ligand, one μ_3-hydorxyl ions (O17), two μ_2-bridged phenolate oxygen atoms and one N-atom of Schiff base. Tb2 and Tb4 are distorted square-antiprismatic coordinate to two μ_3-bridged hydroxyl ions, two oxygen atoms from the acac ligand, two oxygen atoms and one nitrogen atom of Schiff

Dieses Werk ist copyrightgeschützt und darf in keiner Form vervielfältigt werden noch an Dritte weitergegeben werden.
Es gilt nur für den persönlichen Gebrauch.

base ligand. Tb3 is coordinated to seven oxygen atoms and its coordination geometry can be best described as distorted capped octahedron. The Tb-O and Tb-N distances are in the range of 2.189(11)-2.496(10) Å and 2.507(14)-2.540(14) Å respectively. The Tb-Tb distances are in the range of 3.5142(11)-3.8752(12) Å.

Compound **22** crystallizes in the orthorhombic space group $Pna2_1$ with four molecules in the unit cell. It contains a $[Dy_4(\mu_4\text{-}OH)(L^2)_2(acac)_4(MeOH)_2(EtOH)(H_2O)]^+$ cation and a nitrate counter anion. The molecular structure of the cation is shown in Figure 3.31. The charge of the four Dy(III) ions in complex is balanced by four monoanionic acac ligand, two trianionic Schiff base ligands $(L^2)^{3-}$, one hydroxide ion and a nitrate counter anion.

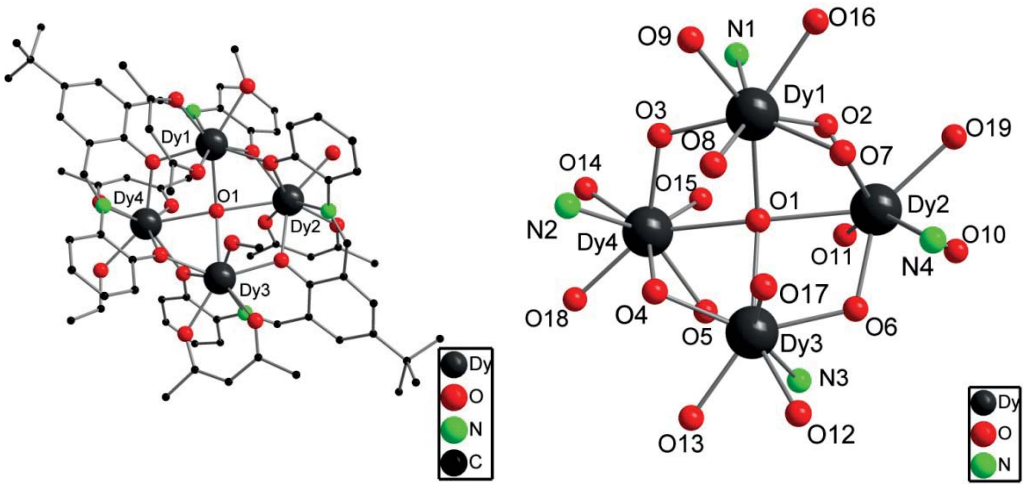

Figure 3.31 Solid state structure of **22** (left) and the metal core (right). Hydrogen atoms have been omitted for clarity.

The central metal core of **22** complex consists of four Dy(III) ions, which are arranged in a square grid shape around the central μ_4-(OH) ion. Such a square grid arrangement is relatively rare $\{[Dy_4(\mu_4\text{-}OH)(Hhpch)_8)]\cdot(ClO_4)_3\}$ (H_2hpch = 2-hydroxylbenzaldehyde (pyridine-4-carbonyl) hydrazone)[46] and $[Dy_4(L1\text{-}2H)_2(L1\text{-}H)_2(N_3)_4(O)]$[47] in the literature. In compound **22** each Schiff base coordinates to four Dy(III) ions with μ_2-bridging phenolate oxygen atoms (O2, O3, O4, O5, O6 and O7) and imine nitrogen atoms (N1, N2, N3 and N4). The eight fold coordination sphere of each Dy(III) ion is completed by the $(L^2)^{3-}$ ligands, one acac ligand and either one methanol (Dy1 and Dy3) or ethanol (Dy4) or water molecule (Dy2). Each Dy(III) ion is coordinated by seven oxygen atoms, one imine nitrogen atom and features a distorted square antiprism coordination geometry. The Dy-(μ_2-O) bond distances (2.288(11)-2.333(11) Å) are slightly shorter than the Dy-(μ_4-OH) bond distances (2.473(11)-2.636(11) Å). The arrangement of the Dy(III) ions and μ_2-bridged phenolate oxygen atoms looks like an octagonal shape, which is shown in metal core of the compound (see Figure 3.31). The four Dy(III) ions are almost planar coordinated. The Dy-N bond

Dieses Werk ist copyrightgeschützt und darf in keiner Form vervielfältigt werden noch an Dritte weitergegeben werden.
Es gilt nur für den persönlichen Gebrauch.

lengths range from 2.503(14)-2.536(15) Å and the Dy-Dy bond lengths range from 3.5346(12)-3.8994(13) Å. The bond lengths of compound **22** are in comparable range to the reported tetranuclear square grid complex $[Dy_4(L1\text{-}2H)_2(L1\text{-}H)_2(N_3)_4(O)]$ which have Dy-N bond lengths of 2.34-2.56 Å and Dy-Dy bond lengths of 3.66-3.69 Å .[47]

The pentanuclear centrosymmetrical compound **23** crystallized in the orthorhombic space group *Pbcn* with half of the molecule in the asymmetric unit. A perspective view of the pentagonal core shaped compound **23** is shown in Figure 3.32. The unique pentanuclear complex consists of a central nitrate anion bridging to five Dy(III) ions, thus a precisely coplanar metal core is formed. A crystallographic inversion center is observed through the central nitrate ion.

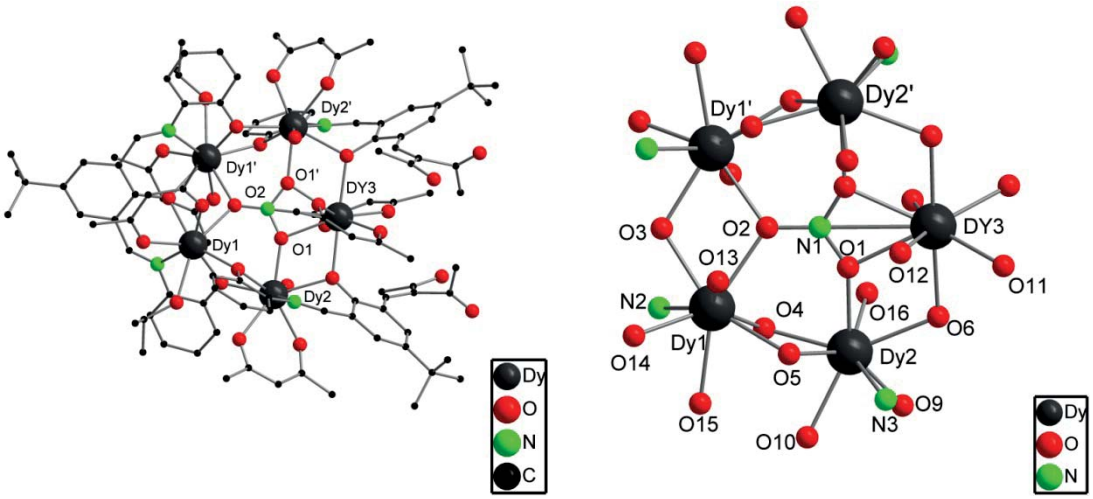

Figure 3.32 Solid state structure of **23** (left), and the metal core (right). Hydrogen atoms have been omitted for clarity.

The complex consists of five Dy(III) ions which are coordinated to six monoanionic acac ligands, a hydroxide ion, a trianionic ligand $(L^2)^{3-}$, two dianionic $(L^{2a})^{2-}$ ligands and a nitrate ion. The nitrate ion of the complex are in the centre and it coordinates to all Dy(III) ions. In the crystal structure a hydroxide ions and a water molecule are disorded and occupying 50:50 positions at Dy2 and Dy2' so to make it simplify in the Scheme 3.5 we fixed their position at parcticlar Dy without knowing their actual position. The central metal core of this complex consists of five Dy(III) ions, which are arranged in a coplanar pentagonal shape around the central μ_5-(NO_3). This nitrate bridging structure is unique in geometrical arrangement of metal atoms. All the phenolate and nitrate O-atoms are in a μ_2-bridging coordination mode with five Dy(III) ions and thus build the central core of Dy_5NO_{10}, which is shown in Figure 3.32. Dy1 and Dy2 are eight fold coordinated by seven oxygen atoms, a nitrogen atom and feature a distorted square antiprism coordination geometry. Dy3 is eight fold coordinated by oxygen atoms and features a distorted dodecahedral coordination geometry. The Dy-(μ_2-O) nitrate bridging distances are Dy2O1 2.247(6) Å, Dy1O2 2.415(4) Å and Dy3O1 2.421(6) Å,

Dieses Werk ist copyrightgeschützt und darf in keiner Form vervielfältigt werden noch an Dritte weitergegeben werden.
Es gilt nur für den persönlichen Gebrauch.

whereas phenolate Dy-(μ_2-O) bridging distance are in the range of 2.336(6)-2.409(6) Å. The Dy-N distances are in the range of 2.483(8)-2.494(7) Å and these bond distances are in the comparable range of other reported pentanuclear compounds $[Dy_5(OH)_5(\alpha\text{-AA})_4(Ph_2acac)_6]$ (α-AA = D-PhGly, L-Trp, L-Pro, Ph_2Gly, Ph_2acac = dibenzoylmethanide).[68, 151] The Dy-Dy distances are between 3.7450(8)-3.9959(8) Å, which are comparable to distances of the reported pentanuclear compound $[Dy_5(\mu_3\text{-}OH)_6(Acc)_6(H_2O)_{10}]^{9+}$ (Acc=1-amino-cyclohexanel-carboxylic acid) 3.7100(5)−3.8721(4).[68]

3.5.2 Magnetic Properties

The magnetic properties of compounds were studied by Dr. Valeriu Mereacre (Prof. Annie K. Powell). The temperature dependent dc magnetic susceptibility data for compounds **17**, **18**, **19** and **23** were collected in the range 300−1.8 K and in an applied magnetic field of 0.1 T. The magnetization (M) data were collected in the 0–70 kOe field range at different temperatures (2-5K). The magnetic measurement of compound **22** is in process of measurement.

The experimental results for complex **17** are plotted at 300 K as shown in Figure 3.33. The $\chi_M T$ value for **17** (44.20 cm^3 K mol^{-1}) is close to that expected for four noninteracting Tb(III) ions 47.2 cm^3 K mol^{-1} (S = 3, L = 3, J = 6, g = 3/2, $^7F_6$). On lowering the temperature, the $\chi_M T$ for **17** remains almost constant until ~ 50 K and then decreases sharply to reach a value of 27.80 cm^3 K mol^{-1} at 1.8 K. This low temperature increase is suggestive of weak antiferromagnetic exchange between the constituent Tb(III) ions.

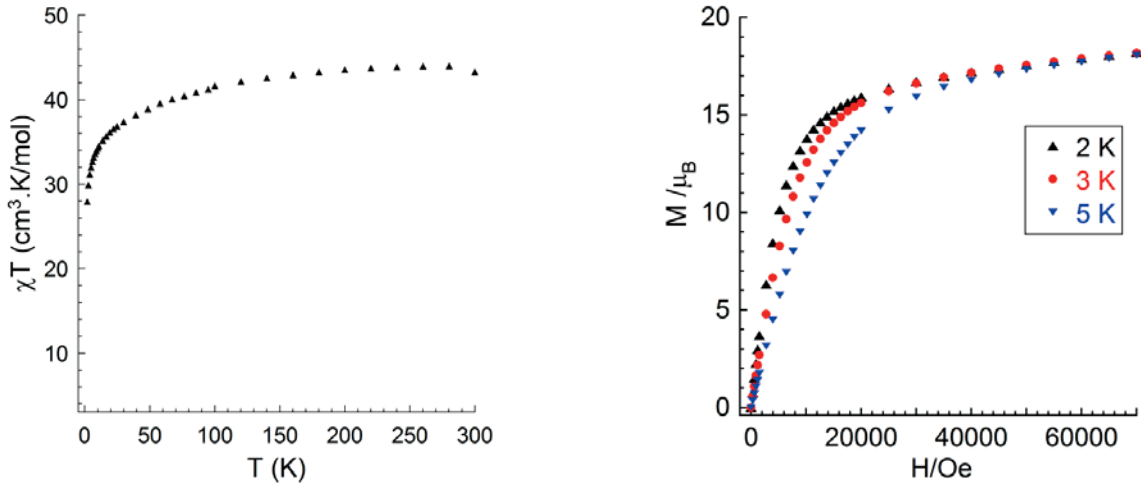

Figure 3.33 Plots of $\chi_M T$ vs. T (left) and M vs. H (right) for compound **17**.

The non-superposition of the M vs. H/T data (Figure 3.33) suggests the presence of a significant magnetic anisotropy and/or low-lying excited states. The magnetization increases rapidly at low field and eventually reaches the value of 18.2 mB at 70 kOe without clear saturation. This value is much lower than the expected saturation value of four noninteracting Tb(III) ions, most likely due to the

Dieses Werk ist copyrightgeschützt und darf in keiner Form vervielfältigt werden noch an Dritte weitergegeben werden.
Es gilt nur für den persönlichen Gebrauch.

crystal-field effect at the Tb(III) ions. Therefore, it is difficult to conclude whether exchange interactions are occurring between the Tb(III) ions.

The experimental results for complex **18** are plotted as shown in Figure 3.34 at 300 K, the $\chi_M T$ value for **18** (51.31 cm^3 K mol^{-1}) slightly differ that expected for four noninteracting Dy(III) ions 56.7 cm^3 K mol^{-1} (S = 5/2, L = 5, J = 15/2, g = 4/3, $^6H_{15/2}$). On lowering the temperature, the $\chi_M T$ for **18** remains almost constant until ~ 50 K then decreases sharply to reach a value of 28.31 cm^3 K mol^{-1} at 1.8 K. This low temperature increase is suggestive of weak antiferromagnetic exchange between the constituent Dy(III) ions.

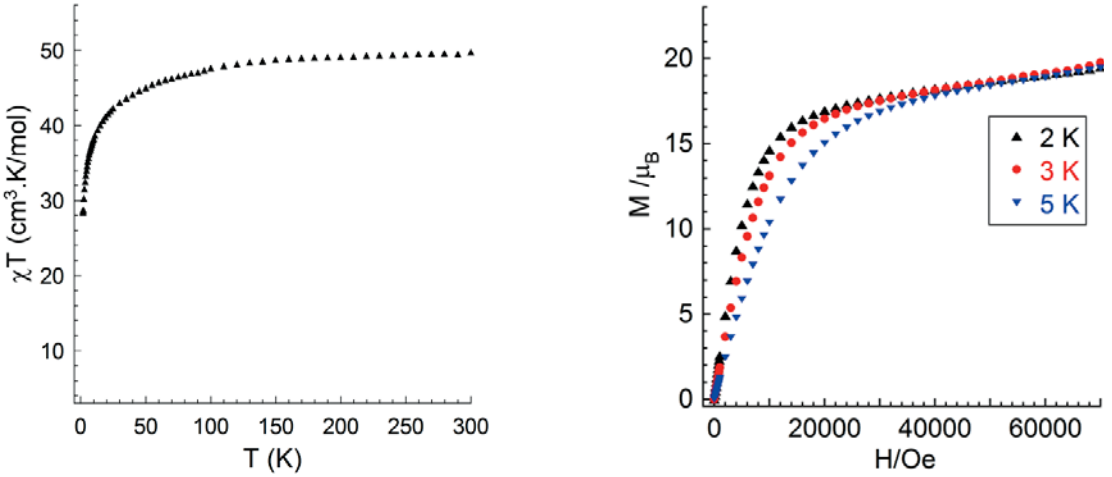

Figure 3.34 Plots of $\chi_M T$ vs. T (left) and M vs. H (right) for compound **18**.

The non-superposition of the M vs. H/T data (Figure 3.34) suggests the presence of a significant magnetic anisotropy and/or low-lying excited states. The magnetization increases rapidly at low field and eventually reaches the value of 19.9 mB at 70 kOe without clear saturation. This value is much lower than the expected saturation value of four noninteracting Dy(III) ions.

The experimental results for complex **19** are plotted as shown in Figure 3.35 at 300 K, the $\chi_M T$ value for **19** (54.67 $cm^3 mol^{-1} K$) is close to that expected for four noninteracting Ho(III) ions of 56.28 cm^3 K mol^{-1} (S = 2, L = 6, J = 8, g = 5/4, $^5I_8$). On lowering the temperature, the $\chi_M T$ for **19** remains almost constant until ~ 50 K and then decreases sharply to reach a value of 26.26 cm^3 K mol^{-1} at 1.8 K. This low temperature increase is suggestive of weak antiferromagnetic exchange between the constituent Ho^{3+} ions.

Dieses Werk ist copyrightgeschützt und darf in keiner Form vervielfältigt werden noch an Dritte weitergegeben werden.
Es gilt nur für den persönlichen Gebrauch.

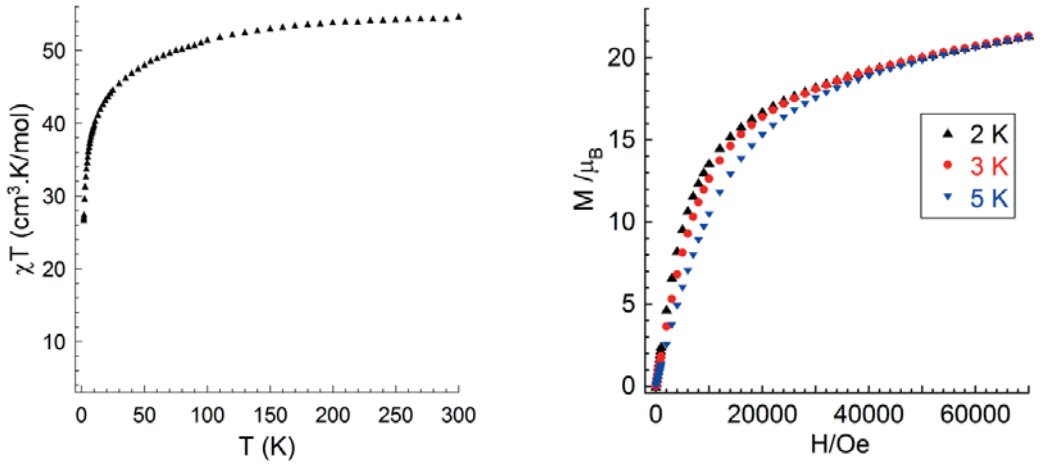

Figure 3.35 Plots of $\chi_M T$ vs. T (left) and M vs. H (right) for compound **19**.

The non-superposition of the M vs. H/T data (Figure 3.35) suggests the presence of a significant magnetic anisotropy and/or low-lying excited states. The magnetization increases rapidly at low field and eventually reaches the value of 21.37 mB at 70 kOe without clear saturation. This value is noticeably lower than the theoretical value expected of four noninteracting Ho(III) ions, indicating a much smaller effective spin**.**

The experimental results for complex **23** are plotted as shown in Figure 3.36 at 300 K, the $\chi_M T$ value for **23** (68.08 cm^3 K mol^{-1}) matches well with that expected for five noninteracting Dy(III) ions of 70.8 cm^3 K mol^{-1} (S = 5/2, L = 5, J = 15/2, g = 4/3, $^6H_{15/2}$). On lowering the temperature, the $\chi_M T$ for **23** remains almost constant until ~ 50 K and then decreases sharply to reach a value of 43.03 cm^3 K mol^{-1} at 1.8 K. This low temperature increase is suggestive of weak antiferromagnetic exchange between the constituent Dy(III) ions.

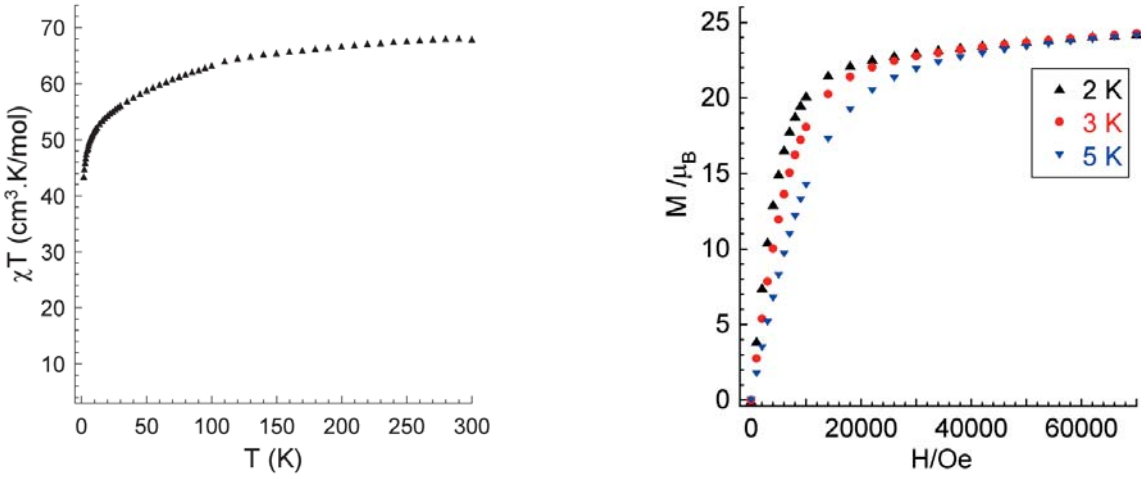

Figure 3.36 Plots of $\chi_M T$ vs. T (left) and M vs. H (right) for compound **23**.

The non-superposition of the M vs. H/T data (Figure 3.36) suggests the presence of a significant magnetic anisotropy and/or low-lying excited states. The magnetization increases rapidly at low field

Dieses Werk ist copyrightgeschützt und darf in keiner Form vervielfältigt werden noch an Dritte weitergegeben werden.
Es gilt nur für den persönlichen Gebrauch.

and eventually reaches the value of 24.24 mB at 70 kOe without clear saturation. This value is noticeably lower than the theoretical value of five noninteracting Dy(III) ions.

Nonetheless, no out-of-phase ac magnetic susceptibility signals were observed for compounds **17**, **18**, **19** and **23** down to 1.8 K, thus ruling out the occurrence of slow magnetic relaxation of the complexes.

In summary, {[$Ln_4(\mu_3\text{-}OH)_2(L^2)(HL^2)(acac)_5(H_2O)$]·($NO_3$)·($HNEt_3$)·2($Et_2O$)} Ln = Tb (**17**), Dy(**18**), Ho(**19**), Er (**20**), Tm (**21**), {[$Dy_4(\mu_4\text{-}OH)(L^2)_2(acac)_4(MeOH)_3(H_2O)$]·($NO_3$)·(MeOH)} (**22**) and {[$Dy_5(\mu_5\text{-}NO_3)(L^2)(L^{2a})_2(acac)_6(iPrOH)_2(H_2O)(OH)$]·4($H_2O$)} (**23**) were prepared by the use of polydentane ligands ($^2L^{3-}$ and $^{2a}L^{2-}$). The tetranuclear compounds **17-21** exhibited a see-saw shaped geometry. Compound (**22**) adopts a planar square grid arrangement and compound (**23**) has a pentagonal shape. The magnetic studies of compounds **17**, **18**, **19** and **23** suggested that they have weak antiferromagnetic magnetic interactions to neighbouring metal ions. No out-of-phase ac magnetic susceptibility signals were observed down to 1.8 K.

3.6 Mononuclear, Pentanculear and Hepatenuclear Complexes of Lanthanides: Synthesis and Magnetism

3.6.1 Synthesis and Structures

The mononuclear compounds {[$Tb(Ph_2acac)_4$]·(Et_3NH)} (**24**) and {[$Dy(Ph_2acac)_4]_2$·2 (Et_3NH)·3(CH_2Cl_2)} (**25**) were prepared with 4:1 ratio of dibenzoylmethane (Ph_2acacH) and $Ln(NO_3)\cdot 6H_2O$ in a 1:1 mixture of methanol and dichloromethane. Previously, tetranuclear [$Ln_4(\mu_3\text{-}OH)_2(Ph_2acac)_8(o\text{-}O_2NC_6H_4O)_2$][Ln=Yb, Lu][146] and pentanuclear $H_5[Y_5(\mu_4\text{-}O)(\mu_3\text{-}O)_4(\mu\text{-}\eta^2\text{-}Ph_2acac)_4(\eta^2\text{-}Ph_2acac)_6]$[145] complexes have been reported by using dibezoylmethane as a ligand.[145, 149, 151] The nuclearity of the metal cluster could be controlled by the variation of reaction time. The Schiff base proligand (H_3L^2) was prepared *in situ* by condensation of 4-tert-butyl-2,6-diformylphenol and 2-aminophenol in methanol. H_3L^2 was reacted with the lanthanide salts [$Ln(NO_3)_3\cdot(H_2O)_m$] (Ln = Tb, Dy) in the presence of dibenzoylmethane and triethylamine. As a result, the compounds{[$Dy_5(\mu_3\text{-}OH)_2(L^2)_3(Ph_2acac)_4(MeOH)_4$]·4(MeOH)} (**26**), {[$Tb_7(\mu_3\text{-}OH)_2(\mu_5\text{-}NO_3)(\mu_3\text{-}NO_3)(L^2)_3(Ph_2acac)_5(H_2N\text{-}Ph\text{-}O)(MeO)_2(MeOH)_3$]·3(MeOH)·(MeCN)·15($H_2O$) (**27**) were isolated as crystalline material with variation in nuclearity of the metal cores. The solubility of compounds **26** and **27** plays a key role in the isolation of these compounds in pure form. Compound **26** was insoluble in methanol and it was separated from the reaction mixture by filtration and recrystallized from a mixture of methanol and dichloromethane to obtain as crystalline material. Compound **27** was soluble in methanol. Thus, single crystals were obtained directly from the reaction solution by diffusion of acetonitrile into the reaction mixture. Compounds **24-27** were characterized by standard

Dieses Werk ist copyrightgeschützt und darf in keiner Form vervielfältigt werden noch an Dritte weitergegeben werden.
Es gilt nur für den persönlichen Gebrauch.

analytical/spectroscopic techniques and the solid state structures were determined by single-crystal X-ray diffraction. The molecular structure of anions in the compounds **24** and **25** were supported by ESI-MS.

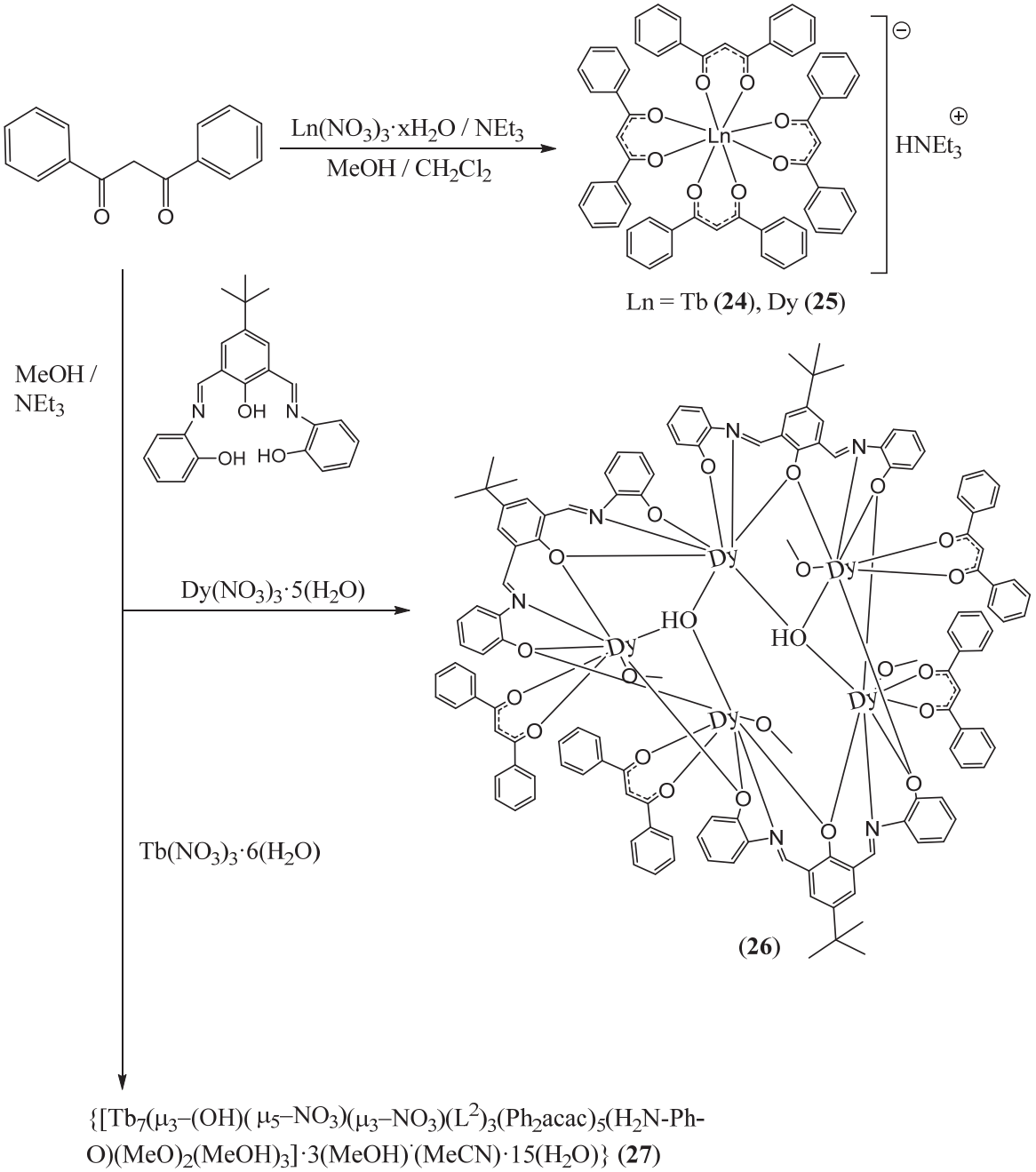

Scheme 3.6 Synthesis of compounds **24-27**

The terbium complex **24** crystallized in the monoclinic space group *Pc* with four molecules in the unit cell, whereas the dysprosium complex **25** crystallized in the monoclinic space group *C*2/*c* with four molecules in the unit cell. A perspective view of complex **25** is shown in Figure 3.37. Compounds **24** and **25** are differing to each other in the number of molecules present in the asymmetric unit. In compound **25**, two isostructural molecules of $\{[Dy(Ph_2acac)_4]\cdot(Et_3NH)\}$ are

Dieses Werk ist copyrightgeschützt und darf in keiner Form vervielfältigt werden noch an Dritte weitergegeben werden.
Es gilt nur für den persönlichen Gebrauch.

present in the asymmetric unit whereas in the structure of **24** only one molecule of $\{[Tb(Ph_2acac)_4]_2 \cdot 2(Et_3NH) \cdot 3(CH_2Cl_2)\}$ is present in the asymmetric unit. The structures of the ionic complexes **24** and **25** consist of a $[Ln(Ph_2acac)_4]^-$ anion and protonated triethyamine $(Et_3NH)^+$ as counter cation as well as dichloromethane (**25**) in the lattice. The molecular structures of the anions were supported by ESI-MS in negative mode.

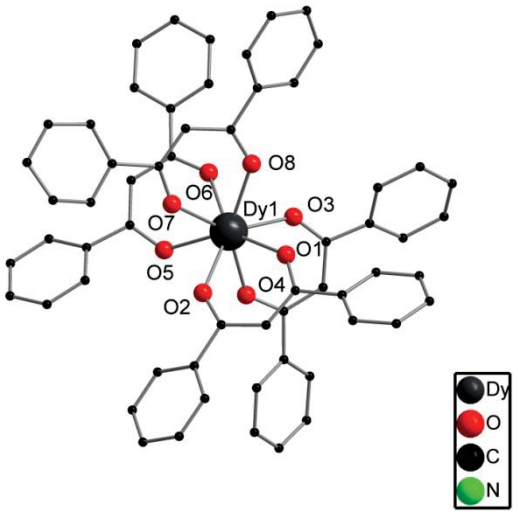

Figure 3.37 Solid state structure of the anion **25**. Hydrogen atoms have been omitted for clarity.

Compound **25** has a crystallographic *C*2-axis thruough the Dy atom. However, the structural parameters of both compounds are similar. The $[Ln(Ph_2acac)_4]^-$ anion consists of one Ln(III) ion coordinated by four monoanionic dibenzoylmethanide ligands. Thus, the metal atom is eight fold coordinated by eight oxygen atoms of the Ph_2acac ligands and resulting in a distorted square anti-prism coordination polyhedron. The Tb-O bond lengths of **24** are in the range of 2.315(6)-2.386(5) Å, which are comparable to the Dy-O bond lengths of **25** [2.3215(19)-2.384(2) Å]. These Ln-O bond lengths are also comparable to our previously reported 1D-coordination polymer $[Cs\{Dy(Ph_2acac)_4\}]$, which have Dy-O bond lengths in the range of 2.340(6)-2.351(6) Å.[154] The bond angles of **24** are (O2-Tb1-O1) 71.9(2)°, (O3-Tb1-O4) 71.4(2)°, (O6-Tb1-O5) 71.9(2)° and (O8-Tb1-O7) 70.7(2)°, which are also comparable to the **25** bond angles (O1-Dy1-O2) 72.06(7)°, (O3-Dy1-O4) 71.78(8)°, (O5-Dy1-O6) 69.76(7)° and (O7-Dy1-O8) 70.81(7)°.

Compound **26** crystallized in the orthorhombic space group *Pbca* with eight molecules in the unit cell. The metal ions are encapsulated by four monoanionic dibenzoylmethanide liagnds, three trianionic ligands $(L^2)^{3-}$ and two hydroxyl ions. A prospective view of complex **26** is shown in Figure 3.38.

Dieses Werk ist copyrightgeschützt und darf in keiner Form vervielfältigt werden noch an Dritte weitergegeben werden.
Es gilt nur für den persönlichen Gebrauch.

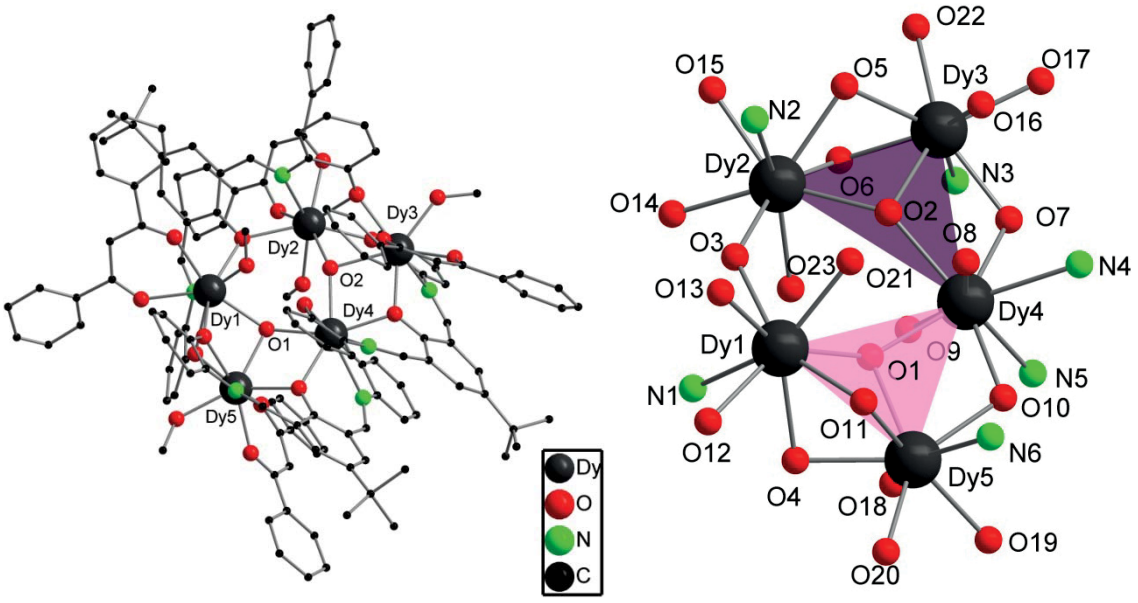

Figure 3.38 Solid state structure of **26** (left) and the metal core (left). Triangle A (rose) and B (plum) are shown in the metal core. Hydrogen atoms have been omitted for clarity.

The pentanuclear complex has an interesting topology. The metal core $[Dy_5(\mu_3\text{-}OH)_2(\mu_2\text{-}O)_7]$ of the compound is precisely coplanar. The structure of complex consist of corner sharing triangles A (Dy1, Dy4, Dy5) and B (Dy2, Dy3, Dy4); and μ_3-(OH) groups are occupying the centre of these triangles. The triangles A and B are shown in metal core by rose and plum color, respectively (see Figure 3.38). Triangles A and B are analogous and connected to each other by the bridging atoms O3 and Dy4. The μ_3-(OH) groups (O1, O2) nearly symmetrical bridge the metal centres and lie 0.524 Å below and 0.532 Å above the plane of the metal cores, respectively. The Dy-(μ_3-O1) bond lengths are in range of 2.363(5)-2.415(5) Å and it is comparable to the Dy-(μ_3-O2) bond lengths 2.374(5)-2.423(5) Å. The central atom (O3) is nearly symmetrically bound to both triangles A and B with regard to the bond lengths Dy1O3 2.408(5) Å and Dy2O3 2.425(6) Å. The phenolate O atoms of the Schiff bases are in μ_2-bridging modes, except O8 and O9 which are in η^1-modes. All O-atoms of the Ph_2acac ligand are in κ^2-modes. Each Dy(III) ion of the complex is eightfold coordinated and the coordination geometry is best described as distorted square antiprism. Dy1, Dy2, Dy3 and Dy5 are coordinated to two O atoms of the Ph_2acac ligand, one O atom from hydroxide, one molecule of methanol, three O atoms and one N atom of the Schiff base ligands. Dy4 complete its coordination sphere (N2O6) by six O atoms and two N atoms of the Schiff base ligands. The Dy-O and Dy-N bond distances are in the range of 2.292(6)-2.425(6) Å and 2.487(6)-2.563(6) Å, respectively. The Dy-Dy distances are in the range of 3.5282(7)-3.7983(9) Å, which are comparable to the reported $[Dy_5(\mu_3\text{-}OH)_6(Acc)_6(H_2O)_{10}]^{9+}$ (Acc=1-amino-cyclohexanel-carboxylic acid) Dy-Dy distances 3.7100(5)−3.8721(4).[68]

Dieses Werk ist copyrightgeschützt und darf in keiner Form vervielfältigt werden noch an Dritte weitergegeben werden.
Es gilt nur für den persönlichen Gebrauch.

Compound $\{[Tb_7(\mu_3\text{-}OH)_2(\mu_5\text{-}NO_3)(\mu_3\text{-}NO_3)(L^2)_3(Ph_2acac)_5(H_2N\text{-}Ph\text{-}O)(MeO)_2(MeOH)_3]\cdot(MeOH)_3\cdot(MeCN)\cdot 15(H_2O)\}$ (**27**) crystallized in the monoclinic space group $P2_1/c$ with four molecules in the unit cell. A perspective view of complex **27** is shown in Figure 3.39. The heptanuclear compound is arranged in an interesting topology with the precisely coplanar metal core. The arrangement of metal atoms is novel for rare earth metals. The seven terbium ions are encapsulated by five monoanionic dibenzoylmethanide ligand, three trianionic Schiff bases, two hydroxyl ions, two nitrate ions, two methoxide and one amine-phenolate. The bonding parameters of compound **27** are not discussed in detail as the crystal data was poor.

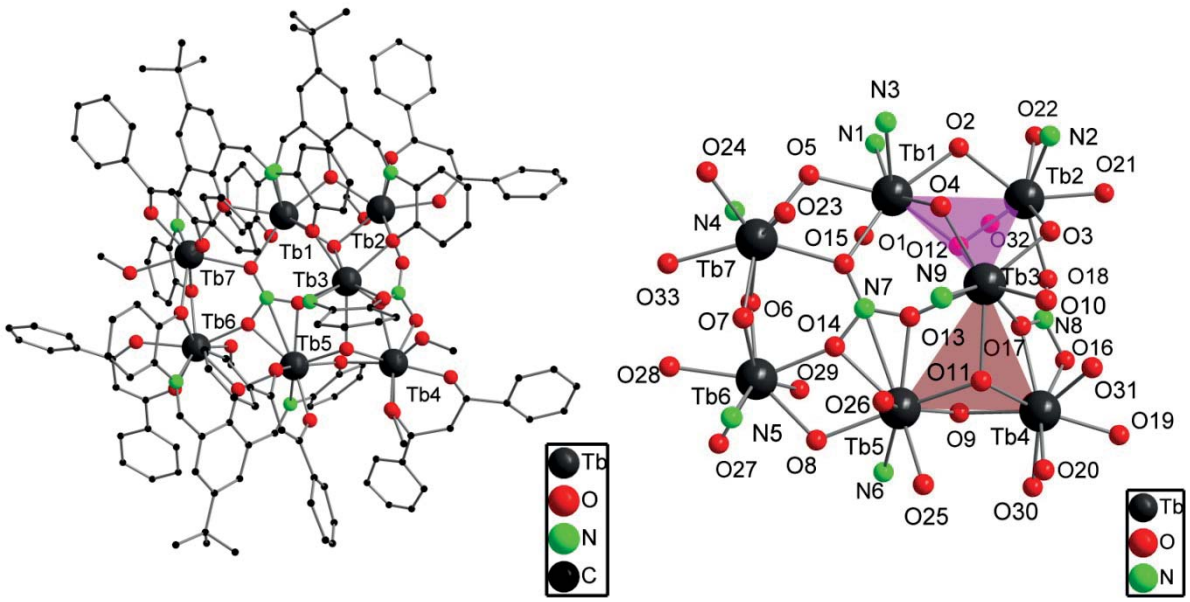

Figure 3.39 Solid state structure of **27** (left) and the metal core (right). Triangle A (pink) and B (light red) are shown in the metal core. Hydrogen atoms have been omitted for clarity.

The metal core of this complex consists of seven Tb(III) ions, the two nitrates and two hydroxyl ions. There are two ways to explain the heptanuclear arrangement of metal atoms: (a). The heptanuclear metal core of the complex has two peripheral linear trinuclear units (Tb1, Tb2, Tb7 and Tb4, Tb5, Tb6) and a central Tb3 atom. The peripheral linear trinuclear units are planar. (b). The five metal atoms (Tb1, Tb3, Tb5, Tb6 and Tb7) adopt a pentagonal geometry μ_5-(NO_3) group in the centre. The edges of this pentagon are fused with μ_3-(OH) group in the centre and connected to Tb2 and Tb4 to form the heptanuclear metal core. The fused Tb(III) ions (Tb2 and Tb4) form the triangles A (Tb1, Tb2 and Tb3) and B (Tb3, Tb4 and Tb5) with the edges of pentagonal. The triangles A and B are shown in metal core by pink and light red color, respectively (see Figure 3.39). Two μ_3-OH groups (O11, O12) in the triangles A and B are nearly symmetrical bridge to the metal centres and lie above and below the plan of metal cores respectively. All the terbium ions in compound **27** are eight fold coordinated. Such a novel heptanuclear arrangement of atoms is unknown for rare earth metals.

Dieses Werk ist copyrightgeschützt und darf in keiner Form vervielfältigt werden noch an Dritte weitergegeben werden.
Es gilt nur für den persönlichen Gebrauch.

3.6.2 Magnetic Properties

The magnetic properties of compounds **24-27** were studied by Dr. Abhishake Mondal (Prof. Annie K. Powell).

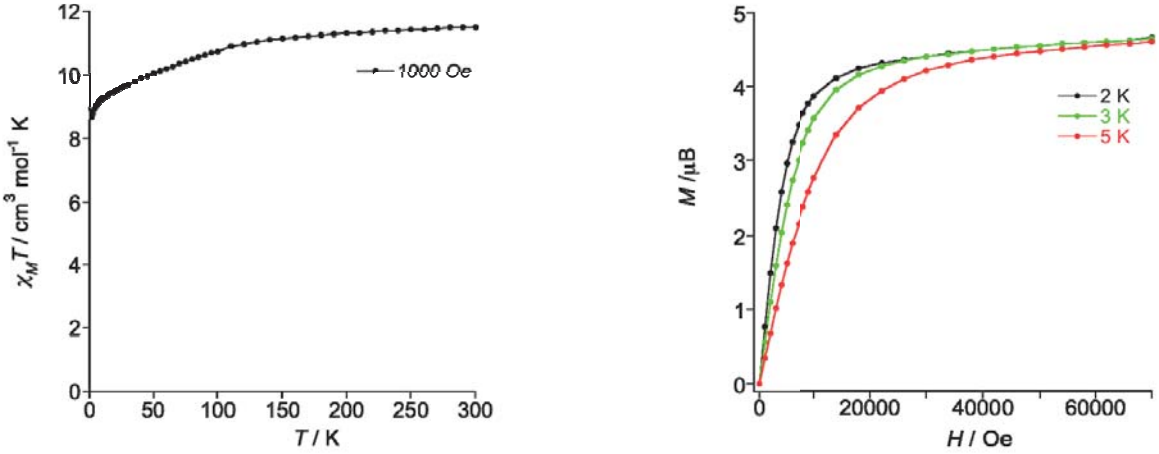

Figure 3.40 Plots of $\chi_M T$ vs. T (left) and M vs. H (right) for compound **24**.

The static dc magnetic susceptibility studies of **24** have been performed in the range of 1.8–300 K under an applied magnetic field of 1000 Oe (Figure 3.40). The $\chi_M T$ value of 11.49 cm^3 K mol^{-1} at 300 K for **24** is close to the calculated value of 11.81 cm^3 K mol^{-1} for the ground state of the Tb(III) ion (S = 3, L = 3, J = 6, g = 3/2, $^7F_6$). On cooling, the $\chi_M T$ product gradually decreases to achieve a value of 8.66 cm^3 K mol^{-1} at 1.8 K. Such behaviour is primarily owing to the depopulation of the Stark sublevels of the terbium ion, which occurs from the splitting of the $^7F_6$ ground term by the ligand field. The M versus H plot at 2-5 K (Figure 3.40) shows a quite fast increase in the magnetization at low field (until 2 T) and then a slow linear increase to achieve a value of 4.68 μ_B at the maximum applied field of 7 T. This value is lower than the expected saturation value for Tb(III) of ~ 9 μ_B and such behaviour is likely due to crystal-field effects leading to significant magnetic anisotropy.

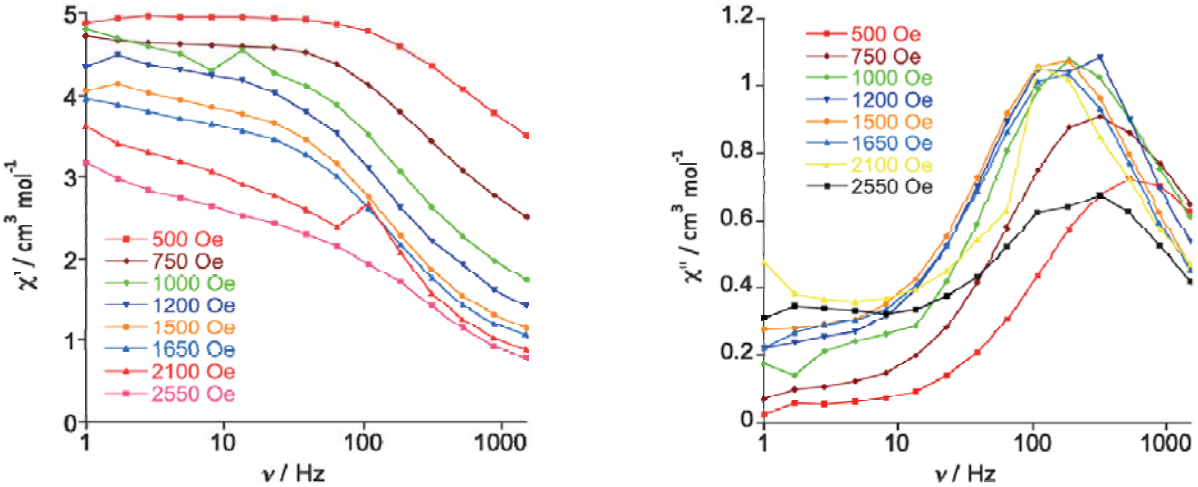

Dieses Werk ist copyrightgeschützt und darf in keiner Form vervielfältigt werden noch an Dritte weitergegeben werden.
Es gilt nur für den persönlichen Gebrauch.

Figure 3.41 Plots of χ' vs. ν (left) and χ" vs. ν (right) at 1.8 K with different applied dc fields for compound **24.**

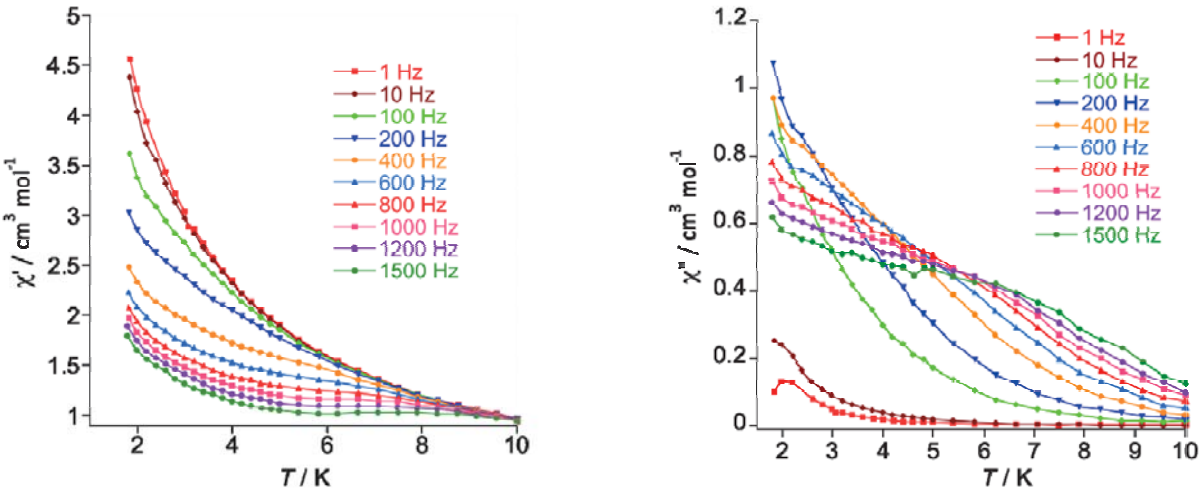

Figure 3.42 Plots of χ' vs. T (left) and χ" vs. T (right) with different frequencies at 1000 Oe dc field for compound **24.**

Due to the presence of magnetic anisotropy, the magnetization relaxation of this system has been probed under zero dc field using ac susceptibility measurements as a function of the temperature at different frequencies. Clearly this compound exhibits non-zero out-of-phase ac susceptibility with a weak intensity (Figure 3.42) indicating an absence of any appreciable barrier to relaxation of the magnetization, which could be due to strong quantum tunnelling resonance at zero dc field. The maximum of out-of-phase signal could not be observed above 1.8 K at a frequency of 1500 Hz. The out-of-phase ac susceptibilities are weakly frequency dependent, indicating that this compound exhibit slow magnetic relaxation, probably being a single-molecule magnet (SMM).

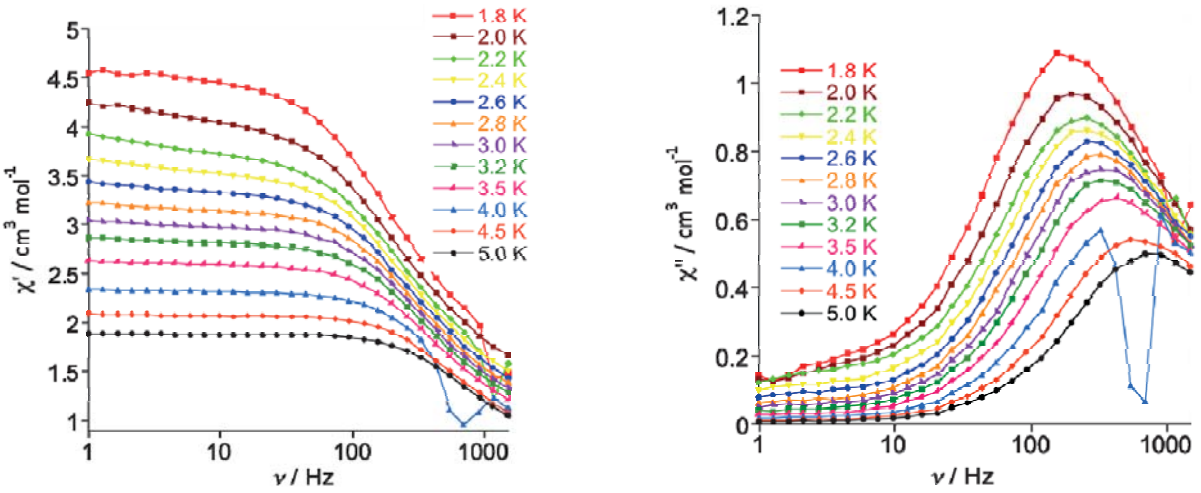

Figure 3.43 Plots of χ' vs. ν (left) and χ" vs. ν (right) with different temperatures at 1000 Oe dc field for compound **24.**

In order to further investigate the dynamic magnetic properties of this complex, ac susceptibility measurements in the presence of a weak dc field were performed. Indeed this compound do show field-induced slow relaxation of the magnetization. With the application of an external dc field, the

Dieses Werk ist copyrightgeschützt und darf in keiner Form vervielfältigt werden noch an Dritte weitergegeben werden.
Es gilt nur für den persönlichen Gebrauch.

intensity of the out-of-phase ac susceptibility is much enhanced (Figure 3.42). This type of behavior further suggests that this complex has a very fast tunneling process in the absence of static field. The tunnelling effect is most efficiently suppressed with a dc field of 1000 Oe (Figure 3.41). Under those fields, the ac response at different temperatures increases by an order of magnitude and shows classic SMM behaviour with strong frequency dependence (Figure 3.43).

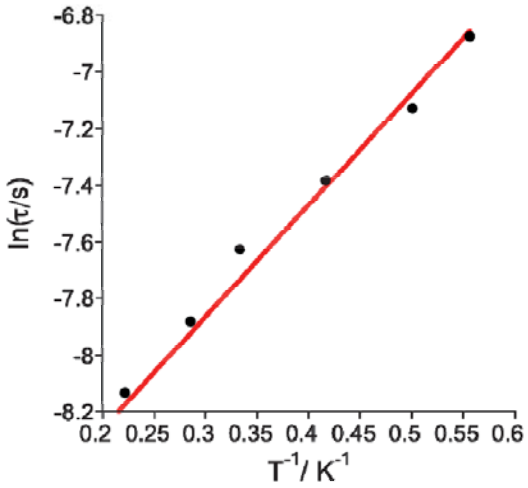

Figure 3.44 The relaxation time of compound **24** under a dc field of 1000 Oe. The solid lines represent the respective Arrhenius law with the parameters discussed in the text.

The data in the χ'' *vs* frequency plot (Figure 3.43) clearly shows one defined peak indicating the presence of one thermally-activated relaxation pathway located in this regime. To extract the characteristic parameters of this relaxation pathway, a plot of the relaxation time ((lnτ) against $^1/_T$ (Arrhenius plot) was constructed (Figure 3.44). The linear fitting resulted in a relaxation time of τ_0 = 1.1 10^{-4} s and a barrier of U_{eff} = 3.94 cm^{-1}, pertaining to the relaxation mechanism assigned to a thermally activated process.

The static dc magnetic susceptibility studies of **25** have been performed in the 1.8–300 K range under an applied magnetic field of 1000 Oe (Figure 3.45). The χ_MT value of 14.32 cm^3 K mol^{-1} at 300 K for **25** is close to the calculated value of 14.17 cm^3 K mol^{-1} for the ground state of the

Dieses Werk ist copyrightgeschützt und darf in keiner Form vervielfältigt werden noch an Dritte weitergegeben werden.
Es gilt nur für den persönlichen Gebrauch.

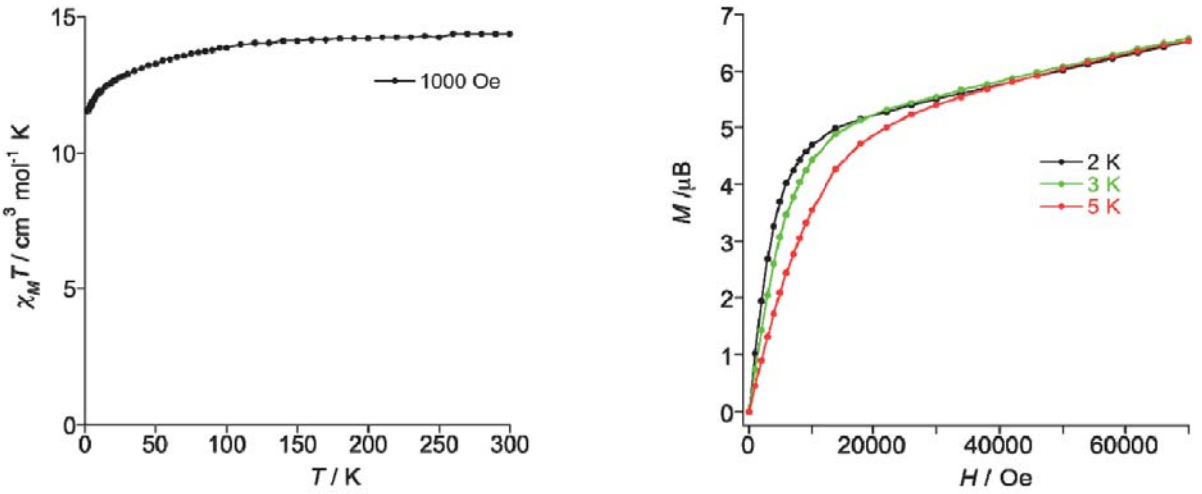

Figure 3.45 Plots of $\chi_M T$ vs. T (left) and M vs. H (right) for compound **25**.

Dy(III) ion ($4f^9$, J = 15/2, S = 5/2, L = 5, g = 4/3, $^6H_{15/2}$). On cooling, the χT product gradually decreases to achieve a value of 11.45 cm^3 K mol^{-1} at 1.8 K. Such behaviour is primarily owing to the depopulation of the Stark sublevels of the dysprosium ion, which occurs from the splitting of the $^6H_{15/2}$ ground term by the ligand field. The M versus H plot at 2-5 K (Figure 3.45) shows a quite fast increase in the magnetization at low field (until 1.5 T) and then a slow linear increase to achieve a value of 6.58 μ_B at the maximum applied field of 7 T. This value is lower than the expected saturation value for Dy(III) of ~10 μ_B and such behaviour is likely due to crystal-field effects leading to significant magnetic anisotropy.

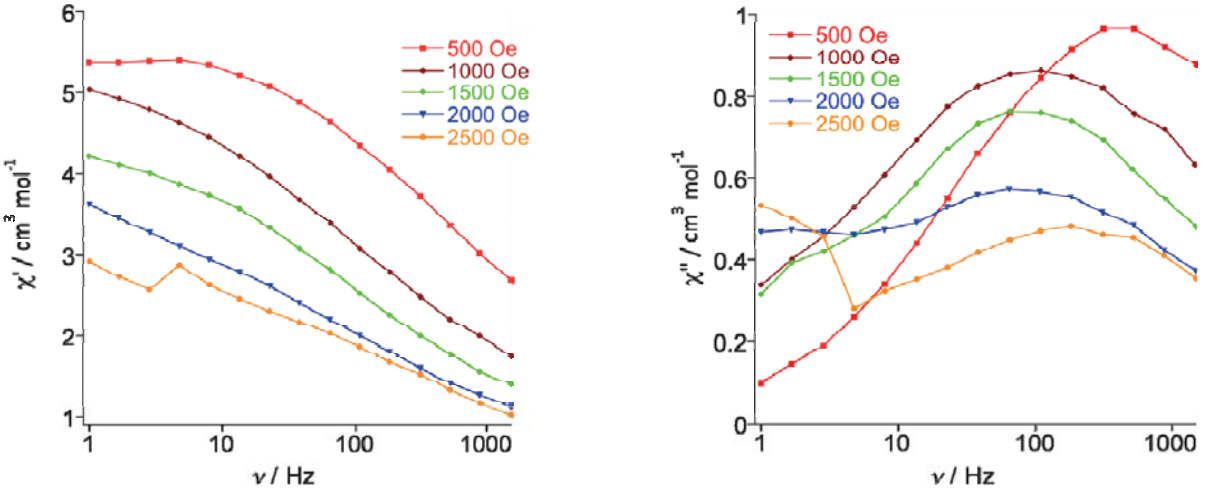

Figure 3.46 Plots of χ' vs. ν (left) and χ'' vs. ν (right) at 1.8 K with different applied dc fields for compound **25.**

Dieses Werk ist copyrightgeschützt und darf in keiner Form vervielfältigt werden noch an Dritte weitergegeben werden.
Es gilt nur für den persönlichen Gebrauch.

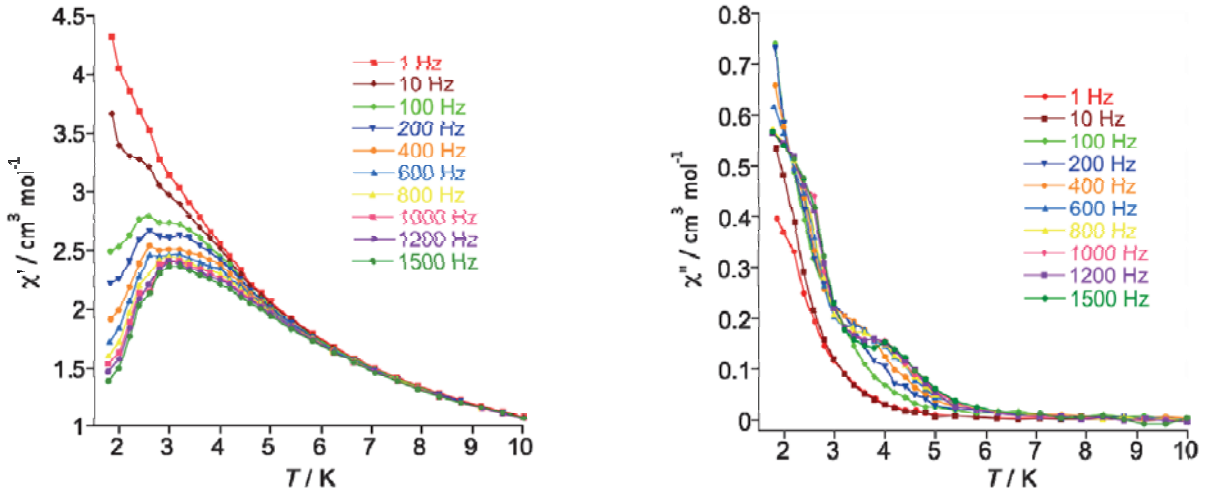

Figure 3.47 Plots of χ' vs. T (left) and χ'' vs. T (right) with different frequencies at 1500 Oe dc field for compound **25.**

Due to the presence of magnetic anisotropy, the magnetization relaxation of this system have been probed under zero dc field using ac susceptibility measurements as a function of the temperature at different frequencies. At zero dc field no maximum could not be observed in out-of-phase signal above 1.8 K at a frequency of 1500 Hz indicating an absence of any appreciable barrier to relaxation of the magnetization, which could be due to strong quantum tunnelling resonance at zero dc field.

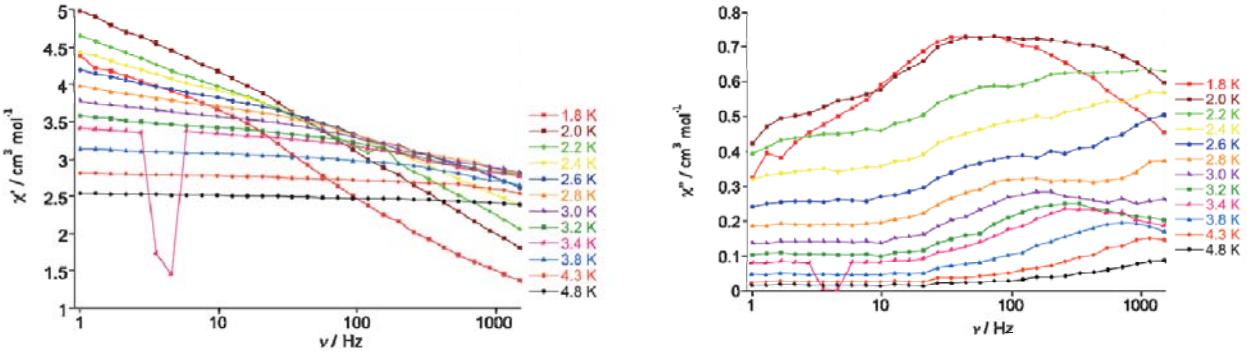

Figure 3.48 Plots of χ' vs. ν (left) and χ'' vs. ν (right) with different temperature at 1500 Oe dc field for compound **25.**

In order to further investigate the dynamic magnetic properties of the complexes, ac susceptibility measurements in the presence of a weak dc field were performed. Indeed both compounds do show field-induced slow relaxation of the magnetization. With the application of an external dc field, the intensity of the out-of-phase ac susceptibility is much enhanced (Figure 3.47). This type of behavior further suggests that these complexe has a very fast tunneling process in the absence of static field. The tunnelling effect is most efficiently suppressed with a dc field of 1500 Oe in both compounds (Figure 3.46). Under those fields, the ac response at different temperatures increases by an order of magnitude and shows classic SMM behaviour with strong frequency dependence (Figure 3.48).

Dieses Werk ist copyrightgeschützt und darf in keiner Form vervielfältigt werden noch an Dritte weitergegeben werden.
Es gilt nur für den persönlichen Gebrauch.

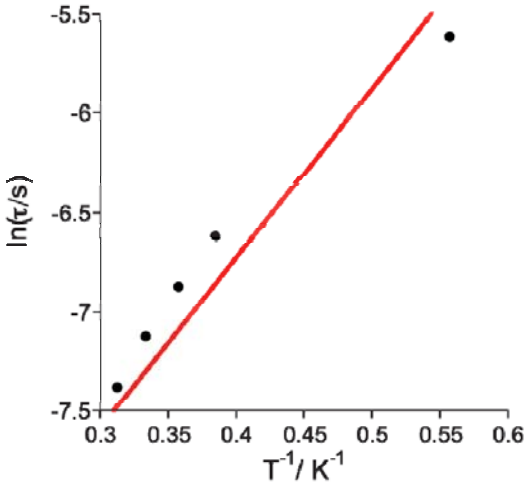

Figure 3.49 The relaxation time of compound **25** under a dc field of 1500 Oe. The solid line represent the respective Arrhenius law with the parameters discussed in the text.

The data in the χ'' *vs* frequency plot (Figure 3.48) clearly shows one defined peak indicating the presence of a thermally-activated relaxation pathway located in this regime. To extract the characteristic parameters of this relaxation pathway, a plot of the relaxation time ((lnτ) against $^{1}/_{T}$ (Arrhenius plot) was constructed (Figure 3.49). The linear fitting resulted in a relaxation time of τ_0 = 3.9 10^{-5} s and a barrier of U_{eff} = 8.53 cm^{-1}, pertaining to the relaxation mechanism assigned to a thermally activated process.

The dc magnetic data for complex **26** shows a temperature dependent value of χ_MT of 72.74 to 65.12 cm^3 K mol^{-1} over the temperature range 300−50 K (Figure 3.50). On lowering the temperature, χ_MT drops abruptly to a minimum value of 43.76 cm^3 K mol^{-1} at 2 K, indicating depopulation of excited Stark sublevels.

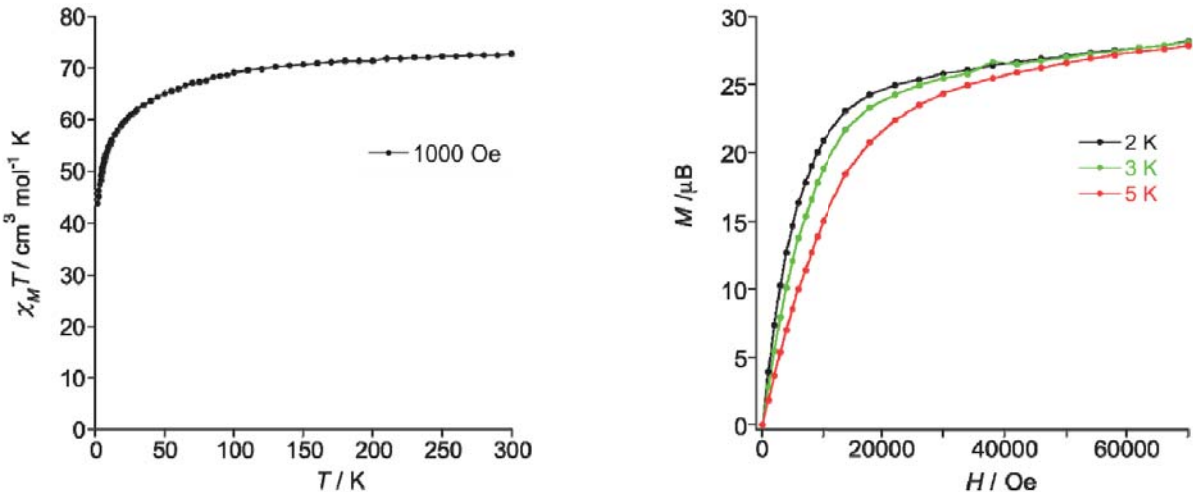

Figure 3.50 Plots of $\chi_M T$ vs. T (left) and M vs. H (right) for compound **26**.

Dieses Werk ist copyrightgeschützt und darf in keiner Form vervielfältigt werden noch an Dritte weitergegeben werden.
Es gilt nur für den persönlichen Gebrauch.

Magnetization data at low temperatures are shown in the Figure 3.50. The magnetization at all temperatures (2 - 5 K) reaches a maximum value of 28.38 μ_B at 70000 Oe, without showing true saturation. This is noticeably lower than the theoretical value for five Dy(III) ions (~ 50 μ_B), indicating a much smaller effective spin and also significant magnetic anisotropy in **26**.

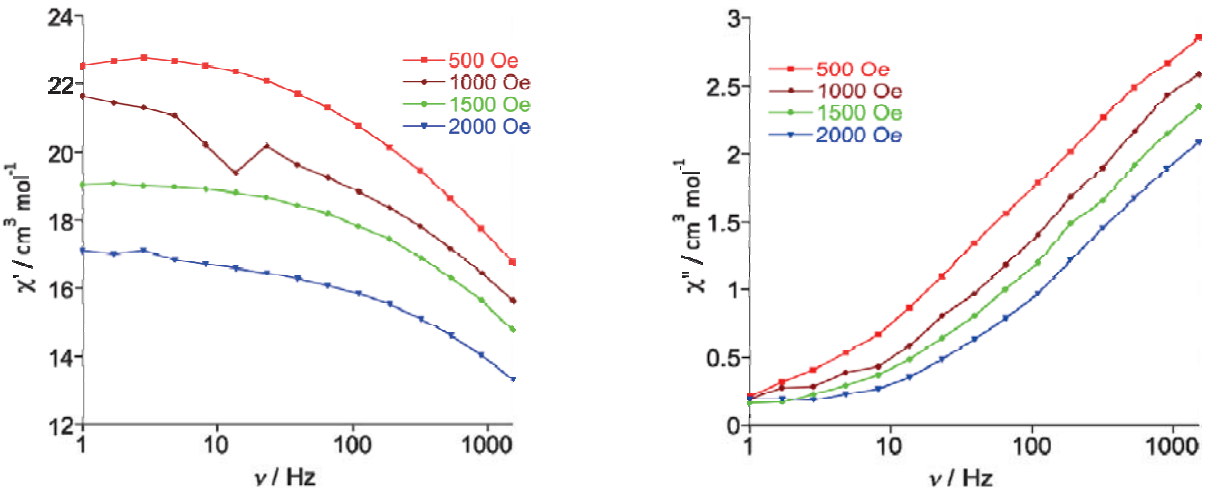

Figure 3.51 Plots of χ' vs. ν (left) and χ'' vs. ν (right) at 1.8 K with different applied dc fields for compound **26.**

Due to the presence of magnetic anisotropy, the magnetization relaxation of this system has been probed under zero dc field using ac susceptibility measurements as a function of the temperature at different frequencies. Clearly this compound exhibits non-zero out-of-phase ac susceptibility with a weak intensity (Figure 3.52) indicating an absence of any appreciable barrier to relaxation of the magnetization, which could be due to strong quantum tunnelling resonance at zero dc field. The maximum of out-of-phase signal could not be observed above 1.8 K at a frequency of 1500 Hz. The out-of-phase ac susceptibilities are weakly frequency dependent, indicating that this compound exhibit slow magnetic relaxation, probably being a single-molecule magnets (SMM).

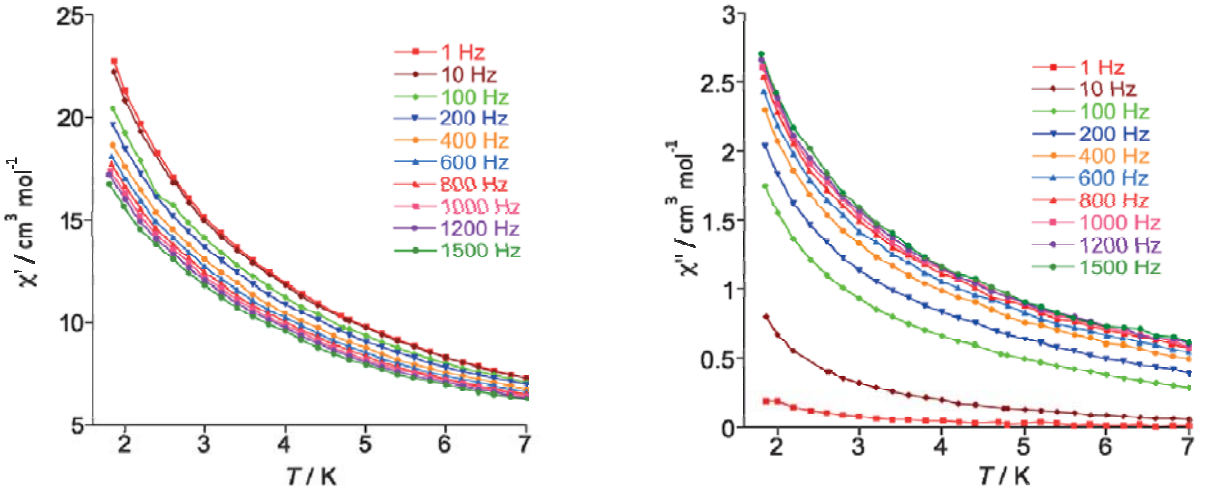

Dieses Werk ist copyrightgeschützt und darf in keiner Form vervielfältigt werden noch an Dritte weitergegeben werden.
Es gilt nur für den persönlichen Gebrauch.

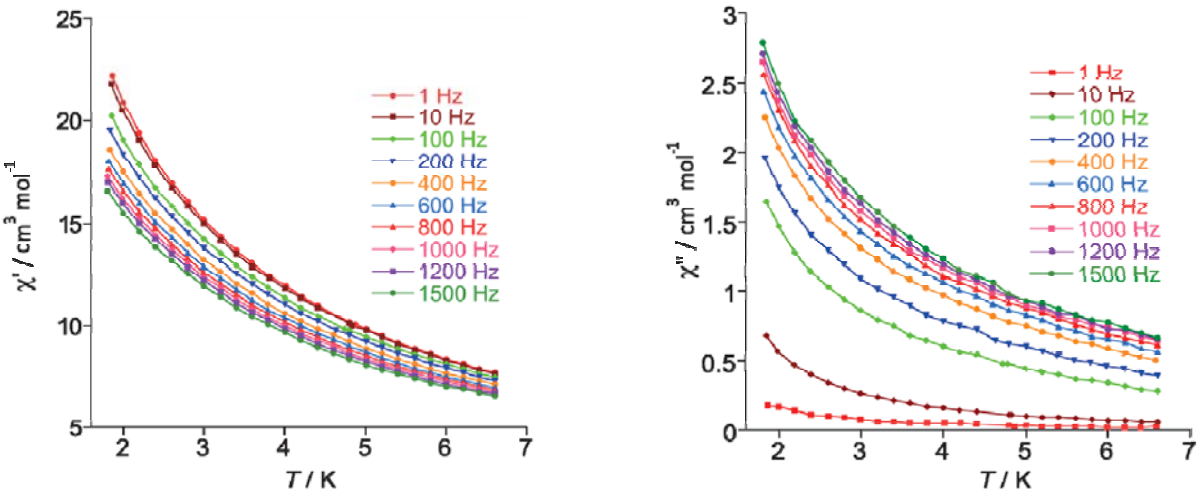

Figure 3.52 Plots of χ' vs. T(left) and χ'' vs. T (right) with different frequencies under zero DC field (above) and 700 Oe Dc field (below) for compound **26.**

In order to further investigate the dynamic magnetic properties of this complex, ac susceptibility measurements in the presence of a weak dc field were performed. Indeed this compound show field-induced slow relaxation of the magnetization. With the application of an external dc field, the intensity of the out-of-phase ac susceptibility is much enhanced (Figure 3.52). This type of behavior further suggests that this complex has a very fast tunnelling process in the absence of static field. The tunnelling effect is most efficiently suppressed with a dc field of 500 Oe (Figure 3.51). Under those fields, the ac response at different temperatures increases by an order of magnitude and shows classic SMM behaviour with strong frequency dependence (Figure 3.52).

The dc magnetic data for complex **27** shows a temperature dependent value of χ_MT of 87.24 to 79.54 cm^3 K mol^{-1} over the temperature range 300−50 K (Figure 3.53). On lowering the temperature, $\chi_M T$ drops abruptly to a minimum value of 57.87 cm^3 K mol^{-1} at 2 K, indicating depopulation of excited Stark sublevels.

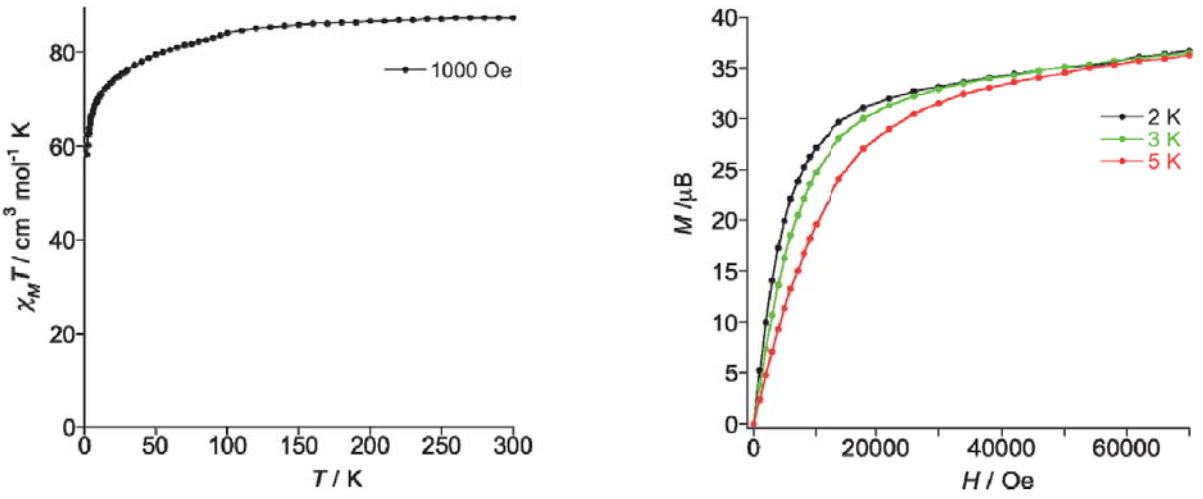

Figure 3.53 Plots of $\chi_M T$ vs. T (left) and M vs. H (right) for compound **27**.

Dieses Werk ist copyrightgeschützt und darf in keiner Form vervielfältigt werden noch an Dritte weitergegeben werden.
Es gilt nur für den persönlichen Gebrauch.

Magnetization data at low temperatures are shown in the Figure 3.53. The magnetization at all temperatures (2-5 K) reaches a maximum value of 36.67 μ_B at 70000 Oe, without showing true saturation. This is noticeably lower than the theoretical value for seven Tb(III) ions (~ 63 μ_B), indicating a much smaller effective spin and also significant magnetic anisotropy in **27**. Dynamic *ac* magnetic susceptibility measurements as a function of the temperature have been carried out, but this complex does not show any out-of-phase signal under zero or dc external field.

In summary, the mononuclear compounds {[Tb(Ph_2acac)$_4$]Et_3NH} (**24**) and {[Dy(Ph_2acac)$_4$]$_2$·2(Et_3NH)·3(CH_2Cl_2)} (**25**) were prepared with dibenzoylmethanide. Further, dibenzoylmethane was used with $(L^2)^{3-}$ to obtain the pentanuclear {[Dy_5(μ_3-OH)$_2$(L^2)$_3$ (Ph_2acac)$_4$(MeOH)$_4$]·4(MeOH)} (**26**) and heptanuclear compounds {[Tb_7(μ_3-OH)$_2$(μ_5-(NO_3)(μ_3-NO_3)(L^2)$_3$(Ph_2acac)$_5$(H_2N-Ph-O)(MeO)$_2$(MeOH)$_3$]·3(MeOH)·(MeCN)·15(H_2O)} (**27**). The solid state structures of compounds were established by single-crystal X-ray diffraction and the anionic structures of **24**, **25** were additionally characterized by ESI-MS. The solubility difference of compounds helps in separation and crystallization from their reaction mixtures. The mononuclear compounds **24**, **25** and pentanuclear compound **26** show the weak antiferromagnetic interactions with SMM behavior under an external weak dc field. Whereas, heptanuclear compound **27** shows weak antiferromagnetic interactions.

3.7 Binuclear and Trinuclear complexes of Dysprosium: Synthesis

3.7.1 Synthesis and Structures

The proligand (HL) was prepared *in situ* by condensation of 4-tert-butyl-2,6-diformylphenol and isoniazid in methanol. It was reacted with the metal salts [Dy(NO_3)$_3$·(H_2O)$_5$] to form the binuclear {[Dy_2L_3]·3(OH)·6(H_2O)·(C_6H_{12})} (**28**) and trinuclear complexes {[Dy_2L_3(OH)][Dy(NO_3)$_3$(H_2O)$_3$]·3(Py)·2(HO)·7(H_2O)·6(MeOH)·($CHCl_3$)} (**29**), {[Dy_2L_3(H_2O)][Dy(NO_3)(H_2O)$_7$]·5(NO_3)·3(MeOH)·7(H_2O)} (**30**). These compounds were isolated as single crystalline material from the reaction mixtures. The reaction conditions such as the amount of the base (triethylamine and pyridine), and the proligand to metal stoichiometric ratio, played a key role in the formation of binuclear and trinuclear complexes. When a proligand to metal ratio of 1:1 was used in the presence of triethylamine, complex **28** was isolated. When this ratio was altered to 1:2 in the presence of pyridine, complex **29** formed. In the next synthesis, the ratio proligand to metal was the same (1:2), but in the absence of a base, under similar reaction conditions complex **30** was isolated. Compounds **28-30** were characterized by standard analytical/spectroscopic techniques and the solid state structures were determined by single-crystal X-ray diffraction. The cationic structures of the compounds **28, 29** and **30** were supported by ESI-MS.

Dieses Werk ist copyrightgeschützt und darf in keiner Form vervielfältigt werden noch an Dritte weitergegeben werden.
Es gilt nur für den persönlichen Gebrauch.

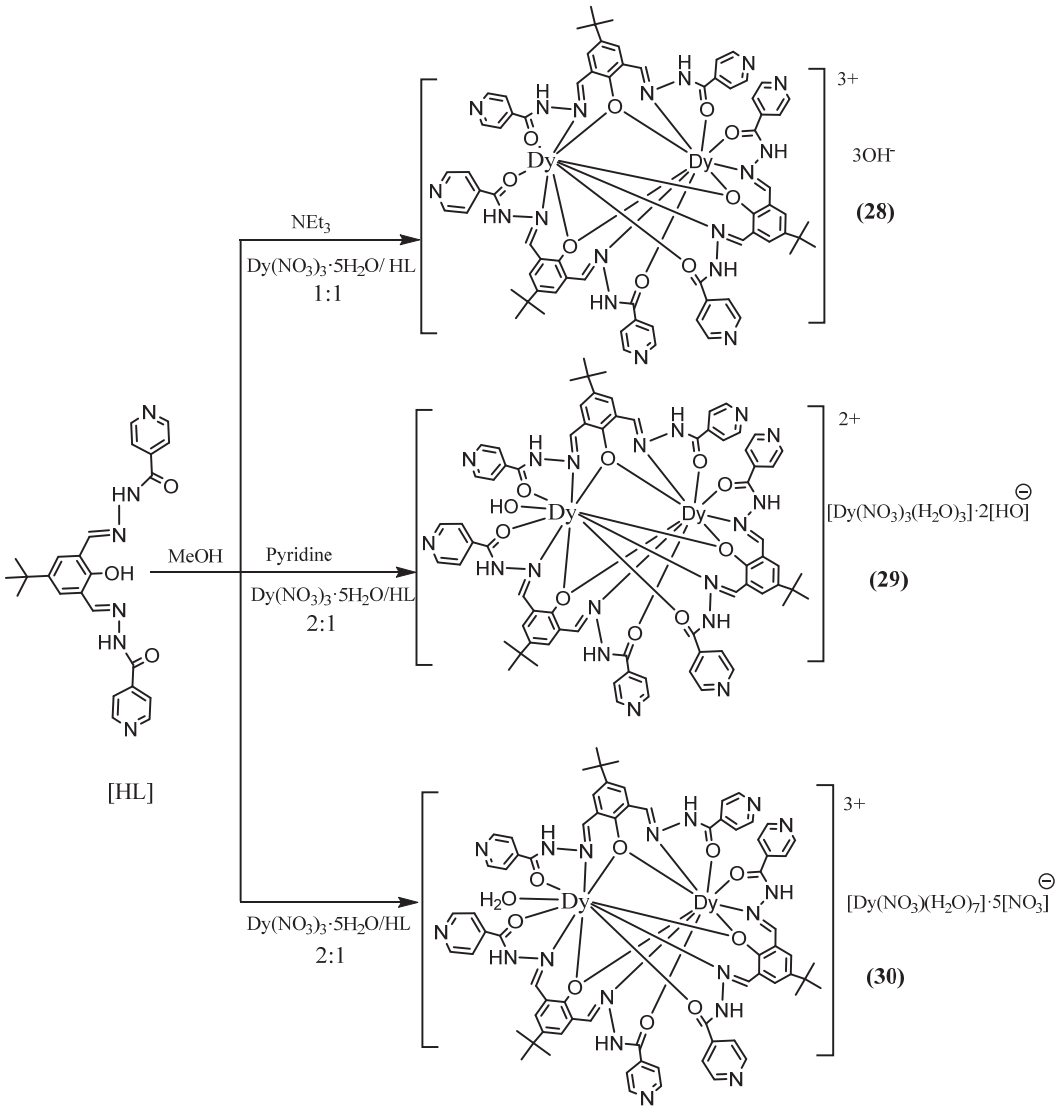

Scheme 3.7 Synthesis of compounds **28-30**

The binuclear complex **28** crystallized in the monoclinic space group *C*2/*c* and the asymmetric unit contains half of the molecule. Single-crystal X-ray analysis shows that the crystal structure of $\{[Dy_2L_3]\cdot 3(OH)\cdot 6(H_2O)\cdot(C_6H_{12})\}$ contains three monoanionic ligands and to balance the charge of the complex, three hydroxide ions are present in the crystal lattice. A perspective view of the complex **28** is shown in Figure 3.54. The structure of the cationic species $[Dy_2L_3]^{3+}$ was supported by ESI-MS. In compound **28** a crystallographic *C2* through the dysprosium atom is observed. Three ligands twist along a pseudo-threefold axis and are coordinated to two metal ions of Dy1 and Dy1'. The structure of the complex consist like a triple-stranded helicates such a helical structure is rarely reported $\{[Dy_2L_3](ClO_4)_3\cdot 6CH_3OH\}$(HL = 2,6-diformyl-4-methylphenol di(benzoylhydrazone) in literature.[155] Two Dy(III) ions have the same coordination environment and are nine coordinate. Dy1

Dieses Werk ist copyrightgeschützt und darf in keiner Form vervielfältigt werden noch an Dritte weitergegeben werden.
Es gilt nur für den persönlichen Gebrauch.

is bound to six oxygen atoms (O1, O1', O2, O3, O4, O5), three nitrogen atoms (N3, N4, N7) of the ligand and the coordination geometry is best described as distorted tricapped trigonal prismatic.

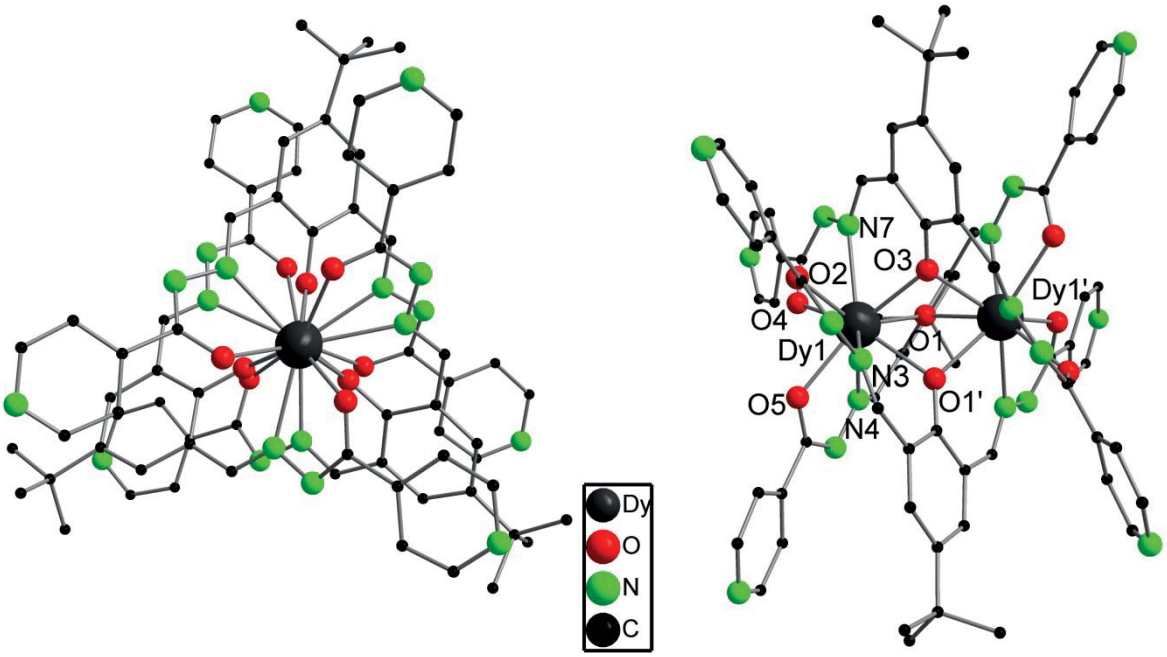

Figure 3.54 Solid state structure of **28** (left), and side view (right). Hydrogen atoms have been omitted for clarity.

The phenolate oxygen atoms of the ligand are in μ_2-bridging modes and the ketonic oxygen atoms are in η^1-modes. The Dy-O bond distances of the μ_2-bridged and η^1-chelating oxygen atoms are in the range of 2.304(3)-2.366(4) Å and 2.313(4)-2.426(4) Å, respectively. The Dy-N and Dy1-Dy1' distances are in the range of 2.572(4)-2.648(4) Å and 3.5181(9) Å respectively. These bond distances are close to the reported compound $\{[Dy_2L_3](ClO_4)_3 \cdot 6CH_3OH\}$.[155]

Complex **29** crystallized in the triclinic space group *P*1 along with $[Dy(NO_3)_3(H_2O)_3]$, which crystallized in the lattice. Single-crystal X-ray analysis shows that the crystal structure of $\{[Dy_2L_3(OH)][Dy(NO_3)_3(H_2O)_3] \cdot 3(Py) \cdot 2(HO) \cdot 7(H_2O) \cdot 6(MeOH) \cdot (CHCl_3)\}$ contains the three monoanionic ligands and the charge of the complex is balanced by two hydroxide ions present in the crystal lattice. A perspective view of complex **29** is shown in Figure 3.55. One methanol and one water molecule present in the lattice were highly disordered so they were SQUEEZE by using PLATON.[156, 157] The structure of the cationic species $[Dy_2L_3(OH)]^{2+}$ was also supported by ESI-MS. The triple-stranded helical structure resembles that of complex **28.** Dy1 is coordinated by six oxygen atoms and three nitrogen atoms of the ligands and its coordination geometry is best described as distorted tricapped trigonal prismatic. Dy2 is ten coordinate and it is bound to one hydroxide ion, six oxygen atoms and three nitrogen atoms of the ligands. Dy3 is present in the lattice, which is nine fold coordinated by three nitrates and three water molecules.

Dieses Werk ist copyrightgeschützt und darf in keiner Form vervielfältigt werden noch an Dritte weitergegeben werden.
Es gilt nur für den persönlichen Gebrauch.

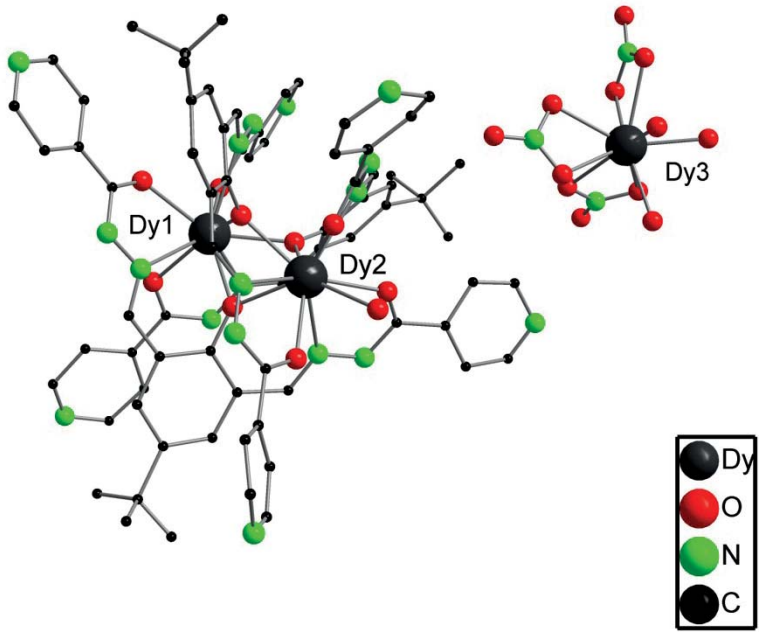

Figure 3.55 Solid state structure of **29**, All hydrogen atoms have been omitted for clarity.

The Dy-O of the μ_2-bridged and η^1-ketonic oxygen atoms oxygen atoms are in the range of 2.308(9)-2.319(9) Å and 2.370(10)-2.424(11) Å, respectively. The Dy-N and Dy1-Dy2 distances are in the range of 2.590(11)-2.670(12) Å and 3.5234(11) Å, respectively.

Complex **30** crystallized in triclinic with space group *P*-1 along with $[Dy(NO_3)(H_2O)_7]$ which crystallized in the crystal lattice, similarly to compound **29.** The binuclear cationic species $[Dy_2L_3]^{n+}$ in all compounds (**28**, **29** and **30**) looks similar to each other**.** The molecular structure of the cationic species ($[Dy_2L_3(H_2O)]^{3+}$) is supported by ESI-MS. A perspective view of complex **30** is shown in Figure 3.56. The triple-stranded helical structure resembles those in compounds **28** and **29**. In compound **29**, Dy3 is nine coordinated by three nitrates and three water molecules, whereas in compound **30**, Dy3 is nine coordinated by one nitrate and seven water molecules. The single-crystal X-ray analysis shows that the crystal structure of $\{[Dy_2L_3(H_2O)]\cdot[Dy(NO_3)(H_2O)_7]\cdot 5(NO_3)\cdot 3(MeOH)\cdot 7(H_2O)\}$ contains three monoanionic ligands and the charge of the complex is balanced by five nitrate molecules present in the crystal lattice. The structural parameters and coordination geometry of the Dy(III) ions are similar to complex **28** and **29**. Dy2 is nine fold coordinated by six oxygen atoms and three nitrogen atoms of the Schiff base ligands and the geometry is best described as distorted tricapped trigonal prismatic. Dy1 is ten fold coordinated by six oxygen atoms and three nitrogen atoms of the ligands and one water molecule.

Dieses Werk ist copyrightgeschützt und darf in keiner Form vervielfältigt werden noch an Dritte weitergegeben werden.
Es gilt nur für den persönlichen Gebrauch.

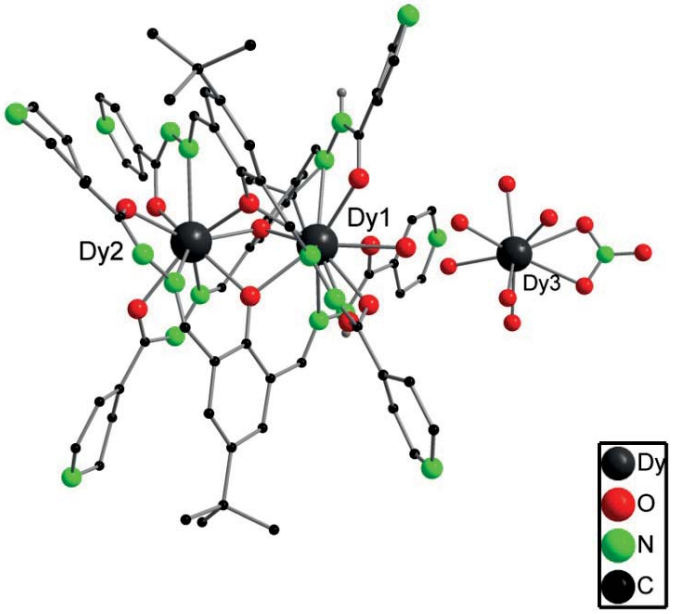

Figure 3.56 Solid state structure of **30,** All hydrogen atoms have been omitted for clarity.

The Dy-O distances between μ_2-bridged oxygen atoms are in the range of 2.330(5)-2.341(4) Å, which is close to compound **28** (2.304(3)-2.366(4) Å), and compound **29** (2.308(9)-2.319(9) Å). The Dy-O η^1-ketonic bond lengths are in the range of 2.323(9)-2.479(10) and it is comparable to the range observed in compound **28** (2.313(4)-2.426(4) Å) and compound **29 (**2.370(10)-2.424(11) Å). The Dy-N distances are in the range of 2.587(6)-2.648(6) Å, similar the range observed in compound **28** (2.572(4)-2.648(4) Å) and compound **29** (2.590(11)-2.670(12) Å). The distance between Dy1-Dy2 is 3.5099(9) Å, similar to compound **28** (3.5181(9) Å) and compound **29** (3.5234(11) Å).

In summary $\{[Dy_2L_3]\cdot(OH)_3\cdot 6(H_2O)\cdot(C_6H_{12})\}$ (**28**), $\{[Dy_2L_3(OH)]\cdot[Dy(NO_3)_3(H_2O)_3]\cdot 3(Py)\cdot 2(HO)\cdot 7(H_2O)\cdot 6(MeOH)\cdot(CHCl_3)\}$ (**29**), $\{[Dy_2L_3(H_2O)]\cdot[Dy(NO_3)(H_2O)_7]\cdot 5(NO_3)\cdot 3(MeOH)\cdot 7(H_2O)\}$ (**30**) were prepared by the use of the polydentane ligand. The molecular structures were established by single crystal X-ray diffraction and characterized by standard analytical/spectroscopic techniques. The molculare structure of cationic species of complex **28, 30** $[Dy_2L_3]^{3+}$ and complex **29** $[Dy_2L_3(OH)]^{2+}$ were additionally characterized by ESI-MS. A dinulcear unit $[Dy_2L_3]$ in all compounds forms a triple standerd helical structure. The bonding parametrs of dinuclear units in all compounds were found close to each other.

Dieses Werk ist copyrightgeschützt und darf in keiner Form vervielfältigt werden noch an Dritte weitergegeben werden.
Es gilt nur für den persönlichen Gebrauch.

3.8 Salen-Based 1-D Coordination Polymers of Manganese and lanthanides: Synthesis and Catalytic sulfoxidation

3.8.1 Synthesis and Structures

The reaction of salen ligand (H_4L) with [$MnCl_2 \cdot 4(H_2O)$] and [$Ln(NO_3)_3 \cdot x(H_2O)$] in the presence of DMF/ pyridine at elevated temperature leads to the formation of chiral 1D-cordination polymer (CP) $\{[Ln_2(MnLClNO_3)_2(dmf)_6(H_2O)_2] \cdot H_2O\}_n$ [Ln = Pr (**31**), Nd (**32**), Sm (**33**) and Gd (**34**) in single crystalline form. The solid state structures of **31-34** were established by single-crystal X-ray diffraction and characterized by standard analytical/spectroscopic techniques. Compound **34** was characterized by TGA to prove the stability of the polymer. Compounds **31-34** were insoluble in common solvents, thus, no NMR data could be acquired. The 1D-cordination polymers were investigated as heterogeneous catalyst for the sulfoxidation reaction and were tested for various alkyl and aryl sulfides. Iodosobenzene was used as an oxidizing agent for sulfoxidation. It was found that the catalysts were active for more than one reaction cycle without significant loss of activity.

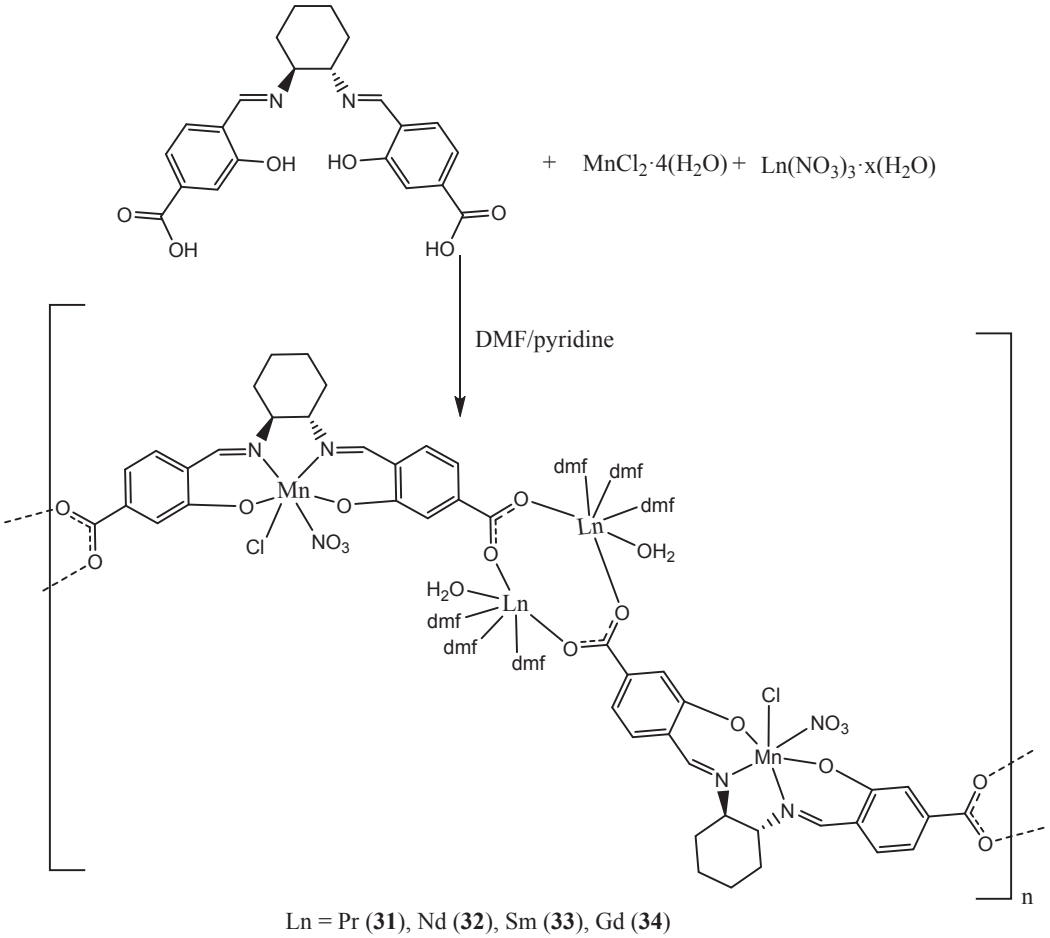

Scheme 3.8 Synthesis of compounds **31-34**.

Compounds **31–34** crystallized in the monoclinic chiral space group *C*2. All compounds are isostructural (as shown in scheme 3.8). Thus, only the representative structural parameters of

Dieses Werk ist copyrightgeschützt und darf in keiner Form vervielfältigt werden noch an Dritte weitergegeben werden.
Es gilt nur für den persönlichen Gebrauch.

complex **34** are discussed in detail. The molecular structure of compound **34** is shown in figure 3.57. The basic building blocks consist of $\{[Ln_2(MnLClNO_3)_2(dmf)_6(H_2O)_2]\cdot H_2O\}_n$. The asymmetric unit is formed by two Mn-salen units ($MnLClNO_3$), two rare earth ions (Ln1 and Ln2), six DMF and two water molecules.

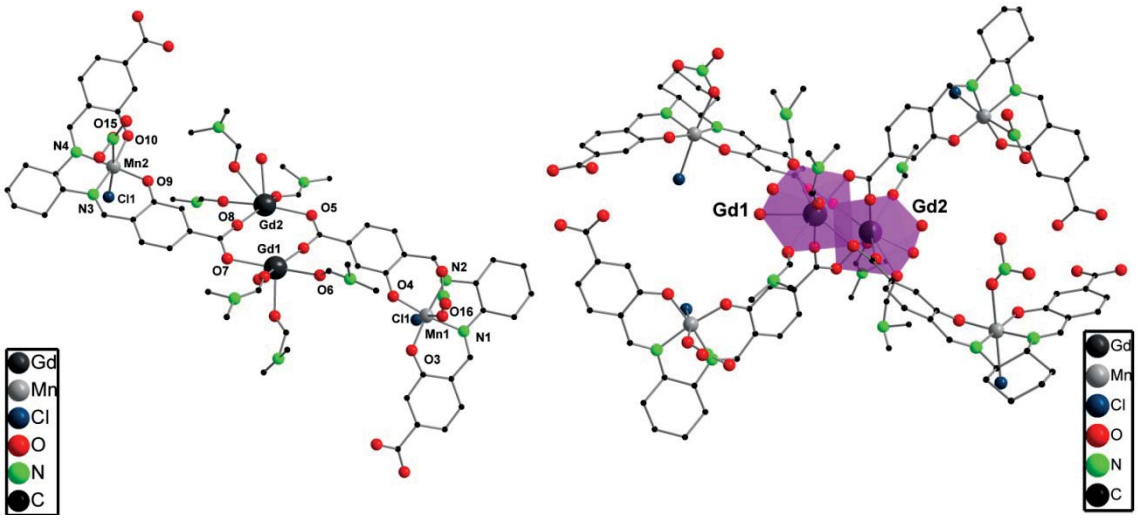

Figure 3.57 Solid state structure of **34** (left) and the SBU is highlighted (right). Hydrogen atoms have been omitted for clarity.

The manganese ions in the salen units ($MnLClNO_3$) are in the centre of a distorted octahedral coordination polyhedron, which is built by the ONNO atoms of the salen ligand, one chloride ion, and one nitrate molecule. The chloride ion and the nitrate ion occupy the apical positions. The ONNO atoms of the salen ligand form an equatorial plane around the Mn atom. Six-fold-coordinated Mn atoms within salen ligands have been reported earlier $\{[Ln_2(MnLCl)_2(NO_3)_2\text{-}(dmf)_5]$ (H_4L = N,N'-bis(4-carboxysalicylidene)ethylenediamine).[129] The Mn–salen units ($MnLClNO_3$) are similar to each other in the structural parameters and the environment near to Mn1 and Mn2 ions. The Mn1-Cl1 and Mn2-Cl2 bond distances are similar and it is 2.600 Å. The$Mn1O_{phenolate}$ bond distances are Mn1O3 1.880(8) Å and Mn1O4 1.884(8) Å, which are comparable to the $Mn2O_{phenolate}$ distances Mn2O9 1.892(8) Å and Mn2O10 1.904(8) Å. The Mn1N1 1.998(8) Å and Mn1N2 1.997(8) Å bond distances are also close to Mn2N3 1.997(9) Å and Mn2N4 1.980(8) Å. The $MnO_{nitrate}$ bond distances are Mn1O16 2.346(10) and Mn2O13 2.363(16).

In the solid-state structure, Mn-salen unit acts as a linker to form the 1D coordination polymers. Each carboxylate group of the Mn–salen unit connects two different lanthanide atoms. Thus, two lanthanide atoms (Ln1 and Ln2) are coordinated together by four Mn–salen units through four bridging carboxylate groups, six DMF and two water molecules, as it is expected due to large size of the lanthanide atoms. This results in a 1D coordination polymer. Two DMF and two water molecules

Dieses Werk ist copyrightgeschützt und darf in keiner Form vervielfältigt werden noch an Dritte weitergegeben werden.
Es gilt nur für den persönlichen Gebrauch.

coordinated to lanthanides are disordered. Thus, bonding parameters near to lanthanides are not discussed in details. The lanthanide atoms Ln1 and Ln2 form the secondary building units (SBUs) and each SBU is based on a $[(Ln)_2(\mu\text{-}O_2CR)_4(dmf)_6(H_2O)_2]$ building block. These SBUs can be considered as a distorted square paddle-wheel built from two rare earth ions which are bridged by four carboxylate groups. The basic structural arrangement of compound **34** looks analogous to our reported 1D-cordination polymers.[129]

The stability of compound **34** was proved by TGA measurements (Figure 3.58). For compound **34**, a weight loss is found at 70 °C. This weight loss is corresponding to one DMF and three water molecules (obs 5.88%, calc 6.8%). At 136 °C, another DMF was lost (obs 3.89%, calc 3.80%) and at 305 °C, remaining four DMF were lost (obs 16.43%, calc 15.19%).

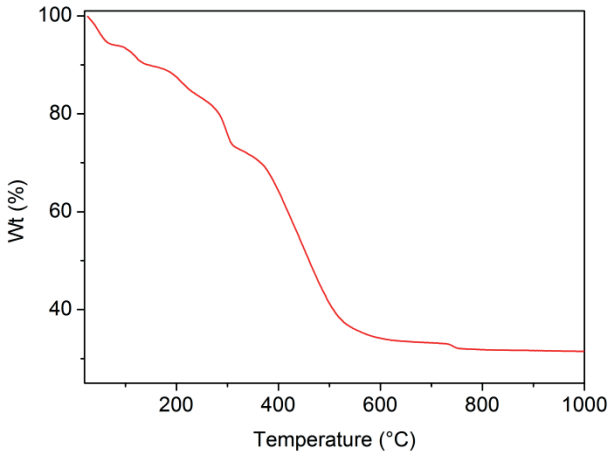

Figure 3.58 TGA curve of **34** in the temperature range of 20 to 1000 °C, under N_2 atmosphere.

The PXRD of compound **34** was measured by Dr. Andreas Eichhöfer. The experimental powder pattern of compound **34** shows a good agreement with the simulated pattern from single crystal, which proves the crystalline purity of the compound (Figure 3.59). The compounds before catalysis process were left at room temperate to get dried. Then its powder measurement was found to be similar except few structural rearrangement of 1D CP, which may be due to the removal of some DMF molecules from its lattice. The reused catalyst was found to be similar to the dry catalyst except small deviations which proves the stability of catalyst.

Dieses Werk ist copyrightgeschützt und darf in keiner Form vervielfältigt werden noch an Dritte weitergegeben werden.
Es gilt nur für den persönlichen Gebrauch.

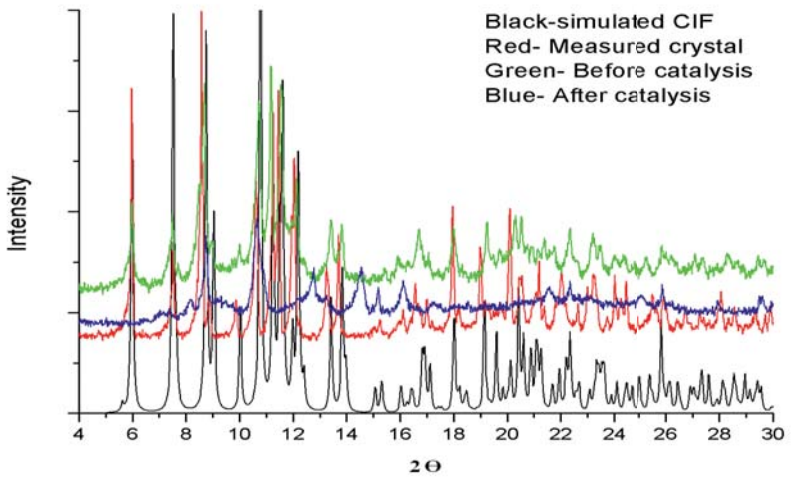

Figure 3.59 Powder X-ray diffractograms of compound **34.**

3.8.2 Catalysis

The characterization of compounds **31–34** shows the chiral Mn–salen based metalloligand in the 1D coordination polymers. Mn-based salen complexes are known to be highly active catalysts in epoxidation and sulfoxidation reactions.[129,131, 140] Polymers should be accessible for catalytic oxidative reactions. Previously, we reported the epoxidation of trans-stilbene with 1D coordination polymers and we found that Mn-Ln based catalyst was active for epoxidation. Molecular oxygen was used as oxidizing agent which does not give any side product.[129] Further extending this work, we synthesized the chiral-1D coordination polymers and then used for sulfoxidation reactions. Compounds **31–34** were shown to be catalytically active and used as solid catalyst materials in the sulfoxidation reactions of aryl and alky sulphides with iodosobenzene as an oxidizing agent. We explored the utilization of compound **31-34** as heterogeneous catalysis and the reaction resulted in the formation of aryl and alkyl sulfoxide as main product and sulfone as the side product.

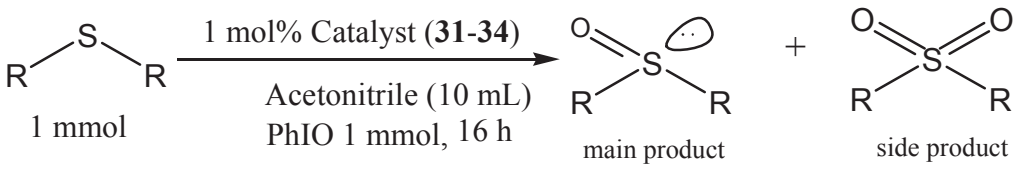

Scheme 3.8.1. Sulfoxidation of aryl and alkyl sulfides with PhIO catalyzed by compounds (**31-34**)

Dieses Werk ist copyrightgeschützt und darf in keiner Form vervielfältigt werden noch an Dritte weitergegeben werden.
Es gilt nur für den persönlichen Gebrauch.

Table 3.1 Catalytic oxidation of sulfides

Entry	Substrate	catalyst	Conversion (%)	Selectivity (%)	Enantiomeric excess ee(%)
1.	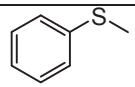	**34**	100	88	7
2.	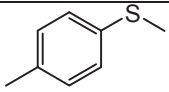	**34**	76	81	7
3.	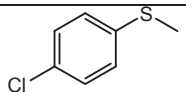	**34**	78	75	10
4.	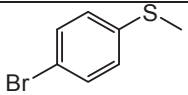	**34**	81	86	8
5.	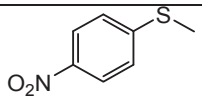	**34**	64	83	25
6.	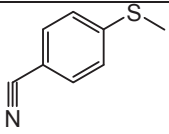	**34**	60	83	19
7.	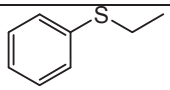	**34**	79	86	n.d
8.	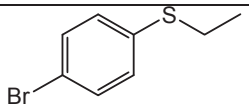	**34**	86	84	6
9.	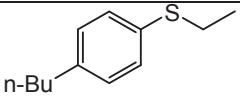	**34**	56	84	3
10.	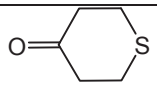	**34**	65	57	n.d
11.	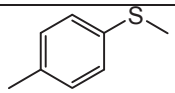	**31**	77	92	8
12.	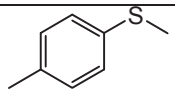	**32**	75	82	8
13.	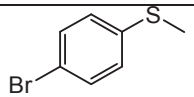	-	4	100	-

Reaction conditions: aryl and alkyl sulfides (1 mmol), PhIO (1 mmol), Acetonitrile (10 mL), catalyst (1 mol %) 16 h. The ee of the resulted sulfoxide was determined by HPLC with Chiralpak-A column and the conversion was determined by ^{1}H-NMR. * n.d – means sulfoxides is not measured for e.e.

Dieses Werk ist copyrightgeschützt und darf in keiner Form vervielfältigt werden noch an Dritte weitergegeben werden.
Es gilt nur für den persönlichen Gebrauch.

For the catalytic screening tests we used compound **34**. The reaction parameters shown in Scheme 3.8.1, were varied to optimize the conversion, selectivity, and enantiomeric excess (ee) for the methylp-tolylsulfide. We examined hydrogen peroxide and iodosobenzene as the oxidizing agent but the conversion was found higher in idosobenzene. The catalytic reactions were also examined for different solvents, such as acetone, hexane, dichloromethane and acetonitrile but the conversion was highest when acetonitrile was used as solvent. Further, we examined the different stoichiometric of an oxidizing agent but 1eq of idosobenzene was found useful to get the maximum conversion of substrates. The acetonitrile as solvent, iodosobenzene (1 eq.) as an oxidizing agent and 1 mol % of the catalyst at room temperature was found as optimized reaction conditions. Thus, all other compounds were tested under the optimized reaction conditions. Using 1 mol% of the catalyst was lead to 56-100% conversion, 57-92 % chemoselectivity and 3-25% ee.

The sulfoxidation of methylsulfide and methylp-tolylsulfide gave a conversion 100% and 76% respectively (Table 3.1, entry 1 and 2), while the 4-chlorophenyl methyl sulfide and 4-bromophenyl methyl sulphide lead to conversion of 78% and 81% respectively (Table 3.1, entry 3 and 4). When the phenyl ring was functionalized with the strong electron-withdrawing -NO_2 and -CN groups, the same reaction conditions lead to slightly lower conversion of 64% and 60% respectively (Table 3.1, entry 5 and 6). When the methyl group of aryl sulphide (PhSMe) is replaced by an ethyl group (PhSEt) the oxidation reaction still gave a conversion of 79%. The introduction of a Br atom in para position of PhSEt gave a conversion of 86 %, but when n-butyl group was introduced in para position (n-BuPhSEt), the conversion decreased to 56%. This is probably due to the slower mass-diffusion of the bulky substrate in the porous media (Table 3.1, entries 9).

We also examined the lanthanides compounds **31** and **32** for methylp-tolylsulfide substrate and a conversion of 75-77% was found. It was proved that the choice of the lanthanide has no impact in sulfoxidation reactions and they are only relevant as node in the chiral 1D CP. Thus, it is a good strategy to get the enantiomericlly pure sulfoxide as chiral part of the 1D CP active for the sulfoxidation. Unfortunately ee of sulfoxide was found to be quite low.

To prove the catalysis as heterogeneous and leaching of the catalyst did not occur, a comparative experiment was carried out. By using methylp-tolylsulfide as substrate performed the two catalytic ractions under similar reaction conditions; the catalyst was removed from the reaction mixtures after 4 h and 8 h. The conversion rates of 4h and 8h reactions were compared with the standard 16 h reaction (Table 3.1, entries 2). Firstly, a standard reaction was carried with duration of 4 h and a conversion of 21% with 100% chemoselectivity was obtained. Then, the solid catalyst was separated out and the fresh iodosobenzene was added to the reaction mixture and other reaction conditions

Dieses Werk ist copyrightgeschützt und darf in keiner Form vervielfältigt werden noch an Dritte weitergegeben werden.
Es gilt nur für den persönlichen Gebrauch.

were maintained as in Scheme 3.8.1. After an additional 14 h, the conversion was found to be 22% with 100% chemoselectivity. Secondly, a standard reaction was carried with the duration of 8 h and a conversion of 44% with 93% chemoselectivity was otained. Then, the solid catalyst was separated out and again fresh idosobenzene was added to the reaction mixture. After an additional 14 h, the conversions of methylp-tolylsulfide were found 50% with 90% chemoselectivity. These results undoubtedly proved that removal of the catalyst after filtration through a regular filter afford very little additional oxidation product. Thus, no active species is leached out from the reaction system as the conversion rates of catalysis after 4h, 8h and 16h in standard conditions were close to each other. A blind test was performed for 4-bromophenyl methyl sulfoxide, under the standard reaction conditions of Table 3.1. Without adding a catalyst, a yield of 4% sulfoxide was obtained after 16 h (entries 13, Table 3.1).

The stability of the catalyst upon recycling was investigated for phenylsulfide substrate. Catalyst was recycled after the first run just by ordinary filtration and reused under exactly the same reaction conditions. It was evaluated that the catalyst was not deactivated under the optimized reaction conditions after two runs. The reused catalyst was characterized by PXRD and it was found that before and after the catalysis powder diffraction pattern of compound **34** was found similar to initial catalyst as shown in Figure 3.45.

In summary, we synthesized and structurally characterized the manganese- and lanthanide-containing chiral 1D CPs (**31-34**) by using trivalent lanthanide nitrates and manganese chloride along with the salen ligand (H_4L). The new manganese–lanthanide compounds, $\{[Ln_2(MnLClNO_3)_2(dmf)_6(H_2O)_2]\cdot(H_2O)\}$ (Ln = Pr, Nd, Sm, Gd), are polymeric materials with defined structures. The polymers consist of manganese–salen-based metalloligands having carboxylate linkers connected to lanthanide atoms to form the chiral 1D CPs. Manganese–gadolinium compound **34** was used as a catalyst in the sulfoxidation reaction and iodosobenzene act as an oxidant, which resulted in the formation of the corresponding sulfoxides. A low catalyst concentration of 1 mol%, in acetonitrile emerged as optimized parameters. In the presence of compound **34**, a maximum conversion of 100% sulfoxide with 88% selectivity was obtained after 16 hours. Under the optimized conditions, the four compounds (**31–34**) showed remarkable activity. A simple filtration test confirmed that the reaction is mainly catalyzed through a heterogeneous pathway, although a minor contribution of homogeneous pathway could not be completely ignored. Compound **34** could be reused without significant loss of activity.

Dieses Werk ist copyrightgeschützt und darf in keiner Form vervielfältigt werden noch an Dritte weitergegeben werden.
Es gilt nur für den persönlichen Gebrauch.

4 Experimental sections

4.1 General considerations:

IR spectra were obtained on a Bruker FTIR Tensor 37 via the Attenuated Total Reflection method (ATR). Elemental analyses were carried out with an Elementar vario EL or Vario Micro Cube. Electrospray ionization mass spectrometry (ESI-MS) was performed in positive and negative ionization mode using an *IonSpec* FT-ICR (7T). NMR spectra were recorded on a Bruker Avance II 300 MHz NMR spectrometer. Chemical shifts are referenced to internal solvent resonances and were reported relative to tetramethylsilane. The enantiomeric ratios of sulfoxides were recorded using high performance liquid chromatography (HPLC) Agilent Technologies 1200 series with a CHIRALPAK-IA column. TGA measurements were made on a Netzsch STA 429 instrument. Aldehydes, ketones, amines, sulphides and solvents were purchased from commercial sources and used without further purification. Schiff bases were synthesized by known and unknown method in the laboratory.

4.2 Photoluminescence (PL) Measurements

Photoluminescence (PL) measurements were performed on a Horiba JobinYvon Fluorolog-322 spectrometer equipped with a closed-cycle optical cryostat (Leybold) operating at ~20-300 K. Hamamatsu R9910 and R5509 photomultipliers (PMT) were used as detectors in the emission spectral range of ~300-850 nm and ~600-1400 nm, respectively. Solid samples (crystalline powders) were dispersed in a thin layer of polyfluoroester oil (ABCR GmbH) between two 1 mm quartz plates. These were mounted on the cold finger of the cryostat. The emission spectra were corrected for the wavelength-dependent response of the spectrometer and detector (in relative photon flux units).

For PL quantum yield (PLQY) measurements (at ambient temperature of 295 K), a 10 cm integrating sphere made of optical PTFE with low auto-luminescence (Berghof GmbH) was installed into the sample chamber of the spectrometer. Samples were inserted into the sphere in 1 mm glass tubes and excited at 420 nm. The emission spectra, relative absorption at the excitation wavelength and, correspondingly, PLQY, were referenced to those of Coumarin 307 laser dye dissolved in methanol, according to a previously described procedure.[158] The PLQY of Coumarin 307 was taken as 0.95.[158] The accuracy of the determination of PLQY was estimated to be ±10%.

4.3 Magnetic Measurements.

The magnetic measurements were carried out using a Quantum Design SQUID magnetometer MPMS. This magnetometer works between 1.8 and 400 K for dc applied fields ranging from −70 to +70 kOe. Measurements were performed on the polycrystalline samples dispersed in Apiezon grease.

Dieses Werk ist copyrightgeschützt und darf in keiner Form vervielfältigt werden noch an Dritte weitergegeben werden.
Es gilt nur für den persönlichen Gebrauch.

4.4 Synthesis of Compounds

4.4.1 Synthesis of {[Ln(HL)$_4$][ETAH]} (1,2).

$Ln(NO_3)_3 \cdot x(H_2O)$ (Ln = Y, Dy) (0.1mmol) was treated with the Schiff-base proligand (H_2L), which was formed *in situ* by condensation of excess of ethanolamine (ETA) (1.5 mmol) and 3-formylsalicylic acid (0.4 mmol) in 10 mL of methanol and the presence of pyridine (0.6 mmol). The slight excess of ethanolamine is essential for the formation of complex. The resulting yellow solution was stirred for 20 min at room temperature and subsequently filtered. The filtrate was left undisturbed to allow slow evaporation of the solvent. Yellow single crystals suitable for X-ray diffraction analysis formed within one week.

{[Y(HL)$_4$][ETAH]·(H$_2$O)} (1).

Yield: 30 mg, (30% based on single crystals). Anal. Calcd. for $C_{42}H_{50}YN_5O_{18}$: C, 50.36; H, 5.03; N, 6.99. Found: C, 49.53; H, 5.01; N, 6.95. ESI-MS: 921.17 $[Y(HL)_4]^-$. IR(ATR): ν 3088(w), 1652(m), 1603(m), 1540(s), 1482(w), 1455(w), 1380(m), 1306(w), 1213(m), 1149(w), 1070(w), 1050(s), 1023(w), 953(w), 920(w), 874(s), 835(w), 791(w), 769(m), 696(w), 646(m), 622(w), 577(w), 538(w), 510(w) cm^{-1}.

{[Dy(HL)$_4$] [ETAH]·(3MeOH)·(H$_2$O)} (2).

Yield: 40 mg, (34% based on single crystals). Anal. Calcd. for $C_{45}H_{60}DyN_5O_{20}$ (corresponds to **2** - H_2O): C, 46.86; H, 5.24; N, 6.07. Found: C, 45.60; H, 4.74; N, 6.47. ESI-MS: 995.0 $[Dy(HL)_4]^-$. IR(ATR): ν 3069(w), 2947(w), 2849(w), 1652(m), 1604(m), 1539(s), 1480(w), 1449(w), 1377(m), 1304(w), 1272(w), 1235(w), 1212(m), 1149(w), 1070(w), 1050(s), 1023(w), 953(w), 920(w), 874(s), 835(w), 791(w), 770(m), 696(w), 646(m), 622(w), 577(w), 538(w), 510(w) cm^{-1}.

4.4.2 Synthesis of {[Y$_4$(HL)$_2$(L)$_4$(μ$_3$-OH)$_2$]·4(MeOH)·4(H$_2$O)} (3).

$[Y(NO_3).6(H_2O)]$ (0.19 mmol) was treated with the Schiff-base proligand (H_2L), which was formed *in situ* by condensation of ethanolamine (0.4 mmol) and 3-formylsalicylic acid (0.4 mmol) in 10 mL of methanol. The resulting yellow solution was stirred for 3 hours at room temperature and then Et_3N (0.1 mmol) was added and the solution was filtered. The filtrate was left undisturbed to allow slow evaporation of the solvent. Yellow single crystals of $\{[Y_4(HL)_2(L)_4(\mu_3\text{-}OH)_2]\cdot 4(MeOH)\cdot 4(H_2O)\}$ (**3**) suitable for X-ray diffraction analysis formed after one week. Yield: 20 mg, (6% based on single crystals). Anal. Calcd. for $C_{64}H_{82}N_6O_{34}Y_4$: C, 41.89; H, 4.50; N, 4.58. Found: C, 40.02 H, 4.10; N, 5.45. IR (ATR): ν 3062(br), 1653(w), 1641(m), 1606(s), 1555(s), 1506(w), 1476(w), 1457(m),

Dieses Werk ist copyrightgeschützt und darf in keiner Form vervielfältigt werden noch an Dritte weitergegeben werden.
Es gilt nur für den persönlichen Gebrauch.

1432(m), 1362(s), 1304(w), 1274(w), 1217(w), 1150(m), 1112 (w), 1077(w) 1048(m), 967(w), 915(w), 872(m), 830(w), 803(w), 755(m),660(w), 645(s), 629(w), 572(w), 536(w) cm^{-1}.

4.4.3 Synthesis of {[$Dy_4(HL)_2(L)_4(\mu_3\text{-}OH)_2$]·5(MeOH)·7($H_2O$)} (4).

$Dy(NO_3)_3·5(H_2O)$ (0.1 mmol) stirred with the Schiff-base proligand (H_2L) formed *in situ* by condensation of ethanolamine (0.3 mmol) and 3-formylsalicylic acid (0.3 mmol) in 10 mL of methanol. The resulting yellow reaction solution was stirred for 3 hours at room temperature and then filtered. The filtrate was left undisturbed to allow slow evaporation of the solvent. After two days, when the reaction volume was around 2 mL, the $Dy(NO_3)_3·5(H_2O)$ (0.05 mmol) and the Et_3N (0.1 mmol) was added to the reaction solution and subsequently closed by parafilm. Yellow single crystals of {[$Dy_4(HL)_2(L)_4(\mu_3\text{-}OH)_2$]·5(MeOH)·7($H_2O$)} (**4**) suitable for X-ray diffraction analysis formed after two days. Yield: 29 mg, (9% based on single crystals). Anal. Calcd. for $C_{65}H_{78}Dy_4N_6O_{31}$ (corresponds to **4** - 7(H_2O)): C, 37.37; H, 3.76; N, 4.02. Found: C, 37.82; H, 3.98; N, 4.45. IR (ATR): ν 3060(w), 2921(Br), 2852(w), 1641(m), 1601(m), 1551(m), 1478(w), 1456(w), 1431(w), 1363(s), 1305(w), 1272(w), 1217(m), 1150(w), 1077(w), 1048(m), 967(w), 872(m), 830(w), 757(w), 645(m), 627(w), 573(w), 553(w) cm^{-1}.

4.4.4 Synthesis of {[$Dy_4(HL)_8(L)_2$]·4(MeOH)·2(H_2O)} (5).

The Schiff-base proligand (H_2L) was formed *in situ* by condensation of ethanolamine (0.4 mmol) and 3-formylsalicylic acid (0.4 mmol) in 10 mL of methanol. The $Dy(NO_3)_3·5(H_2O)$ (0.13 mmol) and Et_3N (0.05 mmol) were added and the reaction mixture was heated for 2 hours at 80 ^oC. Then, the resulting yellow color solution was filtered. The filtrate was left undisturbed to allow slow evaporation of the solvent. Yellow single crystals of {[$Dy_4(HL)_8(L)_2$]·4(MeOH)·2(H_2O)} (**5**) suitable for X-ray diffraction analysis formed within one week. Yield: 32 mg, (8% based on single crystals). Anal. Calcd. for $C_{104}H_{122}Dy_4N_{10}O_{48}$ (corresponds to **5** +2(H_2O)): C, 42.63 H, 4.20; N, 4.78. Found: C, 41.07; H, 3.99; N, 4.93. IR (ATR): ν 3326(Br), 1646(m), 1602(m), 1543(m), 1481(w), 1456(w), 1430(w), 1373(s), 1305(w), 1269(w), 1232(w), 1212(m), 1151(w), 1080(w), 1049(m), 970(w), 912(w), 872(m), 829(w), 764(m), 706(w), 645(w), 623(w), 573(w), 553(w), 509(w) cm^{-1}.

4.4.5 Synthesis of {[$Dy(HL^1)_2(H_2O)_3$]·(NO_3)} (6).

H_2L^1 (0.2 mmol), $Dy(NO_3)_3·5(H_2O)$ (0.1 mmol) and pyridine (0.4 mmol) were stirred for 30 min in 10 mL methanol, resulting give a light yellow color solution. The solution was filtered and left undisturbed to allow slow evaporation of the solvent. Yellow single crystals of **6** suitable for X-ray diffraction analysis formed after one week. Yield: 40 mg, (47% based on single crystals). Anal. Calcd. for $C_{28}H_{26}Dy_1N_7O_{14}$: C, 39.70; H, 3.09; N, 11.58. Found: C, 39.75; H, 3.18; N, 12.40. ESI-

Dieses Werk ist copyrightgeschützt und darf in keiner Form vervielfältigt werden noch an Dritte weitergegeben werden.
Es gilt nur für den persönlichen Gebrauch.

MS: $[Dy(HL)_2]^+$ 732.10. IR(ATR)[cm^{-1}]: 3439(w), 3053(w), 2855(w), 1631(w), 1613(m), 1565(s), 1550(w), 1486(w), 1467(m), 1414(w), 1387(w), 1308(s), 1241(m), 1151(w), 1069(m), 1021(w), 1004(w), 984(w), 903(w), 849(m), 824(w), 766(s), 754(w), 680(s), 609(w), 581(w), 516(m), 467(w), 449(w), 412(w) cm^{-1}.

4.4.6 Synthesis of [NiLnL(acac)2] (7-9).

The Schiff base (H_3L) was synthesized *in situ* by condensation of benzaldehyde (0.3 mmol) and tris(2-aminoethyl)amine (1 mmol) in 10 mL methanol. The solution was refluxed for 1 hour at 80 ^oC and then allowed to cool down to room temperature. $Ni(NO_3)_2 \cdot 6(H_2O)$ (0.1 mmol) and NEt_3 (0.1 mmol) were added to the reaction solution and it was stirred for 5 min giving a orange red color. In another vial $Ln(NO_3)_3 \cdot x(H_2O)$ (0.1 mmol) and acetylacetone (0.3 mmol) were dissolved in 5 mL acetonitrile and poured into the mother solution. The ensuing green solution was observed at room temperature and then filtered. The filtrate was left undisturbed to allow slow evaporation of the solvent. Green single crystals of $[NiLn(L)(acac)_2]$ suitable for X-ray diffraction analysis formed after one week.

$[NiGdL(acac)_2]$ (7).

Yield: 16 mg, (18% based on single crystals). Anal. Calcd. for $C_{37}H_{41}Gd_1Ni_1N_4O_7$: C, 51.10; H, 4.75; N, 6.44. Found: C, 50.09; H, 4.971; N, 6.58. IR (ATR): ν 2978(w), 2924(w), 2866(m), 2822(w), 1628(s), 1595(s), 1549(m), 1513(s), 1473(m), 1446(m), 1426(w), 1394(s), 1340(m), 1329(w), 1298(s), 1258(m), 1221(m),1192(m), 1176(w), 1151(m), 1124(m), 1075(m), 1050(m), 1033(w), 1016(s), 993(w), 970(w), 938(w), 917(s), 890(m), 852(m), 796(m), 781(w), 769(w), 759(s), 746(w), 647(m), 588(s), 553(m), 525(m) cm^{-1}.

$[NiTbL(acac)_2]$ (8).

Yield: 12 mg, (13% based on single crystals). Anal. Calcd. for $C_{37}H_{41}Tb_1Ni_1N_4O_7$: C, 51.00; H, 4.74; N, 6.43. Found: C, 49.82; H, 4.97; N, 6.89. IR (ATR): ν 2978(w), 2924(w), 2866(w), 2822(w), 1628(s), 1595(m), 1549(m), 1513(s), 1473(m), 1446(w), 1425(w), 1392(s), 1339(w), 1297(s), 1259(w), 1221(w),1192(m), 1176(w), 1151(W), 1123(w), 1074(w), 1050(w), 1033(s), 1016(w), 969(w), 939(w), 917(s), 890(m), 851(m), 796(m), 780(w), 769(w), 758(s), 746(w), 647(m), 588(s), 554(m), 525(m) cm^{-1}.

$\{[NiDyL(acac)_2]_2 \cdot 7(MeOH)\}$ (9).

Yield: 14 mg, (14% based on single crystals). Anal. Calcd. for $C_{74}H_{82}Dy_2N_8Ni_2O_{14}$ (corresponds to **9** - 7MeOH) : C, 50.79; H, 4.72; N, 6.40. Found: C, 50.55; H, 4.80; N, 6.51. IR (ATR): ν 2977(w),

Dieses Werk ist copyrightgeschützt und darf in keiner Form vervielfältigt werden noch an Dritte weitergegeben werden.
Es gilt nur für den persönlichen Gebrauch.

2925(w), 2866(w), 2822(w), 1628(s), 1595(m), 1549(w), 1514(s), 1473(s), 1447(w), 1425(w), 1395(s), 1340(w),1329(w), 1299(s), 1260(w), 1222(w),1201(w), 1192(w), 1177(W), 1124(w), 1074(w), 1050(m), 1033(w), 1017(m), 994(w), 970(w), 939(w), 917(m), 890(w), 855(m), 796(w), 780(w), 770(w), 759(s), 746(w), 667(w), 647(w), 589(s), 554(w), 526(m) cm^{-1}.

4.4.7 Synthesis of {[NiDyL(Ph$_2$acac)$_2$]$_2$·4(CH$_2$Cl$_2$)·(MeOH)} (10).

The Schiff base proligand (H_3L) was synthesized *in situ* by condensation of benzaldehyde (0.3 mmol) and tris(2-aminoethyl)amine (1 mmol) in 10 mL methanol. The solution was refluxed for 1 hour at 80 ^oC and then cooled down to room temperature. $Ni(NO_3)_2·6(H_2O)$ (0.1 mmol) and NEt_3 (0.1 mmol) were added and the reaction solution was stirred for 5 min giving a orange red color. In another vial $Dy(NO_3)_3·5(H_2O)$ (0.1 mmol) and dibenzoyl methane (0.3 mmol) was dissolved in 5 ml dichlromethane. Slow diffusion of both the solutions gave green single crystals of {[NiDyL(Phacac)$_2$]$_2$·4(dcm)·(MeOH)} suitable for X-ray diffraction analysis; and they were formed within one week. Yield: 40 mg, (30% based on single crystals). Anal. Calcd. for $C_{115}H_{100}Dy_2N_8Ni_2O_{15}$ (corresponds to **10 –** 4 dcm): C, 60.67; H, 4.43; N, 4.92. Found: C, 60.67; H, 4.41; N, 4.97. IR (ATR): ν 3027(w), 2958(w), 2856(w), 2834(w), 1627(s), 1596(w), 1544(w), 1520(s), 1475(s), 1453(m), 1404(s), 1344(m), 1298(s), 1222(m), 1194(w), 1179(W), 1152(w), 1125(w), 1074(w), 1050(m), 1033(m), 1024(w), 1000(w), 985(w), 967(w), 941(w), 925(m), 891(m), 858(m), 810(w), 785(w), 753(s), 719(s), 684(m), 646(w), 617(w), 608(m), 589(m), 554(w), 524(w) cm^{-1}.

4.4.8 Synthesis of [Ni$_2$Ln(L1)$_2$] (11- 13).

The Schiff base proligand (H_3L^1) was synthesized *in situ* by condensation of 3-methoxysalicylaldehyde (0.6 mmol) and tris(2-aminoethyl)amine (0.2 mmol) in 10 mL methanol. The solution was refluxed for 1 hour at 80 ^oC and then cooled down to room temperature. $Ni(NO_3)_2·6(H_2O)$ (0.2 mmol), $Ln(NO_3)_3·x(H_2O)$ (0.1 mmol) and NEt_3 (4 mmol) were subsequently added and the reaction solution was refluxed for 2 hours. The resulting green solution was then filtered and followed by addition of 5 mL acetonitrile. The solution was left undisturbed to allow slow evaporation of the solvent. Green single crystals of $[Ni_2Ln_1L_2]$ suitable for X-ray diffraction analysis formed after one week.

{[Ni$_2$Gd(L^1)$_2$](NO$_3$)·2(H$_2$O)} (11).

Yield: 28 mg, (19% based on single crystals). ESI-MS $[L_2Ni_2Gd]^+$ 1366.302, Anal. Calcd. for $C_{60}H_{70}Gd_1N_9Ni_2O_{17}$: C, 49.23; H, 4.82; N, 8.61. Found: C, 49.97; H, 4.63; N, 8.62. IR (ATR): ν 3423(w), 2987(w), 2926(w), 2863(w), 2828(m), 2708(w), 1618(s), 1552(m), 1472(s), 1408(m),

Dieses Werk ist copyrightgeschützt und darf in keiner Form vervielfältigt werden noch an Dritte weitergegeben werden.
Es gilt nur für den persönlichen Gebrauch.

1375(w), 1307(s), 1244(m), 1213(s), 1168(m), 1112(w), 1078(m), 1035(s), 976(m), 904(w), 853(m), 827(w), 782(m), 740(s), 630(m), 607(w), 584 (w), 556(w), 517(w) cm^{-1}.

{[$Ni_2Tb(L^1)_2$]$_4$·4(NO_3)·3(MeCN)·5(MeOH)·(H_2O)} (12).

Yield: 38 mg, (25% based on single crystals). ESI-MS $[L_2Ni_2Tb]^+$ 1365.269, Anal. Calcd. for $C_{240}H_{266}Tb_4Ni_8N_{36}O_{61}$ (corresponds to **12 -** 3MeCN, -5MeOH): C, 50.25; H, 4.67; N, 8.79. Found: C, 48.82; H, 4.916; N, 8.86. IR (ATR): ν 3389(w), 3045(w), 3012(w), 2959(w), 2925(w), 2863(m), 2829(w), 1619(s), 1600(w), 1552(m), 1513(w), 1473(s), 1457(w), 1442(w), 1409(w), 1376(w), 1355(w), 1336(w), 1308(m), 1245(m), 1219(s),1169(w), 1112(w), 1077(m), 975(m), 922(w), 891(w), 853(m), 822(w), 781(w), 758(w), 732(s), 631(m), 607(w), 585(w), 548(w), 516(m) cm^{-1}.

{[$Ni_2Dy(L^1)_2$]·(NO_3)·(MeOH)·(H_2O)} (13).

Yield: 32 mg, (22% based on single crystals). ESI-MS $[L_2Ni_2Dy]^+$ 1370.316, Anal. Calcd. for $C_{60}H_{68}DyN_9Ni_2O_{16}$ (corresponds to **13** -MeOH): C, 49.66; H, 4.72; N, 8.69. Found: C, 47.49; H, 4.83; N, 8.99. IR (ATR): ν 3259(w), 3047(w), 2997(w), 2926(w), 2863(w), 2821(m), 1622(s), 1552(w), 1539(m), 1470(s), 1442(m), 1410(m), 1375(w), 1355(w), 1335(w), 1240(m), 1203(s),1169(m), 1110(w), 1074(m), 1055(m), 1036(s), 974(w), 961(s), 855(m), 825(w), 782(w), 746(m), 727(s), 644(w), 631(m), 608(w), 563(m), 516(w) cm^{-1}.

4.4.9 Synthesis of {[$Dy_4(L^2)_3(Ph_2acac)_4$]·(Et_3NH)·4(MeOH)·(MeCN)·(H_2O)} (14).

The Schiff base proligand (H_3L^2) was prepared *in situ* by condensation of 4-tert-butyl-2,6-diformylphenol (0.3 mmol) and 2-aminophenol (0.6 mmol) in 10 mL MeCN. The reaction solution was refluxed for 1 hour at 80 ^oC and then cooled down to room temperature. $Dy(NO_3)_3·5(H_2O)$ (0.4 mmol), dibenzoylmethane (0.4) and Et_3N (0.1 mmol) were subsequently added and the reaction mixture was refluxed for 1 hour resulting a red solution appeared. The solution was filtered and diffused with 0.5 mL methanol. It was left undisturbed to allow slow evaporation of the solvent. Yellow single crystals of **14** suitable for X-ray diffraction analysis formed after three days. Yield: 46 mg, (4% based on single crystals). ESI-MS $[Dy_4(L)_3(Ph_2acac)_4]^-$ 2699.26, Anal. Calcd. for $C_{138}H_{125}Dy_4N_7O_{18}$ (corresponds to **14** -4MeOH, -MeCN): C, 58.79; H, 4.47; N, 3.48. Found: C, 58.58; H, 4.61; N, 3.17. IR (ATR): ν 3057(w), 2955(w), 1619(m), 1597(m),1583(m), 1549(m), 1513(m), 1476(s), 1453(w), 1382(w), 1311(w), 1279(m), 1257(w), 1182(m), 1149(w), 1106(w), 1059(m), 1022(w), 963(w), 940(w), 880(w), 844(w), 822(w), 777(w), 737 (m), 721(s), 687(m), 617(w), 606(m), 589(w), 567(w), 512(s), cm^{-1}.

Dieses Werk ist copyrightgeschützt und darf in keiner Form vervielfältigt werden noch an Dritte weitergegeben werden.
Es gilt nur für den persönlichen Gebrauch.

4.4.10 Synthesis of {[$Ln_5(\mu_3\text{-}OH)_2(L^2)_2(Ph_2acac)_7(Ph_2acacH)]\cdot 7(PhMe)$} (15,16).

The Schiff base (H_3L^2) was synthesized *in situ* by condensation of 4-tert-butyl-2,6-diformylphenol (0.2 mmol) and 2-aminophenol (0.4 mmol) in 10 mL MeOH. The solution was refluxed for 1 hour at 80 °C and then cooled down to room temperature. $Ln(NO_3)_3\cdot x(H_2O)$ (0.5 mmol), dibenzoylmethane (0.8 mmol) and Et_3N (0.15 mmol) were subsequently added and the reaction solution was refluxed for 2 hour, resulting a red solution with precipitate. The precipitate was filtered out and dissolved in toluene then it was left at room temperature for crystallization. After three days, yellow plates of **15** and **16** were obtained suitable for X-ray diffraction analysis.

{[$Tb_5(\mu_3\text{-}OH)_2(L^2)_2(Ph_2acac)_7(Ph_2acacH)]\cdot 7(PhMe)$} (15).

Yield: 52 mg, (2.6 %, based on single crystals). Anal. Calcd. for $C_{168}H_{133}Tb_5N_4O_{24}$ (corresponds to **15** - 7ArMe): C, 59.58; H, 3.96; N, 1.65. Found: C, 58.12; H, 3.76; N, 1.58. IR (ATR): ν 3055(w), 2946(w), 1618(m), 1601(m), 1546(m), 1517(m), 1475(s), 1455(w), 1403(s), 1376(w), 1312(w), 1280(m), 1259(w), 1220(m), 1180(w), 1152(w), 1101(w), 1058(m), 1023(w), 999(w), 961(w), 940(w), 925(w), 926(w), 880(w), 852(w), 815(w), 783(w), 742(m), 717(s), 685(m), 617(w), 607(m) cm^{-1}.

{[$Dy_5(\mu_3\text{-}OH)_2(L^2)_2((Ph_2acac)_7(Ph_2acacH)]\cdot 7(PhMe)$} (16).

Yield: 56 mg, (2.7 % based on single crystals). Anal. Calcd. for $C_{168}H_{133}Dy_5N_4O_{24}$ (corresponds to **16** - 7ArMe): C, 59.27; H, 3.94; N, 1.65. Found: C, 59.38; H, 3.95; N, 1.62. IR (ATR): ν 3054(w), 2945(w), 1617(w), 1601(m), 1546(m), 1518(s), 1475(s), 1456(m), 1405(s), 1377(w), 1312(w), 1281(m), 1260(w), 1221(m), 1179(w), 1152(w), 1102(w), 1059(m), 1023(w), 999(w), 961(w), 940(w), 926(w), 881(w), 852(w), 816(w), 783(w), 742(m), 717(s), 686(m), 618(w), 608(m) cm^{-1}.

4.4.11 Synthesis of {[$Ln_4(\mu_3\text{-}OH)_2(L^2)(HL^2)(acac)_5(H_2O)]\cdot(NO_3)\cdot(HNEt_3)\cdot 2(Et_2O)$} (17-21).

The Schiff base proligand (H_3L^2) was synthesized *in situ* by condensation of 4-tert-butyl-2,6-diformylphenol (0.2 mmol) and 2-aminophenol (0.4 mmol) in 10 mL MeOH. The solution was refluxed for 1 hour at 80 °C and then cooled down to room temperature. $Ln(NO_3)_3\cdot x(H_2O)$ (0.4 mmol), (Ln = Tb, Dy, Ho, Tm), acetylacetone (0.5 mmol) and Et_3N (0.15 mmol) were added and the solution was refluxed for 2 hours. The red solution was evaporated under vacuum and solid precipitate was crystallized with diethylether. Within two days, red crystals were obtained suitable for X-ray diffraction analysis.

Dieses Werk ist copyrightgeschützt und darf in keiner Form vervielfältigt werden noch an Dritte weitergegeben werden.
Es gilt nur für den persönlichen Gebrauch.

{[$Tb_4(\mu_3\text{-}OH)_2(L^2)(HL^2)(acac)_5(H_2O)$]·($NO_3$)·($HNEt_3$)·2($Et_2O$)} (17).

Yield: 36 mg, (4 % based on single crystals). ESI-MS $[Tb_4(\mu_3\text{-}OH)_2(L^2)(HL^2)(acac)_5(H_2O)]^+$ 1951.21, Anal. Calcd. for $C_{79}H_{98}Tb_4N_6O_{22}$ (corresponds to **17** -2Et_2O): C, 44.77; H, 4.66; N, 3.97. Found: C, 43.38; H, 4.39; N, 3.09. IR (ATR): 2957(br), 1584(m), 1559(w), 1540(w), 1515(s), 1477(m), 1455(w), 1379(s), 1293(w), 1258(s), 1203(w), 1150(w), 1108(w), 1060(w), 1018(m), 953(w), 920(w), 880(w), 821(m), 740(s), 667(w), 654(w), 613(w), 588(m), 571(w), 531(w), 507(w) cm^{-1}.

{[$Dy_4(\mu_3\text{-}OH)_2(L^2)(HL^2)(acac)_5(H_2O)$]·($NO_3$)·($HNEt_3$)·2($Et_2O$)} (18).

Yield: 28 mg, (3 % based on single crystals). ESI-MS $[Dy_4(\mu_3\text{-}OH)_2(L^2)(HL^2)(acac)_5(H_2O)]^+$ 1966.05, Anal. Calcd. for $C_{79}H_{98}Dy_4N_6O_{22}$ (corresponds to **18** -2Et_2O): C, 44.47; H, 4.63; N, 3.94. Found: C, 43.89; H, 4.59; N, 3.14. IR (ATR) : 2961(br), 1585(m), 1545(w), 1516(s), 1477(m), 1452(w), 1380(s), 1294(w), 1259(s), 1202(w), 1185(w), 1149(w), 1095(w), 1061(w), 1018(s), 962(w), 920(w), 879(w), 820(s), 798(w), 739(s), 686(w), 656(w), 614(w), 588(m), 572(w), 532(w), 507(w) cm^{-1}.

{[$Ho_4(\mu_3\text{-}OH)_2(L^2)(HL^2)(acac)_5(H_2O)$]·($NO_3$)·($HNEt_3$)·2($Et_2O$)} (19).

Yield: 38 mg, (4 % based on single crystals). ESI-MS $[Ho_4(\mu_3\text{-}OH)_2(L^2)(HL^2)(acac)_5(H_2O)]^+$ 1974.95, Anal. Calcd. for $C_{79}H_{98}Ho_4N_6O_{22}$ (corresponds to **19** -2Et_2O): C, 44.27; H, 4.61; N, 3.92. Found: C, 43.01; H, 4.46; N, 3.64. (ATR): 2958(br), 1585(m), 1559(w), 1540(w), 1517(s), 1477(m), 1456(m), 1437(w), 1419(w), 1383(s), 1295(w), 1258(s), 1236(w), 1185(w), 1152(w), 1108(w), 1061(w), 1018(m), 952(w), 921(w), 880(m), 849(w), 822(s), 740(s), 667(w), 655(w), 614(w), 589(m), 571(w), 532(w), 504(w) cm^{-1}.

{[$Er_4(\mu_3\text{-}OH)_2(L^2)(HL^2)(acac)_5(H_2O)$]·($NO_3$)·($HNEt_3$)·2($Et_2O$)} (20).

Yield: 42 mg, (4.5 % based on single crystals). ESI-MS $[Er_4(\mu_3\text{-}OH)_2(L^2)(HL^2)(acac)_5(H_2O)]^+$ 1984.91, Anal. Calcd. for $C_{79}H_{98}Er_4N_6O_{22}$ (corresponds to **20** -2Et_2O): C, 44.08; H, 4.59; N, 3.90. Found: C, 43.87; H, 4.37; N, 2.86. IR (ATR) : 2961(br), 1586(m), 1544(w), 1479(m), 1454(w), 1385(s), 1298(w), 1259(s), 1236(w), 1202(w), 1184(w), 1148(w), 1098(m), 1057(m), 1017(s), 961(w), 920(w), 879(w), 852(w), 821(w), 797(m), 740(s), 688(w), 656(w), 614(w), 590(m), 570(w), 532(w), 505(w) cm^{-1}.

{[$Tm_4(\mu_3\text{-}OH)_2(L^2)(HL^2)(acac)_5(H_2O)$]·($NO_3$)·($HNEt_3$)·2($Et_2O$)} (21).

Yield: 46 mg, (5 % based on single crystals). ESI-MS $[Tm_4(\mu_3\text{-}OH)_2(L^2)(HL^2)(acac)_5(H_2O)]^+$ 1991.13, Anal. Calcd. for $C_{79}H_{98}Tm_4N_6O_{22}$ (corresponds to **21** -2Et_2O): C, 43.94; H, 4.57; N, 3.89.

Dieses Werk ist copyrightgeschützt und darf in keiner Form vervielfältigt werden noch an Dritte weitergegeben werden.
Es gilt nur für den persönlichen Gebrauch.

Found: C, 43.31; H, 4.42; N, 3.56 IR : 2958(br), 1586(m), 1559(w), 1541(w), 1517(s), 1479(m), 1456(w), 1384(s), 1283(w), 1260(m), 1236(w), 1204(w), 1185(w), 1152(w), 1107(w), 1059(w), 1019(m), 961(w), 921(w), 880(w), 849(w), 824(m), 740(s), 688(w), 655(w), 613(w), 590(w), 572(w), 532(w), 504(w) cm^{-1}.

4.4.12 Synthesis of {[$Dy_4(\mu_4$-OH)(L^2)$_2$(acac)$_4$(MeOH)$_2$(EtOH)(H_2O)]·(NO_3)·2(MeOH)·3(EtOH)} (22).

The Schiff base proligand (H_3L^2) was synthesized *in situ* by condensation of 4-tert-butyl-2,6-diformylphenol (0.2 mmol) and 2-aminophenol (0.4 mmol) in 10 mL MeOH. The solution was refluxed for 1 hour at 80 ^oC and then cooled down to room temperature. $Dy(NO_3)_3 \cdot 5(H_2O)$ (0.4 mmol), acetylacetone (0.5 mmol) and Et_3N (0.1 mmol) were subsequently added and the reaction solution was stirred for 2 minutes. The resulting red solution was filtered and then 1 ml ethanol was added. The solution was left at room temperature for crystallization. After one week, yellow-orange color crystals were obtained. Yield: 40 mg, (4.5% based on single crystals). ESI-MS {[$Dy_4(\mu_4$-OH)(L)$_2$(acac)$_4$(MeOH)(EtOH)(H_2O)]$^+$ 1930.17, Anal. Calcd. for $C_{80}H_{112}Dy_4N_5O_{27}$: C, 43.17; H, 5.07; N, 3.15. Found: C, 43.15; H, 4.33; N, 3.41, IR (ATR) : 3612(w), 3055(w), 2954(w), 2865(w), 1619(w), 1582(s), 1548(w), 1516(s), 1475(s), 1453(w), 1374(s), 1305(w), 1286(w), 1259(s), 1182(w), 1154(w), 1108(w), 1061(w), 1035(w), 1019(m), 965(w), 950(w), 921(m), 878(m), 845(w), 823(s), 776(m), 748(s), 655(w), 590(m), 570(w), 507(s), 478(m), 448(w) cm^{-1}.

4.4.13 Synthesis of {[$Dy_5(\mu_5$-NO_3)(L^2) (L^{2a})$_2$(acac)$_6$(iPrOH)$_2$(HO)(H_2O)]·4(H_2O)} (23).

H_3L^2 and H_2L^{2a} proligands were synthesized *in situ* by condensation of 4-tert-butyl-2,6-diformylphenol (0.2 mmol), 2-aminophenol (0.26 mmol) and acetlyacetone (0.7 mmol) in presence of Et_3N (0.1 mmol) and 10 mL iPrOH. The solution was refluxed for 1 hour at 80 ^oC and then cooled down to room temperature. $Dy(NO_3)_3 \cdot 5(H_2O)$ (0.4 mmol) was added and the reaction solution was stirred for 2 minutes. The red solution was filtered and left at room temperate for crystallization. Red crystals suitable for X-ray diffraction analysis formed after two weeks. Yield: 50 mg, (4 % based on single crystals). Anal. Calcd. for $C_{106}H_{136}Dy_5N_5O_{34}$: C, 44.88; H, 4.83; N, 2.47. Found: C, 44.41; H, 4.76; N, 2.18. IR (ATR): 3611(w), 3054(w), 2954(w), 2864(w), 2864(w), 2363(w), 1619(w), 1883(s), 1548(w), 1517(s), 1476(m), 1453(w), 1376(s), 1305(w), 1287(w), 1260(s), 1182(w), 1154(w), 1109(w), 1062(w), 1034(w), 1020(m), 965(w), 950(w), 921(m), 879(m), 845(w), 823(s), 776(w), 749(s), 656(w), 590(m), 570(w), 508(m), 479(w), 448(w) cm^{-1}.

Dieses Werk ist copyrightgeschützt und darf in keiner Form vervielfältigt werden noch an Dritte weitergegeben werden.
Es gilt nur für den persönlichen Gebrauch.

4.4.14 Synthesis of {[Ln(Ph$_2$acac)$_4$](Et$_3$NH)}(24, 25).

The dibenzoylmethane (0.4 mmol) and Ln(NO$_3$)$_3$·x(H$_2$O) (0.1 mmol) were stirred for 5 minutes in 6 mL a mixture of 1:1 ratio of methanol and dichloromethane and then Et$_3$N (0.1 mmol) was added to reaction mixture. Then, it was filtered and left at room temperature for crystallization. After four days, colourless single crystals of **24** and **25** obtained that were suitable for X-ray diffraction analysis.

{[Tb(Ph$_2$acac)$_4$]·(Et$_3$NH)} (24).

Yield: 60 mg, (52% based on single crystals). ESI-MS [Tb(Phacac)$_4$]$^-$ 1051.26, Anal. Calcd. for C$_{66}$H$_{60}$N$_1$O$_8$Tb$_1$: C, 68.69; H, 5.24; N, 1.21. Found: C, 67.41; H, 5.20; N, 1.58. IR (ATR): 3056(w), 3026(w), 2986(w), 1595(s), 1550(m), 1509(s), 1475(w), 1456(s), 1396(m), 1305(w), 1278(m), 1217(m), 1177(w), 1100(w), 1066(m), 1022(m), 939(w), 835(w), 809(w), 782(w), 745(w), 720(s), 688(m), 607(s), 507(m), 428(w) cm^{-1}.

{[Dy(Ph$_2$acac)$_4$]$_2$·2(Et$_3$NH)·3(CH$_2$Cl$_2$)} (25)

Yield: 62 mg, (48% based on single crystals). ESI-MS [Dy(Phacac)$_4$]$^-$ 1056.19, Anal. Calcd. for C$_{132}$H$_{120}$Dy$_2$N$_2$O$_{16}$ (corresponds to **25** – 3CH$_2$Cl$_2$): C, 68.47; H, 5.22; N, 1.21. Found: C, 68.16; H, 5.29; N, 1.33. IR (ATR): 3056(w), 2361(w), 2337(w), 1595(m), 1551(m), 1513(s), 1476(m), 1455(w), 1398(m), 1306(w), 1279(w), 1218(w), 1178(w), 1155(w), 1066(w), 1022(w), 999(w), 973(w), 939(w), 835(w), 809(w), 782(w), 745(w), 720(s), 688(m), 608(m), 510(w), 429(w) cm^{-1}.

4.4.15 Synthesis of {[Dy$_5$(μ$_3$-OH)$_2$(L^2)$_3$(Ph$_2$acac)$_4$(MeOH)$_4$]·4(MeOH)} (26)

H$_3$L^2 was synthesized *in situ* by condensation of 4-tert-butyl-2,6-diformylphenol (0.2 mmol) and 2-aminophenol (0.4 mmol) in 15 mL methanol. The solution was refluxed for 1 hour at 80 ^{o}C and then cooled down to room temperature. Dy(NO$_3$)$_3$·5(H$_2$O) (0.35 mmol), dibenzoylmethane (0.32 mmol) and Et$_3$N (0.10 mmol) were then added and the solution was refluxed for 3 hours, giving the red solution with precipitate. The precipitate was filtered out then dissolved in methanol and dichloromethane and left at room temperature for crystallization. Within one week, yellow crystal of **26** obtained that were suitable for X-ray diffraction analysis. Yield: 42 mg, (4% based on single crystals). Anal. Calcd. for C$_{136}$H$_{122}$Dy$_5$N$_6$O$_{23}$ (corresponds to **26** -4MeOH): C, 54.07; H, 4.07; N, 2.78. Found: C, 52.88; H, 4.07; N, 3.68. IR (ATR): 3059(w), 2958(w), 2361(w), 1619(w), 1597(s), 1549(m), 1518(s), 1453(m), 1282(s), 1258(w), 1182(w), 1150(w), 1107(w), 1062(s), 1025(m), 1001(w), 962(w), 942(w), 921(w), 880(m), 843(w), 823(s), 776(w), 741(s), 721(w), 688(m), 632(w), 609(m), 589(w), 569(w), 511(s), 474(m), 446(w) cm^{-1}.

Dieses Werk ist copyrightgeschützt und darf in keiner Form vervielfältigt werden noch an Dritte weitergegeben werden.
Es gilt nur für den persönlichen Gebrauch.

4.4.16 Synthesis of {[$Tb_7(\mu_3\text{-}OH)_2(\mu_5\text{-}(NO_3)(\mu_3\text{-}NO_3)(L^2)_3(Ph_2acac)_5(H_2N\text{-}Ph\text{-}O)(MeO)_2(MeOH)_3]\cdot(MeOH)_3\cdot(MeCN)\cdot 15(H_2O)$} (27).

H_3L^2 was synthesized *in situ* by condensation of 4-tert-butyl-2,6-diformylphenol (0.2 mmol) and 2-aminophenol (0.4 mmol) in 15 mL methanol. The solution was refluxed for 1 hour at 80 ^oC and then cooled down to room temperature. $Tb(NO_3)_3\cdot 6(H_2O)$ (0.35 mmol), dibenzoylmethane (0.32 mmol) and Et_3N (0.10 mmol) were then added and the solution was refluxed for 3 hours, giving the red solution with precipitate. The solution was filtered and mixed with 5 ml acetonitrile. It was left undisturbed to allow slow evaporation of the solvent. Yellow-orange single crystals of **27** suitable for X-ray diffraction analysis formed after four days. Yield: 32 mg, (2% based on single crystals). Anal. Calcd. for $C_{163}H_{188}N_{10}O_{51}Tb_7$: C, 46.44; H, 4.49; N, 3.32. Found: C, 46.63; H, 3.79; N, 2.85. IR (ATR): 3058(w), 2955(w), 2362(w), 1596(w), 1549(m), 1453(m), 1289(s), 1257(m), 1180(w), 1155(w), 1109(w), 1061(m), 1023(m), 1000(w), 964(w), 941(w), 923(w), 880(w), 821(s), 783(w), 740(s), 721(s), 688(s), 609(m), 588(m), 512(s), 476(m), 445(w) cm^{-1}.

4.4.17 Synthesis of {[Dy_2L_3]·3(OH)·6(H_2O)·(C_6H_{12})} (28).

The Schiff base (HL) was synthesized *in situ* by condensation of 4-tert-butyl-2,6-diformyl phenol (0.2 mmol) and isoniazid (0.4 mmol) in 10 mL methanol. The solution was refluxed for 2 hours at 80 ^oC and then cooled down to room temperature. $Dy(NO_3)_3\cdot 5(H_2O)$ (0.2 mmol) and Et_3N (0.15 mmol) were added and the reaction solution was stirred for 2 hours at room temperature. The orange solution was filtered and left at room temperature for slow evaporation of solvent. Then, the reaction volume was reduced and dichloromethane was added to it. Within day, yellow color plates of **28** obtained that were suitable for X-ray diffraction analysis. Yield: 42 mg, (11% based on single crystals). ESI-MS $[Dy_2L_3]^+$ 1653, Anal. Calcd. for $C_{72}H_{84}N_{18}O_{18}Dy_2$ (corresponds to **28** –C_6H_{12}): C, 47.66; H, 4.67; N, 13.89. Found: C, 43.90; H, 4.99; N, 13.85. IR (ATR): 3034(w), 2953(w), 2863(w), 1658(w), 1614(m), 1585(w), 1549(m), 1513(s), 1446(w), 1381(s), 1361(w), 1322(m), 1305(w), 1241(w), 1228(w), 1156(w), 1068(m), 1018(m), 962(w), 905(w), 842(s), 779(m), 751(m), 717(w), 680(s), 662(w), 634(w), 587(w), 533(w), 455(w), 427(w) cm^{-1}.

4.4.18 Synthesis of{$[Dy_2L_3(OH)]\cdot[Dy(NO_3)_3(H_2O)_3]\cdot 3(Py)\cdot 2(HO)\cdot 7(H_2O)\cdot 6(MeOH)\cdot(CHCl_3)$} (29).

The Schiff base proligand (HL) was synthesized *in situ* by condensation of 4-tertbutyl-2,6-diformyl phenol (0.2 mmol) and isoniazid (0.4 mmol) in 10 mL methanol. The solution was refluxed for 2 hours at 80 ^oC and then cooled down to room temperature. $Dy(NO_3)_3\cdot 5(H_2O)$ (0.4 mmol) and pyridine (0.3 mmol) were subsequently added and the reaction solution was stirred for 1 hour at room temperature. The orange solution was filtered and dichloromethane added to it in a ratio of 2:1

Dieses Werk ist copyrightgeschützt und darf in keiner Form vervielfältigt werden noch an Dritte weitergegeben werden.
Es gilt nur für den persönlichen Gebrauch.

(CH_2Cl_2: MeOH). The reaction mixture was left at room temperature for slow evaporation of solvent. Slow diffusion of pentane in reaction mixture was helpful to obtain the suitable crystal for X-ray diffraction and analysis. Yield: 40 mg, (4% based on single crystals). ESI-MS $[Dy_2L_3]^{2+}$ 825.84, Anal. Calcd. for $C_{94}H_{132}Cl_3Dy_3N_{24}O_{37}$: C, 40.55; H, 4.78; N, 12.07. Found: C, 39.30; H, 4.52; N, 11.61. IR (ATR): 3034(w), 2959(w), 2862(w), 1614(m), 1587(w), 1569(m), 1548(m), 1506(w), 1446(w), 1410(m), 1383(m), 1362(w), 1305(s), 1245(w), 1230(w), 1156(w), 1068(m), 1028(w), 963(w), 904(m), 841(s), 778(m), 747(s), 714(w), 683(m), 634(w), 587(w), 539(w), 518(w), 494(w), 473(w) cm^{-1}.

4.4.19 Synthesis of {$[Dy_2L_3(H_2O)]\cdot[Dy(NO_3)(H_2O)_7]\cdot 5(NO_3)\cdot 3(MeOH)\cdot 7(H_2O)$} (30).

The Schiff base proligand (HL) was synthesized *in situ* by condensation of 4-tert-butyl-2,6-diformyl phenol (0.2 mmol) and isoniazid (0.4 mmol) in 10 mL methanol. The solution was refluxed for 2 hours at 80 ^oC and cooled down to room temperature. $Dy(NO_3)_3\cdot 5(H_2O)$ (0.4 mmol) was added and then the reaction solution was stirred for 2 hours at room temperature. The orange solution was filtered and mixed with dichloromethane in a ratio of 2:1 (CH_2Cl_2:MeOH). The reaction mixture was left at room temperature for slow evaporation of solvent. Yellow suitable crystal for X-ray diffraction analysis was obtained after slow diffusion of pentane in the reaction mixture. Yield: 61 mg, (6% based on single crystals). ESI-MS $[Dy_2L_3]^+$ 1654, Anal. Calcd. for $C_{75}H_{104}Dy_3N_{24}O_{42}$ (corresponds to **30** $-3H_2O$): C, 36.01; H, 4.19; N, 13.44. Found: C, 36.10; H, 3.68; N, 14.63. IR (ATR): 2961(w), 2863(w), 1613(s), 1585(w), 1545(m), 1501(s), 1383(m),1304(s), 1245(w), 1155(w), 1071(m), 1036(m), 964(m), 900(s), 841(s), 777(m), 748(m), 714(m), 680(s), 633(w), 586(w), 519(w), 492(w), 454(w), 429(w) cm^{-1}.

4.4.20 General procedure for the synthesis of complexes (31- 34).

H_4L (0.055mmol) and $MnCl_2\cdot 4(H_2O)$ (0.055 mmol) were stirred in DMF (2 mL) for 5 min than $Ln(NO_3)_3\cdot(H_2O)m$ (0.1 mmol) and pyridine (0.15 mL) was added to the reaction mixture. Black resulting solution was stirred for 2 hours at room temperature and then filtered in 10 mL glass vial. The glass vial was heated at 90^o C for two days in an oven and during the heating crystal was formed in vial then cooled down to room temperature. The red block shaped crystals were collected suitable for single-crystal X-ray diffraction and washed three times with DMF followed by diethyl ether and dried in air for further analysis.

{$[Pr_2(MnLClNO_3)_2(dmf)_6(H_2O)_2]\cdot(H_2O)\}_n$ (31).

Yield: 20 mg (21% based on single crystals), Anal. Calcd. for $C_{59}H_{77}Cl_2Mn_2N_{11}Pr_2O_{26}$ (corresponds to loss of one DMF molecules): C, 38.96; H, 4.27; N, 8.47. Found: C, 37.96; H, 4.89; N, 8.52 IR

Dieses Werk ist copyrightgeschützt und darf in keiner Form vervielfältigt werden noch an Dritte weitergegeben werden.
Es gilt nur für den persönlichen Gebrauch.

(ATR): 2939 (w), 2861 (w), 1613 (m), 1559 (m), 1515(m) , 1479 (m), 1397 (s), 1338 (s), 1300 (s), 1269 (s), 1198 (m), 1140 (w), 1109 (w), 1022 (w), 977(m), 895 (w), 862 (w), 819 (w), 777 (s), 736 (w), 637 (w), 606(s), 520 (w), 493(w), 467 (w), 441(w) cm^{-1}.

$\{[Nd_2(MnLClNO_3)_2(dmf)_6(H_2O)_2]\cdot(H_2O)\}_n$ (32).

Yield: 19 mg (20% based on single crystals), Anal. Calcd. for $C_{62}H_{84}Cl_2Mn_2N_{12}Nd_2O_{27}$: C, 39.22; H, 4.46; N, 8.85. Found: C, 38.12; H, 4.85; N, 8.59 IR(ATR): 2940 (w), 2861 (w), 1647 (m), 1615 (s), 1565 (s), 1521(w) , 1476 (w), 1389 (s), 1337 (w), 1299 (m), 1269 (m), 1198 (m), 1139 (w), 1106 (w), 1023 (w), 974 (m), 897 (w), 860 (w), 817 (m), 775 (s), 736 (w), 662 (w), 634 (s), 601 (w), 520 (w), 494(w), 467 (w), 442(w), 418 (w) cm^{-1}.

$\{[Sm_2(MnLClNO_3)_2(dmf)_6(H_2O)_2]\cdot(H_2O)\}_n$ (33).

Yield: 20 mg (21% based on single crystals), Anal. Calcd. for $C_{62}H_{84}Cl_2Sm_2Mn_2N_{12}O_{27}$: C, 38.97; H, 4.43; N, 8.80. Found: C, 38.31; H, 4.43; N, 8.91 IR (ATR): 2939 (w), 2861 (w), 1651 (m), 1617 (s), 1564 (s), 1519(w) , 1477 (w), 1391 (s), 1337 (w), 1299 (m), 1269 (m), 1197 (m), 1139 (w), 1106 (w), 1022 (w), 975(m), 897 (w), 860 (w), 813 (m), 777 (s), 737 (w), 635 (s), 602(w), 520 (w), 494(w), 467 (w), 441(w) cm^{-1}.

$\{[Gd_2(MnLClNO_3)_2(dmf)_6(H_2O)_2]\cdot(H_2O)\}_n$ (34).

Yield: 18 mg (18% based on single crystals), Anal. Calcd. for $C_{56}H_{70}Cl_2Gd_2Mn_2N_{10}O_{25}$ (corresponds to loss of two DMF molecules): C, 37.82; H, 3.97; N, 7.88. Found: C, 36.75; H, 4.52; N, 7.81 IR (ATR): IR (ATR): 2939 (w), 2861 (w), 1647 (m), 1616 (s), 1566 (s), 1521(w) , 1477 (w), 1394 (s), 1337 (w), 1300 (m), 1270 (m), 1198 (m), 1139 (w), 1107 (w), 1023 (w), 975(m), 898 (w), 861 (w), 819 (m), 776 (s), 738 (w), 667 (w), 634 (s), 602(w), 519 (w), 494(w), 467 (w), 443(w), 419 (w) cm^{-1}.

4.4.21 General procedure for catalysis

The catalyst **30-34** (20 mg) and the affiliated sulfide (1 mmol) were combined in acetonitrile (10 mL) and followed by addition of phenyliodosobenzene (1 mmol). The combined reaction mixture was stirred for 16 hours at room temperature. The reaction progress was monitored by TLC (eluent: EtOAc/hexane). The catalyst was separated out from reaction mixture by ordinary filtration. The catalyst was recycled and performed in the similar way.

4.4.22 NMR data of Sulfoxides

1. **phenyl methyl sulfoxide.**

^1H NMR (300 MHz, $CDCl_3$) δ 7.73 – 7.66 (m, 2H), 7.61 – 7.53 (m, 2H), 2.77 (s, 3H).

Dieses Werk ist copyrightgeschützt und darf in keiner Form vervielfältigt werden noch an Dritte weitergegeben werden.
Es gilt nur für den persönlichen Gebrauch.

2. 4-tolyl methyl sulfoxide.

^{1}H NMR (300 MHz, $CDCl_3$) δ 7.57 (d, *J* = 8.2 Hz, 2H), 7.36 (d, *J* = 8.0 Hz, 2H), 2.73 (s, 3H), 2.45 (s, 3H).

3. 4-chlorophenyl methyl sulfoxide.

^{1}H NMR (300 MHz, $CDCl_3$) δ 7.65 – 7.60 (m, 2H), 7.58 – 7.51 (m, 2H), 2.75 (s, 3H).

4. 4-bromophenyl methyl sulfoxide.

^{1}H NMR (300 MHz, $CDCl_3$) δ 7.74 – 7.69 (m, 2H), 7.59 – 7.54 (m, 2H), 2.76 (s, 3H).

5. 4-nitrophenyl methyl sulfoxide.

^{1}H NMR (300 MHz, $CDCl_3$) δ 8.50 – 8.38 (m, 2H), 7.93 – 7.82 (m, 2H), 2.84 (s, 3H).

6. 4-nitrile methyl sulfoxide.

^{1}H NMR (300 MHz, $CDCl_3$) δ 7.86 (d, *J* = 8.4 Hz, 2H), 7.79 (d, *J* = 8.3 Hz, 2H), 2.78 (s, 3H).

7. Phenyl ethyl sulfoxide.

^{1}H NMR (300 MHz, $CDCl_3$) δ 7.68 – 7.59 (m, 2H), 7.58 – 7.49 (m, 2H), 3.00 – 2.87 (m, 1H), 2.86 – 2.72 (m, 1H), 1.22 (t, *J* = 7.4 Hz, 3H).

8. 4-bromophenyl ethyl sulfoxide.

^{1}H NMR (300 MHz, $CDCl_3$) δ 7.70 – 7.64 (m, 2H), 7.53 – 7.47 (m, 2H), 2.92 (dq, *J* = 13.4, 7.4 Hz, 1H), 2.76 (dq, *J* = 13.3, 7.4 Hz, 1H), 1.23 (dt, *J* = 14.8, 7.3 Hz, 3H).

9. 4-n-butylphenyl ethyl sulfoxide.

^{1}H NMR (300 MHz, $CDCl_3$) δ 7.61 – 7.49 (m, 2H), 7.36 (d, *J* = 8.3 Hz, 2H), 2.98 – 2.76 (m, 2H), 2.71 (dd, *J* = 14.3, 6.6 Hz, 2H), 1.71 – 1.58 (m, 2H), 1.46 – 1.34 (m, 2H), 1.23 (t, *J* = 7.4 Hz, 3H), 0.97 (t, *J* = 7.3 Hz, 3H).

Dieses Werk ist copyrightgeschützt und darf in keiner Form vervielfältigt werden noch an Dritte weitergegeben werden.
Es gilt nur für den persönlichen Gebrauch.

5 Crystal Structure Measurements

5.1 Data collection and refinement

The crystal structures were measured with Imaging Plate Detection System (IPDS) X-ray diffractometer (STOE). A suitable crystal was covered in mineral oil (Aldrich) and mounted on a glass fiber. The crystal was transferred directly to the cold stream of a diffractometer. The oil freezes upon cooling in a flow of cold nitrogen protecting the crystal. The structural analyses were carried out at low temperatures (-100 to -173) on STOE IPDS II MoKα (λ = 0.71073 Å) equipped with an imaging plate area detector. All structures were solved using the program SHELXS-2013.[159] The remaining non-hydrogen atoms were located from successive difference in Fourier map calculations. The refinements were carried out by using full-matrix least-squares techniques on F^2, minimizing the function $(F_o\text{-}F_c)^2$, where the weight is defined as $4F_0^2/2(F_o^2)$ and F_o and F_c are the observed and calculated structure factor amplitudes using the program SHELXL-2013.[157, 159] The final values of refinement parameters are given in crystal data. In few compounds disordered molecules were SQUEEZED by using the PLATON.[156],[157] The locations of the largest peaks in the final difference Fourier map calculation as well as the magnitude of the residual electron densities in each case were of no chemical significance. The graphical representation was done by using the program DIAMOND.

Dieses Werk ist copyrightgeschützt und darf in keiner Form vervielfältigt werden noch an Dritte weitergegeben werden.
Es gilt nur für den persönlichen Gebrauch.

5.1.1 {[Y(HL)$_4$][ETAH]·(H$_2$O)} (1).

Chemical formula	$C_{42}H_{50}Y_1N_5O_{18}$
Formula mass	1001.78
Crystal system	Monoclinic
Space group	*C2/c*
a/Å, b/Å, c/Å	23.955(5), 14.600(3), 16.930(3)
β/°	134.97(3)
Unit cell volume/Å^3	4189(2)
Temperature/K	150
No. of formula units per unit cell, Z	4
Absorption coefficient, μ/mm^{-1}	1.480
No. of reflections measured	11960
No. of independent reflections	3886
R_{int}	0.0818
Final R1values (I >2σ(I))	0.0549
Final wR_2values (all data)	0.1337
Goodness of fit	0.885

5.1.2 {[Dy(HL)$_4$][ETAH]·(3MeOH)·(H$_2$O)} (2).

Chemical formula	$C_{45}H_{62}Dy_1N_5O_{21}$
Formula mass	1171.49
Crystal system	Monoclinic
Space group	$P2_1/c$
a/Å, b/Å, c/Å	14.035(3), 25.654(4), 17.380(3)
β/°	123.94(2)
Unit cell volume/Å^3	5192.0(3)
Temperature/K	150(2)
No. of formula units per unit cell, Z	4
Absorption coefficient, μ/mm^{-1}	1.521
No. of reflections measured	18971
No. of independent reflections	9652
R_{int}	0.0486
Final R1values (I >2σ(I))	0.0728
Final wR_2values (all data)	0.1929
Goodness of fit	1.128

Dieses Werk ist copyrightgeschützt und darf in keiner Form vervielfältigt werden noch an Dritte weitergegeben werden.
Es gilt nur für den persönlichen Gebrauch.

5.1.3 {[$Y_4(HL)_2(L)_4(\mu_3\text{-}OH)_2$]·4(MeOH)·4($H_2O$)} (3).

Chemical formula	$C_{64}H_{82}N_6O_{34}Y_4$
Formula mass	1834.99
Crystal system	Monoclinic
Space group	$P2_1/c$
a/Å, b/Å, c/Å	12.2239(5), 16.5807(5), 18.8528(8)
β/°	92.471(3)
Unit cell volume/Å^3	3817.5(3)
Temperature/K	150(2)
No. of formula units per unit cell, Z	2
Absorption coefficient, μ/mm^{-1}	3.102
No. of reflections measured	29236
No. of independent reflections	7110
R_{int}	0.0813
Final R1values (I >2σ(I))	0.0558
Final wR_2values (all data)	0.1467
Goodness of fit	1.032

5.1.4 {[$Dy_4(HL)_2(L)_4(\mu_3\text{-}OH)_2$]·5(MeOH)·7($H_2O$)} (4).

Chemical formula	$C_{65}H_{92}Dy_4N_6O_{38}$
Formula mass	2215.45
Crystal system	Monoclinic
Space group	$P2_1/c$
a/Å, b/Å, c/Å	12.262(3), 16.562(3), 18.889(4)
β/°	92.60(3)
Unit cell volume/Å^3	3832.1(14)
Temperature/K	150(2)
No. of formula units per unit cell, Z	2
Absorption coefficient, μ/mm^{-1}	3.954
No. of reflections measured	26541
No. of independent reflections	7527
R_{int}	0.0375
Final R1values (I >2σ(I))	0.0296
Final wR_2values (all data)	0.0719
Goodness of fit	1.065

Dieses Werk ist copyrightgeschützt und darf in keiner Form vervielfältigt werden noch an Dritte weitergegeben werden.
Es gilt nur für den persönlichen Gebrauch.

5.1.5 {[$Dy_4(HL)_8(L)_2$]·4(MeOH)·2(H_2O)} (5).

Chemical formula	$C_{104}H_{118}Dy_4N_{10}O_{46}$
Formula mass	2894.08
Crystal system	Monoclinic
Space group	$P2_1/n$
a/Å, b/Å, c/Å	14.6078(4), 15.2410(6), 25.4038(8)
β/°	94.884(2)
Unit cell volume/$Å^3$	5635.3(3)
Temperature/K	100(2)
No. of formula units per unit cell, Z	2
Absorption coefficient, μ/mm^{-1}	2.717
No. of reflections measured	26018
No. of independent reflections	10994
R_{int}	0.0989
Final R1values (I >2σ(I))	0.0591
Final wR_2values (all data)	0.1598
Goodness of fit	0.947

5.1.6 {[$Dy(HL^1)_2(H_2O)_3$](NO_3)} (6).

Chemical formula	$C_{28}H_{26}DyN_7O_{14}$
Formula mass	847.06
Crystal system	Monoclinic
Space group	$P2/n$
a/Å, b/Å, c/Å	9.2319(18), 13.092(3), 13.009(3)
β/°	98.58(3)
Unit cell volume/$Å^3$	1554.7(5)
Temperature/K	205
No. of formula units per unit cell, Z	2
Absorption coefficient, μ/mm^{-1}	2.487
No. of reflections measured	9189
No. of independent reflections	3054
R_{int}	0.0563
Final R1values (I >2σ(I))	0.0345
Final wR_2values (all data)	0.0652
Goodness of fit	0.933

Dieses Werk ist copyrightgeschützt und darf in keiner Form vervielfältigt werden noch an Dritte weitergegeben werden.
Es gilt nur für den persönlichen Gebrauch.

5.1.7 {NiGdL(acac)$_2$} (7).

Chemical formula	$C_{37}H_{41}GdN_4NiO_7$
Formula mass	869.70
Crystal system	Monoclinic
Space group	$P2_1/n$
a/Å, b/Å, c/Å	13.524(3), 18.310(4), 14.989(3)
β/°	97.59(3)
Unit cell volume/Å^3	3679.0(13)
Temperature/K	200
No. of formula units per unit cell, Z	4
Absorption coefficient, μ/mm^{-1}	2.351
No. of reflections measured	49865
No. of independent reflections	6860
R_{int}	0.0605
Final R1values (I >2σ(I))	0.0271
Final wR_2values (all data)	0.0461
Goodness of fit	0.880

5.1.8 {NiTbL(acac)$_2$} (8).

Chemical formula	$C_{37}H_{41}N_4NiO_7Tb$
Formula mass	871.37
Crystal system	Monoclinic
Space group	$P2_1/n$
a/Å, b/Å, c/Å	13.472(3), 18.261(4), 14.932(3)
β/°	97.92(3)
Unit cell volume/Å^3	3638.6(13)
Temperature/K	150
No. of formula units per unit cell, Z	4
Absorption coefficient, μ/mm^{-1}	2.498
No. of reflections measured	31435
No. of independent reflections	7710
R_{int}	0.0987
Final R1values (I >2σ(I))	0.0375
Final wR_2values (all data)	0.0934
Goodness of fit	1.021

Dieses Werk ist copyrightgeschützt und darf in keiner Form vervielfältigt werden noch an Dritte weitergegeben werden.
Es gilt nur für den persönlichen Gebrauch.

5.1.9 {[NiDyL(acac)$_2$]$_2$·7(MeOH)} (9).

Chemical formula	$C_{81}H_{110}Dy_2N_8Ni_2O_{21}$
Formula mass	1974.09
Crystal system	Triclinic
Space group	*P*-1
a/Å, b/Å, c/Å	11.702(2), 13.640(3), 15.385(3)
α/°, β/°, γ/°	66.13(3), 71.73(3), 80.90(3)
Unit cell volume/Å^3	2131.0(9)
Temperature/K	150
No. of formula units per unit cell, Z	1
Absorption coefficient, μ/mm^{-1}	2.242
No. of reflections measured	57926
No. of independent reflections	9035
R_{int}	0.1146
Final R1values (I >2σ(I))	0.0304
Final wR_2values (all data)	0.0792
Goodness of fit	1.035

5.1.10 {[NiDyL(Ph$_2$acac)$_2$]$_2$·4(CH$_2$Cl$_2$)·(MeOH)} (10).

Chemical formula	$C_{119}H_{108}Cl_8Dy_2N_8Ni_2O_{15}$
Formula mass	2616.15
Crystal system	Triclinic
Space group	*P*-1
a/Å, b/Å, c/Å	13.756(3), 15.416(3), 16.240(3)
α/°, β/°, γ/°	64.39(3), 66.71(3), 71.99(3)
Unit cell volume/Å^3	2812.4(14)
Temperature/K	206
No. of formula units per unit cell, Z	1
Absorption coefficient, μ/mm^{-1}	1.900
No. of reflections measured	21619
No. of independent reflections	10424
R_{int}	0.0602
Final R1values (I >2σ(I))	0.0333
Final wR_2values (all data)	0.0827
Goodness of fit	0.994

Dieses Werk ist copyrightgeschützt und darf in keiner Form vervielfältigt werden noch an Dritte weitergegeben werden.
Es gilt nur für den persönlichen Gebrauch.

5.1.11 {[$Ni_2Gd(L^1)_2$]·(NO_3)·2(H_2O)} (11).

Chemical formula	$C_{60}H_{70}GdN_9Ni_2O_{17}$
Formula mass	1463.90
Crystal system	Triclinic
Space group	*P*-1
a/Å, b/Å, c/Å	13.428(3), 15.368(3), 17.645(4)
α/°, β/°, γ/°	73.84(3), 89.14(3), 66.29(3)
Unit cell volume/Å^3	3182.6(14)
Temperature/K	205
No. of formula units per unit cell, Z	2
Absorption coefficient, μ/mm^{-1}	1.690
No. of reflections measured	37767
No. of independent reflections	11857
R_{int}	0.0594
Final R1values (I >2σ(I))	0.0498
Final wR_2values (all data)	0.1521
Goodness of fit	1.018

5.1.12 {[$Ni_2Tb(L^1)_2$]$_4$·4(NO_3)·3(MeCN)·5(MeOH)·(H_2O)} (12).

Chemical formula	$C_{251}H_{295}N_{39}Ni_8O_{66}Tb_4$
Formula mass	6019.58
Crystal system	Triclinic
Space group	*P*-1
a/Å, b/Å, c/Å	15.528(3), 17.496(4), 25.019(5)
α/°, β/°, γ/°	82.15(3), 79.04(3), 75.47(3)
Unit cell volume/Å^3	6431(3)
Temperature/K	150
No. of formula units per unit cell, Z	1
Absorption coefficient, μ/mm^{-1}	1.744
No. of reflections measured	64580
No. of independent reflections	23901
R_{int}	0.0609
Final R1values (I >2σ(I))	0.0532
Final wR_2values (all data)	0.1477
Goodness of fit	1.025

Dieses Werk ist copyrightgeschützt und darf in keiner Form vervielfältigt werden noch an Dritte weitergegeben werden.
Es gilt nur für den persönlichen Gebrauch.

5.1.13 {[$Ni_2Dy(L^1)_2$]·(NO_3)(MeOH)·(H_2O)} (13).

Chemical formula	$C_{61}H_{72}DyN_9Ni_2O_{17}$
Formula mass	1483.14
Crystal system	Monoclinic
Space group	$P2_1/n$
a/Å, b/Å, c/Å	13.574(3), 27.231(5), 17.588(4)
β/°	91.21(3)
Unit cell volume/$Å^3$	6500(2)
Temperature/K	100
No. of formula units per unit cell, Z	4
Absorption coefficient, μ/mm^{-1}	1.785
No. of reflections measured	79802
No. of independent reflections	12114
R_{int}	0.1086
Final R1values (I >2σ(I))	0.0669
Final wR_2values (all data)	0.1834
Goodness of fit	1.088

5.1.14 {[$Dy_4(L^2)_3(Ph_2acac)_4$](Et_3NH)·4(MeOH)·(MeCN)·(H_2O)} (14).

Chemical formula	$C_{144}H_{144}Dy_4N_8O_{22}$
Formula mass	2988.66
Crystal system	Triclinic
Space group	*P*-1
a/Å, b/Å, c/Å	12.229(2), 19.215(4), 29.152(6)
α/°, β/°, γ/°	104.58(3)°, 96.87(3)°, 95.90(3)°,
Unit cell volume/$Å^3$	6519.0(2)
Temperature/K	150(2)
No. of formula units per unit cell, Z	2
Absorption coefficient, μ/mm^{-1}	2.338
No. of reflections measured	61771
No. of independent reflections	23782
R_{int}	0.0768
Final R1values (I >2σ(I))	0.0412
Final wR_2values (all data)	0.0811
Goodness of fit	0.891

Dieses Werk ist copyrightgeschützt und darf in keiner Form vervielfältigt werden noch an Dritte weitergegeben werden.
Es gilt nur für den persönlichen Gebrauch.

5.1.15 {[$Tb_5(\mu_3\text{-}OH)_2(L^2)_2(Ph_2acac)_7(Ph_2acacH)$]·7(PhMe)} (15).

Chemical formula	$C_{217}H_{189}N_4O_{24}Tb_5$
Formula mass	4031.45
Crystal system	Monoclinic
Space group	*C2/c*
a/Å, b/Å, c/Å	42.715(16), 28.526(6), 34.279(7)
β/°	123.14
Unit cell volume/$Å^3$	34974(18)
Temperature/K	150(2)
No. of formula units per unit cell, Z	8
Absorption coefficient, μ/mm^{-1}	2.066
No. of reflections measured	405628
No. of independent reflections	37242
R_{int}	0.1085
Final R1values (I >2σ(I))	0.0516
Final wR_2values (all data)	0.1408
Goodness of fit	1.048

5.1.16 {[$Dy_5(\mu_3\text{-}OH)_2(L^2)_2((Ph_2acac)_7(Ph_2acacH)$]·7(PhMe)} (16).

Chemical formula	$C_{217}H_{189}N_4O_{24}Dy_5$
Formula mass	4049.33
Crystal system	Monoclinic
Space group	*C2/c*
a/Å, b/Å, c/Å	42.6(6), 28.4441(11), 34.0627(6)
β/°	123.3(10)
Unit cell volume/$Å^3$	34497(58)
Temperature/K	100(2)
No. of formula units per unit cell, Z	8
Absorption coefficient, μ/mm^{-1}	2.210
No. of reflections measured	90805
No. of independent reflections	32037
R_{int}	0.1085
Final R1values (I >2σ(I))	0.0552
Final wR_2values (all data)	0.1432
Goodness of fit	0.996

Dieses Werk ist copyrightgeschützt und darf in keiner Form vervielfältigt werden noch an Dritte weitergegeben werden.
Es gilt nur für den persönlichen Gebrauch.

5.1.17 {[$Tb_4(\mu_3\text{-}OH)_2(L^2)(HL^2)(acac)_5(H_2O)]\cdot(NO_3)\cdot(HNEt_3)\cdot 2(Et_2O)$} (17).

Chemical formula	$C_{87}H_{118}N_6O_{24}Tb_4$
Formula mass	2267.55
Crystal system	Triclinic
Space group	*P-1*
a/Å, b/Å, c/Å	13.9775(5), 17.7557(5), 21.8287(8)
α/°, β/°, γ/°	68.762(2), 85.665(3), 72.449(2)
Unit cell volume/Å^3	4811.0(3)
Temperature/K	150
No. of formula units per unit cell, Z	2
Absorption coefficient, μ/mm^{-1}	2.975
No. of reflections measured	31657
No. of independent reflections	16371
R_{int}	0.1350
Final R1values (I >2σ(I))	0.0815
Final wR_2values (all data)	0.1652
Goodness of fit	0.902

5.1.18 {[$Dy_4(\mu_3\text{-}OH)_2(L^2)(HL^2)(acac)_5(H_2O)]\cdot(NO_3)\cdot(HNEt_3)\cdot 2(Et_2O)$} (18).

Chemical formula	$C_{87}H_{118}N_6O_{24}Dy_4$
Formula mass	2281.87
Crystal system	Triclinic
Space group	*P-1*
a/Å, b/Å, c/Å	13.9386(5), 17.7302(5), 21.7811(8)
α/°, β/°, γ/°	68.213(2), 85.236(3), 72.539(2)
Unit cell volume/Å^3	4765.6(3)
Temperature/K	150
No. of formula units per unit cell, Z	2
Absorption coefficient, μ/mm^{-1}	3.172
No. of reflections measured	29926
No. of independent reflections	15531
R_{int}	0.0529
Final R1values (I >2σ(I))	0.0401
Final wR_2values (all data)	0.0743
Goodness of fit	0.775

Dieses Werk ist copyrightgeschützt und darf in keiner Form vervielfältigt werden noch an Dritte weitergegeben werden.
Es gilt nur für den persönlichen Gebrauch.

5.1.19 {[$Ho_4(\mu_3\text{-}OH)_2(L^2)(HL^2)(acac)_5(H_2O)]\cdot(NO_3)\cdot(HNEt_3)\cdot 2(Et_2O)$} (19).

Chemical formula	$C_{87}H_{118}N_6O_{24}Ho_4$
Formula mass	2291.61
Crystal system	Triclinic
Space group	*P-1*
a/Å, b/Å, c/Å	13.9761(5), 17.7491(5), 21.7385(8)
α/°, β/°, γ/°	68.770(2), 85.545(3), 72.455(2)
Unit cell volume/Å^3	4789.7(3)
Temperature/K	150
No. of formula units per unit cell, Z	2
Absorption coefficient, μ/mm^{-1}	3.339
No. of reflections measured	46201
No. of independent reflections	16619
R_{int}	0.1522
Final R1values (I >2σ(I))	0.0783
Final wR_2values (all data)	0.1694
Goodness of fit	0.936

5.1.20 {[$Er_4(\mu_3\text{-}OH)_2(L^2)(HL^2)(acac)_5(H_2O)]\cdot(NO_3)\cdot(HNEt_3)\cdot 2(Et_2O)$} (20).

Chemical formula	$C_{87}H_{118}N_6O_{24}Er_4$
Formula mass	2300.89
Crystal system	Triclinic
Space group	*P-1*
a/Å, b/Å, c/Å	13.961(3), 17.703(4), 21.717(4)
α/°, β/°, γ/°	68.27(3), 85.26(3), 72.44(3)
Unit cell volume/Å^3	4751(2)
Temperature/K	120
No. of formula units per unit cell, Z	2
Absorption coefficient, μ/mm^{-1}	3.569
No. of reflections measured	69512
No. of independent reflections	37666
R_{int}	0.1021
Final R1values (I >2σ(I))	0.0634
Final wR_2values (all data)	0.1326
Goodness of fit	0.862

Dieses Werk ist copyrightgeschützt und darf in keiner Form vervielfältigt werden noch an Dritte weitergegeben werden.
Es gilt nur für den persönlichen Gebrauch.

5.1.21 {[$Tm_4(\mu_3\text{-}OH)_2(L^2)(HL^2)(acac)_5(H_2O)$]·($NO_3$)·($HNEt_3$)·2($Et_2O$)} (21).

Chemical formula	$C_{87}H_{118}N_6O_{24}Tm_4$
Formula mass	2307.63
Crystal system	Triclinic
Space group	*P-1*
a/Å, b/Å, c/Å	13.9186(5), 17.6449(5), 21.6536(8)
α/°, β/°, γ/°	68.463(2), 85.537(3), 72.381(2)
Unit cell volume/Å^3	4711.3(3)
Temperature/K	100
No. of formula units per unit cell, Z	2
Absorption coefficient, μ/mm^{-1}	3.802
No. of reflections measured	101737
No. of independent reflections	16606
R_{int}	0.1169
Final R1values (I >2σ(I))	0.0350
Final wR_2values (all data)	0.0903
Goodness of fit	1.022

5.1.22 {[$Dy_4(\mu_4\text{-}OH)(L^2)_2(acac)_4(MeOH)_2(EtOH)(H_2O)$]·($NO_3$)·2(MeOH)·3(EtOH)} (22).

Chemical formula	$C_{80}H_{112}Dy_4N_5O_{27}$
Formula mass	2225.72
Crystal system	orthorhombic
Space group	*Pna2$_1$*
a/Å, b/Å, c/Å	31.154(6), 11.549(2), 24.197(5)
Unit cell volume/Å^3	8706(3)
Temperature/K	100
No. of formula units per unit cell, Z	4
Absorption coefficient, μ/mm^{-1}	3.472
No. of reflections measured	44012
No. of independent reflections	14746
R_{int}	0.0843
Final R1values (I >2σ(I))	0.0555
Final wR_2values (all data)	0.1419
Goodness of fit	0.979

Dieses Werk ist copyrightgeschützt und darf in keiner Form vervielfältigt werden noch an Dritte weitergegeben werden.
Es gilt nur für den persönlichen Gebrauch.

5.1.23 {[$Dy_5(\mu_5\text{-}NO_3)(L^2)(L^{2a})_2(acac)_6(iPrOH)_2(HO)(H_2O)]\cdot 4(H_2O)$} (23).

Chemical formula	$C_{106}H_{136}Dy_5N_5O_{34}$
Formula mass	2836.62
Crystal system	orthorhombic
Space group	*Pbcn*
a/Å, b/Å, c/Å	16.782(3), 32.447(7), 23.459(5)
Unit cell volume/Å^3	12774(4)
Temperature/K	150
No. of formula units per unit cell, Z	4
Absorption coefficient, μ/mm^{-1}	2.959
No. of reflections measured	39361
No. of independent reflections	12399
R_{int}	0.0699
Final R1values (I >2σ(I))	0.0449
Final wR_2values (all data)	0.1266
Goodness of fit	0.818

5.1.24 {[$Tb(Ph_2acac)_4]\cdot(Et_3NH)$} (24).

Chemical formula	$C_{66}H_{60}NO_8Tb$
Formula mass	1154.07
Crystal system	Monoclinic
Space group	*Pc*
a/Å, b/Å, c/Å	25.117(5), 8.9748(18), 27.450(6)
β/°	112.44(3)
Unit cell volume/Å^3	5719(2)
Temperature/K	150
No. of formula units per unit cell, Z	4
Absorption coefficient, μ/mm^{-1}	1.292
No. of reflections measured	43343
No. of independent reflections	20339
R_{int}	0.0584
Final R1values (I >2σ(I))	0.0341
Final wR_2values (all data)	0.0806
Goodness of fit	0.939

Dieses Werk ist copyrightgeschützt und darf in keiner Form vervielfältigt werden noch an Dritte weitergegeben werden.
Es gilt nur für den persönlichen Gebrauch.

5.1.25 {[Dy(Ph$_2$acac)$_4$]$_2$·2(Et$_3$NH)·3(CH$_2$Cl$_2$)} (25).

Chemical formula	$C_{135}H_{126}Cl_6Dy_2N_2O_{16}$
Formula mass	2570.07
Crystal system	Monoclinic
Space group	*C2/c*
a/Å, b/Å, c/Å	35.757(7), 17.628(4), 25.201(5)
β/°	131.15(3)
Unit cell volume/Å^3	11962(6)
Temperature/K	150
No. of formula units per unit cell, Z	4
Absorption coefficient, μ/mm^{-1}	1.440
No. of reflections measured	36501
No. of independent reflections	11755
R_{int}	0.0489
Final R1values (I >2σ(I))	0.0279
Final wR_2values (all data)	0.0592
Goodness of fit	0.835

5.1.26 {[Dy$_5$(μ$_3$-OH)$_2$(L^2)$_3$(Ph$_2$acac)$_4$(MeOH)$_4$]·4(MeOH)} (26).

Chemical formula	$C_{140}H_{138}Dy_5N_6O_{27}$
Formula mass	3149.11
Crystal system	orthorhombic
Space group	*Pbca*
a/Å, b/Å, c/Å	27.378(6), 29.921(6), 32.547(7)
Unit cell volume/Å^3	26662(9)
Temperature/K	150
No. of formula units per unit cell, Z	8
Absorption coefficient, μ/mm^{-1}	2.841
No. of reflections measured	90588
No. of independent reflections	23834
R_{int}	0.0865
Final R1values (I >2σ(I))	0.0469
Final wR_2values (all data)	0.0870
Goodness of fit	0.868

□ieses □ er□ist c□p□rightgeschütt□t und darf in □einer □□r□ □er□ielf□ltigt □erden n□ch an □ritte □eitergegeben □erden.
Es gilt nur für den persönlichen Gebrauch.

5.1.27{[$Tb_7(\mu_3\text{-}OH)_2(\mu_5\text{-}NO_3)(\mu_3\text{-}NO_3)(L^2)_3(Ph_2acac)_5(H_2N\text{-}PhO)(MeO)_2(MeOH)_3$]·3(MeOH)·(MeCN)·15($H_2O$) (27).

Chemical formula	$C_{163}H_{188}N_{10}O_{51}Tb_7$
Formula mass	4214.46
Crystal system	Monoclinic
Space group	*$P2_1/c$*
a/Å, b/Å, c/Å	22.245(4), 28.913(6), 27.360(5)
β/°	94.40(3)
Unit cell volume/$Å^3$	17545(6)
Temperature/K	200
No. of formula units per unit cell, Z	4
Absorption coefficient, μ/mm^{-1}	2.864
No. of reflections measured	107786
No. of independent reflections	37054
R_{int}	0.1690
Final R1values (I >2σ(I))	0.0846
Final wR_2values (all data)	0.2155
Goodness of fit	0.883

5.1.28 {[Dy_2L_3]·3(OH)·6(H_2O)·(C_6H_{12})}(28).

Chemical formula	$C_{78}H_{96}Dy_2N_{18}O_{18}$
Formula mass	1898.70
Crystal system	Monoclinic
Space group	*C2/c*
a/Å, b/Å, c/Å	12.933(3), 26.701(5), 26.623(5)
β/°	93.27(3)
Unit cell volume/$Å^3$	9179(3)
Temperature/K	200
No. of formula units per unit cell, Z	4
Absorption coefficient, μ/mm^{-1}	1.686
No. of reflections measured	39721
No. of independent reflections	8547
R_{int}	0.0615
Final R1values (I >2σ(I))	0.0392
Final wR_2values (all data)	0.1131
Goodness of fit	0.954

□ieses □ er□ist c□p□rightgeschütt□t und darf in □einer □□r□ □er□ielf□ltigt □erden n□ch an □ritte □eitergegeben □erden.
Es gilt nur für den persönlichen Gebrauch.

5.1.29 {[$Dy_2L_3(OH)$]·[$Dy(NO_3)_3(H_2O)_3$]·3(Py)·2(HO)·7(H_2O)·6(MeOH)·($CHCl_3$)} (29).

Chemical formula	$C_{94}H_{132}Cl_3Dy_3N_{24}O_{37}$
Formula mass	2784.05
Crystal system	Triclinic
Space group	*P1*
a/Å, b/Å, c/Å	16.742(2), 16.742(2), 13.056(3)
α/°, β/°, γ/°	90, 90, 120
Unit cell volume/Å^3	3169.1(9)
Temperature/K	295
No. of formula units per unit cell, Z	1
Absorption coefficient, μ/mm^{-1}	1.893
No. of reflections measured	52338
No. of independent reflections	24870
R_{int}	0.0863
Final R1values (I >2σ(I))	0.0579
Final wR_2values (all data)	0.1455
Goodness of fit	0.979

5.1.30 {[$Dy_2L_3(H_2O)$][$Dy(NO_3)(H_2O)_7$]·5(NO_3)·3(MeOH)·7(H_2O)} (30).

Chemical formula	$C_{75}H_{110}Dy_3N_{24}O_{45}$
Formula mass	2555.31
Crystal system	Triclinic
Space group	*P-1*
a/Å, b/Å, c/Å	12.843(3), 19.472(4), 21.186(4)
α/°, β/°, γ/°	92.95(3), 90.32(3), 90.30(3)
Unit cell volume/Å^3	5291.0(18)
Temperature/K	150
No. of formula units per unit cell, Z	2
Absorption coefficient, μ/mm^{-1}	2.194
No. of reflections measured	48558
No. of independent reflections	23072
R_{int}	0.0514
Final R1values (I >2σ(I))	0.0484
Final wR_2values (all data)	0.1276
Goodness of fit	0.841

□ieses □ er□ist c□p□rightgeschütt□t und darf in □einer □□r□ □er□ielf□ltigt □erden n□ch an □ritte □eitergegeben □erden.
Es gilt nur für den persönlichen Gebrauch.

5.1.31 $\{[Pr_2(MnLClNO_3)_2(dmf)_6(H_2O)_2]\cdot(H_2O)\}_n$ (31).

Chemical formula	$C_{62}H_{84}Cl_2Mn_2N_{12}O_{27}Pr_2$
Formula mass	1891.99
Crystal system	Monoclinic
Space group	*C2*
a/Å, b/Å, c/Å	32.726(7), 10.721(2), 25.497(5)
β/°	114.88(3)
Unit cell volume/Å^3	8116(3)
Temperature/K	150
No. of formula units per unit cell, Z	4
Absorption coefficient, μ/mm^{-1}	1.629
No. of reflections measured	58171
No. of independent reflections	17201
R_{int}	0.0400
Final R1values (I >2σ(I))	0.0744
Final wR_2values (all data)	0.1860
Goodness of fit	1.270

5.1.32 $\{[Nd_2(MnLClNO_3)_2(dmf)_6(H_2O)_2]\cdot(H_2O)\}_n$ (32).

Chemical formula	$C_{62}H_{84}Cl_2Mn_2N_{12}O_{27}Nd_2$
Formula mass	1898.65
Crystal system	Monoclinic
Space group	*C2*
a/Å, b/Å, c/Å	32.768(7), 10.801(2), 25.553(5)
β/°	114.82(3)
Unit cell volume/Å^3	8208(3)
Temperature/K	190
No. of formula units per unit cell, Z	4
Absorption coefficient, μ/mm^{-1}	1.688
No. of reflections measured	45633
No. of independent reflections	16582
R_{int}	0.1013
Final R1values (I >2σ(I))	0.0805
Final wR_2values (all data)	0.1691
Goodness of fit	0.974

□ieses □ er□ist c□p□rightgeschütt□t und darf in □einer □□r□ □er□ielf□ltigt □erden n□ch an □ritte □eitergegeben □erden.
Es gilt nur für den persönlichen Gebrauch.

5.1.33 $\{[Sm_2(MnLClNO_3)_2(dmf)_6(H_2O)_2]\cdot(H_2O)\}_n$ (33).

Chemical formula	$C_{62}H_{84}Cl_2Mn_2N_{12}O_{27}Sm_2$
Formula mass	1910.89
Crystal system	Monoclinic
Space group	*C2*
a/Å, b/Å, c/Å	32.570(7), 10.734(2), 25.464(5)
β/°	114.71(3)
Unit cell volume/Å^3	8087(3)
Temperature/K	150
No. of formula units per unit cell, Z	4
Absorption coefficient, μ/mm^{-1}	1.882
No. of reflections measured	31488
No. of independent reflections	17138
R_{int}	0.0581
Final R1values (I >2σ(I))	0.0969
Final wR_2values (all data)	0.2391
Goodness of fit	1.204

5.1.34 $\{[Gd_2(MnLClNO_3)_2(dmf)_6(H_2O)_2]\cdot(H_2O)\}_n$ (34).

Chemical formula	$C_{62}H_{84}Cl_2Mn_2N_{12}O_{27}Gd_2$
Formula mass	1924.67
Crystal system	Monoclinic
Space group	*C2*
a/Å, b/Å, c/Å	32.393(7), 10.749(2), 25.390(5)
β/°	114.29(3)
Unit cell volume/Å^3	8058(3)
Temperature/K	150
No. of formula units per unit cell, Z	4
Absorption coefficient, μ/mm^{-1}	2.077
No. of reflections measured	138229
No. of independent reflections	21739
R_{int}	0.0578
Final R1values (I >2σ(I))	0.0642
Final wR_2values (all data)	0.1764
Goodness of fit	1.048

□ieses □ er□ist c□p□rightgeschütt□t und darf in □einer □□r□ □er□ielf□ltigt □erden n□ch an □ritte □eitergegeben □erden.
Es gilt nur für den persönlichen Gebrauch.

6 Summary/ Zusammenfassung

6.1 Summary

This work explored the synthesis of homo- and heterometallic complexes of transition and rare earth metals. Various novel compounds were synthesized by using the Schiff bases ligands and investigated for magnetic, luminescent and catalytic properties. The Schiff bases used in this work are 2-aminoethyl-hydroxybenzoic acid (H_2L), 2-hydroxy-3-(pyridine-4-carbonyl)-hydrazonomethyl-benzoic acid (H_2L^1), tris-((2-hydroxybenzyliden)-aminoethyl)amine (H_3L), tris-((2-hydroxy-3-methoxybenzyliden)-aminoethyl)amine (H_3L^1), 4-tert-butyl-2,6-bis-[(2-hydroxy-phenylimino)-methyl]-phenol (H_3L^2), (3-{5-tert-butyl-2-hydroxy-3-[(2-hydroxy-phenylimino)-methyl]-benzy-lidene}-pentane-2,4-dione) (H_2L^{2a}), 4-tert-butyl-2,6-bis-[(pyridine-4-cabonyl)-hydrazonomethyl]-phenol (HL) and *N,N'*-bis(4-carboxysalicylidene)cyclohexanediamine (H_4L).

By using the proligand H_2L, five new rare earth compounds were obtained as single crystalline material. These included the mononuclear complexes {[Y(HL)$_4$][ETAH]·(H_2O)} (**1**) and {[Dy(HL)$_4$][ETAH]·(3MeOH)·(H_2O)} (**2**), and the tetranuclear complexes {[Y_4(HL)$_2$(L)$_4$(μ_3-OH)$_2$]·4(MeOH)·4(H_2O)} (**3**), {[Dy_4(HL)$_2$(L)$_4$(μ_3-OH)$_2$]·5(MeOH)$_2$·7(H_2O)} (**4**) and {[Dy_4(HL)$_8$(L)$_2$]·4(MeOH)·2(H_2O)} (**5**). The clusters are either in a butterfly or in a rectangular scaffold arrangement. The proligand H_2L exhibits fluorescence and all of the all yttrium complexes also show fluorescence with quantum yields of up to 13%. In contrast, the dysprosium compound **4** only shows weak fluorescence due to quenching effects. The dysprosium compounds were explored for magnetic studies, the tetranuclear compound **4,** which has a butterfly structure, shows SMM behaviour with two relaxation processes; one with an effective energy barrier of U_{eff} = 84 cm^{-1} and a pre-exponential factor of τ_0 = 5.1 10^{-9} s, other fast relaxation with an effective energy barrier U_{eff} = 3 cm^{-1} and pre-exponential factor τ_0 = 2.5 10^{-3} s. In contrast to compound **4**, the mononuclear compound **2** and the tetranuclear compound **5,** which has a rectangular arrangement, do not show slow relaxation of the magnetization.

From the proligand H_2L^1, the mononuclear compound {[Dy(HL^1)$_2$(H_2O)$_3$](NO_3)} (**6**) was obtained as single crystalline material. This compound shows significant intermolecular and intramolecular hydrogen bonding.

The proligands H_3L and H_3L^1 were used for the synthesis of seven new Ni-Ln compounds. Four binuclear compounds containing (L^{3-}) were obtained {NiGdL(acac)$_2$} (**7**), {NiTbL(acac)$_2$} (**8**), {[NiDyL(acac)$_2$]$_2$·7(MeOH)} (**9**) and {[NiDyL(Ph_2acac)$_2$]$_2$·4(CH_2Cl_2)·(MeOH)} (**10**). The remaining three trinuclear compounds are ligated by the corresponding methoxy derivative of the

□ieses □ er□ist c□p□rightgeschütt□t und darf in □einer □□r□ □er□ielf□ltigt □erden n□ch an □ritte □eitergegeben □erden.
Es gilt nur für den persönlichen Gebrauch.

ligand $(L^1)^{3-}$. They are $\{[Ni_2Gd(L^1)_2]\cdot(NO_3)\cdot 2(H_2O)\}$ (**11**), $\{[Ni_2Tb(L^1)_2]_4\cdot 4(NO_3)\cdot 3(MeCN)\cdot 5(MeOH)\cdot(H_2O)\}$ (**12**), and $\{[Ni_2Dy(L^1)_2]\cdot(NO_3)\cdot(MeOH)\cdot(H_2O)\}$ (**13**). The lanthanide contraction was observed in all these binuclear and trinuclear compounds. In the binuclear compounds, the lanthanide ions are seven-coordinate, whereas in the trinuclear complexes the lanthanide ions are six-coordinate and have an interaction with the methoxy group of the Schiff base ligand. The coordination environment around the nickel ions is similar in all compounds.

The proligand H_3L^2 was used with dibenzoylmethane to obtain three new rare earth compounds: $\{[Dy_4(L^2)_3(Ph_2acac)_4](Et_3NH)\cdot 4(MeOH)\cdot(MeCN)\cdot(H_2O)\}$ (**14**) and $\{[Ln_5(\mu_3\text{-}OH)_2(L^2)_2(Ph_2acac)_7(Ph_2acacH)]\cdot 7(PhMe)\}$ Ln = Tb (**15**), Dy (**16**). The tetranuclear compound **14** shows a precisely linear arrangement of four dysprosium ions, while the pentanuclear compounds **15** and **16** are isostructural with each other and feature a delta wing shaped arrangement of five lanthanide ions. Compounds **14** and **15** show weak ferromagnetic interactions, whereas compound **16** exhibits antiferromagnteic interactions between neighboring metal ions. In addition, compound **14** shows the SMM behavior with the application of an external dc field.

The proligands H_3L^2 and H_3L^{2a} were used with acetylacetone to obtain seven new rare earth compounds. Five of the tetranuclear compounds, $\{[Ln_4(\mu_3\text{-}OH)_2(L^2)(HL^2)(acac)_5(H_2O)]\cdot(NO_3)\cdot(HNEt_3)\cdot 2(Et_2O)\}$ (Ln = Tb (**17**), Dy (**18**), Ho (**19**), Er (**20**), Tm (**21**)) were found to have a see saw shaped arrangement of metal ions. Another tetranuclear compound $\{[Dy_4(\mu_4\text{-}OH)(L^2)_2(acac)_4(MeOH)_2(EtOH)(H_2O)]\cdot(NO_3)\cdot 2(MeOH)\cdot 3(EtOH)\}$ (**22**) adopts a square planar grid arrangement. The pentanuclear compound $\{[Dy_5(\mu_5\text{-}NO_3)(L^2)(L^{2a})_2(acac)_6(iPrOH)_2(H_2O)(OH)]\cdot 4(H_2O)\}$ (**23**) has a unique pentagonal planar arrangement of the dysprosium ions in which a central nitrate ion is coordinated to all of the dysprosium ions. Magnetic studies of compounds **17**, **18**, **19** and **23** suggest weak antiferromagnetic interactions between neighbouring metal ions and no slow relaxation of the magnetization was observed to 1.8 K.

By using dibenzoylmethane as a proligand in synthesis, two mononuclear compounds $\{[Tb(Ph_2acac)_4]\cdot(Et_3NH)\}$ (**24**), and $\{[Dy(Ph_2acac)_4]_2\cdot 2(Et_3NH)\cdot 3(CH_2Cl_2)\}$ (**25**), were obtained. When dibenzoylmethane was used together with the H_3L^2 proligand, the pentanuclear compound $\{[Dy_5(\mu_3\text{-}OH)_2(L^2)_3(Ph_2acac)_4(MeOH)_4]\cdot 4(MeOH)\}$ (**26**) and the heptanuclear compound $\{[Tb_7(\mu_3\text{-}OH)_2(\mu_5\text{-}NO_3)(\mu_3\text{-}NO_3)(L^2)_3(Ph_2acac)_5(H_2N\text{-}Ph\text{-}O)(MeO)_2(MeOH)_3]\cdot 3(MeOH)\cdot(MeCN)\cdot 15(H_2O)$ (**27**) were obtained. The pentanuclear and heptanuclear compounds are unique in the structural arrangement of the metal ions and their different solubilities played an important role in separating them. The mononuclear terbium compound **24** shows the SMM behavior with a relaxation time of τ_0 = 1.1 10^{-4} s and an energy barrier of U_{eff} = 8.53 cm^{-1}. The mononuclear dysprosium compound **25**

□ieses □ er□ist c□p□rightgeschütt□t und darf in □einer □□r□ □er□ielf□ltigt □erden n□ch an □ritte □eitergegeben □erden.
Es gilt nur für den persönlichen Gebrauch.

shows SMM behavior with a relaxation time of τ_0 = 3.9 10^{-5} s and an energy barrier of U_{eff} = 3.94 cm^{-1}. A thermally activated relaxation mechanism was assigned for compounds **24** and **25**. The pentanuclear compound **26** shows SMM behavior under a weak external dc field, whereas the heptanuclear compound **27** shows weak antiferromagnetic interactions with no slow relaxation of the magnetization.

The proligand HL was used for the synthesis of the binuclear complex {$[Dy_2L_3]\cdot 3(OH)\cdot 6(H_2O)\cdot(C_6H_{12})$} (**28)** and the trinuclear complexes {$[Dy_2L_3(OH)]\cdot[Dy(NO_3)_3\ (H_2O)_3]\cdot 3(Py)\cdot 2(HO)\cdot 7(H_2O)\cdot 6(MeOH)\cdot(CHCl_3)$} (**29**), and {$[Dy_2L_3(H_2O)]\cdot[Dy(NO_3)(H_2O)_7]\cdot\ 5(NO_3)\cdot 3(MeOH)\cdot 7(H_2O)$} (**30**). The binuclear cationic unit $[Dy_2L_3]$ has similar in bonding parameters in all compounds. It consists of three ligands which twist along a pseudo-threefold axis and form a unique triple-stranded helical structure.

Four new 1D-cordination polymers were synthesized using solvothermal process. The reactions of the salen ligand (H_4L) with $MnCl_2\cdot 4(H_2O)$ and $Ln(NO_3)_3\cdot xH_2O$ led to the formation of the 1D-cordination polymers $\{[Ln_2(MnLClNO_3)_2(dmf)_6(H_2O)_2]\cdot(H_2O)\}_n$ (Ln = Pr (**31**), Nd (**32**), Sm (**33**) and Gd (**34**)). TGA studies of compound **34** proved the stability of the polymer. Catalytic studies of compounds **31-34** suggest that they are active for the sulfoxidation of alkyl and aryl sulphides in the presence of the oxidizing agent iodosobenzene. The heterogeneous nature of the catalytic process was demonstrated by a simple filtration test. The powder diffraction patterns of compound **34** before and after the catalysis were found to be similar suggesting that compounds **31-34** could be reused for catalysis without significant loss of structural arrangement.

□ieses □ er□ist c□p□rightgeschütt□t und darf in □einer □□r□ □er□ielf□ltigt □erden n□ch an □ritte □eitergegeben □erden.
Es gilt nur für den persönlichen Gebrauch.

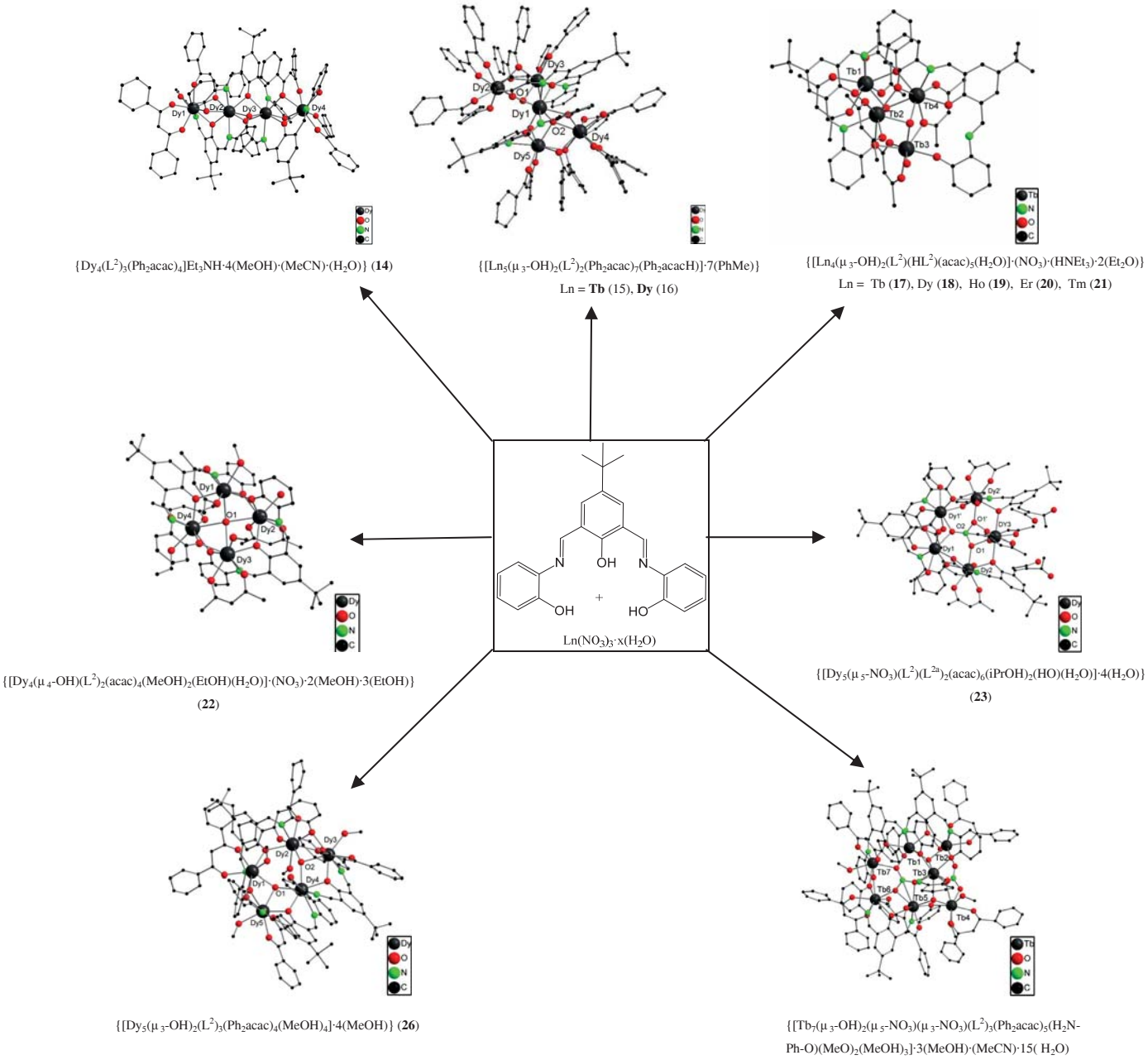

Scheme 6.1 A brief summary of compounds which were synthesized by the H_3L^2 proligand.

□ieses □ er□ist c□p□rightgeschütt□t und darf in □einer □□r□ □er□ielf□ltigt □erden n□ch an □ritte □eitergegeben □erden.
Es gilt nur für den persönlichen Gebrauch.

6.2 Zusammenfassung

Diese Arbeit befasst sich mit der Synthese homo- und heterometallischer Komplexe der Übergangs- sowie der Seltenerdmetalle. Verschiedene neuartige Verbindungen wurden durch Verwendung Schiff´scher Basen als Ligand hergestellt und auf ihre magnetischen, lumineszierenden und katalytischen Eigenschaften untersucht. Bei den in dieser Arbeit verwendeten Schiff´schen Basen handelt es sich um die 2-Aminoethyl-hydroxybenzoylsäure (H_2L^1), Tris-((2-hydroxybenzyliden)-aminoethyl)amin (H_3L), Tris-((2-hydroxy-3-methoxybenzyliden)-aminoethyl)amin (H_3L^1), 4-Tert-butyl-2,6-bis-[(2-hydroxy-phenylimino)-methyl]-phenol (H_3L^2), (3-{5-Tert-butyl-2-hydroxy-3-[(2-hydroxy-phenylimino)-methyl]-benzyliden}-pentan-2,4-dion) (H_2L^{2a}), 4-Tert-butyl-2,6-bis-[(pyridin-4-cabonyl)-hydrazonomethyl]-phenol (HL) und *N,N′*-bis(4-carboxysalicyliden)cyclohexandiamin (H_4L).

Durch Verwendung des Proliganden H_2L, konnten fünf neue Seltenerdverbindungen als kristallines Material erhalten werden. Diese beinhalten die mononuklearen Komplexe {[$Y(HL)_4$][ETAH]·(H_2O)} (**1**) und {[$Dy(HL)_4$] [ETAH]·(3MeOH)·(H_2O)} (**2**), und die tetranuklearen Komplexe {[$Y_4(HL)_2(L)_4(\mu_3\text{-}OH)_2$]·4(MeOH)·4($H_2O$)} (**3**), {[$Dy_4(HL)_2(L)_4(\mu_3\text{-}OH)_2$]·5$(MeOH)_2$·7($H_2O$)} (**4**) und {[$Dy_4(HL)_8(L)_2$]·4(MeOH)·2($H_2O$)} (**5**) Verbindungen. Die Cluster nehmen entweder eine Schmetterlings- oder eine rechteckige Anordnung des Grundgerüsts ein. Der Proligand H_2L sowie alle Yttriumkomplexe zeigen Fluoreszenz mit Quantenausbeuten bis zu 13 %. Im Gegensatz dazu zeigt die Dysprosiumverbindung **4** nur schwache Fluoreszenz aufgrund von auslöschenden Effekten. Die Dysprosiumverbindung **4** wurde hinsichtlich ihrer magnetischen Eigenschaften untersucht. Die tetranukleare Verbindung **4**, welche eine Schmetterlingsstruktur besitzt, zeigt SMM Verhalten mit zwei Relaxationsprozessen. Einer mit einer effektiven Energiebarriere U_{eff} = 84 cm^{-1} und einem präexponentiellen Faktor τ_0 = 5.1 10^{-9} s, der andere mit einer schnellen Relaxation mit einer effektiven Energiebarriere U_{eff} = 3 cm^{-1} und einem präexponentiellen Faktor τ_0 = 2.5 10^{-3} s. Im Gegensatz zu der tetranuklearen Verbindung **4**, zeigen die mononukleare Verbindung **2** und die tetranukleare Verbindung **5**, welche beide eine rechteckige Anordnung besitzen, keine langsame Relaxation der Magnetisierung.

Durch Verwendung des Proliganden H_2L^1 wurde die mononukleare Verbindung {[$Dy(HL^1)_2(H_2O)_3$](NO_3)}(**6**) als einkristallines Material erhalten. Diese Verbindung zeigt signifikante inter- und intramolekulare Wasserstoffbrückenbindungen.

Die Proliganden H_3L und H_3L^1 wurden zur Synthese von sieben neuen Ni-Ln Verbindungen verwendet. Vier binukleare Verbindungen, die den Liganden L^3 enthalten, konnten erhalten werden: {$NiGdL(acac)_2$} (**7**), {$NiTbL(acac)_2$} (**8**), {[$NiDyL(acac)_2]_2$·7(MeOH)} (**9**), {[$NiDyL(Phacac)_2]_2$·

□ieses □ er□ist c□p□rightgeschütt□t und darf in □einer □□r□ □er□ielf□ltigt □erden n□ch an □ritte □eitergegeben □erden.
Es gilt nur für den persönlichen Gebrauch.

$4(CH_2Cl_2)\cdot(MeOH)\}$ (**10**). Die restlichen drei trinuklearen Verbindungen bestehen aus dem entsprechendem Methoxyderivat des Liganden $(L^1)^{3-}$. Diese sind $\{[Ni_2Gd(L^1)_2]\cdot(NO_3)\cdot 2(H_2O)\}$(**11**), $\{[Ni_2Tb(L^1)_2]_4\cdot 4(NO_3)\cdot 3(MeCN)\cdot 5(MeOH)\cdot(H_2O)\}$ (**12**), $\{[Ni_2Dy(L^1)_2]\cdot(NO_3)\cdot(MeOH)\cdot (H_2O)\}$(**13**). In all diesen bi- und trinuklearen Verbindungen wurden Effekte der Lanthanoidenkontraktion beobachtet. In den binuklearen Komplexen sind die Lanthanoidionen siebenfach koordiniert. In den dreikernigen Komplexen sind die Lanthanoidionen sechsfach koordiniert und wechselwirken mit den Methoxygruppen der Schiffbase. Die Umgebung in der Nähe des Nickelions ist in allen Verbindungen ähnlich.

Der Proligand H_3L^2 wurde zusammen mit Dibenzoylmethan verwendet um drei neue Seltenerdverbindungen $\{Dy_4(L^2)_3(Ph_2acac)_4](Et_3NH)\cdot 4(MeOH)\cdot(MeCN)\cdot(H_2O)\}$(**14**), $\{[Tb_5(\mu_3\text{-}OH)_2(L^2)_2(Ph_2acac)_7(Ph_2acacH)]\cdot 7(PhMe)\}$(**15**), und $\{[Dy_5(\mu_3\text{-}OH)_2(L^2)_2((Ph_2acac)_7(Ph_2acacH)]\cdot 7(PhMe)\}$(**16**) zu erhalten. Die tetranukleare Verbindung **14** zeigt eine präzise lineare Anordnung der vier Dysprosiumionen. Die beiden fünfkernigen Verbindungen **15** und **16** sind isostruktruell, wobei sich die fünf Lanthanoidionen in Form eines Deltaflügels anordnen. Die Verbindungen **14** und **15** zeigen schwache ferromagnetische Wechselwirkungen, wohingegen bei Verbindung **16** antiferromagnetische Wechselwirkungen zwischen den benachbarten Metallionen beobachtet werden. Zusätzlich zeigt Verbindung **14** durch Anlegen eines externen Gleichfelds SMM Verhalten.

Die Proliganden H_3L^2 und H_3L^{2a} wurde zusammen mit Acetylaceton zur Darstellung von sieben neuen Seltenerdverbindungen verwendet. Fünf der tetranuklearen Verbindungen $\{[Ln_4(\mu_3\text{-}OH)_2(L^2)(HL^2)(acac)_5(H_2O)]\cdot(NO_3)\cdot(HNEt_3)\cdot 2(Et_2O)\}$ Ln = Tb (**17**), Dy (**18**), Ho (**19**), Er (**20**), Tm (**21**) besitzen eine "Sägezahn"-Anordnung der Metallionen. Eine andere tetranukleare Verbindung $\{[Dy_4(\mu_4\text{-}OH)(L^2)_2(acac)_4(MeOH)_2(EtOH)(H_2O)]\cdot(NO_3)\cdot 2(MeOH)\cdot 3(EtOH)\}$ (**22**) bildet ein quadratisch planares Gitter aus. Die pentanukleare Verbindung $\{[Dy_5(\mu_5\text{-}NO_3)(L^2)(L^{2a})_2(acac)_6(iPrOH)_2(H_2O)(OH)]\cdot 4(H_2O)\}$ (**23**) besitzt eine einzigartige pentagonal planare Anordnung der Dysprosiumionen, in welcher das zentrale Nitration an alle Dysprosiumatome koordiniert. Magnetische Studien der Verbindungen **17**, **18**, **19** und **23** lassen auf schwache antiferromagnetische Wechselwirkungen zwischen benachbarten Metallionen schließen, zudem wird keine langsame Relaxation der Magnetisierung bei Temperaturen bis 1.8 K beobachtet.

Durch Verwendung von Dibenzoylmethan als Proligand konnten zwei mononukleare Verbindungen $\{[Tb(Phacac)_4]\cdot(Et_3NH)\}$ **(24)**, und $\{[Dy(Phacac)_4]_2\cdot 2(Et_3NH)\cdot 3(CH_2Cl_2)\}$ **(25)** erhalten werden. Wurde Dibenzoylmethan zusammen mit dem H_3L^2 Proliganden verwendet, wurde die pentanukleare Verbindung $\{[Dy_5(\mu_3\text{-}OH)_2(L^2)_3(Ph_2acac)_4(MeOH)_4]\cdot 4(MeOH)\}$ **(26)** und die heptanukleare Verbindng $\{[Tb_7(\mu_3\text{-}OH)_2(\mu_5\text{-}NO_3)(\mu_3\text{-}NO_3)(L^2)_3(Ph_2acac)_5(H_2N\text{-}Ph\text{-}O)(MeO)_2(MeOH)_3]\cdot 3(MeOH)\cdot$

□ieses □ er□ist c□p□rightgeschütt□t und darf in □einer □□r□ □er□ielf□ltigt □erden n□ch an □ritte □eitergegeben □erden.
Es gilt nur für den persönlichen Gebrauch.

(MeCN)·15(H_2O) **(27)** erhalten. Die penta- und heptanukleare Verbindung sind in ihrer strukturellen Anordnung der Metallionen einzigartig und ihre unterschiedlichen Löslichkeiten spielten eine große Rolle hinsichtlich ihrer Isolierung. Die mononukleare Terbiumverbindung **24** zeigt SMM Verhalten mit einer Relaxationszeit τ_0 = 1.1 10^{-4} s und einer Energiebarriere U_{eff} = 8.53 cm^{-1}. Die mononukleare Dysprosiumverbindung **25** zeigt SMM Verhalten mit einer Relaxationszeit τ_0 = 3.9 10^{-5} und einer Energiebarriere U_{eff} = 3.94 cm^{-1} Den Verbindungen **24** und **25** wird ein thermisch aktivierter Relaxationsmechanismus zugeschrieben. Die pentanukleare Verbindung **26** zeigt SMM Verhalten bei Anlegen eines schwachen externen Gleichfelds. Die heptanukleare Verbindung **27** zeigt schwache antiferromagnetische Wechselwirkungen ohne langsame Relaxation der Magnetisierung.

Der Proligand HL wurde zur Synthese des binuklearen Komplexes {[Dy_2L_3]·3(OH)·6(H_2O)·(C_6H_{12})} (**28**) und der trinuklearen Komplexe {[Dy_2L_3(OH)]·[$Dy(NO_3)_3(H_2O)_3$]·3(Py)·2(HO)·7(H_2O)·6(MeOH)·($CHCl_3$)} **(29**) and {[$Dy_2L_3(H_2O)$]·[$Dy(NO_3)(H_2O)_7$]·5(NO_3)·3(MeOH)·7(H_2O)} **(30)** verwendet. Die binukleare kationische [Dy_2L_3] Einheit besitzt in allen Verbindungen ähnliche Strukturparameter. Sie besteht aus drei Liganden welche sich um eine pseudo-dreizähnige Achse schlängeln und eine einzigartige dreifachsträngige helikale Struktur ausbilden.

Vier neue 1D-Koordinationspolymere konnten durch solvothermal Prozesse dargestellt werden. Die Reaktionen des Salen Liganden (H_4L) mit $MnCl_2·4(H_2O)$ und $Ln(NO_3)_3·xH_2O$ führt zu 1D-Koordinationspolymeren $\{[Ln_2(MnLClNO_3)_2(dmf)_6(H_2O)_2]·(H_2O)\}_n$ (Ln = Pr (**31**), Nd (**32**), Sm (**33**) and Gd (**34**). Die Stabilität des Polymers **34** wurde durch TGA Studien belegt. Katalytischen Studien der Verbindungen **31-34** zeigen, dass es sich in Anwesenheit des oxidierenden Agens Iodosobenzol, um aktive Katalysatoren in der Sulfoxidierung von Alkyl- und Arylsulfiden handelt. Die heterogene Natur des katalytischen Prozesses konnte durch einen einfachen Filtrationstest gezeigt werden. Die Ergebnisse aus der Pulverdiffraktometrie von Verbindung **34** vor und nach der Katalyse unterschieden sich nur geringfügig , wodurch die Verbindungen **31-34** ohne Verlust der strukturellen Anordnung wiederholt in der Katalyse eingesetzt werden konnten.

□ieses □ er□ist c□p□rightgeschütt□t und darf in □einer □□r□ □er□ielf□ltigt □erden n□ch an □ritte □eitergegeben □erden.
Es gilt nur für den persönlichen Gebrauch.

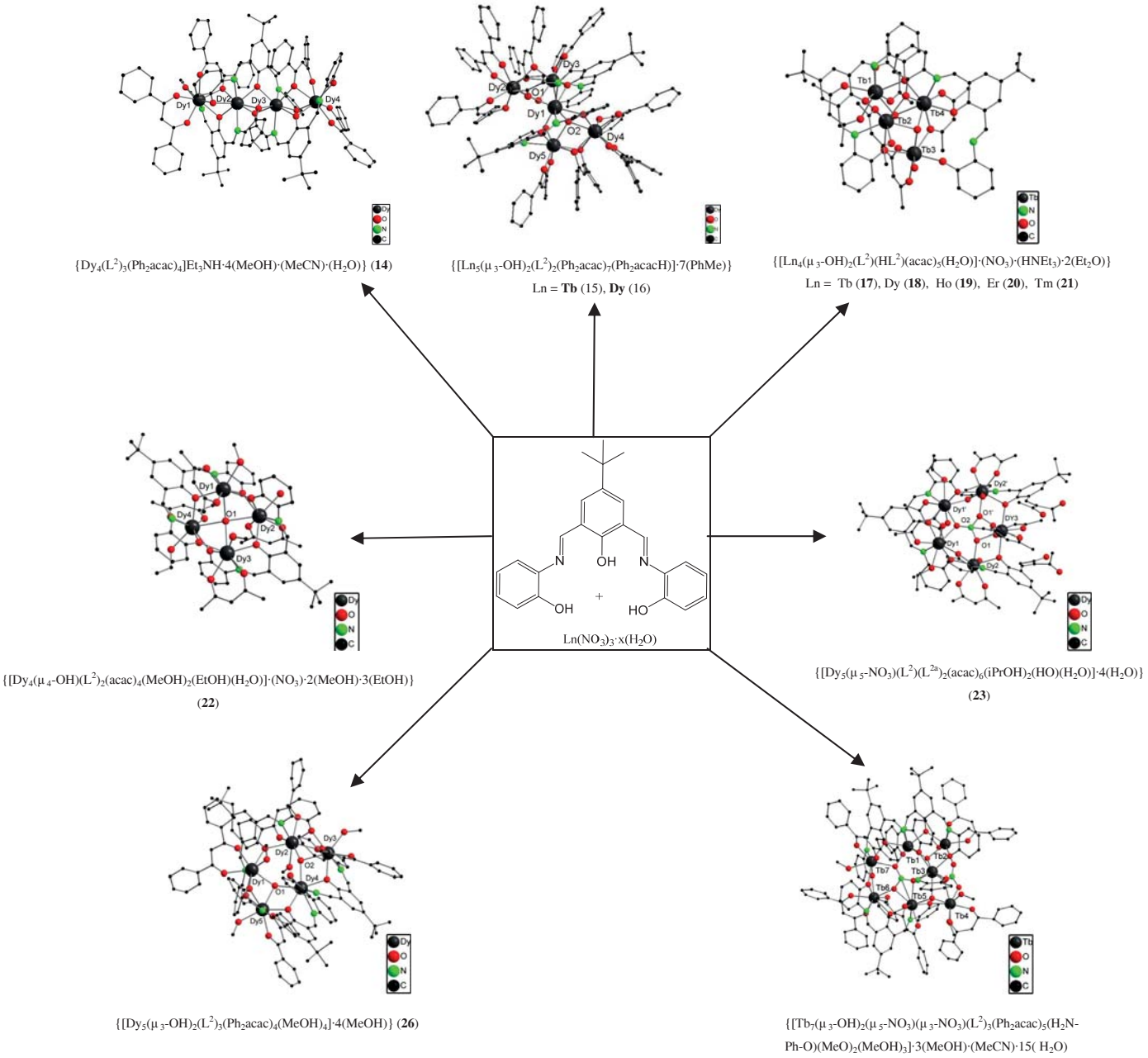

Schema 6.1 Eine kurze zusammenfassung der verbindungen des H_3L^2 proliganden.

□ieses □ er□ist c□p□rightgeschütt□t und darf in □einer □□r□ □er□ielf□ltigt □erden n□ch an □ritte □eitergegeben □erden.
Es gilt nur für den persönlichen Gebrauch.

7 References

1. Hakala, R. W., *J. Chem. Educ.* **1952,** *29*, 581-582.
2. Huheey, J. E., *Inorganic chemistry : principles of structure and reactivity*. 4th ed.; Harper Collins College Publishers: New York, NY :, 1993.
3. Douglas, B. E., *J. Chem. Educ.* **1954,** *31*, 598.
4. Shannon, R., *Acta Crystallogr. Sect. A* **1976,** *32*, 751-767.
5. Chandrasekhar, V.; Pandian, B. M.; Boomishankar, R.; Steiner, A.; Vittal, J. J.; Houri, A.; Clérac, R., *Inorg. Chem.* **2008,** *47*, 4918-4929.
6. Cui, Y.; Yue, Y.; Qian, G.; Chen, B., *Chem. Rev.* **2011,** *112*, 1126-1162.
7. Choppin, G. R.; Peterman, D. R., *Coord. Chem. Rev.* **1998,** *174*, 283-299.
8. Binnemans, K., *Chem. Rev.* **2009,** *109*, 4283-4374.
9. Eliseeva, S. V.; Bunzli, J.-C. G., *Chem. Soc. Rev.* **2010,** *39*, 189-227.
10. Handl, H. L.; Gillies, R. J., *Life Sci.* **2005,** *77*, 361-371.
11. O'Keeffe, M.; Yaghi, O. M., *Chem. Rev.* **2011,** *112*, 675-702.
12. Sabbatini, N.; Guardigli, M.; Lehn, J.-M., *Coord. Chem. Rev.* **1993,** *123*, 201-228.
13. Oude Wolbers, M. P.; van Veggel, F. C. J. M.; Peters, F. G. A.; van Beelen, E. S. E.; Hofstraat, J. W.; Geurts, F. A. J.; Reinhoudt, D. N., *Chem. Eur. J.* **1998,** *4*, 772-780.
14. Beeby, A.; Bushby, L. M.; Maffeo, D.; Gareth Williams, J. A., *Dalton Trans.* **2002**, 48-54.
15. Carlos, L. D.; Ferreira, R. A. S.; de Zea Bermudez, V.; Julian-Lopez, B.; Escribano, P., *Chem. Soc. Rev.* **2011,** *40*, 536-549.
16. Hwang, S.-H.; Moorefield, C. N.; Newkome, G. R., *Chem. Soc. Rev.* **2008,** *37*, 2543-2557.
17. Maspoch, D.; Ruiz-Molina, D.; Veciana, J., *Chem. Soc. Rev.* **2007,** *36*, 770-818.
18. Champion, G.; Escax, V.; Cartier dit Moulin, C.; Bleuzen, A.; Villain, F.; Baudelet, F.; Dartyge, E.; Verdaguer, M., *J. Am. Chem. Soc.* **2001,** *123*, 12544-12546.
19. Park, S.-H.; Oh, I.-H.; Park, S.; Park, Y.; Kim, J. H.; Huh, Y.-D., *Dalton Transactions* **2012,** *41*, 1237-1242.
20. Gatteschi, D.; Sessoli, R.; Cornia, A., *Chem. Commun.* **2000**, 725-732.
21. Sessoli, R.; Gatteschi, D.; Caneschi, A.; Novak, M. A., *Nature* **1993,** *365*, 141-143.
22. Sessoli, R.; Tsai, H. L.; Schake, A. R.; Wang, S.; Vincent, J. B.; Folting, K.; Gatteschi, D.; Christou, G.; Hendrickson, D. N., *J. Am. Chem. Soc.* **1993,** *115*, 1804-1816.
23. Thomas, L.; Lionti, F.; Ballou, R.; Gatteschi, D.; Sessoli, R.; Barbara, B., *Nature* **1996,** *383*, 145-147.
24. Gatteschi, D.; Sessoli, R., *Angew. Chem. Int. Ed.* **2003,** *42*, 268-297.

□ieses □ er□ist c□p□rightgeschüt□t und darf in □einer □□r□ □er□ielf□ltigt □erden n□ch an □ritte □eitergegeben □erden.
Es gilt nur für den persönlichen Gebrauch.

25. Sorace, L.; Benelli, C.; Gatteschi, D., *Chem. Soc. Rev.* **2011,** *40*, 3092-3104.
26. Rinehart, J. D.; Long, J. R., *Chem. Sci.* **2011,** *2*, 2078-2085.
27. Yamashita, A.; Watanabe, A.; Akine, S.; Nabeshima, T.; Nakano, M.; Yamamura, T.; Kajiwara, T., *Angew. Chem. Int. Ed.* **2011,** *50*, 4016-4019.
28. Ishikawa, N.; Sugita, M.; Ishikawa, T.; Koshihara, S.-y.; Kaizu, Y., *J. Am. Chem. Soc.* **2003,** *125*, 8694-8695.
29. Ishikawa, N.; Sugita, M.; Ishikawa, T.; Koshihara, S.-y.; Kaizu, Y., *J. Phys. Chem. B* **2004,** *108*, 11265-11271.
30. Volcker, F.; Lan, Y.; Powell, A. K.; Roesky, P. W., *Dalton Trans.* **2013,** *42*, 11471-11475.
31. Car, P.-E.; Perfetti, M.; Mannini, M.; Favre, A.; Caneschi, A.; Sessoli, R., *Chem. Commun.* **2011,** *47*, 3751-3753.
32. Luo, F.; Liao, Z.-w.; Song, Y.-m.; Huang, H.-x.; Tian, X.-z.; Sun, G.-m.; Zhu, Y.; Yuan, Z.-Z.; Luo, M.-b.; Liu, S.-j.; Xu, W.-y.; Feng, X.-F., *Dalton Trans.* **2011,** *40*, 12651-12655.
33. Ruiz, J.; Mota, A. J.; Rodriguez-Dieguez, A.; Titos, S.; Herrera, J. M.; Ruiz, E.; Cremades, E.; Costes, J. P.; Colacio, E., *Chem. Commun.* **2012,** *48*, 7916-7918.
34. Campbell, V. E.; Guillot, R.; Riviere, E.; Brun, P.-T.; Wernsdorfer, W.; Mallah, T., *Inorg. Chem.* **2013,** *52*, 5194-5200.
35. Fortea-Pérez, F. R.; Vallejo, J.; Julve, M.; Lloret, F.; De Munno, G.; Armentano, D.; Pardo, E., *Inorg. Chem.* **2013,** *52*, 4777-4779.
36. Lin, P.-H.; Korobkov, I.; Burchell, T. J.; Murugesu, M., *Dalton Trans.* **2012,** *41*, 13649-13655.
37. Rinehart, J. D.; Fang, M.; Evans, W. J.; Long, J. R., *J. Am. Chem. Soc.* **2011,** *133*, 14236-14239.
38. Fatila, E. M.; Rouzières, M.; Jennings, M. C.; Lough, A. J.; Clérac, R.; Preuss, K. E., *J. Am. Chem. Soc.* **2013,** *135*, 9596-9599.
39. Mei, X.-L.; Liu, R.-N.; Wang, C.; Yang, P.-P.; Li, L.-C.; Liao, D.-Z., *Dalton Trans.* **2012,** *41*, 2904-2909.
40. Vallejo, J.; Cano, J.; Castro, I.; Julve, M.; Lloret, F.; Fabelo, O.; Canadillas-Delgado, L.; Pardo, E., *Chem. Commun.* **2012,** *48*, 7726-7728.
41. Li, X.-L.; Chen, C.-L.; Gao, Y.-L.; Liu, C.-M.; Feng, X.-L.; Gui, Y.-H.; Fang, S.-M., *Chem. Eur. J.* **2012,** *18*, 14632-14637.
42. Lin, P.-H.; Sun, W.-B.; Yu, M.-F.; Li, G.-M.; Yan, P.-F.; Murugesu, M., *Chem. Commun.* **2011,** *47*, 10993-10995.
43. Chibotaru, L. F.; Ungur, L.; Soncini, A., *Angew. Chem. Int. Ed.* **2008,** *47*, 4126-4129.

□ieses □ er□ist c□p□rightgeschütz□t und darf in □einer □□r□ □er□ielf□ltigt □erden n□ch an □ritte □eitergegeben □erden.
Es gilt nur für den persönlichen Gebrauch.

44. Hewitt, I. J.; Lan, Y.; Anson, C. E.; Luzon, J.; Sessoli, R.; Powell, A. K., *Chem. Commun.* **2009**, 6765-6767.
45. Lin, S.-Y.; Zhao, L.; Guo, Y.-N.; Zhang, P.; Guo, Y.; Tang, J., *Inorg. Chem.* **2012,** *51*, 10522-10528.
46. Xue, S.; Zhao, L.; Guo, Y.-N.; Chen, X.-H.; Tang, J., *Chem. Commun.* **2012,** *48*, 7031-7033.
47. Anwar, M. U.; Thompson, L. K.; Dawe, L. N.; Habib, F.; Murugesu, M., *Chem. Commun.* **2012,** *48*, 4576-4578.
48. Zheng, Y.-Z.; Lan, Y.; Anson, C. E.; Powell, A. K., *Inorg. Chem.* **2008,** *47*, 10813-10815.
49. Yan, P.-F.; Lin, P.-H.; Habib, F.; Aharen, T.; Murugesu, M.; Deng, Z.-P.; Li, G.-M.; Sun, W.-B., *Inorg. Chem.* **2011,** *50*, 7059-7065.
50. Chandrasekhar, V.; Das, S.; Dey, A.; Hossain, S.; Sutter, J.-P., *Inorg. Chem.* **2013,** *52*, 11956-11965.
51. Chandrasekhar, V.; Hossain, S.; Das, S.; Biswas, S.; Sutter, J.-P., *Inorg. Chem.* **2013,** *52*, 6346-6353.
52. Blagg, R. J.; Muryn, C. A.; McInnes, E. J. L.; Tuna, F.; Winpenny, R. E. P., *Angew. Chem. Int. Ed.* **2011,** *50*, 6530-6533.
53. Gamer, M. T.; Lan, Y.; Roesky, P. W.; Powell, A. K.; Clérac, R., *Inorg. Chem.* **2008,** *47*, 6581-6583.
54. Hussain, B.; Savard, D.; Burchell, T. J.; Wernsdorfer, W.; Murugesu, M., *Chem. Commun.* **2009**, 1100-1102.
55. Roesky, P. W.; Bhunia, A.; Lan, Y.; Powell, A. K.; Kureti, S., *Chem. Commun.* **2011,** *47*, 2035-2037.
56. Chandrasekhar, V.; Bag, P.; Colacio, E., *Inorg. Chem.* **2013,** *52*, 4562-4570.
57. Demir, S.; Zadrozny, J. M.; Nippe, M.; Long, J. R., *J. Am. Chem. Soc.* **2012,** *134*, 18546-18549.
58. Jiang, S.-D.; Wang, B.-W.; Su, G.; Wang, Z.-M.; Gao, S., *Angew. Chem. Int. Ed.* **2010,** *49*, 7448-7451.
59. Cucinotta, G.; Perfetti, M.; Luzon, J.; Etienne, M.; Car, P.-E.; Caneschi, A.; Calvez, G.; Bernot, K.; Sessoli, R., *Angew. Chem. Int. Ed.* **2012,** *51*, 1606-1610.
60. Batchelor, L. J.; Cimatti, I.; Guillot, R.; Tuna, F.; Wernsdorfer, W.; Ungur, L.; Chibotaru, L. F.; Campbell, V. E.; Mallah, T., *Dalton Trans.* **2014**.
61. Tuna, F.; Smith, C. A.; Bodensteiner, M.; Ungur, L.; Chibotaru, L. F.; McInnes, E. J. L.; Winpenny, R. E. P.; Collison, D.; Layfield, R. A., *Angew. Chem. Int. Ed.* **2012,** *51*, 6976-6980.

□ieses □ er□ist c□p□rightgeschütt□t und darf in □einer □□r□ □er□ielf□ltigt □erden n□ch an □ritte □eitergegeben □erden.
Es gilt nur für den persönlichen Gebrauch.

62. Guo, Y.-N.; Xu, G.-F.; Wernsdorfer, W.; Ungur, L.; Guo, Y.; Tang, J.; Zhang, H.-J.; Chibotaru, L. F.; Powell, A. K., *J. Am. Chem. Soc.* **2011,** *133*, 11948-11951.

63. Lin, P.-H.; Burchell, T. J.; Ungur, L.; Chibotaru, L. F.; Wernsdorfer, W.; Murugesu, M., *Angew. Chem. Int. Ed.* **2009,** *48*, 9489-9492.

64. Guo, Y.-N.; Xu, G.-F.; Gamez, P.; Zhao, L.; Lin, S.-Y.; Deng, R.; Tang, J.; Zhang, H.-J., *J. Am. Chem. Soc.* **2010,** *132*, 8538-8539.

65. Hewitt, I. J.; Tang, J.; Madhu, N. T.; Anson, C. E.; Lan, Y.; Luzon, J.; Etienne, M.; Sessoli, R.; Powell, A. K., *Angew. Chem. Int. Ed.* **2010,** *49*, 6352-6356.

66. Shen, S.; Xue, S.; Lin, S.-Y.; Zhao, L.; Tang, J., *Dalton Trans.* **2013,** *42*, 10413-10416.

67. Tian, H.; Zhao, L.; Lin, H.; Tang, J.; Li, G., *Chem. Eur. J.* **2013,** *19*, 13235-13241.

68. Peng, J.-B.; Kong, X.-J.; Ren, Y.-P.; Long, L.-S.; Huang, R.-B.; Zheng, L.-S., *Inorg. Chem.* **2012,** *51*, 2186-2190.

69. Canaj, A. B.; Tzimopoulos, D. I.; Philippidis, A.; Kostakis, G. E.; Milios, C. J., *Inorg. Chem.* **2012,** *51*, 7451-7453.

70. Zaleski, C. M.; Depperman, E. C.; Kampf, J. W.; Kirk, M. L.; Pecoraro, V. L., *Angew. Chem. Int. Ed.* **2004,** *43*, 3912-3914.

71. Stamatatos, T. C.; Teat, S. J.; Wernsdorfer, W.; Christou, G., *Angew. Chem. Int. Ed.* **2009,** *48*, 521-524.

72. Kong, X.-J.; Wu, Y.; Long, L.-S.; Zheng, L.-S.; Zheng, Z., *J. Am. Chem. Soc.* **2009,** *131*, 6918-6919.

73. Bhunia, A.; Gamer, M. T.; Ungur, L.; Chibotaru, L. F.; Powell, A. K.; Lan, Y.; Roesky, P. W.; Menges, F.; Riehn, C.; Niedner-Schatteburg, G., *Inorg. Chem.* **2012,** *51*, 9589-9597.

74. Gu, X.; Xue, D., *Inorg. Chem.* **2007,** *46*, 3212-3216.

75. Westin, L. G.; Kritikos, M.; Caneschi, A., *Chem. Commun.* **2003**, 1012-1013.

76. Tian, H.; Zhao, L.; Guo, Y.-N.; Guo, Y.; Tang, J.; Liu, Z., *Chem. Commun.* **2012,** *48*, 708-710.

77. Blagg, R. J.; Ungur, L.; Tuna, F.; Speak, J.; Comar, P.; Collison, D.; Wernsdorfer, W.; McInnes, E. J. L.; Chibotaru, L. F.; Winpenny, R. E. P., *Nat Chem* **2013,** *5*, 673-678.

78. Tang, J.; Hewitt, I.; Madhu, N. T.; Chastanet, G.; Wernsdorfer, W.; Anson, C. E.; Benelli, C.; Sessoli, R.; Powell, A. K., *Angew. Chem. Int. Ed.* **2006,** *45*, 1729-1733.

79. Luzon, J.; Bernot, K.; Hewitt, I. J.; Anson, C. E.; Powell, A. K.; Sessoli, R., *Phys. Rev. Lett.* **2008,** *100*, 247205.

80. McLellan, R.; Palacios, M. A.; Beavers, C. M.; Teat, S. J.; Brechin, E. K.; Dalgarno, S. J., *Chem. Commun.* **2013,** *49*, 9552-9554.

□ieses □ er□ist c□p□rightgeschütz□t und darf in □einer □□r□ □er□ielf□ltigt □erden n□ch an □ritte □eitergegeben □erden.
Es gilt nur für den persönlichen Gebrauch.

81. Ke, H.; Xu, G.-F.; Guo, Y.-N.; Gamez, P.; Beavers, C. M.; Teat, S. J.; Tang, J., *Chem. Commun.* **2010,** *46*, 6057-6059.

82. Lin, S.-Y.; Zhao, L.; Ke, H.; Guo, Y.-N.; Tang, J.; Guo, Y.; Dou, J., *Dalton Trans.* **2012,** *41*, 3248-3252.

83. Rinehart, J. D.; Fang, M.; Evans, W. J.; Long, J. R., *Nat Chem* **2011,** *3*, 538-542.

84. Gonidec, M.; Luis, F.; Vílchez, À.; Esquena, J.; Amabilino, D. B.; Veciana, J., *Angew. Chem. Int. Ed.* **2010,** *49*, 1623-1626.

85. Gonidec, M.; Biagi, R.; Corradini, V.; Moro, F.; De Renzi, V.; del Pennino, U.; Summa, D.; Muccioli, L.; Zannoni, C.; Amabilino, D. B.; Veciana, J., *J. Am. Chem. Soc.* **2011,** *133*, 6603-6612.

86. Jiang, S.-D.; Wang, B.-W.; Sun, H.-L.; Wang, Z.-M.; Gao, S., *J. Am. Chem. Soc.* **2011,** *133*, 4730-4733.

87. Watanabe, A.; Yamashita, A.; Nakano, M.; Yamamura, T.; Kajiwara, T., *Chem. Eur. J.* **2011,** *17*, 7428-7432.

88. Yamaguchi, T.; Sunatsuki, Y.; Ishida, H.; Kojima, M.; Akashi, H.; Re, N.; Matsumoto, N.; Pochaba, A.; Mroziński, J., *Inorg. Chem.* **2008,** *47*, 5736-5745.

89. Bhunia, A.; Yadav, M.; Lan, Y.; Powell, A. K.; Menges, F.; Riehn, C.; Niedner-Schatteburg, G.; Jana, P. P.; Riedel, R.; Harms, K.; Dehnen, S.; Roesky, P. W., *Dalton Trans.* **2013,** *42*, 2445-2450.

90. Pasatoiu, T. D.; Sutter, J.-P.; Madalan, A. M.; Fellah, F. Z. C.; Duhayon, C.; Andruh, M., *Inorg. Chem.* **2011,** *50*, 5890-5898.

91. Gheorghe, R.; Madalan, A. M.; Costes, J.-P.; Wernsdorfer, W.; Andruh, M., *Dalton Trans.* **2010,** *39*, 4734-4736.

92. Visinescu, D.; Madalan, A. M.; Andruh, M.; Duhayon, C.; Sutter, J.-P.; Ungur, L.; Van den Heuvel, W.; Chibotaru, L. F., *Chem. Eur. J.* **2009,** *15*, 11808-11814.

93. Andruh, M.; Costes, J.-P.; Diaz, C.; Gao, S., *Inorg. Chem.* **2009,** *48*, 3342-3359.

94. Kajiwara, T.; Nakano, M.; Takahashi, K.; Takaishi, S.; Yamashita, M., *Chem. Eur. J.* **2011,** *17*, 196-205.

95. Xu, G.-F.; Gamez, P.; Tang, J.; Clérac, R.; Guo, Y.-N.; Guo, Y., *Inorg. Chem.* **2012,** *51*, 5693-5698.

96. Chandrasekhar, V.; Pandian, B. M.; Boomishankar, R.; Steiner, A.; Clerac, R., *Dalton Trans.* **2008**, 5143-5145.

97. Schray, D.; Abbas, G.; Lan, Y.; Mereacre, V.; Sundt, A.; Dreiser, J.; Waldmann, O.; Kostakis, G. E.; Anson, C. E.; Powell, A. K., *Angew. Chem. Int. Ed.* **2010,** *49*, 5185-5188.

□ieses □ er□ist c□p□rightgeschütt□t und darf in □einer □□r□ □er□ielf□ltigt □erden n□ch an □ritte □eitergegeben □erden.
Es gilt nur für den persönlichen Gebrauch.

98. Chandrasekhar, V.; Pandian, B. M.; Azhakar, R.; Vittal, J. J.; Clérac, R., *Inorg. Chem.* **2007,** *46*, 5140-5142.

99. Cimpoesu, F.; Dahan, F.; Ladeira, S.; Ferbinteanu, M.; Costes, J.-P., *Inorg. Chem.* **2012,** *51*, 11279-11293.

100. Costes, J.-P.; Yamaguchi, T.; Kojima, M.; Vendier, L., *Inorg. Chem.* **2009,** *48*, 5555-5561.

101. Barta, C. A.; Bayly, S. R.; Read, P. W.; Patrick, B. O.; Thompson, R. C.; Orvig, C., *Inorg. Chem.* **2008,** *47*, 2280-2293.

102. Yamaguchi, T.; Sunatsuki, Y.; Kojima, M.; Akashi, H.; Tsuchimoto, M.; Re, N.; Osa, S.; Matsumoto, N., *Chem. Commun.* **2004**, 1048-1049.

103. Rocha, A. R.; Garcia-suarez, V. M.; Bailey, S. W.; Lambert, C. J.; Ferrer, J.; Sanvito, S., *Nat. Mater.* **2005,** *4*, 335-339.

104. Bogani, L.; Wernsdorfer, W., *Nat. Mater.* **2008,** *7*, 179-186.

105. Affronte, M., *J. Mater. Chem.* **2009,** *19*, 1731-1737.

106. Leuenberger, M. N.; Loss, D., *Nature* **2001,** *410*, 789-793.

107. Ardavan, A.; Rival, O.; Morton, J. J. L.; Blundell, S. J.; Tyryshkin, A. M.; Timco, G. A.; Winpenny, R. E. P., *Phys. Rev. Lett.* **2007,** *98*, 057201.

108. Stamp, P. C. E.; Gaita-Arino, A., *J. Mater. Chem.* **2009,** *19*, 1718-1730.

109. Tomic, E. A., *J. Appl. Polym. Sci.* **1965,** *9*, 3745-3752.

110. Robson, R., *J. Chem. Soc., Dalton Trans.* **2000**, 3735-3744.

111. Eddaoudi, M.; Kim, J.; Rosi, N.; Vodak, D.; Wachter, J.; O'Keeffe, M.; Yaghi, O. M., *Science* **2002,** *295*, 469-472.

112. Chae, H. K.; Siberio-Perez, D. Y.; Kim, J.; Go, Y.; Eddaoudi, M.; Matzger, A. J.; O'Keeffe, M.; Yaghi, O. M., *Nature* **2004,** *427*, 523-527.

113. Zhou, H.-C.; Long, J. R.; Yaghi, O. M., *Chem. Rev.* **2012,** *112*, 673-674.

114. Li, H.; Eddaoudi, M.; O'Keeffe, M.; Yaghi, O. M., *Nature* **1999,** *402*, 276-279.

115. Getman, R. B.; Bae, Y.-S.; Wilmer, C. E.; Snurr, R. Q., *Chem. Rev.* **2011,** *112*, 703-723.

116. Sumida, K.; Rogow, D. L.; Mason, J. A.; McDonald, T. M.; Bloch, E. D.; Herm, Z. R.; Bae, T.-H.; Long, J. R., *Chem. Rev.* **2011,** *112*, 724-781.

117. Yoon, M.; Srirambalaji, R.; Kim, K., *Chem. Rev.* **2011,** *112*, 1196-1231.

118. Heitbaum, M.; Glorius, F.; Escher, I., *Angew. Chem. Int. Ed.* **2006,** *45*, 4732-4762.

119. Fujita, M.; Kwon, Y. J.; Washizu, S.; Ogura, K., *J. Am. Chem. Soc.* **1994,** *116*, 1151-1152.

120. Sawaki, T.; Dewa, T.; Aoyama, Y., *J. Am. Chem. Soc.* **1998,** *120*, 8539-8540.

121. Jung Soo, S.; Dongmok, W.; Hyoyoung, L.; Sung Im, J.; Jinho, O.; Young Jin, J.; Kimoon, K., *Nature* **2000,** *404*, 982-986.

□ieses □ er□ist c□p□rightgeschütz□t und darf in □einer □□r□ □er□ielf□ltigt □erden n□ch an □ritte □eitergegeben □erden.
Es gilt nur für den persönlichen Gebrauch.

122. Evans, O. R.; Ngo, H. L.; Lin, W., *J. Am. Chem. Soc.* **2001,** *123*, 10395-10396.

123. Hu, A.; Ngo, H. L.; Lin, W., *J. Am. Chem. Soc.* **2003,** *125*, 11490-11491.

124. Wu, C.-D.; Hu, A.; Zhang, L.; Lin, W., *J. Am. Chem. Soc.* **2005,** *127*, 8940-8941.

125. Cho, S.-H.; Ma, B.; Nguyen, S. T.; Hupp, J. T.; Albrecht-Schmitt, T. E., *Chem. Commun.* **2006**, 2563-2565.

126. Banerjee, M.; Das, S.; Yoon, M.; Choi, H. J.; Hyun, M. H.; Park, S. M.; Seo, G.; Kim, K., *J. Am. Chem. Soc.* **2009,** *131*, 7524-7525.

127. Ma, L.; Falkowski, J. M.; Abney, C.; Lin, W., *Nat Chem* **2010,** *2*, 838-846.

128. Lun, D. J.; Waterhouse, G. I. N.; Telfer, S. G., *J. Am. Chem. Soc.* **2011,** *133*, 5806-5809.

129. Bhunia, A.; Gotthardt, M. A.; Yadav, M.; Gamer, M. T.; Eichhöfer, A.; Kleist, W.; Roesky, P. W., *Chem. Eur. J.* **2013,** *19*, 1986-1995.

130. Falkowski, J. M.; Sawano, T.; Zhang, T.; Tsun, G.; Chen, Y.; Lockard, J. V.; Lin, W., *J. Am. Chem. Soc.* **2014,** *136*, 5213-5216.

131. Yang, Z.; Zhu, C.; Li, Z.; Liu, Y.; Liu, G.; Cui, Y., *Chem. Commun.* **2014,** *50*, 8775-8778.

132. Wojaczyńska, E.; Wojaczyński, J., *Chem. Rev.* **2010,** *110*, 4303-4356.

133. Bentley, R., *Chem. Soc. Rev.* **2005,** *34*, 609-624.

134. Falkowski, J. M.; Liu, S.; Wang, C.; Lin, W., *Chem. Commun.* **2012,** *48*, 6508-6510.

135. Bogaerts, T.; Van Yperen-De Deyne, A.; Liu, Y.-Y.; Lynen, F.; Van Speybroeck, V.; Van Der Voort, P., *Chem. Commun.* **2013,** *49*, 8021-8023.

136. Wang, C.; Wang, J.-L.; Lin, W., *J. Am. Chem. Soc.* **2012,** *134*, 19895-19908.

137. Zhu, C.; Chen, X.; Yang, Z.; Du, X.; Liu, Y.; Cui, Y., *Chem. Commun.* **2013,** *49*, 7120-7122.

138. Legros, J.; Bolm, C., *Chem. Eur. J.* **2005,** *11*, 1086-1092.

139. Liao, S.; List, B., *Adv. Synth. Catal.* **2012,** *354*, 2363-2367.

140. Wang, X.; Wang, X.; Guo, H.; Wang, Z.; Ding, K., *Chem. Eur. J.* **2005,** *11*, 4078-4088.

141. Maurya, M. R.; Kumar, U.; Manikandan, P., *Eur. J. Inorg. Chem.* **2007,** *2007*, 2303-2314.

142. Langley, S. K.; Chilton, N. F.; Gass, I. A.; Moubaraki, B.; Murray, K. S., *Dalton Trans.* **2011,** *40*, 12656-12659.

143. Jiang, S.-D.; Liu, S.-S.; Zhou, L.-N.; Wang, B.-W.; Wang, Z.-M.; Gao, S., *Inorg. Chem.* **2012,** *51*, 3079-3087.

144. Meihaus, K. R.; Rinehart, J. D.; Long, J. R., *Inorg. Chem.* **2011,** *50*, 8484-8489.

145. Roesky, P. W.; Canseco-Melchor, G.; Zulys, A., *Chem. Commun.* **2004**, 738-739.

146. Datta, S.; Baskar, V.; Li, H.; Roesky, P. W., *Eur. J. Inorg. Chem.* **2007**, 4216-4220.

147. Baskar, V.; Roesky, P. W., *Z. Anorg. Allg. Chem.* **2005,** *631*, 2782-2785.

□ieses □ er□ist c□p□rightgeschüt□t und darf in □einer □□r□ □er□ielf□ltigt □erden n□ch an □ritte □eitergegeben □erden.
Es gilt nur für den persönlichen Gebrauch.

148. Andrews, P. C.; Beck, T.; Forsyth, C. M.; Fraser, B. H.; Junk, P. C.; Massi, M.; Roesky, P. W., *Dalton Trans.* **2007**, 5651-5654.

149. Gamer, M. T.; Lan, Y.; Roesky, P. W.; Powell, A. K.; Clérac, R., *Inorg. Chem.* **2008,** *47*, 6581-6583.

150. Thielemann, D. T.; Wagner, A. T.; Rösch, E.; Kölmel, D. K.; Heck, J. G.; Rudat, B.; Neumaier, M.; Feldmann, C.; Schepers, U.; Bräse, S.; Roesky, P. W., *J. Am. Chem. Soc.* **2013,** *135*, 7454-7457.

151. Thielemann, D. T.; Wagner, A. T.; Lan, Y.; Anson, C. E.; Gamer, M. T.; Powell, A. K.; Roesky, P. W., *Dalton Trans.* **2013,** *42*, 14794-14800.

152. Osa, S.; Kido, T.; Matsumoto, N.; Re, N.; Pochaba, A.; Mrozinski, J., *J. Am. Chem. Soc.* **2004,** *126*, 420-421.

153. Goura, J.; Walsh, J. P. S.; Tuna, F.; Chandrasekhar, V., *Inorg. Chem.* **2014,** *53*, 3385-3391.

154. Thielemann, D. T.; Klinger, M.; Wolf, T. J. A.; Lan, Y.; Wernsdorfer, W.; Busse, M.; Roesky, P. W.; Unterreiner, A.-N.; Powell, A. K.; Junk, P. C.; Deacon, G. B., *Inorganic Chemistry* **2011,** *50*, 11990-12000.

155. Lin, S.-Y.; Xu, G.-F.; Zhao, L.; Guo, Y.-N.; Guo, Y.; Tang, J., *Dalton Trans.* **2011,** *40*, 8213-8217.

156. van der Sluis, P.; Spek, A. L., *Acta Crystallogr. Sect. A* **1990,** *46*, 194-201.

157. Spek, A., *Acta Crystallogr. Sect. A* **1990,** *46*, c34.

158. Lebedkin, S.; Langetepe, T.; Sevillano, P.; Fenske, D.; Kappes, M. M., *J. Phys. Chem. B* **2002,** *106*, 9019-9026.

159. Sheldrick, G. M., *Acta Crystallogr. Sect. A* **2008,** *64*, 112-122.

□ieses □ er□ist c□p□rightgeschüt□t und darf in □einer □□r□ □er□ielf□ltigt □erden n□ch an □ritte □eitergegeben □erden.
Es gilt nur für den persönlichen Gebrauch.

8 Appendices

8.1 Directory of Abbreviations

Ln	Lanthanide
Me	Methyl
Ar	Aryl group
Py	Pyridine
Et	Ethyl
Ph	Phenyl
PhMe	Toluene
MeCN	Acetonitrile
iPrOH	Isopropanol
dcm	Dichloromethane
DMF	Dimethylformamide
Tren	Tris(2-aminoethyl)amine
ETAH	Protonated ethanolamine
acac	dimethylmethanide
acacH	acetylacetone
Phacac	dibenzoylmethanide
PhacacH	dibenzoylmethane
$HNEt_3$	Protonated triethylamine
NEt_3	Triethylamine
R	Organic group
Calcd	Calculated

□ieses □ er□ist c□p□rightgeschütt□t und darf in □einer □□r□ □er□ielf□ltigt □erden n□ch an □ritte □eitergegeben □erden.
Es gilt nur für den persönlichen Gebrauch.

Obsd	Observed
M	Metal atom
Ln	Lanthanide
L	Ligand
mg	milligram
mL	millilitre
mmol	millimole
NMR	Nuclear magnetic resonance
EI-MS	Electron-ionization mass spectrometry
IR	Infrared
TGA	Thermogravimetric analysis
MOFs	Metal organic frameworks
CMOFs	Chiral metal organic frameworks
MCPs	Microporous coordination polymers
UMCs	Unsaturated metal centers
ICPs	Infinite coordination polymers
SMMs	Single molecule magnets

8.1.1 NMR Abbreviations

δ	Chemical shift
ppm	Parts per million
s	Singlet
d	Doublet

□ieses □ er□ist c□p□rightgeschütt□t und darf in □einer □□r□ □er□ielf□ltigt □erden n□ch an □ritte □eitergegeben □erden.
Es gilt nur für den persönlichen Gebrauch.

t	Triplet
m	Multiplet

8.1.2 IR Abbreviations

br	Broad
w	Weak
m	Medium
s	Strong

8.1.3 Magnetic Abbreviations

SQUID	Super-conducting quantum interference device
ac	Alternating current
dc	Direct current
D	zero-field splitting parameter
K	Kelvin
Oe	Oersted
H	Field
Hz	Hertz
M	Magnetisation
T	Tesla
Tb	Blocking temperature
Tc	Critical temperature
h	Hour
χ	Molar magnetic susceptibility
χ'	In-phase magnetic susceptibility
χ''	Out-of-phase magnetic susceptibility

□ieses □ er□ist c□p□rightgeschütt□t und darf in □einer □□r□ □er□ielf□ltigt □erden n□ch an □ritte □eitergegeben □erden.
Es gilt nur für den persönlichen Gebrauch.

τ	Relaxation rate
μB	Bohr magneton
U_{eff}	Effective energy barrier
cm^3	Cubic centimetres

8.2 Directory of Compounds

1	$\{[Y(HL)_4][ETAH]\cdot(H_2O)\}$
2	$\{[Dy(HL_{)4}]\ [ETAH]\cdot(3MeOH)\cdot(H_2O)\}$
3	$\{[Y_4(HL)_2(L)_4(\mu_3\text{-}OH)_2]\cdot 4(MeOH)\cdot 4(H_2O)\}$
4	$\{[Dy_4(HL)_2(L)_4(\mu_3\text{-}OH)_2]\cdot 5(MeOH)\cdot 7(H_2O)\}$
5	$\{[Dy_4(HL)_8(L)_2]\cdot 4(MeOH)\cdot 2(H_2O)\}$
6	$\{[Dy(HL^1)_2(H_2O)_3](NO_3)\}$
7	$\{NiGdL(acac)_2\}$
8	$\{NiTbL(acac)_2\}$
9	$\{[NiDyL(acac)_2]_2\cdot 7(MeOH)\}$
10	$\{[NiDyL(Phacac)_2]_2\cdot 4(CH_2Cl_2)\cdot(MeOH)\}$
11	$\{[Ni_2Gd(L^1)_2]\cdot(NO_3)\cdot 2(H_2O)\}$
12	$\{[Ni_2Tb(L^1)_2]_4\cdot 4(NO_3)\cdot 3(MeCN)\cdot 5(MeOH)\cdot(H_2O)\}$
13	$\{[Ni_2Dy(L^1)_2]\cdot(NO_3)\cdot(MeOH)\cdot(H_2O)\}$
14	$\{Dy_4(L^2)_3(Ph_2acac)_4](Et_3NH)\cdot 4(MeOH)\cdot(MeCN)\cdot(H_2O)\}$
15	$\{[Tb_5(\mu_3\text{-}OH)_2(L^2)_2(Ph_2acac)_7(Ph_2acacH)]\cdot 7(PhMe)\}$
16	$\{[Dy_5(\mu_3\text{-}OH)_2(L^2)_2((Ph_2acac)_7(Ph_2acacH)]\cdot 7(PhMe)\}$
17	$\{[Tb_4(\mu_3\text{-}OH)_2(L^2)(HL^2)(acac)_5(H_2O)]\cdot(NO_3)\cdot(HNEt_3)\cdot 2(Et_2O)\}$
18	$\{[Dy_4(\mu_3\text{-}OH)_2(L^2)(HL^2)(acac)_5(H_2O)]\cdot(NO_3)\cdot(HNEt_3)\cdot 2(Et_2O)\}$

□ieses □ er□ist c□p□rightgeschütt□t und darf in □einer □□r□ □er□ielf□ltigt □erden n□ch an □ritte □eitergegeben □erden.
Es gilt nur für den persönlichen Gebrauch.

19 $\{[Ho_4(\mu_3\text{-}OH)_2(L^2)(HL^2)(acac)_5(H_2O)]\cdot(NO_3)\cdot(HNEt_3)\cdot 2(Et_2O)\}$

20 $\{[Er_4(\mu_3\text{-}OH)_2(L^2)(HL^2)(acac)_5(H_2O)]\cdot(NO_3)\cdot(HNEt_3)\cdot 2(Et_2O)\}$

21 $\{[Tm_4(\mu_3\text{-}OH)_2(L^2)(HL^2)(acac)_5(H_2O)]\cdot(NO_3)\cdot(HNEt_3)\cdot 2(Et_2O)\}$

22 $\{[Dy_4(\mu_4\text{-}OH)(L^2)_2(acac)_4(MeOH)_2(EtOH)(H_2O)]\cdot(NO_3)\cdot 2(MeOH)\cdot 3(EtOH)\}$

23 $\{[Dy_5(\mu_5\text{-}NO_3)(L^2)(L^{2a})_2(acac)_6(iPrOH)_2(HO)(H_2O]\cdot 4(H_2O)\}$

24 $\{[Tb(Phacac)_4]\cdot(Et_3NH)\}$

25 $\{[Dy(Phacac)_4]_2\cdot 2(Et_3NH)\cdot 3(CH_2Cl_2)\}$

26 $\{[Dy_5(\mu_3\text{-}OH)_2(L^2)_3(Ph_2acac)_4(MeOH)_4]\cdot 4(MeOH)\}$

27 $\{[Tb_7(\mu_3\text{-}OH)_2(\mu_5\text{-}NO_3)(\mu_3\text{-}NO_3)(L^2)_3(Ph_2acac)_5(H_2N\text{-}Ph\text{-}O)(MeO)_2(MeOH)_3]\cdot 3(MeOH)\cdot(MeCN)\cdot(15H_2O)$

28 $\{[Dy_2L_3]\cdot 3(OH)\cdot 6(H_2O)\cdot(C_6H_{12})\}$

29 $\{[Dy_2L_3(OH)]\cdot[Dy(NO_3)_3(H_2O)_3]\cdot 3(Py)\cdot 2(HO)\cdot 7(H_2O)\cdot 6(MeOH)\cdot(CHCl_3)\}$

30 $\{[Dy_2L_3(H_2O)]\cdot[Dy(NO_3)(H_2O)_7]\cdot 5(NO_3)\cdot 3(MeOH)\cdot 7(H_2O)\}$

31 $\{[Pr_2(MnLClNO_3)_2(dmf)_6(H_2O)_2]\cdot(H_2O)\}_n$

32 $\{[Nd_2(MnLClNO_3)_2(dmf)_6(H_2O)_2]\cdot(H_2O)\}_n$

33 $\{[Sm_2(MnLClNO_3)_2(dmf)_6(H_2O)_2]\cdot(H_2O)\}_n$

34 $\{[Gd_2(MnLClNO_3)_2(dmf)_6(H_2O)_2]\cdot(H_2O)\}_n$

□ieses □ er□ist c□p□rightgeschütt□t und darf in □einer □□r□ □er□ielf□ltigt □erden n□ch an □ritte □eitergegeben □erden.
Es gilt nur für den persönlichen Gebrauch.

□ieses □ er□ist c□p□rightgeschütt□t und darf in □einer □□r□ □er□ielf□ltigt □erden n□ch an □ritte □eitergegeben □erden.
Es gilt nur für den persönlichen Gebrauch.

Acknowledgements

First and above all, I praise God, the almighty for providing me this opportunity and granting me the capability to proceed successfully. There are a number of people without whom this thesis might not have been written, and to whom I am greatly indebted.

Foremost I take this opportunity to express my deepest gratitude and sincere thanks to my PhD supervisor Prof. Dr. Peter W. Roesky. I will never forget his enthusiastic encouragement, valuable suggestions, jolly nature and continuous support during my research work and writing of my thesis. He always gave me new ideas as well as the liberty to work on my own ideas. His constructive criticism was invaluable. His advice and extensive discussions of my work always helped me and I could not have imagined a better supervisor for my PhD thesis.

I would like to convey my sincere thanks to Prof. Dr. Dieter Fenske and Dr. Olaf Fuhr who suggested and recommended me to join Prof. Roesky's research group. I appreciate Dr. Olaf for all the help he provided and helping me with crystallographic problems. I am very thankful to Prof. Dr. Jai Deo Singh for introducing me to research and recommending me for a DAAD fellowship during my master's program. Without him it would have been difficult to come to Germany and pursue my master's thesis here.

I would like to thank Dr. Valeriu Mereacre, Dr. Abhishake Mondal for their help with magnetic measurements; Dr.Sergei Lebedkin and Prof. Dr. Manfred M. Kappes for their assistance with photoluminescence measurements. Apart from her cooperation in magnetic measurements, I found Prof. Fr. Annie K. Powell to be a friendly colleague and good badminton player.

I would like to further express my gratitude towards Dr. Andreas Eichhöfer for his assistance in PXRD measurements; Dr. Michael Gamer and Dr. Sebastian Marks who always gave me valuable suggestions in crystallography. I would like to thank Schneider Sibylle and Petra Smie for the single crystal, mass spectroscopy and HPLC measurements. They have always been friendly in their advice and jolly in nature.

I am grateful to thank Monika Kayas and Angie Pendl for all the paperwork they assisted me with. I am also especially thankful to Rory Kelly, Tessa Wagner, Claude Kiefer, Ashok, Amritesh, Salil, Marie Fustier-Boutignon, Sebastian Bestgen and Kamini for proofreading and thesis correction during my thesis writing.

I would like to thank Dr. Ralf Köppe, Nicholas Arleth, Tobias Brunner, Sebastian Schäfer, Franziska Völcker, Eugenia Tausch, David Schrader, Christoph Schoo, He Meng, Neda Kazeminejad,

□ieses □ er□ist c□p□rightgeschüt□t und darf in □einer □□r□ □er□ielf□ltigt □erden n□ch an □ritte □eitergegeben □erden.
Es gilt nur für den persönlichen Gebrauch.

Christoph Kaub, Larissa Hartenstein, Christoph Götz, Matthias Schmid, Denise Girnt, Tanja Sanden and Tianshu Li for their help during my PhD. I am grateful to Asmanjoy Bhunia and Sanjay Singh for their kind suggestions. I am thankful to Paul Benndorf and Jochen Kratsch for helping me with software related problems.

Thanks to Frau Berberich (NMR), Frau Lude (elementalanalysis), Herr Müller (mass spectrometry) Herr Rieß, Herr Lampert and Herr Kastner (mechanical workshop), Herr Schlachter (electrical workshop), Frau Leichle (chemical store), Herr Munshi (glassblowing) and Frau Maurer.

I thank my friends, Ravi, Nilesha, Ashok, Amritesh, Bhawana, Partha, Robbin, Tapas, Biplab, Sulabh, Nayan, uncle Ashok and aunty Eva for their great company during my stay in Karlsruhe. Whenever I needed support, whenever I was lost in dark and needed directions, I always found my brother Kailash standing by my side, guiding me; I thank him and wish he would always remain so. Finally, my wholehearted thanks to parents, my sister, cousins, Bhabhi, niece, friends and relatives for believing in me and providing the continuous support and encouragement which made my work possible. Thanks to Pankaj for his friendship. Thanks to my wife Kamini for her love and support.

□ieses □ er□ist c□p□rightgeschüt□t und darf in □einer □□r□ □er□ielf□ltigt □erden n□ch an □ritte □eitergegeben □erden.
Es gilt nur für den persönlichen Gebrauch.

Curriculum vitae

Name:	Munendra Yadav
Date of birth:	7th July 1986
Place of birth:	Etah (Uttar Pradesh), India
Parents	Mr. Ghanraj Singh and Mrs. Kanta Devi
Marital status:	Married
Nationality:	Indian

Education

Ph. D. in Chemistry (Sep. 2011- Oct. 2014) Department of Chemistry, Karlsruhe Institute of Technology, Germany.

Thesis Supervisor	Prof. Dr. Peter W. Roesky
Thesis Title	Synthesis of 4f and 3d-4f Homo and Hetrometallic Complexes: Magnetsim, Photoluminescence and Catalytic Studies.

Master of Technology (2011) Department of Chemistry, Indian Institute of Technology Delhi, India.

Master of Science (2008) Department of Chemistry, Aligarh Muslim University, Aligarh, India.

Bachelor of Science (2005) Department of Chemistry, Aligarh Muslim University, Aligarh, India.

Master Projects:

June-August – (2010) Summer project under Prof. Dr. Jai Deo Singh in the Department of Chemistry. I.I.T, Delhi, India

September(2010)-May (2011) Master project under Prof. Dr. Dieter Fenske and Dr. Olaf Fuhr in Institute of Nanotechnology, K.I.T. Karlsruhe Germany, India.

□ieses □ er□ist c□p□rightgeschütt□t und darf in □einer □□r□ □er□ielf□ltigt □erden n□ch an □ritte □eitergegeben □erden.
Es gilt nur für den persönlichen Gebrauch.

List of Publications

1. Sanjay K. Singh, **Munendra Yadav**, Silke Behrens and Peter W. Roesky "Au-based bimetallic nanoparticles for the intramolecular aminoalkene hydroamination" ***Dalton Trans.,* 2013**, *42*, 10404-10408.

2. Asamanjoy Bhunia, **Munendra Yadav**, Yanhua Lan, Annie K. Powell, Fabian Menges, Christoph Riehn, Gereon Niedner-Schatteburg, Partha P. Jana, Radostan Riedel, Klaus Harms, Stefanie Dehnen and Peter W. Roesky "Trinuclear nickel–lanthanide compounds" ***Dalton Trans.,* 2013, *42***, 2445-2450.

3. Asamanjoy Bhunia, Meike A. Gotthardt, **Munendra Yadav**, Michael T. Gamer,Andreas Eichhçfer,Wolfgang Kleist and Peter W. Roesky "Salen-Based Coordination Polymers of Manganese and the Rare-Earth Elements: Synthesis and Catalytic Aerobic Epoxidation of Olefins" ***Chem. Eur. J.* 2013*, 19, 1***986 – 1995.

4. Robert Langer, **Munendra Yadav**, Bastian Weinert, Dieter Fenske, Olaf Fuhr "Fluorescence in Functionalized Copper Thiolate Clusters: Synthesis and Structural Effects" ***Eur. J. Inorg. Chem.* 2013**, *21*, 3623–3631.

5**. Munendra Yadav**, Valeriu Mereacre, Sergei Lebedkin, Manfred M. Kappes, Annie K. Powell, and Peter W. Roesky "Mononuclear and Tetranuclear Compounds of Yttrium and Dysprosium ligated by a Salicylic Schiff-Base Derivative: Synthesis, Photoluminescence and Magnetism" ***Inorg. Chem.* 2015**, *54*, 773-781.

Participation and Poster Presentation in Conferences

1. 16 vortragstagung der Wohler-Vereinigung 26-28, Septmeber, 2012, Gottingen, Germany.
2. Heidelberg Forum of Molecular catalysis June 28, 2013 Heidelberg, Germany.
3. 2nd international conference on Bimetallic complexes 23-25, 2013 Karlsruhe, Germany.
4. XXV. Tage der Seltenen Erden –Terrae Rarae-Universitat Stuttgart 05.12-07.12.2013 Stuttgart, Germany.
5. XXVI. Tage der Seltenen Erden –Terrae Rarae- Universität zu Köln 06.07-08.07.2014 Stuttgart, Germany.

□ieses □ er□ist c□p□rightgeschüt□t und darf in □einer □□r□ □er□ielf□ltigt □erden n□ch an □ritte □eitergegeben □erden.
Es gilt nur für den persönlichen Gebrauch.

□ieses □ er□ist c□p□rightgeschütt□t und darf in □einer □□r□ □er□ielf□ltigt □erden n□ch an □ritte □eitergegeben □erden.
Es gilt nur für den persönlichen Gebrauch.

□ieses □ er□ist c□p□rightgeschütt□t und darf in □einer □□r□ □er□ielf□ltigt □erden n□ch an □ritte □eitergegeben □erden.
Es gilt nur für den persönlichen Gebrauch.